JULIUS-MAXIMILIANS-UNIVERSITÄT
WÜRZBURG

Synthesis and Reactivity of Pseudohalide-substituted Boranes and Borylenes

DISSERTATION ZUR ERLANGUNG DES
NATURWISSENSCHAFTLICHEN DOKTORGRADES

Stephan Hagspiel

Würzburg 2021

Synthesis and Reactivity of Pseudohalide-substituted Boranes and Borylenes

Dissertation zur Erlangung
des naturwissenschaftlichen Doktorgrades
der
Julius-Maximilians-Universität Würzburg

vorgelegt von

Stephan Alexander Hagspiel
aus
Memmingen

Würzburg 2021

Eingereicht bei der Fakultät für Chemie und Pharmazie der Julius-Maximilians-Universität Würzburg am 21. September 2021.

Gutachter der schriftlichen Arbeit:

1. Gutachter: Prof. Dr. Holger Braunschweig

2. Gutachter: Prof. Dr. Maik Finze

Prüfer des öffentlichen Promotionskolloquiums:

1. Prüfer: Prof. Dr. Holger Braunschweig

2. Prüfer: Prof. Dr. Maik Finze

3. Prüfer: Prof. Dr. Ingo Fischer

4. Prüfer: Prof. Dr. Matthias Lehmann

5. Prüfer: PD Dr. Florian Beuerle

Datum des öffentlichen Promotionskolloquiums: 12. November 2021

Doktorurkunde ausgehändigt am: _____

Die vorliegende Arbeit wurde in der Zeit von Oktober 2018 bis September 2021 am Institut für Anorganische Chemie der Julius-Maximilians-Universität Würzburg unter der Leitung von Prof. Dr. Holger Braunschweig angefertigt.

Die vorliegende Arbeit wurde auszugsweise veröffentlicht unter:

Reduction of a dihydroboryl cation to a boryl anion and its air-stable, neutral hydroboryl radical through hydrogen shuttling

S. Hagspiel, M. Arrowsmith, F. Fantuzzi, A. Hermann, V. Paprocki, R. Drescher, I. Krummenacher, H. Braunschweig, *Chem. Sci.* **2020**, *11*, 551–555.

Highly Colored Boron-Doped Thiazolothiazoles from the Reductive Dimerization of Boron Isothiocyanates

S. Hagspiel, M. Arrowsmith, F. Fantuzzi, A. Vargas, A. Rempel, A. Hermann, T. Brückner, H. Braunschweig, *Angew. Chem. Int. Ed.* **2021**, *60*, 6446–6450; *Angew. Chem.* **2021**, *133*, 6519–6524.

Adducts of the Parent Boraphosphaketene H_2BPCO and their Decarbonylative Insertion Chemistry

S. Hagspiel, F. Fantuzzi, R. D. Dewhurst, A. Gärtner, F. Lindl, A. Lamprecht, H. Braunschweig, *Angew. Chem. Int. Ed.* **2021**, *60*, 13666–13670; *Angew. Chem.* **2021**, *133*, 13780–13784.

Reactivity of cyano- and isothiocyanatoborylenes: metal coordination, one-electron oxidation and boron-centred Brønsted basicity

S. Hagspiel, D. Elezi, M. Arrowsmith, F. Fantuzzi, A. Vargas, A. Rempel, M. Härterich, I. Krummenacher, H. Braunschweig, *Chem. Sci.* **2021**, *12*, 7937–7942.

Weitere Beiträge zu Publikationen während der Promotion:

Facile Synthesis of a Stable Dihydroboryl $\{BH_2\}^-$ Anion

M. Arrowsmith, J. D. Mattock, S. Hagspiel, I. Krummenacher, A. Vargas, H. Braunschweig, *Angew. Chem. Int. Ed.* **2018**, *57*, 15272–15275; *Angew. Chem.* **2018**, *130*, 15493–15497.

Synthesis of unsymmetrical B_2E_2 and B_2E_3 heterocycles by borylene insertion into boradichalcogeniranes

S. Liu, M.-A. Légaré, A. Hofmann, A. Rempel, S. Hagspiel, H. Braunschweig, *Chem. Sci.* **2019**, *10*, 4662–4666.

Vorbemerkung

In der eigens am Lehrstuhl für Anorganische Chemie II der Julius-Maximilians-Universität Würzburg unter der Leitung von Herrn Prof. Dr. Holger Braunschweig angefertigten Arbeit zur Erlangung des akademischen Grades *Master of Science* mit dem Titel „Synthese und Reaktivität neuer Borylene“ wurde bereits über die Darstellung des Triflatoborans ($CAAC^{Me}$)BH_2(OTf) (**1^{Me}**) sowie dessen Umsetzungen zu Boroniumkationen der Form [($CAAC^{Me}$)(L)BH_2]OTf (**2-L**) (L = $CAAC^{Me}$, PMe_3, DMAP, Pyr) und [($CAAC^{Me}$H)(L)$_2$BH]OTf (**3-L**) (L = DMAP, Pyr) berichtet.[1] Aufgrund unvollständiger Charakterisierungen wurde dieses Themengebiet im Rahmen der vorliegenden Arbeit erneut bearbeitet und findet hier ebenfalls Erwähnung (Kapitel II 2.1).

Darüber hinaus wurde in der eigenen Masterarbeit die Synthese sowie das Reduktionsverhalten $CAAC^{Me}$-stabilisierter Isothiocyanatoborane beschrieben, wobei die im Folgenden als **9^{Me}**, **10^{Me}** und **16^{Me}** bezeichneten Verbindungen röntgenkristallographisch sowie teilweise NMR-spektroskopisch untersucht werden konnten. Aufgrund ausstehender Analysen und wissenschaftlicher Fragestellungen wurde dieses Themengebiet in der vorliegenden Arbeit weiterführend bearbeitet. Aus Gründen der Vollständigkeit und Übersichtlichkeit werden die bereits erhaltenen Ergebnisse erneut beschrieben (Kapitel II 2.2 und II 2.3).

In den letzten Jahren wurde in der Literatur zwiegespalten über den Formalismus für die Beschreibung der elektronischen Struktur von Hauptgruppenelementverbindungen diskutiert.[2-4] Dabei kann grundsätzlich zwischen einer dativen (D→A) und einer kovalenten, zwitterionischen (D^+–A^-) Schreibweise zwischen einem Donor (D) und einem Akzeptor (A) unterschieden werden. In der vorliegenden Arbeit wird ausschließlich die dative „Pfeilschreibweise“ verwendet, wobei ein ganzer Pfeil ein Elektronenpaar und ein halber (gestrichelter) Pfeil ein einzelnes Elektron repräsentiert.

List of Abbreviations

Å	Ångström (10^{-10} m)
atm	atmosphere(s)
$BAr^{Cl}{}_4$	tetrakis(3,5-dichlorophenyl)borate
$BAr^{F}{}_4$	tetrakis[3,5-bis(trifluoromethyl)phenyl]borate
Bipy	4,4'-bipyridine
br	broad
°C	degree Celsius
CAAC	cyclic alkyl(amino)carbene
$CAAC^{Cy}$	2-(2,6-di*iso*propylphenyl)-3,5-dimethyl-2-azaspiro[4.5]decan-1-ylidene
$CAAC^{Et}$	1-(2,6-di*iso*propylphenyl)-3,3-diethyl-5,5-dimethyl-pyrrolidin-2-ylidene
$CAAC^{Me}$	1-(2,6-di*iso*propylphenyl)-3,3,5,5-tetramethyl-pyrrolidin-2-ylidene
calcd.	calculated
Cat	catecholato
CCDC	Cambridge Crystallographic Data Center
cm	centimeter
Cp*	pentamethylcyclopentadienyl
CV	cyclic voltammetry
Cy	cyclohexyl
d	doublet (NMR); day(s)
DCD	Dewar-Chatt-Duncanson
DFT	density functional theory
Dipp	2,6-di*iso*propylphenyl
DMAP	4-dimethylaminopyridine
Dur	2,3,5,6-tetramethylphenyl
E	energy
E	main group element
e.g.	lat. "*exempli gratia*", engl. „for example"
EPR	electron paramagnetic resonance
equiv	equivalent(s)
Et	ethyl
eV	electronvolt

Fc	ferrocene
FT	Fourier transformation
g	gram
h	Planck constant = $6.62607015 \cdot 10^{-34}$ Js
h	hour(s)
HOMO	highest occupied molecular orbital
HRMS	high resolution mass spectrometry
Hz	Hertz
i	*ipso*
i.e.	lat. "*id est*", engl. "that is"
IDipp	1,3-bis(2,6-di*iso*propylphenyl)imidazol-2-ylidene
I*i*Pr	1,3-di*iso*propylimidazol-2-ylidene
*i*Pr	*iso*propyl
IMe	1,3-dimethylimidazol-2-ylidene
IMe^{Me}	1,3,4,5-tetramethylimidazol-2-ylidene
IR	infrared
J	coupling constant (NMR)
J	Joule
K	Kelvin
kcal	kilocalories
L	neutral donor ligand, Lewis base
LUMO	lowest unoccupied molecular orbital
m	*meta*
m	multiplet (NMR)
M	(transition) metal
Me	methyl
MeOTf	methyl trifluoromethanesulfonate
MHz	megahertz
min	minute(s)
mL	milliliter
mmol	millimole
*n*Bu	*n*-butyl

NHC	*N*-heterocyclic carbene
NMR	nuclear magnetic resonance
o	*ortho*
OTf	trifluoromethanesulfonate
p	*para*
Ph	phenyl
Pyr	pyridine
q	quartet (NMR)
R	anionic substituent, specified in text
rt	ambient temperature
s	singlet (NMR)
sept	septet (NMR)
SOMO	singly occupied molecular orbital
t	triplet (NMR)
T	temperature
TMS	trimethylsilyl
Tn	2-thienyl
TS	transition state
UV-vis	ultraviolet-visible
V	Volt
VT	variable temperature
vide infra	see below
vide supra	see above
X	halogen, specified in text
xs	excess
Xyl	2,6-dimethylphenyl
Y	pseudohalogen, specified in text
δ	chemical shift (NMR) in ppm
Φ_{fl}	fluorescence quantum yield
λ	wavelength [nm], absorption maximum
λ_{max}	global absorption maximum
$\tilde{\nu}$	wavenumber [cm^{-1}]

Table of Contents

I Introduction

1.1 Advent and Historical Development of Borylenes

The last few decades have been characterized by a tremendous upswing in low-valent main group chemistry. Foremost among these is the chemistry of subvalent group 14 species, in particular carbenes RR'C: (R, R' = anionic substituent). While carbenes were long thought to be short-lived due to their lack of electronic and coordinative saturation, over the last thirty years they have evolved from reactive intermediates to isolable compounds with numerous applications.[5,6] The first structural evidence for carbon atoms with an electron sextet was obtained by the groups of Fischer and Schrock by stabilizing the carbene center in the coordination sphere of transition metals.[7,8] Since the synthesis and isolation of the first free carbene by Arduengo in 1991,[9] the class of *N*-heterocyclic carbenes (NHC) has evolved to become an integral part of modern organometallic chemistry.[10] Their remarkable development and influence in fields such as pharmaceuticals,[11] photoactive materials[12] or homogeneous catalysis[13] have been reviewed in numerous articles.[5,14,15] Applications in homogeneous catalysis include commercially important processes such as cross-coupling reactions[16] and asymmetric syntheses.[17] Likewise, Grubbs catalysts, used in olefin metathesis reactions, underwent a literal generation change owing to the systematic replacement of phosphines by NHCs.[18,19]

In NHCs stabilization of the low-valent carbene carbon atom is achieved by π donation of the two vicinal nitrogen atoms into its vacant p orbital. Formally, the non-bonding electron pair is localized in a sp^2 hybrid orbital with σ symmetry. Depending on the hybridization of the imidazole backbone, NHCs are in general subdivided into unsaturated (*e.g.* I*i*Pr = 1,3-di*iso*propylimidazol-2-ylidene) and saturated NHCs (*e.g.* SIDipp = 1,3-bis(2,6-di*iso*propyl-phenyl)imidazolidin-2-ylidene), with the latter having a slightly smaller HOMO–LUMO gap in comparison (Figure 1).

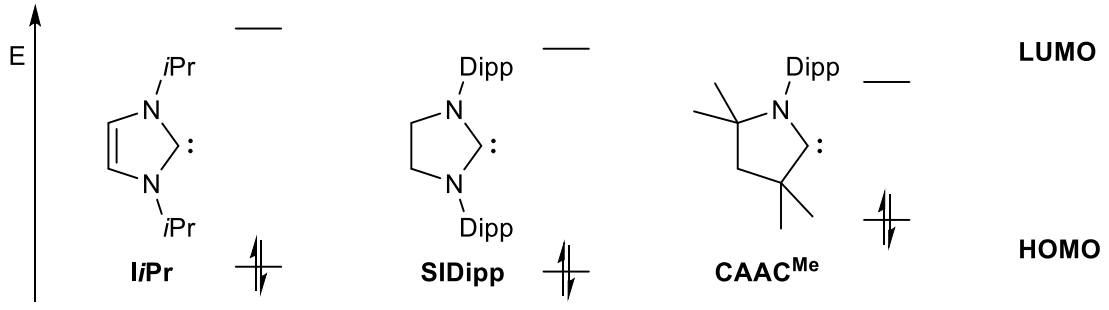

Figure 1. Schematic representation of the relative HOMO and LUMO energies of selected NHCs and $CAAC^{Me}$. I*i*Pr = 1,3-di*iso*propylimidazol-2-ylidene. SIDipp = 1,3-bis(2,6-di*iso*propylphenyl)imidazolidin-2-ylidene. $CAAC^{Me}$ = 1-(2,6-di*iso*propylphenyl)-3,3,5,5-tetramethylpyrrolidin-2-ylidene.

In 2005 the series of singlet carbenes was extended by Bertrand and co-workers to include cyclic alkyl(amino)carbene (CAAC) ligands, in which one amino functionality of the imidazole ring is replaced by an alkyl moiety.[20] This substitution results in an increase in the energy of the HOMO and a decrease in that of the LUMO. Thus, CAAC ligands (*e.g.* $CAAC^{Me}$ = 1-(2,6-di*iso*propylphenyl)-3,3,5,5-tetramethylpyrrolidin-2-ylidene) are both better σ donors and π acceptors than NHCs. This allows unprecedented reactivity patterns of CAACs such as the activation of small molecules (*e.g.* CO, CO_2, NH_3, H_2)[21,22] as well as the stabilization of previously inaccessible compounds.[23-26]

In contrast to carbenes and their heavier homologues,[27] the range of group 13 carbenoids L_nRE: (E = group 13 element, L = neutral donor ligand, R = anionic substituent) is still small and the synthesis of stable borylenes is the subject of current research.[28] While in organoboron compounds the boron atom usually adopts the oxidation state +3 and reacts as an electron acceptor, borylenes adopt the oxidation state +1, which makes them particularly electron-rich nucleophiles. According to theoretical studies free borylenes (RB:) exhibit a singlet ground state, with the non-bonding electron pair localized in a hybrid sp orbital.[29,30] With only one substituent and two vacant p orbitals orthogonal to each other, free borylenes have a larger electron deficit compared to carbenes (Figure 2).[31]

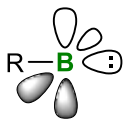

Figure 2. Schematic representation of the electronic structure of a free borylene in the singlet ground state.

The electronic structure accounts for the high reactivity of free borylenes and the difficulties associated with their characterization, which is limited to investigations by microwave and infrared spectroscopy in inert gas matrices at 4 to 10 K.[31-36] The transient formation of free borylenes has also been postulated using suitable trapping reagents.[37-39] In pioneering work by Timms and co-workers in the late 1960s,[33,40] the putative generation of the fluoroborylene (FB:) (**I**), which calculations have shown to be the most stable diatomic borylene,[30] was described for the first time. Boron fluoride (**I**) was generated from the comproportionation of BF_3 with elemental boron at 1850 °C and trapped with a variety of small molecules,[33] *e.g.* acetylene, yielding 1,4-difluoro-1,4-diborinine (**II**) (Scheme 1, top).[40] Nearly 20 years later, Pachaly and West reported the photolysis of tris(triphenylsilyl)borane (**III**) in the presence of an alkyne.[41] The isolated product was authenticated as the borirene **V**, the formation of which presumably proceeded *via* a 1,2-addition of the *in-situ* generated (triphenylsilyl)borylene (**IV**) to the C≡C triple bond of the alkyne (Scheme 1, bottom). To date, the synthesis and

characterization of free borylenes still remain limited to a few examples. Moreover, the inert gas conditions required for their isolation hamper an extensive study of the reactivity of these low-valent boron species.

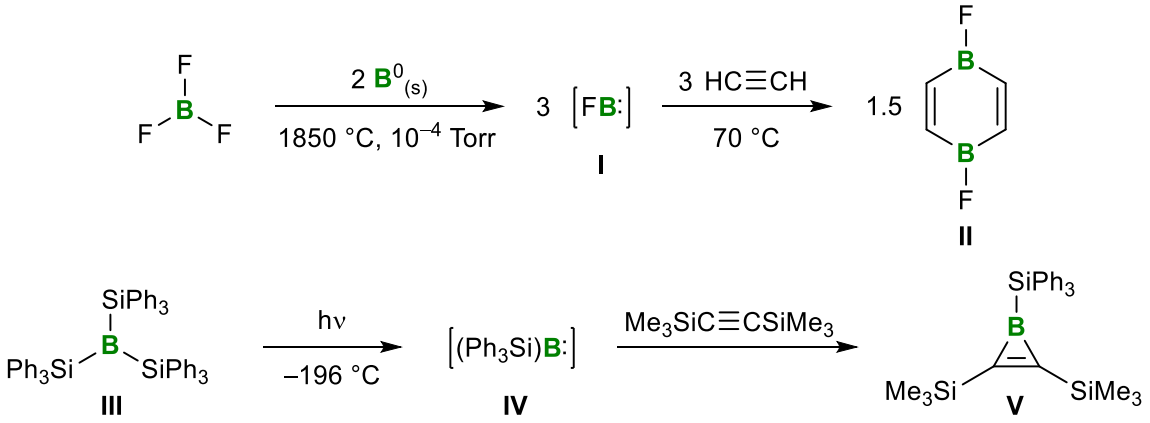

Scheme 1. *In-situ* generation and trapping of the free borylenes **I** and **IV**.

Using the first metal carbene complexes of Fischer and Schrock as a model,[7,8] our group succeeded in 1995 in synthesizing the first metal borylene complex stable at ambient temperature, in which the low-valent borylene fragment is stabilized in the coordination sphere of two manganese centers.[42] Analogously, the first terminal borylene complexes were isolated a few years later, the borylene unit of which is stabilized *via* a push-pull effect of the respective group 6 metal carbonyl fragment and the bis(trimethylsilyl)amino substituent.[43] Since then metal borylene complexes have been widely explored.[44] In contrast, the chemistry of metal-free borylenes is much more recent. In 2007 Robinson and co-workers reported the reduction of the NHC-stabilized tribromoborane (IDipp)BBr_3 (IDipp = 1,3-bis(2,6-di*iso*propyl-phenyl)imidazol-2-ylidene), resulting in the isolation of the first doubly NHC-stabilized dihydrodiborene.[45] Inspired by this reactivity, Bertrand and co-workers exchanged the NHC against a much more σ-donating and π-accepting CAAC ligand. Upon reduction of ($CAAC^{Cy}$)BBr_3 (**VI^{Cy}**) ($CAAC^{Cy}$ = 2-(2,6-di*iso*propylphenyl)-3,5-dimethyl-2-azaspiro[4.5]de-can-1-ylidene) with an excess of potassium graphite (KC_8) the first stable metal-free borylene, the parent borylene ($CAAC^{Cy}$)$_2$BH (**VII**), was isolated (Scheme 2).[46]

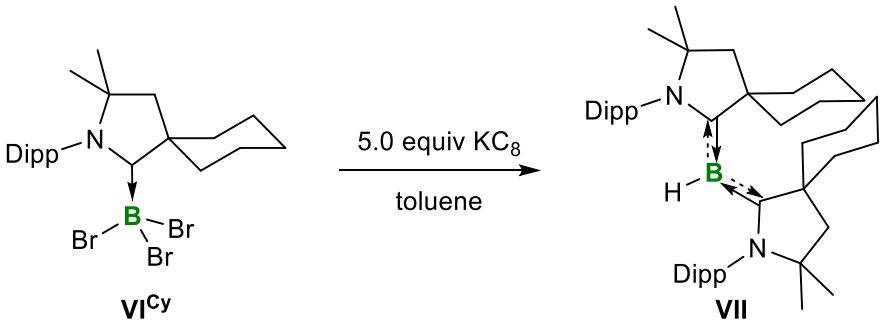

Scheme 2. Synthesis of the first metal-free borylene, compound **VII**, by Bertrand. Dipp = 2,6-di*iso*propylphenyl.

The parent borylene **VII** owes its stability to the two CAAC^{Cy} ligands, which stabilize the vacant p orbitals of the borylene through σ donation and the boron-centered lone pair through π backdonation to the π-acidic carbene carbon atoms. It is noteworthy that the former bromide substituent at boron was replaced by a hydride, likely to result from a radical hydrogen abstraction.[46] On the one hand the synthetic route to **VII** described by Bertrand is not fully understood, on the other it does not allow for variation of the stabilizing Lewis bases. The sterics and electronics of the latter could exert a considerable influence on the stability and reactivity of the borylene moiety. In view of this the same group reported an efficient, stepwise route to unsymmetrical doubly carbene-stabilized borylenes of the form (CAAC^{Et})(L)BH (**XII-L**) (CAAC^{Et} = 1-(2,6-di*iso*propylphenyl)-3,3-diethyl-5,5-dimethylpyrrolidin-2-ylidene; L = BI^{iPr}, BAC^{iPr}) (Scheme 3).[47]

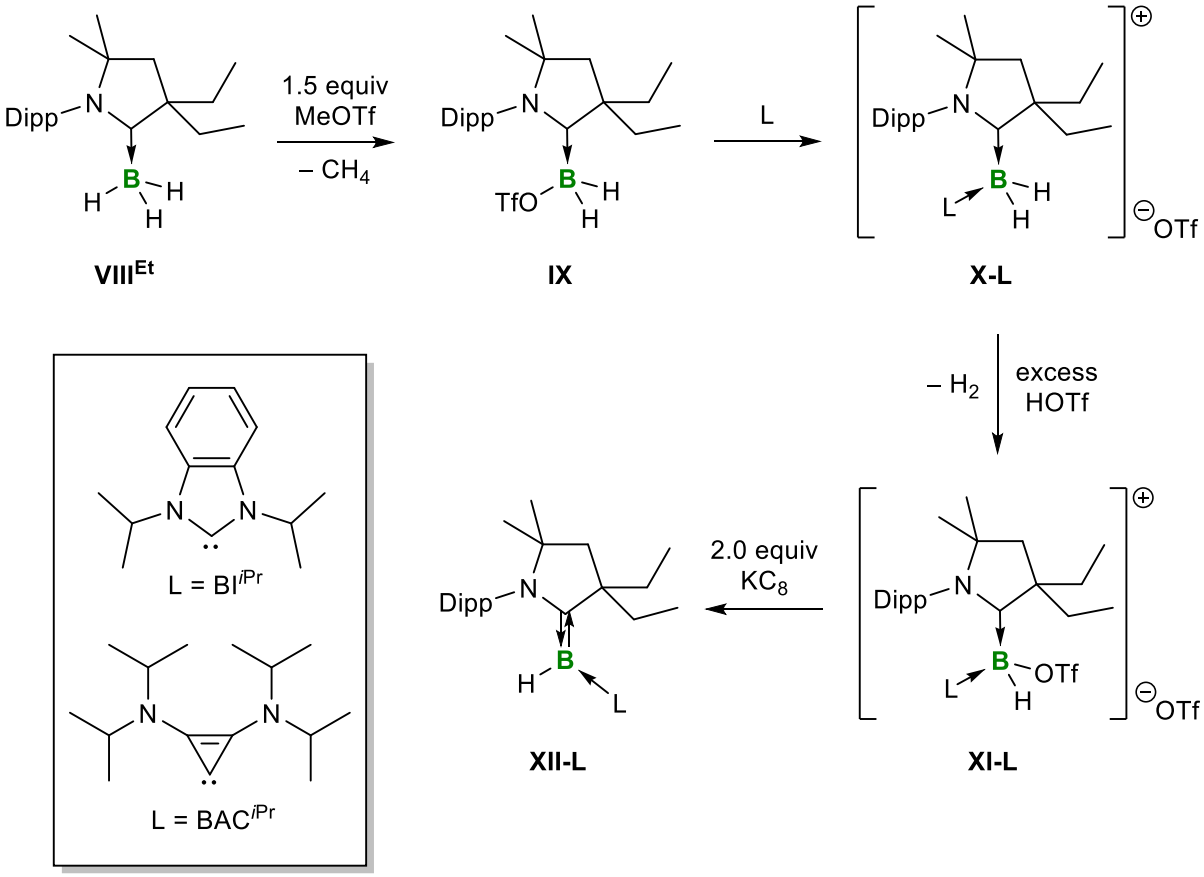

Scheme 3. Stepwise synthetic route to the unsymmetrical doubly Lewis-base-stabilized hydroborylenes **XII-L**. OTf = OSO_2CF_3.

Starting from the (CAAC^{Et})BH_3 adduct (**VIII^{Et}**), methyl trifluoromethanesulfonate (MeOTf) was employed to abstract a hydride, forming the CAAC^{Et}-stabilized triflatoborane **IX** by elimination of methane. The addition of a second Lewis base, L, displaced the triflate substituent, yielding the corresponding unsymmetrical doubly carbene-stabilized dihydroboronium cations [(CAAC^{Et})(L)BH_2]OTf (**X-L**). After the abstraction of a second

hydride with an excess of triflic acid (HOTf), the boronium cations **XI-L** were reduced with two equivalents of KC_8, generating the unsymmetrical doubly carbene-stabilized hydroborylenes **XII-L**.

In the same year Kinjo and co-workers developed an elegant route to synthesize a tricoordinate phenylborylene (Scheme 4).[48] Instead of CAAC ligands two oxazolinyl groups were attached to the boron center by reacting 2-lithio-4,4'-dimethyl-2-oxazolide (**XIII**) with dichlorophenylborane. The twofold *N*-methylation of borate **XIV** with two equivalents of MeOTf afforded the corresponding boronium salt **XV**, which was subsequently reduced with KC_8 to the doubly oxazol-2-ylidene-stabilized phenylborylene (**XVI**). This synthetic approach is remarkable in that the N,O-heterocycles are first introduced as anionic substituents and then transformed to the corresponding neutral, π-accepting donor ligands by the final reduction step.

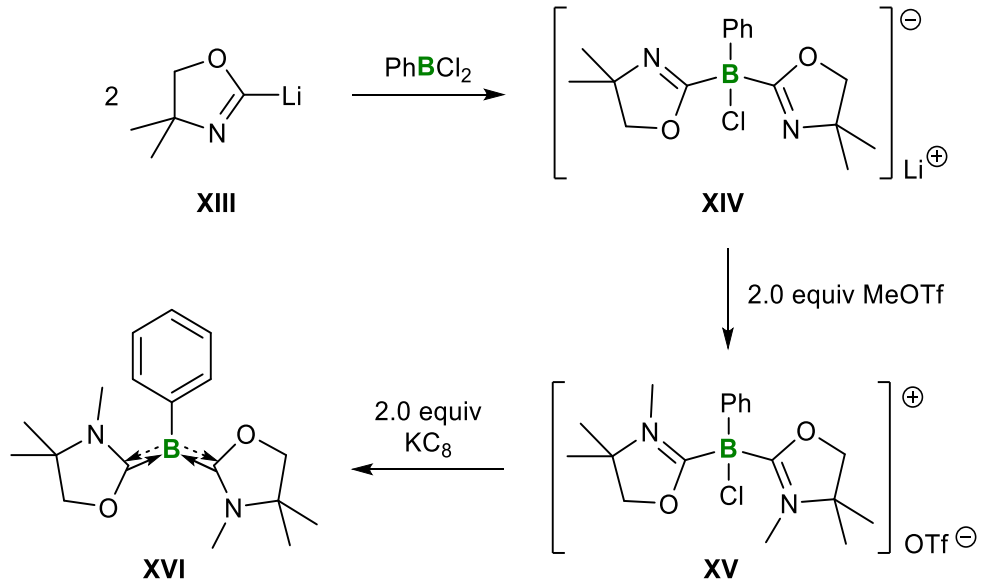

Scheme 4. Synthesis of the doubly oxazol-2-ylidene-stabilized phenylborylene **XVI** by Kinjo.

Our group also reported the preparation of metal-free arylborylenes using a completely different synthetic approach. Previous work had shown that metal borylene complexes are excellent precursors for releasing a borylene fragment.[49] When the terminal borylene transition-metal complex **XVII-Cr** was heated at 80 °C under an atmosphere of CO the terphenylborylene **XVIIIa**, stabilized by two CO ligands, was obtained (Scheme 5).[50] Similarly, the room temperature reactions of **XVII-Mo** with methyl isocyanide and the considerably more bulky 2,6-di*iso*propylphenyl isocyanide afforded the related bis(CNMe)- and (CO)(CNDipp)-stabilized terphenylborylenes **XVIIIb** and **XVIIIc**, respectively.

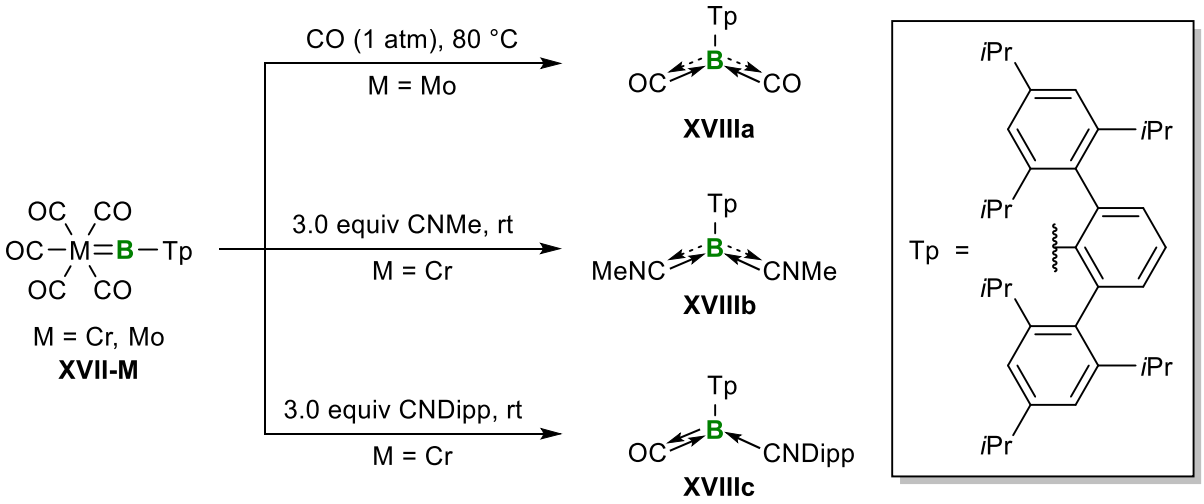

Scheme 5. Synthesis of the doubly Lewis-base-stabilized terphenylborylenes **XVIIIa-c** by Braunschweig.

Following this approach, a similar terminal iron borylene complex **XIX** was treated with the Lewis base $CAAC^{Me}$, releasing the durylborylene (duryl, Dur = 2,3,5,6-tetramethylphenyl) fragment and generating the $(CAAC^{Me})$(CO)-stabilized durylborylene (**XX-CO**) (Scheme 6a).[51] Although this synthetic protocol allows for the isolation of unsymmetrical doubly Lewis-base-stabilized borylenes, both the challenging synthesis of the transition-metal borylene complex and the subsequent release of the borylene unit limit the substitution pattern at boron and the nature of Lewis bases employed.

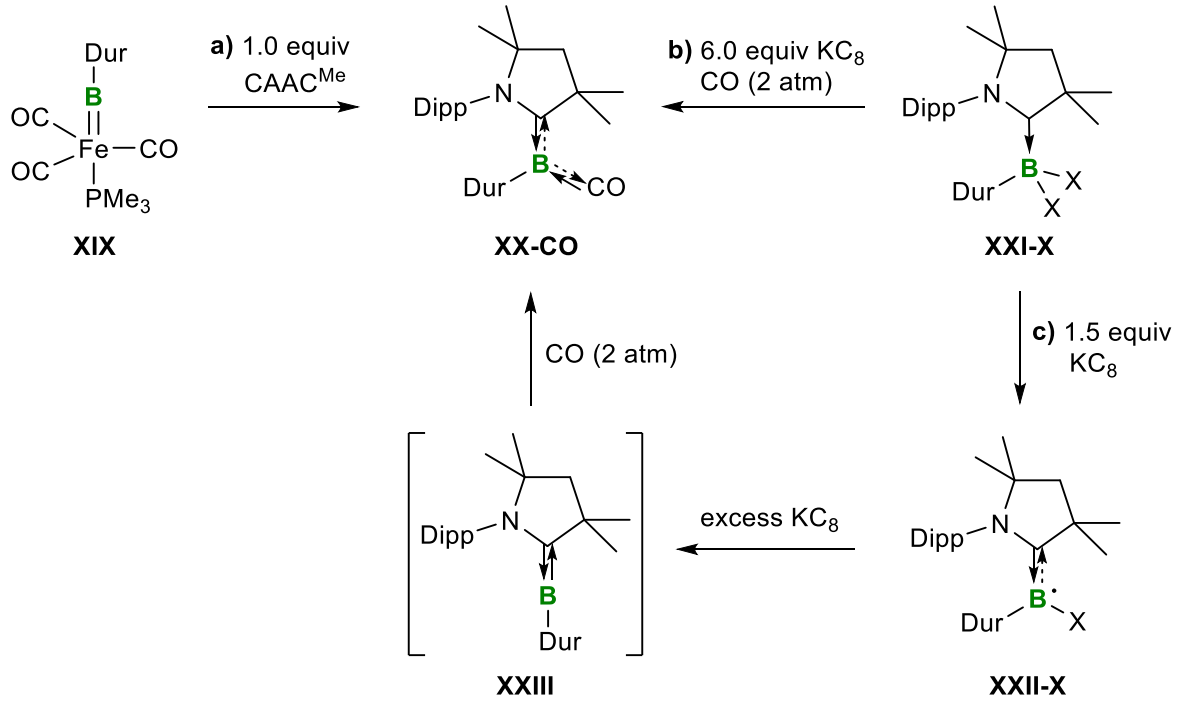

Scheme 6. a) Liberation of a durylborylene from the iron carbonyl complex **XIX**. **b)** + **c)** One- and two-electron reduction of **XXI-X**, yielding the durylboryl radicals **XXII-X** and the $(CAAC^{Me})$(CO)-stabilized durylborylene **XX-CO**. Dur = 2,3,5,6-tetramethylphenyl.

To remedy this our group designed a fully metal-free synthetic route, which is also based on the reduction of CAAC-stabilized dihaloboranes, analogous to the route of Bertrand and co-workers described previously (see Scheme 2). The reduction of $CAAC^{Me}$ adducts of the dihalodurylboranes **XXI-X** (X = Cl, Br) with 1.5 equivalents of KC_8 yielded the corresponding $CAAC^{Me}$-stabilized boryl radicals **XXII-X** (Scheme 6c), which could be isolated and stored as solids.[52,53] Further reduction of the radicals **XXII-X** with a vast excess of KC_8 under an atmosphere of CO ultimately provided the durylborylene **XX-CO**, the latter presumably being formed *via* trapping of the transient dicoordinate durylborylene **XXIII** with CO.[53]

Based on the isoelectronic structure of dinitrogen (N_2) and CO, and following studies by Bettinger and co-workers, who reported the generation of a free phenylborylene under matrix conditions, as well as its reactivity towards CO and N_2,[54] our group also investigated the ability of the transient durylborylene **XXIII** to activate N_2. Analogously to the above-mentioned preparation of **XX-CO**, the durylboryl radical **XXII-Br** was reduced with KC_8 under a dinitrogen atmosphere (Scheme 7).[53]

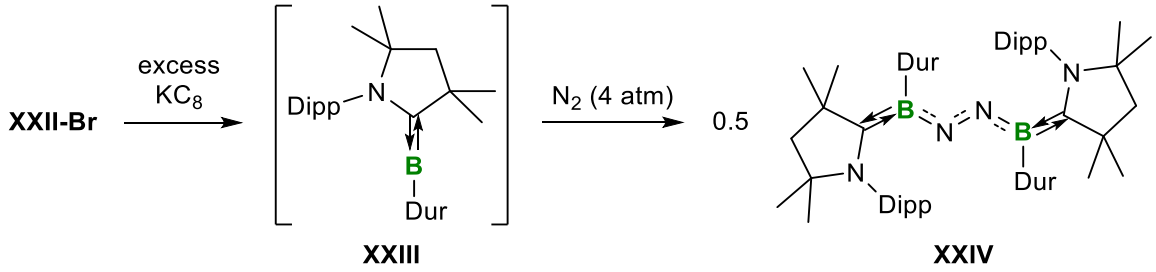

Scheme 7. Borylene-mediated activation of N_2 yielding the μ_2-N_2-bridged compound **XXIV**.

The resulting N_2-activation product **XXIV** can be viewed as two $CAAC^{Me}$-stabilized durylborylene units stabilized *via* a bridging μ_2-N_2 ligand. The activation of the exceptionally strong N≡N triple bond of N_2 has long been the preserve of transition-metal complexes, which can interact with one or more dinitrogen ligands owing to the combination of occupied and vacant d orbitals with suitable energetic levels.[55] The resulting synergism of σ donation and π backdonation, described with the aid of the Dewar-Chatt-Duncanson model,[56] has long since found its way into the textbooks of modern organometallic chemistry. Due to a suitable combination of occupied and vacant orbitals, free and singly base-stabilized borylenes afford reactivity patterns similar to those of transition-metal complexes, and are therefore referred to as metallomimetic.[51,57] In recent years, the concept of metallomimetic chemistry was also applied to other low-valent main-group compounds.[58] In addition to the activation of dinitrogen by a borylene fragment, which has also been achieved recently with a free fluoroborylene under matrix conditions,[59] our group reported the borylene-mediated coupling of two N_2 units,[60] a reaction that is unprecedented even in transition-metal chemistry.

Furthermore, the borylene-mediated activation of N_2 recently culminated in its functionalization und subsequent release as ammonium chloride, which ultimately highlights the synthetic power of borylenes.[61]

As described above, the two- and one-electron reduction of CAAC-stabilized dihaloboranes and the corresponding haloboryl radicals, respectively, have become the methods of choice for the synthesis of metal-free borylenes. In addition to hydro- and various arylborylenes, our group extended the series of metal-free borylenes to several tricoordinate cyanoborylenes.[62] The room temperature reduction of the carbene-borane adduct ($CAAC^{Me}$)BBr_2(CN) (**XXV**) with KC_8 in the presence of an excess of PEt_3 afforded the corresponding cyanoborylene ($CAAC^{Me}$)(PEt_3)B(CN) (**XXVI-PEt$_3$**), presumably formed *via* trapping of the transient dicoordinate cyanoborylene ($CAAC^{Me}$)B(CN) by the phosphine (Scheme 8a).

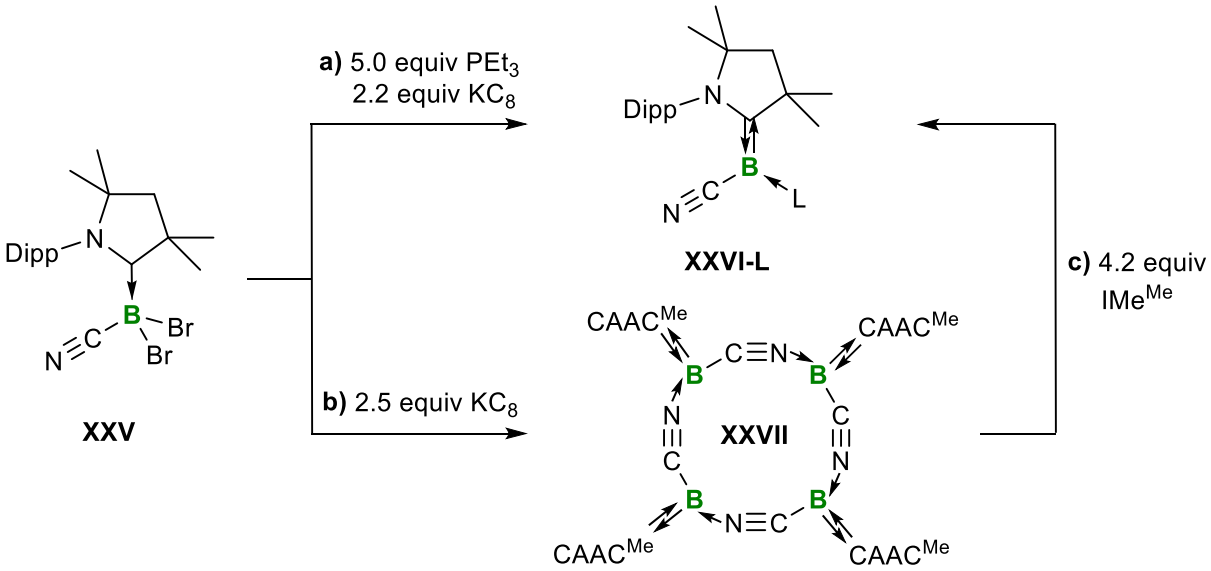

Scheme 8. a) + **c)** Syntheses of the tricoordinate cyanoborylenes **XXVI-L**. **b)** Generation of the cyanoborylene tetramer **XXVII**. IMe^{Me} = 1,3,4,5-tetramethylimidazol-2-ylidene.

It is noteworthy that the reduction of **XXV** in the absence of another stabilizing Lewis base cleanly yielded the tetrakis(cyanoborylene) [($CAAC^{Me}$)B(CN)]$_4$ (**XXVII**), which presents a twelve-membered $(BCN)_4$ ring (Scheme 8b). Interestingly, the cyano ligand in the tetramer **XXVII** acts both as a monoanionic electron-withdrawing substituent and a neutral nitrile donor to another borylene unit, making the addition of a second donor ligand redundant. Furthermore, **XXVII** could be employed as a synthetic equivalent of four dicoordinate ($CAAC^{Me}$)B(CN) cyanoborylene units, as the reaction with IMe^{Me} (IMe^{Me} = 1,3,4,5-tetramethylimidazol-2-ylidene) induced a fragmentation of **XXVII**, generating the tricoordinate ($CAAC^{Me}$)(IMe^{Me})-stabilized cyanoborylene **XXVI-IMe^{Me}** (Scheme 8c).

Isolable metal-free haloborylenes are of particular interest due to their potentially reactive B–X bond. However, these species long remained elusive. Indeed, the twofold reduction of (CAAC^{Cy})BBr$_3$ (**VI^{Cy}**) yielded the parent borylene **VII** rather than the corresponding bromoborylene, presumably due to radical hydrogen abstraction (*vide supra*). In 2017 Xie and co-workers reported the synthesis of the first bromoborylene, compound **XXIX**, from the reduction of an *ortho*-carborane-based bis(silylene) tribromoborane adduct with three equivalents of KC_8 (Scheme 9).[63] Due to the relatively weak π acidity of the silylene donor ligands the borylene lone pair of electrons remains essentially localized at boron. The rigidity of the bespoke carborane-bridged bis(silylene) scaffold **XXVIII**, however, allows virtually no variation in the sterics or electronics of such a bromoborylene.

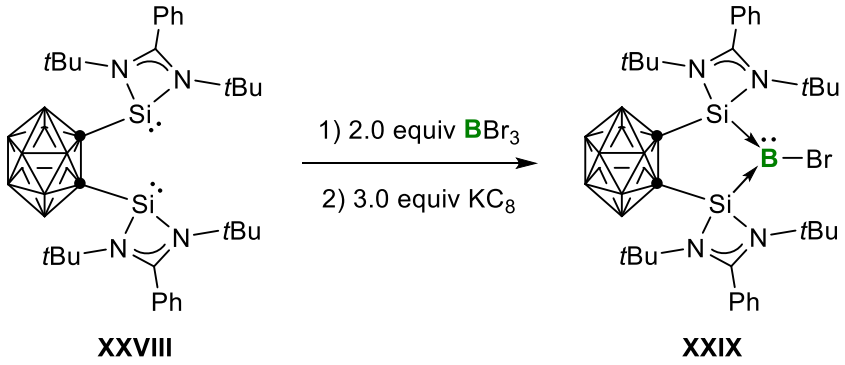

Scheme 9. Synthesis of the bis(silylene)-stabilized bromoborylene **XXIX** by Xie.

Our group recently presented a facile route towards mixed-Lewis-base-stabilized chloroborylenes.[64] Similar to the above-mentioned two-electron reductions of carbene-stabilized dihalo- and trihaloborane adducts, the room temperature reduction of (CAAC^{Me})BCl$_3$ (**XXX**) with KC_8 in the presence of a second donor ligand L provided a series of (un)symmetrically stabilized chloroborylenes of the form (CAAC^{Me})(L)BCl (**XXXI-L**) (L = CAAC^{Me}, IMes (IMes = 1,3-bis(2,4-6-trimethylphenyl)imidazol-2-ylidene), SIMes (SIMes = 1,3-bis(2,4-6-trimethylphenyl)imidazolidin-2-ylidene), PEt$_3$, PMe$_3$) (Scheme 10).

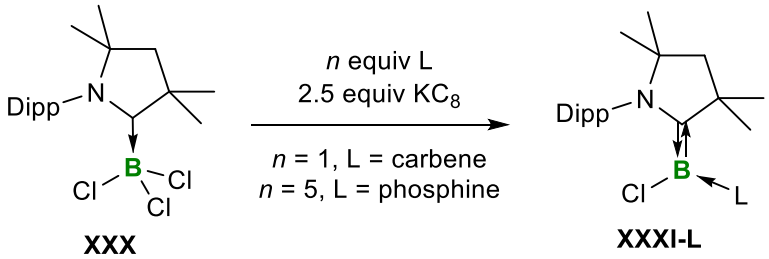

Scheme 10. Synthesis of the mixed-Lewis-base-stabilized chloroborylenes **XXXI-L** by Braunschweig. L = CAAC^{Me}, IMes (IMes = 1,3-bis(2,4-6-trimethylphenyl)imidazol-2-ylidene), SIMes (SIMes = 1,3-bis(2,4-6-trimethylphenyl)imidazolidin-2-ylidene), PEt$_3$, PMe$_3$.

The introduction of different Lewis bases allows for the adjustment of the electron density at the low-valent boron atom. Accordingly, the ^{11}B NMR resonances of the tricoordinate chloroborylenes (CAAC^{Me})(L)BCl (**XXXI-L**) range between 19 and 3 ppm, depending on the overall donor strength of the ligand (CAAC > NHC > phosphine). In addition to the electronics, the steric influence of the second Lewis base can also be selectively varied, allowing the borylene center to be either strongly shielded (L = CAAC) or comparatively exposed (L = small NHC or phosphine). Consequently, the stability and nucleophilicity of the chloroborylene becomes highly tunable. Furthermore, small phosphines are (photo)labile ligands, the cleavage or exchange of which enables versatile follow-up chemistry (*vide infra*). The strong influence of the second donor ligand on the electronic properties can also be observed in the colors of the chloroborylenes **XXXI-L**, which cover almost the entire visible spectrum, ranging from blue (L = CAAC^{Me}) *via* purple (L = SIMes) and red (L = IMe^{Me}) to yellow (L = PMe_3).

Shortly after the preparation of various chloroborylenes by our group Roesky and co-workers also used a similar approach for the synthesis of the first metal-free fluoroborylene.[65] The reduction of (CAAC^{Me})BF_3 (**XXXII**) with KC_8 in the presence of a second equivalent of CAAC^{Me} afforded the corresponding doubly CAAC^{Me}-stabilized fluoroborylene **XXXIII** (Scheme 11).

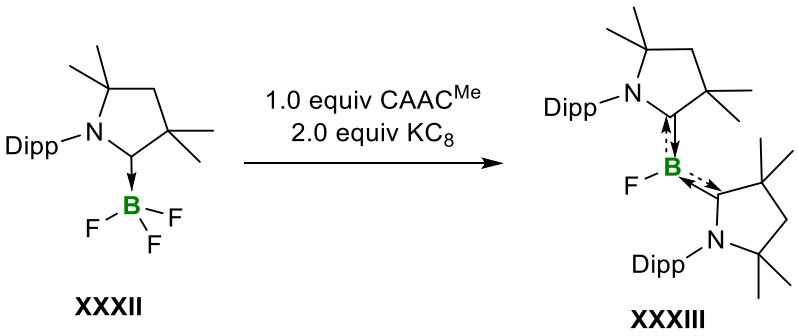

XXXII **XXXIII**

Scheme 11. Synthesis of the doubly CAAC^{Me}-stabilized fluoroborylene **XXXIII** by Roesky.

Beyond the reduction of base-stabilized dihaloboranes, our group has recently developed another synthetic strategy for the generation of borylenes. Starting from Lewis-base-stabilized (aminoboryl)aminoborenium cations **XXXIV-L** (L = SIMes, CAAC^{Me}), the transition-metal-based reduction with Collman's reagent ($Na_2[Fe(CO)_4]$) led to the isolation of the iron complexes **XXXV-L** (Scheme 12a).[66] These species can be viewed as aminoborylene-stabilized metal aminoborylenes. In contrast to aforementioned CAAC-stabilized borylenes, the non-bonding electron pair of the boron center in **XXXV-CAAC^{Me}** is not stabilized *via* π backdonation to the π-acidic CAAC^{Me} ligand. The aminoborylene-stabilized aminoborylenes,

in turn, coordinate as exceptionally strong σ donor ligands to the iron carbonyl complex, enabling the stabilization of the lone pair through the dative boron–iron bond.

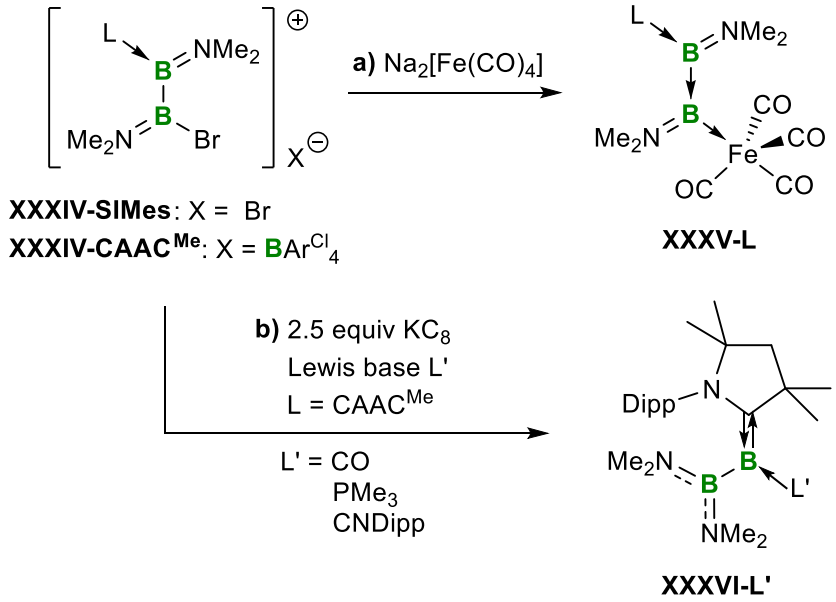

Scheme 12. Synthesis of the aminoborylene-stabilized aminoborylenes **XXXV-L** (**a**) and the (diaminoboryl)borylenes **XXXVI-L'** (**b**) by Braunschweig. BAr^{Cl}_4 = tetrakis(3,5-dichlorophenyl)borate.

Furthermore, the $CAAC^{Me}$-stabilized borenium cation **XXXIV-CAAC^{Me}** could also be reduced with KC_8 in the presence of a stabilizing Lewis base L' (L' = CO, PMe_3, CNDipp) (Scheme 12b).[66] Surprisingly, this resulted in migration of one dimethylamino group to the adjacent boron atom and formation of the corresponding tricoordinate (diaminoboryl)borylenes **XXXVI-L'**. In these compounds the borylene lone pair is solely delocalized across the C_{CAAC}–B bond without any contribution of the neighboring boryl substituent, as the vacant p orbital of the latter is populated by the two π-donating NMe_2 groups.

Another, albeit very specific, example of a tricoordinate borylene was reported by Yamamoto and co-workers in 2017. The reduction of the aminodichloroborane (TMP)BCl_2 (**XXXVII**) (TMP = 2,2,6,6-tetramethylpiperidinyl) with sodium naphthalenide ([Na][$C_{10}H_8$]) provided the triaminotriborane(3) **XXXVIII** (Scheme 13).[67] This boron species, in which three [TMP–B:] units formed a bent B_3 catenated structure, can be viewed as a bis(borylene)-stabilized aminoborylene, the HOMO of which is localized on the central boron chain.

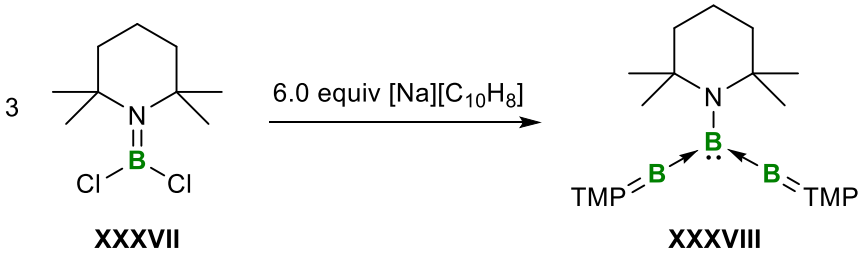

Scheme 13. Synthesis of the bis(borylene)-stabilized borylene **XXXVIII**. TMP = 2,2,6,6-tetramethylpiperidinyl.

While the variety of tricoordinate metal-free borylenes has increased steadily, only a few examples of dicoordinate borylenes are known to date.[28] The first one was reported by Bertrand, Stephan and co-workers in 2014, who based its stabilization on the substitution pattern of the first stable terminal metal borylene complex[43] and consequently chose an electron-donating bis(trimethylsilyl)amino substituent at boron.[68] The CAAC^{Cy}-borane adduct **XXXIX** was initially reduced with one equivalent of decamethylcobaltocene ($Co(Cp^*)_2$) (Cp^* = pentamethylcyclopentadienyl), yielding the corresponding neutral boryl radical **XL** (Scheme 14). A second one-electron reduction of the latter with $Co(Cp^*)_2$ afforded the dicoordinate aminoborylene **XLI**. The solid-state structure of **XLI** revealed an almost linear environment of the boron center, in which the C–B–N unit exhibits an allenic structure **XLIa**. DFT calculations, however, showed that bending of the C_{CAAC}–B–N unit incurs a negligible energetic cost of 5.7 kcal mol^{-1} only, providing the bent structure **XLIb** with a highly electrophilic borylene center.

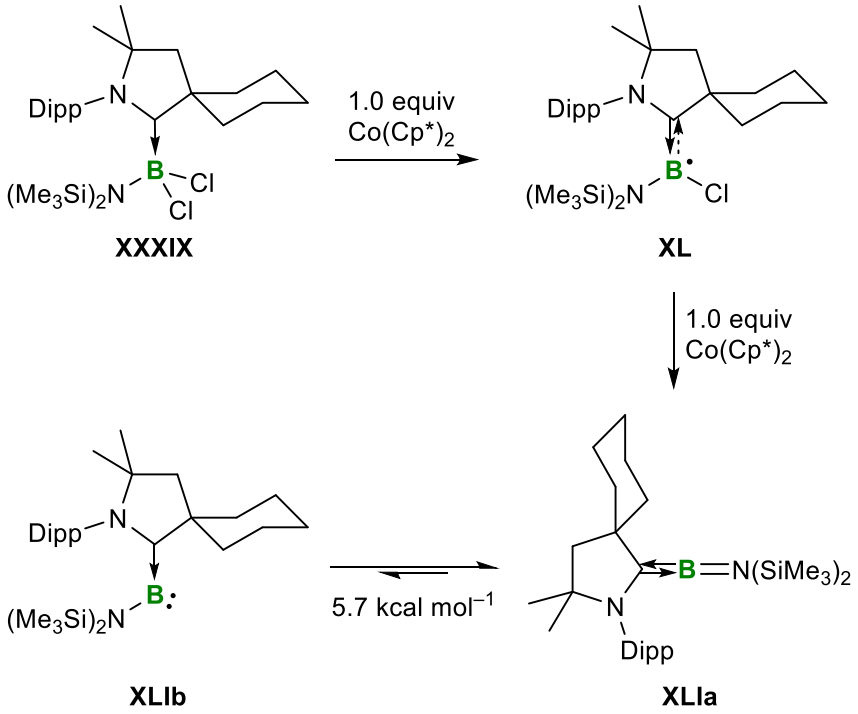

Scheme 14. Synthesis of the first dicoordinate aminoborylene **XLI** by Bertrand and Stephan. Cp* = pentamethylcyclopentadienyl.

Hudnall and co-workers presented another very similar example of a dicoordinate borylene, the stabilization of which was ensured by a strongly σ-donating and π-accepting DAC ligand (DAC = diamidocarbene) and a comparable π-donating amino substituent.[69] Mono- and dicoordinate borylenes are in general extremely reactive species, making their generation and the study of their reactivity very difficult. In contrast, tricoordinate borylenes exhibit much higher stability, which is often offset by a loss of reactivity. However, metal-free borylenes of

all types have demonstrated impressive reactivity patterns over recent years, including the activation of small molecules and of various σ bonds. As electron-rich species they are also capable of acting as one-electron reducing agents and serving as ligands for transition-metal and main-group element complexes (*vide infra*).

1.2 Reactivity of Metal-Free Borylenes

Ligand Exchange Reactions and Activations of σ Bonds and Small Molecules

As described above, the existence of intermediately formed borylenes has often been postulated with the aid of suitable trapping reagents.[37-39] Thus, numerous examples of insertion reactions of an *in-situ* generated borylene fragment into inter- and intramolecular C–C and C–H bonds have been described in the literature.[50,70-73] In 2017 our group reported the metal-like reactivity of the (CAAC^{Me})(CO)-stabilized durylborylene (**XX-CO**), the metallomimetic properties of which were demonstrated by photolytic cleavage of the labile CO ligand.[51] Compared to the isolable aminoborylene **XLI**,[68] which is stabilized *via* a push-pull system, the transiently formed dicoordinate durylborylene **XXIII** exhibits a significantly lower stability and consequently an increased reactivity. Irradiation of a benzene solution of **XX-CO** led to the formation of the intramolecular C–H activation product **XLII**, in which the durylborylene **XXIII** formally inserted into one *iso*propyl group of the Dipp substituent, followed by a 1,2-hydride migration from the boron center to the carbene carbon atom, which is frequently observed in CAAC-stabilized hydroboranes (Scheme 15).[74]

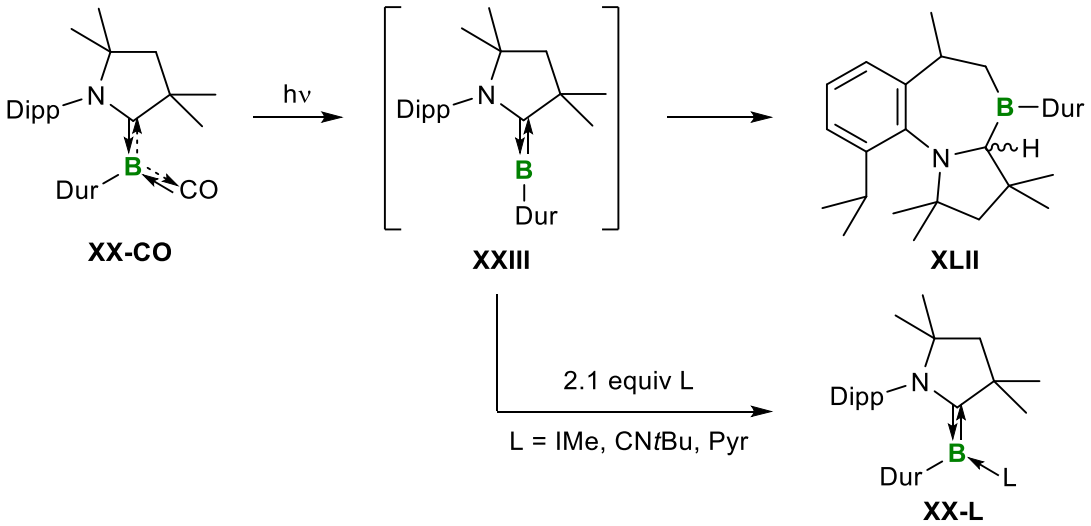

Scheme 15. Photolytic ligand exchange reactions of the durylborylene **XX-CO**. IMe = 1,3-dimethylimidazol-2-ylidene.

Although **XXIII** could not be isolated, trapping of the dicoordinate borylene fragment was achieved by photolysis of **XX-CO** in the presence of a stabilizing Lewis base, L (L = IMe

(IMe = 1,3-dimethylimidazol-2-ylidene), CN*t*Bu, pyridine), producing the corresponding tricoordinate durylborylenes **XX-L**. A major advantage of this ligand exchange is that the photolytic expulsion of CO at an already existing tricoordinate borylene allows for the installation of Lewis bases that would not tolerate the reduction conditions usually employed for the preparation of (CAAC)(L)BR borylenes from dihaloboranes.

This concept of ligand exchange has recently also been applied to phosphine-stabilized borylenes. The ($CAAC^{Me}$)(PMe_3)-stabilized chloroborylene (**XXXI-PMe$_3$**) can be quantitatively converted into the corresponding bis(carbene)-stabilized derivative **XXXI-IMe^{Me}** by the reaction with one equivalent of IMe^{Me} at room temperature (Scheme 16).[64] It is noteworthy that this ligand exchange reaction does not require photolytic conditions, thus representing a very mild synthetic route for the generation of unsymmetric tricoordinate borylenes.

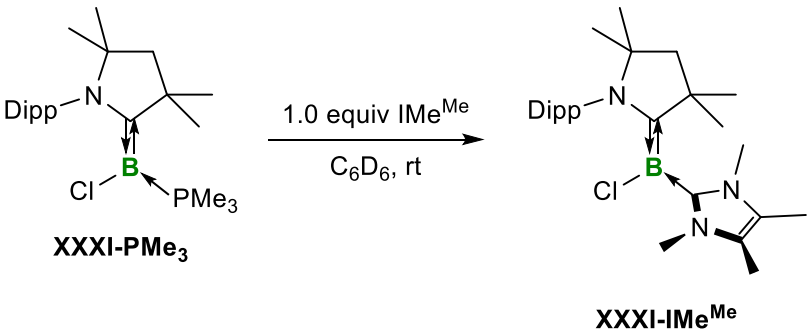

Scheme 16. Ligand exchange reaction of the chloroborylene **XXXI-PMe$_3$**.

Following this method, our group also reported the ability of the ($CAAC^{Me}$)(PMe_3)-stabilized (diaminoboryl)borylene (**XXXVI-PMe$_3$**) to serve as stable source of a fleeting dicoordinate borylene.[75] Depending on the work-up procedure, the borylene **XXXVI-PMe$_3$** was either obtained as (*Z*)-isomer, in which the Dipp moiety and the boryl substituent are oriented on the same side of the C_{CAAC}–B double bond, or as (*E*)-isomer, in which the Dipp and ($B(NMe_2)_2$) units point in opposite directions. As phosphines already proved to be very labile, heating of **(*Z*)-XXXVI-PMe$_3$** at 60 °C in the presence of a stronger donor ligand L (L = CNXyl (Xyl = 2,6-dimethylphenyl), CO, DMAP (DMAP = 4-dimethylaminopyridine)) induced the displacement of the PMe_3 ligand by the respective Lewis base, affording the corresponding borylenes **(*Z*)-XXXVI-L** (Scheme 17).

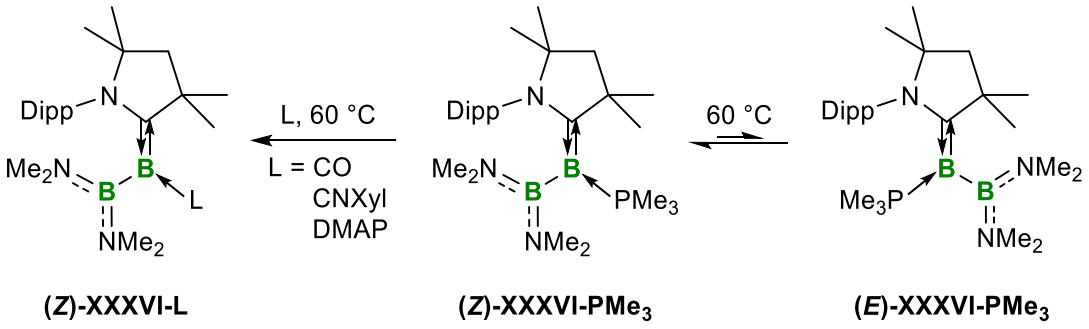

Scheme 17. Isomerization and ligand exchange reactions of the borylene **XXXVI-PMe3**. Xyl = 2,6-dimethylphenyl. DMAP = 4-dimethylaminopyridine.

Heating of a C_6D_6 solution of **(*Z*)-XXXVI-PMe3** at 60 °C in the absence of another stabilizing donor ligand, in turn, resulted in a 23% conversion to the (*E*)-isomer **(*E*)-XXXVI-PMe3** over the course of thirty minutes, likely *via* a dissociation-isomerization-association process of the phosphine-stabilized borylene.

Bertrand's and Stephan's aminoborylene **XLI** is an impressive example of a borylene that combines both high stability and reactivity. Similar to CAAC and diamidocarbene ligands that are capable of binding CO,[22,76] the carbene-like reactivity of the aminoborylene **XLI** was demonstrated by stirring a solution of the latter under one atmosphere of CO at room temperature (Scheme 18a). The resulting product (CAAC^{Cy})(CO)B(N(SiMe$_3$)$_2$) (**XLIII**) can be viewed as doubly Lewis-base-stabilized aminoborylene, in which the electron density is delocalized from the boron center to both π-acidic donor ligands.

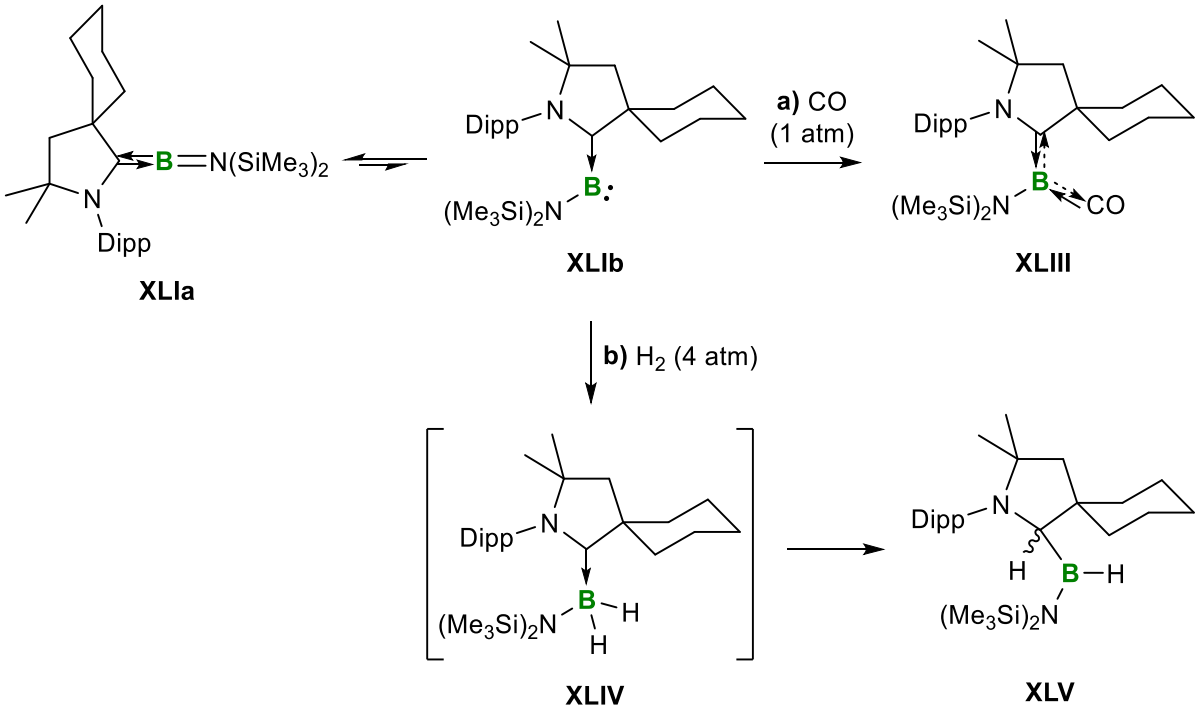

Scheme 18. Activation of CO (**a**) and H_2 (**b**) at the dicoordinate aminoborylene **XLI**.

To further illustrate the electrophilic character of the aminoborylene **XLI** it was reacted with 4 atmospheres of dihydrogen (H_2) yielding monoborane **XLV** (Scheme 18b). The formation of **XLV** presumably proceeds *via* an oxidative addition of H_2 at the borylene center forming intermediate **XLIV**, which then undergoes a 1,2-hydride migration from boron to the adjacent carbene carbon atom. It is noteworthy that both the activation of CO and H_2 likely take place *via* the bent structure of **XLIb** with its highly electrophilic boron center. In **XLIb** the boron-centered lone pair and the vacant p orbitals can cooperatively interact with antibonding and bonding orbitals of CO and H_2, respectively, thus mimicking the bond-activating synergism of transition-metal complexes.

In contrast to the aforementioned (transient) dicoordinate borylenes, tricoordinate borylenes are usually hampered in their nucleophilicity due to electronic saturation and steric shielding of the low-valent boron center by the two stabilizing Lewis bases. Nevertheless, tricoordinate borylenes are isoelectronic with amines and phosphines and can therefore react as nucleophiles and Brønsted bases. Bertrand's parent borylene **VII**, for instance, was protonated with an equimolar amount of HOTf, resulting in the generation of the boronium cation **XLVI** (Scheme 19a). The protonation of **VII** has also been proven to be reversible as treatment of the boronium cation **XLVI** with sodium ethoxide regenerated the starting borylene **VII** (Scheme 19b).

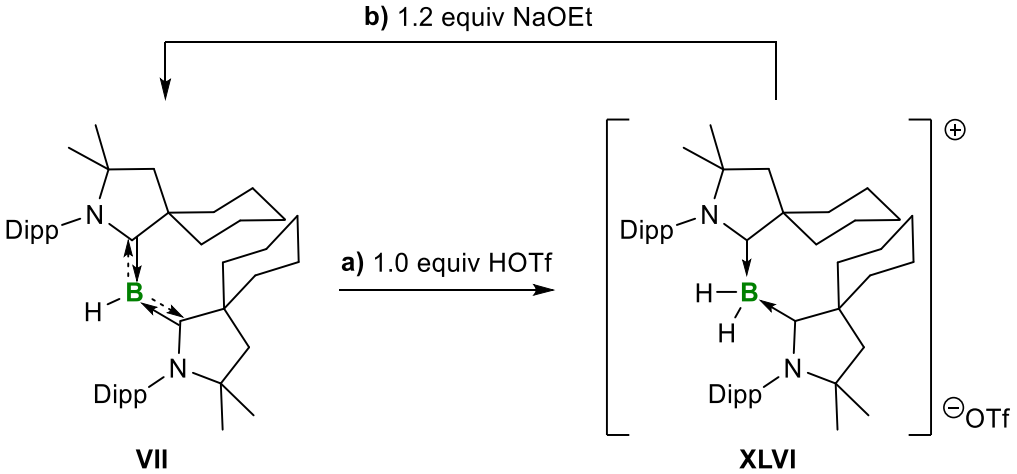

Scheme 19. Reversible protonation of the parent borylene **VII**.

While **VII** does not react with TMSOTf (TMS = trimethylsilyl) and MeOTf, presumably due to the bulky $CAAC^{Cy}$ ligands, Kinjo's phenylborylene **XVI** reacts with both HOTf and MeOTf, and inserts into the C–Cl σ bond of dichloromethane (DCM), forming the corresponding cationic species **[XVI-E$^+$][X$^-$]** (E = H, Me, CH_2Cl; X = OTf, Cl) (Scheme 20). The significantly

increased nucleophilicity of **XVI** is owed to the sterically less demanding oxazol-2-ylidene ligands.

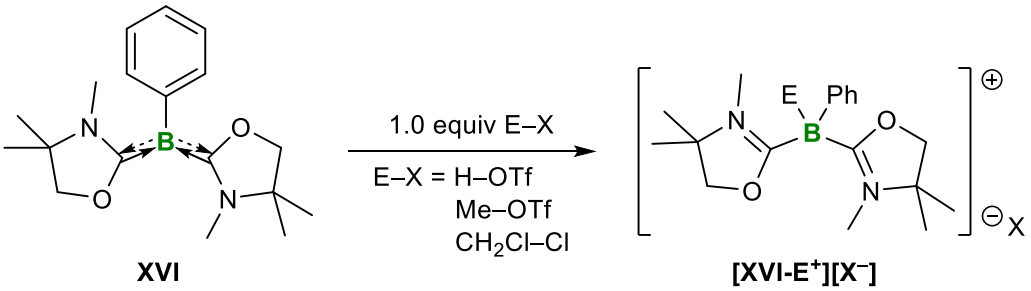

Scheme 20. Boron-centered nucleophilic reactivity of the phenylborylene **XVI**.

One-Electron Oxidation

The boron center of borylenes adopts the formal oxidation state +1, making these boron species exceptionally electron-rich. Cyclic voltammetry experiments performed on isolated tricoordinate borylenes such as Bertrand's bis(CAAC^{Cy})-stabilized hydroborylene **VII** revealed a fully reversible electrochemical oxidation event. Accordingly, the reaction of the parent borylene **VII** with two equivalents of $GaCl_3$ selectively resulted in one-electron oxidation of the former and formation of the corresponding hydroboryl radical cation **[VII$^{\bullet+}$][GaCl$_4^-$]** (Scheme 21).

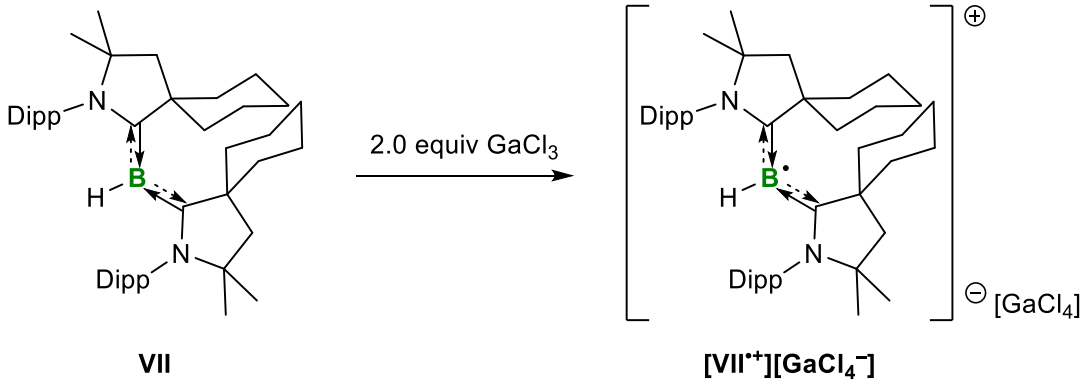

Scheme 21. One-electron oxidation of the parent hydroborylene **VII** to the boryl radical cation **[VII$^{\bullet+}$][GaCl$_4^-$]**.

Alternatively, the related unsymmetrical doubly base-stabilized hydroboryl radical cation [(CAAC^{Et})(BAC^{iPr})BH$^{\bullet+}$][OTf$^-$] was obtained *via* selective one-electron reduction of the boronium cation [(CAAC^{Et})(BAC^{iPr})BH(OTf)][OTf$^-$] (**XI-BAC^{iPr}**, see Scheme 3).[47] In both boryl radical cations, the unpaired electron is mainly delocalized over the C_{CAAC}–B fragment, with only very little contribution by the BAC^{iPr} ligand of the latter. In addition to the electronic stabilization, the bulky CAAC and BAC^{iPr} ligands provide effective encapsulation of the reactive BH$^{\bullet+}$ moiety.

As mentioned above, haloborylenes are of particular interest due to their potentially reactive B–X bond. When Roesky and co-workers attempted to abstract the fluoride substituent of the bis(CAAC^{Me})-stabilized fluoroborylene **XXXIII** with one equivalent of Li[B(C_6F_5)$_4$] in order to generate a cationic boron(I) species, a one-electron oxidation of **XXXIII** occurred instead, selectively yielding the boryl radical cation **[XXXIII$^{\bullet+}$][B(C_6F_5)$_4^-$]** (Scheme 22).[65] The latter is electronically and kinetically stabilized by the two π-acidic, bulky CAAC^{Me} ligands, similar to the parent boryl radical cation **[VII$^{\bullet+}$][GaCl$_4^-$]**.

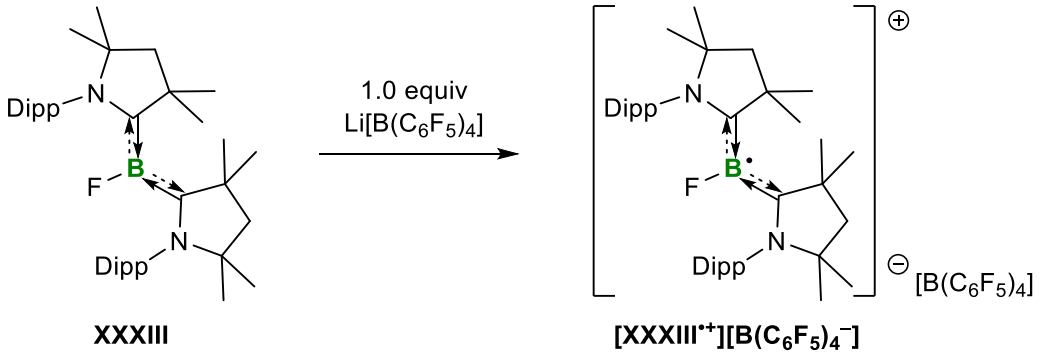

XXXIII **[XXXIII$^{\bullet+}$][B(C_6F_5)$_4^-$]**

Scheme 22. One-electron oxidation of the bis(CAAC^{Me})-stabilized fluoroborylene **XXXIII** to the boryl radical cation **[XXXIII$^{\bullet+}$][B(C_6F_5)$_4^-$]**.

In contrast, the reaction of Kinjo's phenylborylene **XVI** with one equivalent of silver triflate (AgOTf) did not lead to the formation of the boryl radical cation **[XVI$^{\bullet+}$][OTf$^-$]** but to its dimer, the diborane(6) dication **XLVII** (Scheme 23).[77] The coupling of the two boryl radical cation fragments likely occurs due to the lack of steric shielding by the relatively small oxazol-2-ylidene (Oxz) ligands. The cyclic voltammogram of **XVI** showed an irreversible one-electron oxidation. The twofold reduction of the diboron dication **XLVII** with KC_8, however, regenerated the starting phenylborylene, thus providing a novel synthetic method for the preparation of a tricoordinate borylene by reductive B–B bond cleavage of a diboron dication.

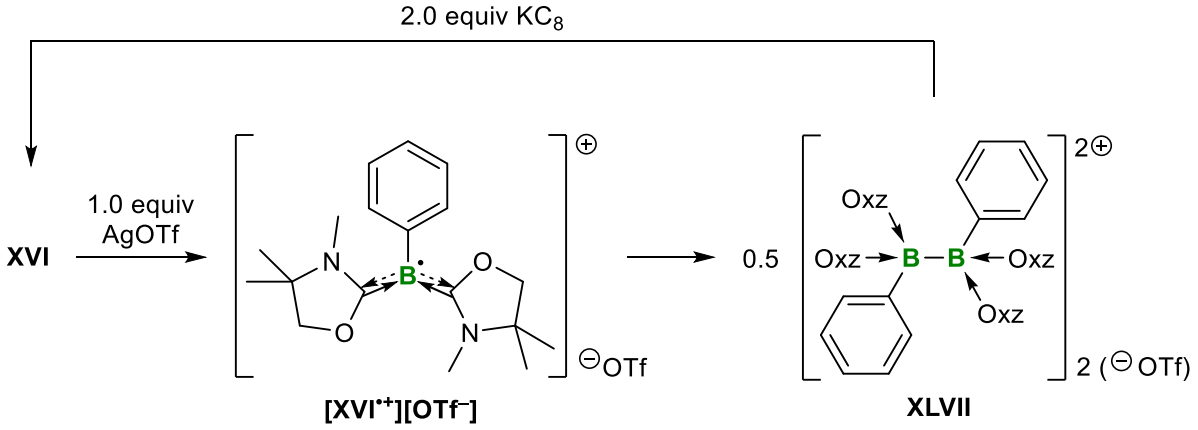

[XVI$^{\bullet+}$][OTf$^-$] **XLVII**

Scheme 23. One-electron oxidation of Kinjo's phenylborylene **XVI** and subsequent dimerization of the resulting boryl radical cation **[XVI$^{\bullet+}$][OTf$^-$]**. Oxz = oxazol-2-ylidene.

Coordination Chemistry

Tricoordinate borylenes are isoelectronic with amines and phosphines, and due to the lower electronegativity of boron compared to that of nitrogen und phosphorus they can act as strong σ donor ligands for transition metals. Whereas the nucleophilicity of the parent borylene **VII** is hampered by the sterically crowded CAAC^{Cy} ligands,[46] Kinjo's phenylborylene **XVI**, which is stabilized by two significantly smaller oxazol-2-ylidene ligands, shows a much more pronounced propensity for coordination. The reaction of **XVI** with a freshly prepared solution of [Cr(CO)$_5$(thf)] induced the replacement of the weakly bound THF molecule, generating the transition-metal borylene complex **XVI-Cr** (Scheme 24).[48] The now tetracoordinate boron atom coordinates as a σ donor to the chromium(0) center in an η^1 fashion without π backbonding from the metal center.

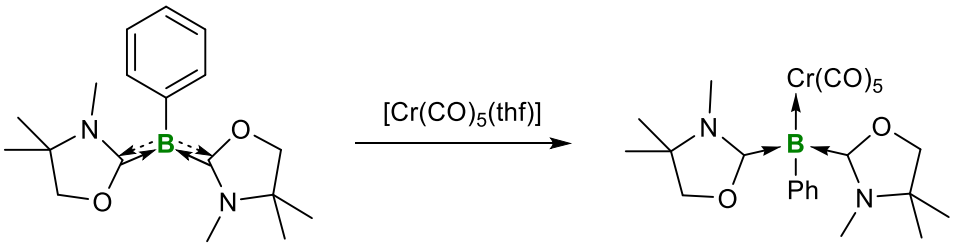

Scheme 24. Coordination of the phenylborylene **XVI** to chromium pentacarbonyl.

These results prompted Kinjo and co-workers to further investigate the reactivity of the phenylborylene **XVI** towards metal precursors. Besides the coordination of **XVI** to group 9 metal complexes, they succeeded in isolating various coinage metal borylene complexes.[78] The reactions of the phenylborylene **XVI** with MCl (M = Cu, Ag, Au) each resulted in the reduction of the respective coinage metal ion, showing again the strong reduction potential of these electron-rich boron(I) species. However, Lewis-base-stabilized gold(I) chloride complexes exhibit a sufficiently high electron density at the metal center to enable the coordination of **XVI** rather than its oxidation. The reaction of **XVI** with [(IDipp)AuCl] resulted in the displacement of the chloride substituent, yielding the heteroleptic cationic gold complex **[XVI-Au$^+$][Cl$^-$]** (Scheme 25a). The addition of phenylborylene **XVI** to [(PPh$_3$)AuCl], in turn, provided the neutral complex **XVI-Au**, in which the labile phosphine ligand was exchanged by the significantly stronger σ-donating borylene unit (Scheme 25b).

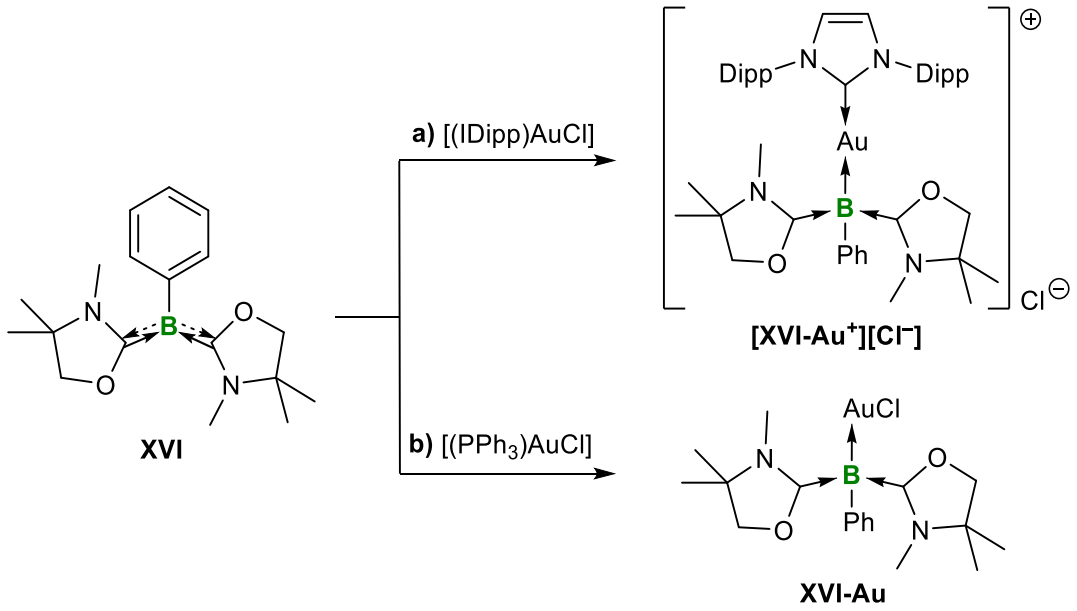

Scheme 25. Coordination of the phenylborylene **XVI** to base-stabilized gold(I) chlorides.

After the generation of doubly Lewis-base-stabilized borylenes by base-induced liberation of an arylborylene fragment from transition-metal borylene complexes (see Scheme 5),[50] our group also reported the coordination behavior of the bis(CNDipp)-stabilized durylborylene **XLVIII** towards main-group Lewis acids.[79] The reaction of **XLVIII** with $AlCl_3$ afforded adduct **XLIX**, in which the nitrogen atom of one of the isonitrile ligands coordinates to the aluminium center, forming the respective push-pull-stabilized 1,3-azaboraallene (Scheme 26a).

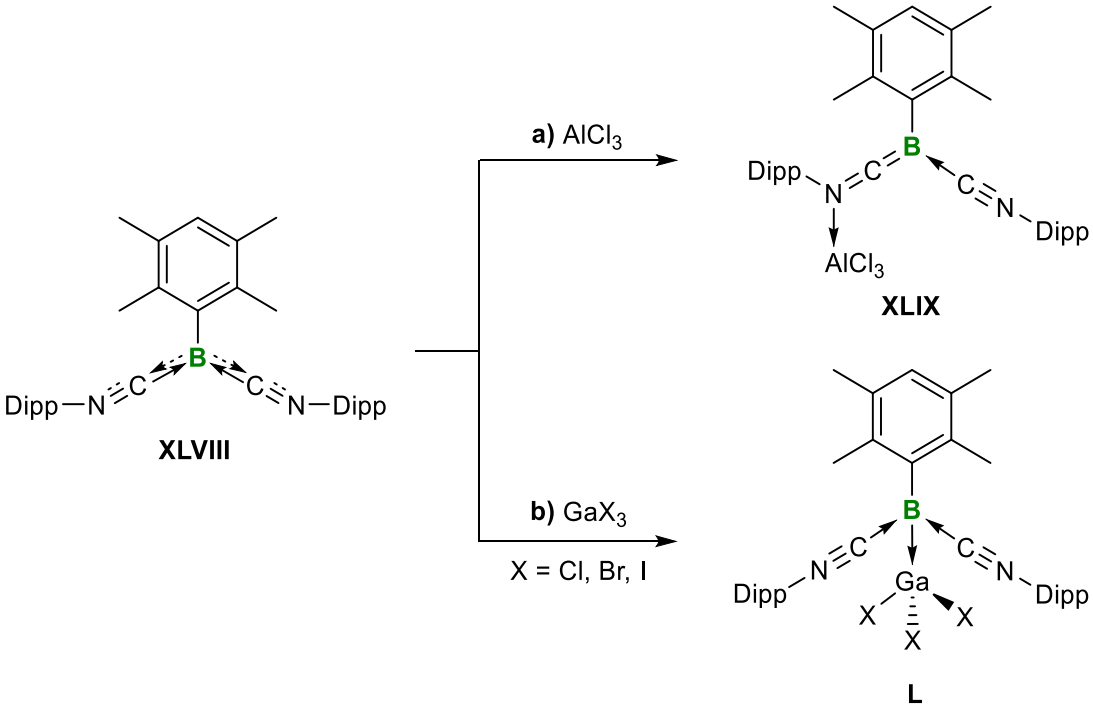

Scheme 26. Ditopic coordination chemistry of the bis(CNDipp)-stabilized durylborylene **XLVIII** towards group 13 Lewis acids.

The adduct formation between **XLVIII** and Lewis-acidic trihalogallanes GaX_3 (X= Cl, Br, I), however, was boron-centered *via* B→Ga σ donation (Scheme 26b). The resulting borylene-gallane adducts **L** evidence not only the Lewis basicity of the bis(isonitrile)-stabilized boron(I) compound **XLVIII**, but also highlight its ditopic nature towards main-group Lewis acids. Consequently, the use of ligands with multiple donor sites (*e.g.* isonitriles) could enable tuning of both the Lewis basicity and the coordination behavior of tricoordinate borylenes.

In the last ten years, a large number of variously functionalized and stabilized metal-free borylenes has been synthesized. Both di- and tricoordinate borylenes have demonstrated versatile reactivity patterns and thus give an idea of their wide range of future applications. The aim of this work involves the synthesis of new pseudohalide-substituted borylenes. (Un)symmetrically doubly Lewis-base-stabilized pseudohaloborylenes could potentially function as ditopic ligands due to the ambiphilic nature of the pseudohalogen substituent. Moreover, the latter could enable self-stabilization of the dicoordinate pseudohaloborylene similar to that in the cyanoborylene tetramer **XXVII**, thus potentially enabling the isolation of synthetic equivalents for fleeting dicoordinate borylenes.

II Results and Discussion

2.1 Synthesis of Novel Boryl Anions and a Neutral Hydroboryl Radical[1]

Tricoordinate borylenes of the form (L)(L')BR are formally isoelectronic to amines and phosphines. Since the coordination ability of the parent borylene $(CAAC^{Cy})_2BH$ (**VII**) is blocked by the steric demands of the two bulky stabilizing $CAAC^{Cy}$ ligands, Bertrand and co-workers developed a stepwise and more versatile synthetic route to access the unsymmetrically substituted borylenes $(CAAC^{Et})(L)BH$ (**XII-L**) (see Scheme 3).[47] Inspired by these results, the initial work of this thesis focused on the preparation of new boronium cations of the form $[(CAAC^{Me})(L)BH_2]OTf$, in which the second Lewis base L is either a carbene, a phosphine or a nitrogen donor. These would be used as precursors for the synthesis of novel $(CAAC^{Me})(L)BH$ borylenes, in which the donor ligand L is either sterically less demanding and/or labile, thus increasing its reactivity and coordination ability, and/or enabling the *in-situ* generation of the dicoordinate parent borylene $(CAAC^{Me})BH$.

2.1.1 Synthesis of Boronium Cations

Following to the procedure reported by Bertrand and co-workers,[47] methyl triflate was employed to abstract a hydride from $(CAAC^{Me})BH_3$ (**VIII^{Me}**) and $(CAAC^{Cy})BH_3$ (**VIII^{Cy}**). The addition of 1.5 equivalents of MeOTf to a solution of **VIII^{Me}** or **VIII^{Cy}** in benzene resulted in gas evolution (CH_4) in both cases (Scheme 27).

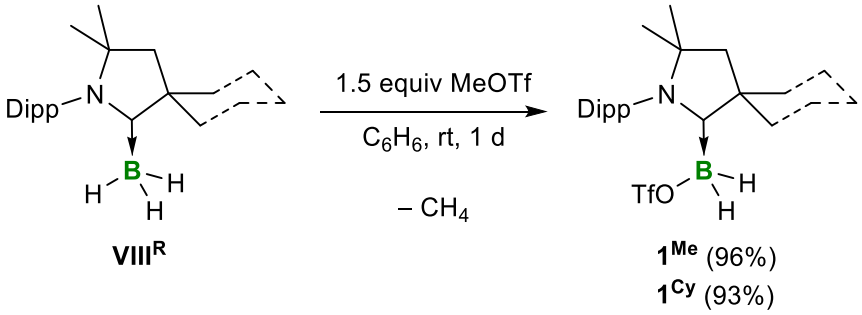

Scheme 27. Synthesis of the triflatoboranes **1^{Me}** and **1^{Cy}**. Isolated yields in parentheses.

The reaction mixtures were stirred at room temperature overnight and after workup, **1^{Me}** and **1^{Cy}** were isolated as white solids in 96% and 93% yield, respectively. The ^{11}B and ^{19}F NMR spectra of **1^{Me}** (δ_{11B} = –6.3, δ_{19F} = –76.2 ppm) and **1^{Cy}** (δ_{11B} = –6.1, δ_{19F} = –76.2 ppm) were essentially identical to those reported by Bertrand,[47] indicating that the triflate moiety is

[1] The results presented herein were published in "S. Hagspiel, M. Arrowsmith, F. Fantuzzi, A. Hermann, V. Paprocki, R. Drescher, I. Krummenacher, H. Braunschweig, Reduction of a dihydroboryl cation to a boryl anion and its air-stable, neutral hydroboryl radical through hydrogen shuttling, *Chem. Sci.* **2020**, *11*, 551–555."

covalently bound to a quaternary boron center, which is stabilized by the respective CAAC^{R} ligand. Colorless single crystals suitable for X-ray diffraction analyses were obtained by vapor diffusion of hexane into saturated benzene solutions of **1^{Me}** and **1^{Cy}** (Figure 3). The solid-state structures confirm the formation of **1^{Me}** and **1^{Cy}**, the bonding parameters of which are similar to Bertrand's analogue.[47]

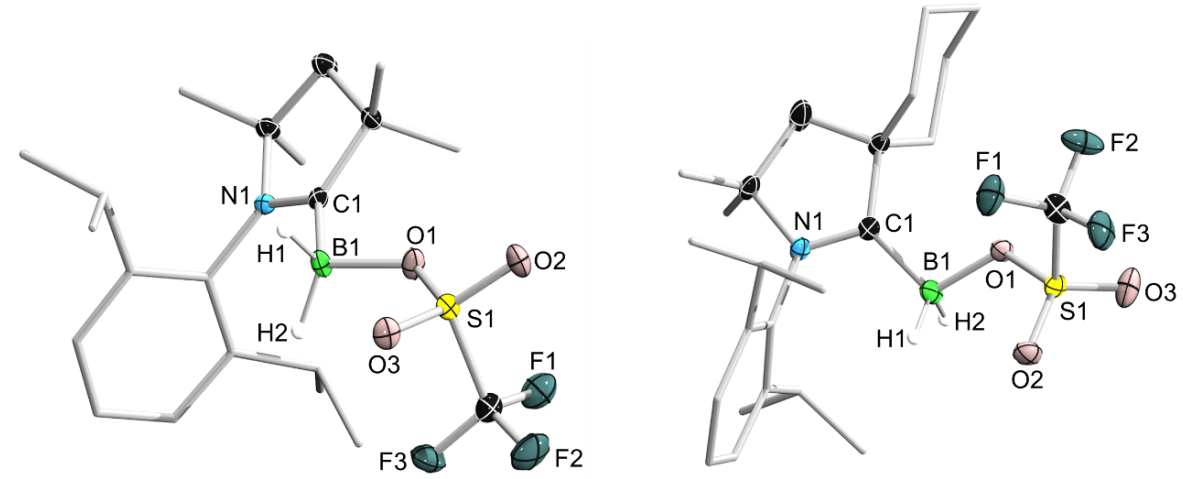

Figure 3. Crystallographically-derived molecular structures of **1^{Me}** (left) and **1^{Cy}** (right). Atomic displacement ellipsoids are shown at the 50% probability level. Ellipsoids of the CAAC ligand periphery and hydrogen atoms, except those bound to boron, have been omitted for clarity. Selected bond lengths (Å) for **1^{Me}**: N1–C1 1.300(2), C1–B1 1.598(2), B1–O1 1.562(2); for **1^{Cy}**: N1–C1 1.3025(19), C1–B1 1.602(2), B1–O1 1.5626(19).

Inspired by Bertrand's studies on the replacement of the triflate substituent in (CAAC^{Et})BH$_2$(OTf) (**IX**) by a carbene (see Scheme 3),[47] the triflatoborane **1^{Me}** was combined with one equivalent of CAAC^{Me} in benzene (Scheme 28a).

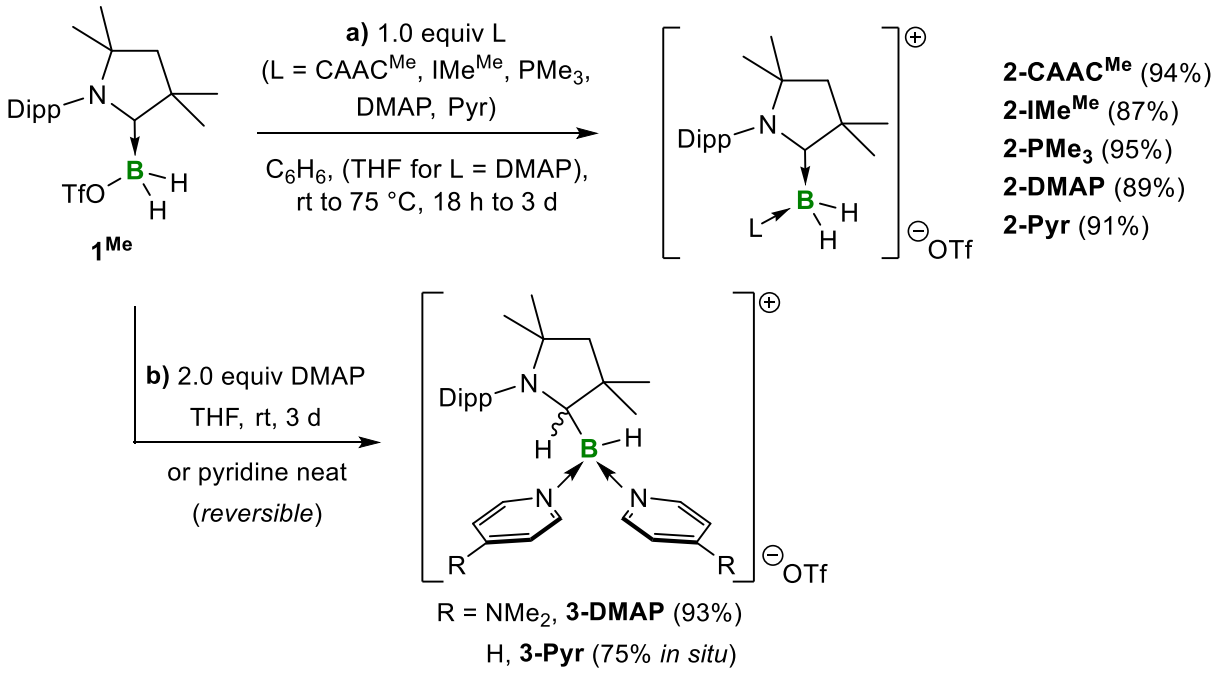

Scheme 28. Synthesis of the boronium cations **2-L** (L = CAAC^{Me}, IMe^{Me}, PMe$_3$, DMAP, Pyr) and the bis(base) adducts **3-L** (L = DMAP, Pyr). Isolated yields in parentheses. DMAP = 4-dimethylaminopyridine; Pyr = pyridine.

Stirring at 75 °C for two days provided a colorless suspension, and after workup **2-CAAC^{Me}** was isolated as a colorless solid in 94% yield. The ^{11}B NMR spectrum of **2-CAAC^{Me}** showed a triplet at –22.4 ppm ($^{1}J_{BH}$ = 85.4 Hz), indicating the formation of a boronium cation with a non-coordinating triflate counteranion (δ_{19F} = –78.0 ppm).[47] The broadened resonances in the ^{1}H NMR spectrum suggest hindered rotation of the CAAC^{Me} ligands at room temperature and sharpen upon cooling to –15 °C into one symmetrical set of signals. Vapor diffusion of hexane into a saturated chloroform solution of **2-CAAC^{Me}** afforded colorless single crystals suitable for X-ray diffraction analysis (Figure 4).

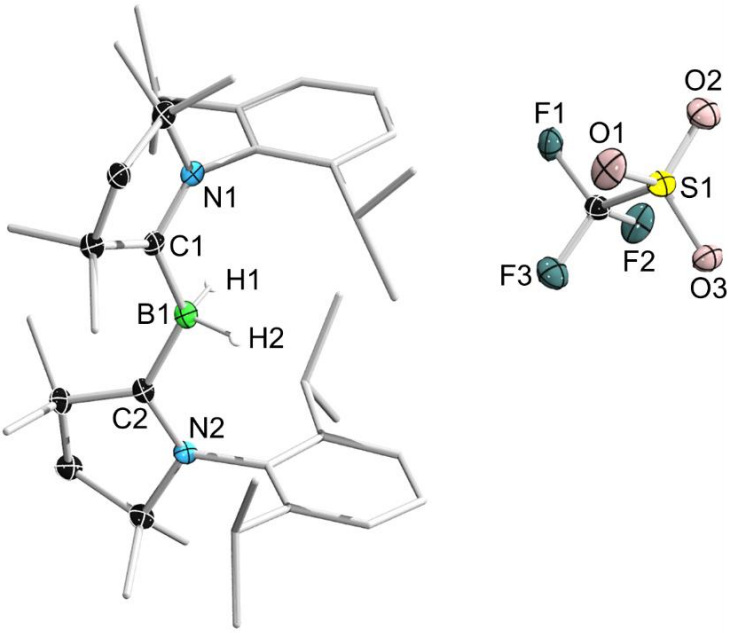

Figure 4. Crystallographically-derived molecular structure of **2-CAAC^{Me}**. Atomic displacement ellipsoids are shown at the 50% probability level. Ellipsoids of the CAAC ligand periphery and hydrogen atoms, except those bound to boron, have been omitted for clarity. Selected bond lengths (Å): N1–C1 1.316(6), C1–B1 1.597(7), B1–H1 1.11(6), B1–H2 1.16(6), C2–B1 1.607(7), N2–C2 1.310(6).

The solid-state structure confirms the formation of the boronium cation **2-CAAC^{Me}**, the bonding parameters of which are essentially identical to those of the CAAC^{Cy} derivative **XLVI** reported by Bertrand, which was obtained by protonation of the bis(CAAC^{Cy})-stabilized parent borylene **VII** with triflic acid (HOTf).[46] The two CAAC^{Me} ligands of **2-CAAC^{Me}** coordinate as pure σ donors to the cationic BH_2 unit (C1–B1 1.597(7) Å and C2–B1 1.607(7) Å), while the triflate counterion is not bound to the boron center. Similarly, the reaction of **1^{Me}** with IMe^{Me} required heating at 60 °C overnight until full conversion of **1^{Me}** was observed by ^{11}B NMR-spectroscopic analysis (Scheme 2a). After workup, **2-IMe^{Me}** was obtained as a colorless solid in 87% yield, its NMR-spectroscopic data (δ_{11B} = –29.2 ppm, t, $^{1}J_{BH}$ = 85.4 Hz; δ_{19F} = –78.1 ppm) being similar to its **2-CAAC^{Me}** analogue. Despite phosphines being much weaker Lewis base than carbenes,[80] the reaction of **1^{Me}** with PMe_3 proceeded at room temperature,

presumably due to the smaller steric demands of the latter (Scheme 28a).[81] The boronium cation **2-PMe$_3$** was isolated as a colorless solid in 95% yield. The ^{11}B NMR spectrum showed a doublet of triplets at –27.8 ppm, indicative of pronounced coupling between the ^{11}B and ^{1}H ($^{1}J_{BH}$ = 89.8 Hz) and the ^{11}B and ^{31}P ($^{1}J_{BP}$ = 81.5 Hz) nuclei, respectively, which was determined by selective ^{1}H- and ^{31}P-decoupling experiments. A broad multiplet was observed at –10.6 ppm in the ^{31}P NMR spectrum, which is ca. 50 ppm downfield-shifted from free PMe$_3$.[82] Since both carbenes and phosphines proved capable of replacing the triflate moiety in **1^{Me}**, it was of interest to determine whether the donor strength of nitrogen donors would also be sufficient for this substitution reaction (Scheme 2b). A THF solution of **1^{Me}** and one equivalent of 4-dimethylaminopyridine (DMAP) was stirred for three days at room temperature, yielding **2-DMAP** as a colorless solid in 89% yield. The boronium cation **2-DMAP** showed a broad singlet at –10.6 ppm in the ^{11}B NMR spectrum, as well as a ^{19}F NMR resonance at –78.0 ppm, similar to the previously described cations **2-L**. The analogous reaction of **1^{Me}** with one equivalent of pyridine afforded the corresponding boronium salt **2-Pyr** in 91% yield, the NMR spectra of which (δ_{11B} = –9.3 ppm, δ_{19F} = –78.1 ppm) were essentially identical to the DMAP derivative. Single crystals of **2-Pyr** and **2-DMAP** suitable for X-ray diffraction analyses were obtained by vapor diffusion of hexane into saturated THF solutions (Figure 5).

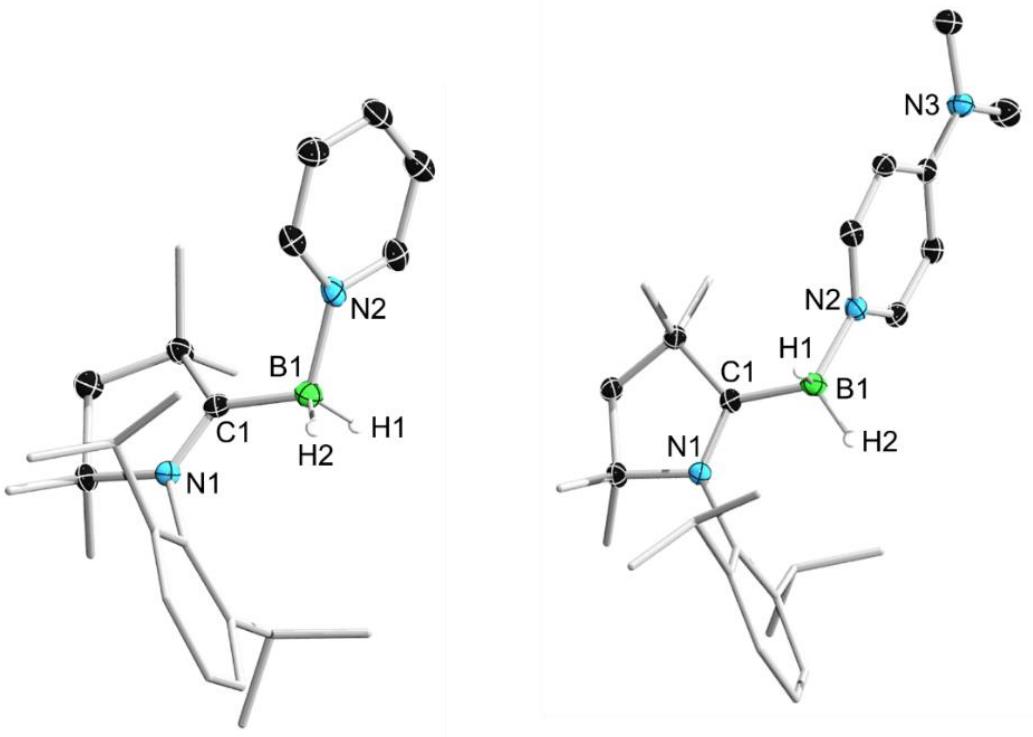

Figure 5. Crystallographically-derived molecular structures of **2-Pyr** (left) and **2-DMAP** (right). Atomic displacement ellipsoids are shown at the 50% probability level. Ellipsoids of the CAAC ligand periphery, the triflate counterion and hydrogen atoms, except those bound to boron, have been omitted for clarity. Selected bond lengths (Å) for **2-Pyr**: N1–C1 1.302(2), C1–B1 1.608(3), B1–N2 1.589(2); for **2-DMAP**: N1–C1 1.308(3), C1–B1 1.616(3), B1–N2 1.574(3).

Both in **2-Pyr** and **2-DMAP**, the CAAC^{Me} ligand acts as a pure σ donor with typical N1–C1 (ca. 1.30 Å) and C1–B1 (ca. 1.61 Å) bond lengths. The presence of the electron-donating NMe_2 group in **2-DMAP** affects only little the B1–N2 bond length of 1.589(2) Å compared to the one in **2-Pyr** (B1–N2 1.589(2) Å), both representing boron–nitrogen single bonds.

It is noteworthy that the same reaction of **1^{Me}** with one equivalent of DMAP carried out in benzene instead of THF resulted in the formation of the bis(DMAP) adduct **3-DMAP**, in which a second DMAP molecule has promoted a typical 1,2-migration of one hydrogen atom from boron to the carbene carbon atom of the CAAC^{Me} ligand (Scheme 28b).[74] While **3-DMAP** crystallized quantitatively, 50% of **1^{Me}** remained unreacted in solution. Alternatively, **3-DMAP** could be synthesized in 93% yield by treatment of a THF solution of **1^{Me}** with two equivalents of DMAP. Colorless single crystals were obtained by vapor diffusion of hexane into a saturated THF solution. The solid-state structure of **3-DMAP** evidences the binding of the DMAP residues and the migration of H1 to C1, the latter being now sp^3-hybridized (Σ(∠C1) 331.9(9)°) (Figure 6). Furthermore, the protonation of the CAAC^{Me} ligand is supported by the ^{1}H NMR spectrum of **3-DMAP**, for which a characteristic doublet at 3.51 ppm ($^3J_{HH}$ = 5.7 Hz) was observed, indicative of coupling between the hydrogen atoms bound to the former carbene carbon (C1) and the boron center. The corresponding ^{11}B NMR resonance at 4.2 ppm appears as a broad singlet that sharpens only slightly in selectively decoupled ^{11}B{^{1}H} NMR experiments.

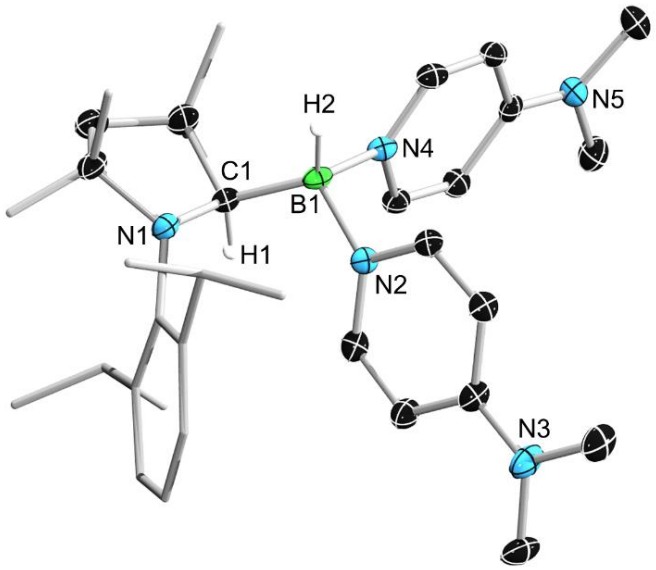

Figure 6. Crystallographically-derived molecular structure of **3-DMAP**. Atomic displacement ellipsoids are shown at the 50% probability level. Ellipsoids of the CAAC ligand periphery, the triflate counterion and hydrogen atoms, except H1 and H2, have been omitted for clarity. Selected bond lengths (Å) and angles (°): N1–C1 1.490(3), C1–B1 1.619(4), B1–N2 1.597(3), B1–N4 1.585(3), Σ(∠C1) 331.9(9).

In contrast, the binding of a second equivalent of pyridine to **2-Pyr** led only to a 1:1 mixture of **2-Pyr** (δ_{11B} = –9.1 ppm) and a second species with a very broad ^{11}B NMR resonance at 6.9 ppm, attributable to the pyridine analogue of **3-DMAP**, [(CAAC^{Me}H)BH(Pyr)$_2$]OTf (**3-Pyr**) (Scheme 28b). Heating at 80 °C for one day resulted in a maximum conversion of ca. 75% to **3-Pyr**, but unfortunately, all attempts to isolate this compound failed as removal of the pyridine solvent also resulted in removal of the second adducted pyridine ligand and regeneration of **2-Pyr**. The reversibility of the formation of **3-Pyr** is in line with the reversible binding of pyridine to (CAAC^{Me})BH$_3$ (**VIII^{Me}**), which induces a reversible hydride shuttling from the boron center to the adjacent carbene carbon atom.[74] Since pyridine derivatives are able to displace the triflate group in **1^{Me}**, the extension of this reactivity to the bifunctional Lewis base 4,4'-bipyridine was investigated, in order to obtain two connected cationic boron centers (Scheme 29).

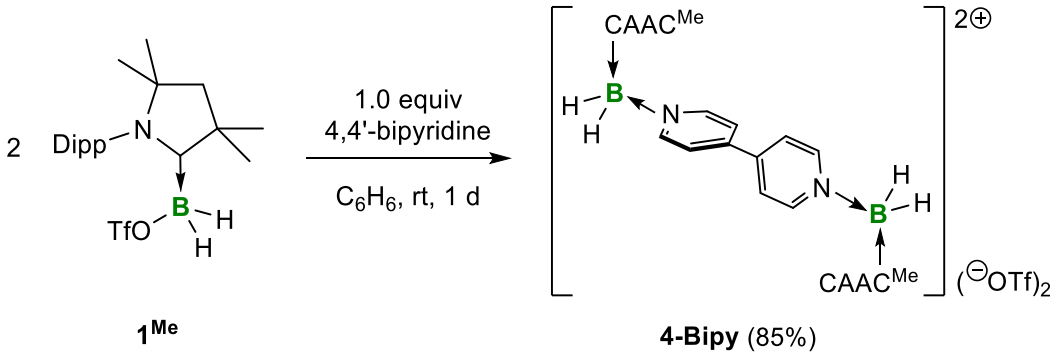

1^{Me} **4-Bipy** (85%)

Scheme 29. Synthesis of the bis(boronium) cation **4-Bipy**. Isolated yield in parentheses.

The reaction mixture of **1^{Me}** instantly turned red upon addition of half an equivalent of 4,4'-bipyridine accompanied by the formation of a colorless precipitate. After workup, the 4,4'-bipyridine-bridged bis(boronium) species **4-Bipy** was isolated in 85% yield as an off-white solid. The ^{11}B NMR spectrum showed a broad singlet at –8.5 ppm, in agreement with those of the monocationic derivatives **2-L** (L = DMAP, Pyr), as did the ^{19}F NMR resonance at –78.2 ppm. Attempts to synthesize other bis(Lewis base)-stabilized boronium cations, *i.e.* the **2-THF** derivative by stirring a THF solution of **1^{Me}** resulted in ring-opening polymerization of the solvent within two days at room temperature, as usually observed for alkyl-substituted triflate esters.[83] In contrast, the reaction of **1^{Me}** with one atmosphere of carbon monoxide did not show any conversion to the corresponding **2-CO** species, even after prolonged heating at 80 °C. In conclusion, the replacement of the triflate substituent in (CAAC^{Me})BH$_2$(OTf) (**1^{Me}**) is not solely limited to strong Lewis bases such as carbenes, but can be further extended to weaker σ donors, including trimethylphosphine, pyridine and derivatives thereof.

2.1.2 Synthesis and Reactivity of (Alkyl)hydroboryl Anions

Following the synthetic procedure to unsymmetrical hydroborylenes reported by Bertrand and co-workers,[47] the aforementioned boronium cations of the form [(CAAC^{Me})(L)BH$_2$]OTf were tested towards their ability to ultimately form analogue (CAAC^{Me})(L)BH borylenes. The advantage of this synthetic route would be the introduction of labile Lewis bases (L = phosphine, pyridine), which could potentially be removed photolytically or thermally, yielding the transient dicoordinate hydroborylene (CAAC^{Me})BH. To investigate the general viability of these Lewis bases to withstand reducing conditions and to stabilize the resulting low-valent boron species, the boronium cations presented above were reduced prior to the intended second exchange of a hydride with a triflate moiety. While the reductions of **2-L**, **3-L** and **4-L** all yielded complex mixtures of unidentifiable products, the reduction of **2-CAAC^{Me}** with an excess of KC_8 in benzene selectively afforded the intensely red (alkyl)hydroboryl anion **5** by 1,2-migration of one hydrogen atom from the boron center to the CAAC^{Me} ligand (Scheme 30a).

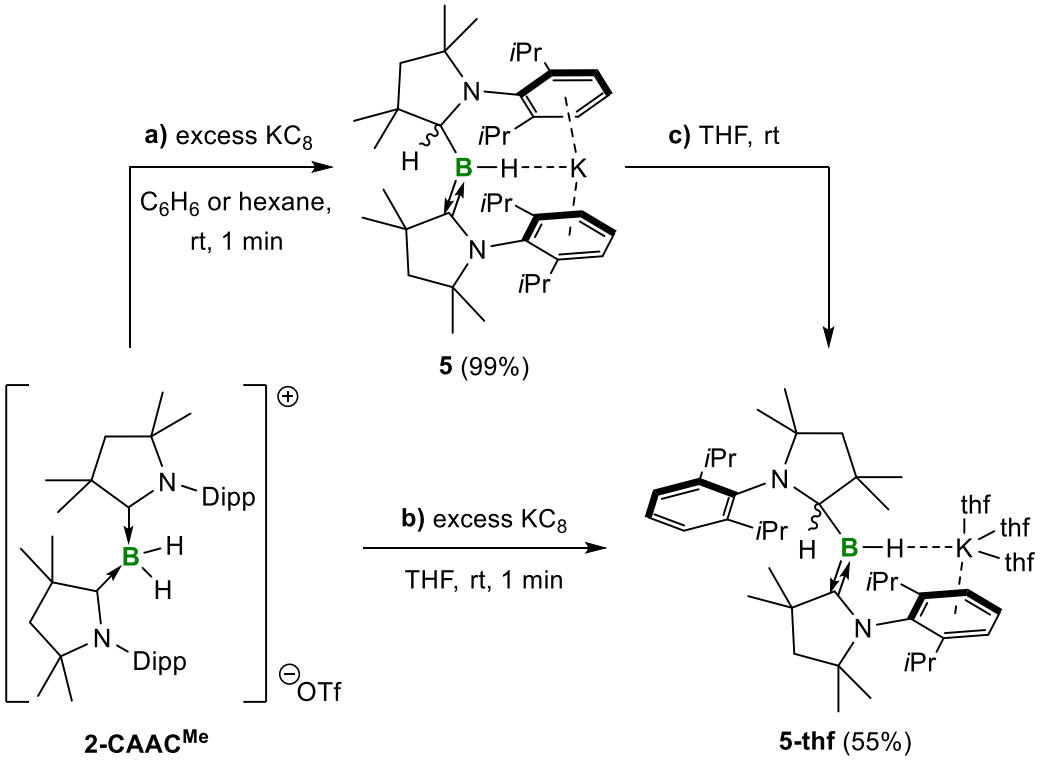

Scheme 30. Reduction of **2-CAAC^{Me}** to the (alkyl)hydroboryl anions **5** and **5-thf**. Isolated yields in parentheses.

The ^{11}B NMR spectrum of **5** showed a single broad resonance at 16.7 ppm, which is significantly downfield-shifted compared to that of other CAAC-stabilized boryl anions,[84-86] likely due to the electron-withdrawing nature of the aminoalkyl substituent CAAC^{Me}H. The ^{1}H{^{11}B} NMR spectrum displayed two sets of unsymmetrical CAAC^{Me} ligand resonances, as well as a B*H* doublet at 1.90 ppm ($^{3}J_{HH}$ = 6.6 Hz) due to coupling to the BC*H* resonance of the

CAAC^{Me}H moiety at 4.38 ppm. The presence of the boron-bound hydrogen atom was further evidenced by solid-state IR spectroscopy, which revealed an absorption band at 2329 cm^{-1} corresponding to the B–H stretching mode. The respective B–H vibrational frequency of 2352 cm^{-1} calculated at the ωB97XD/6-31+G* level of theory agrees well with the experimental data. It is noteworthy that evaporation of the solvent *in vacuo* resulted in some protonation of **5** to the known compound [(CAAC^{Me})BH$_2$(CAAC^{Me}H)],[74] the generation of which could be prevented by conducting the reduction of **2-CAAC^{Me}** to **5** in hexane. Subsequent evaporation of the solvent under atmospheric pressure afforded boryl anion **5** in essentially quantitative yield of 99%. Additionally, the reduction of **2-CAAC^{Me}** in C_6D_6 also yielded **5** in analytically pure quality sufficient for NMR-spectroscopic analysis. Slow evaporation of a benzene solution afforded red single crystals of **5**, an X-ray diffraction analysis of which revealed a monomeric structure with a trigonal-planar boron center (Σ(∠B1) 359.4(12)°) (Figure 7, left).

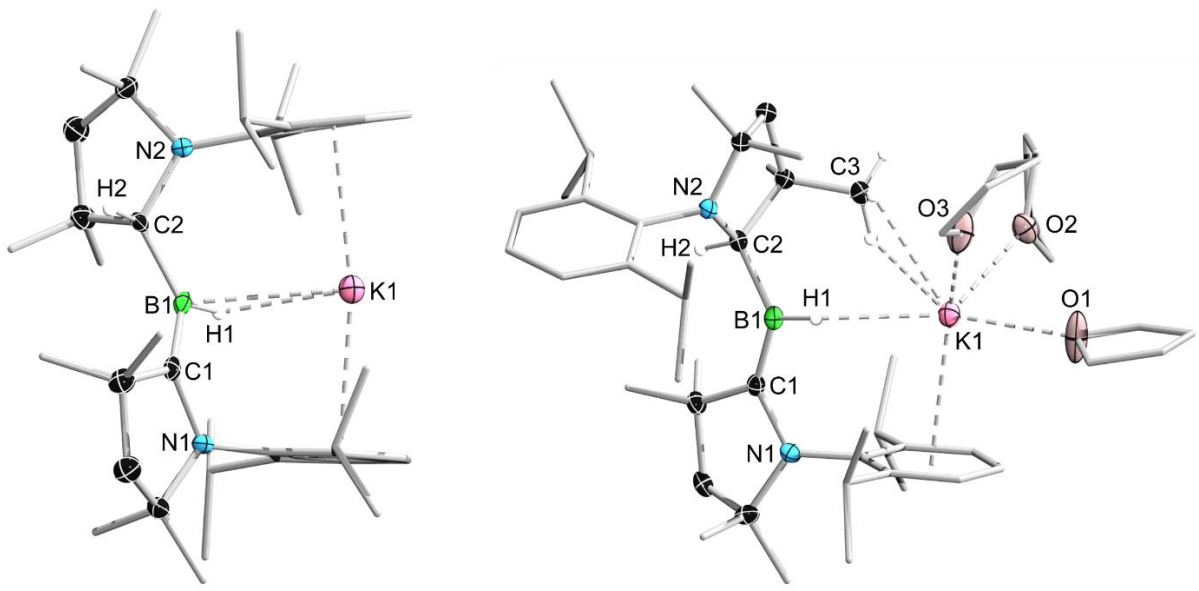

Figure 7. Crystallographically-derived molecular structures of **5** (left) and **5-thf** (right). Atomic displacement ellipsoids are shown at the 50% probability level. Ellipsoids of the CAAC ligand peripheries and hydrogen atoms, except H1, H2, and those bound to C3, have been omitted for clarity. Selected bond lengths (Å) and angles (°) for **5**: N1–C1 1.450(7), C1–B1 1.439(11), B1–C2 1.633(9), C2–N2 1.520(8), B1–H1 1.14(3), K1···H1 2.53(3), K1···B1 3.141(4), K1···centroid 2.91, Σ(∠B1) 359.4(12), Σ(∠C1) 359.7(5), Σ(∠C2) 330.1(9), B1–H1–K1 111.8(12); for **5-thf**: N1–C1 1.4601(18), C1–B1 1.452(2), B1–N2 1.620(2), C2–N2 1.5076(19), B1–H1 1.159(17), K1···H1 2.653(16), K1···B1 3.599(2), K1···centroid 2.95, K1···C3 3.2922(17), Σ(∠B1) 359.9(1), Σ(∠C1) 359.9(1), Σ(∠C2) 334.7(6), B1–H1–K1 138(1).

The potassium cation strongly interacts with the B*H* hydride (K1···H2 2.53(3) Å) and is encapsulated by the ligand sphere through π coordination of the Dipp substituents of both the CAAC^{Me} and CAAC^{Me}H ligands in a η^6 fashion. The B1–C1 distance of 1.439(11) Å is significantly shorter than those in the **2-CAAC^{Me}** precursor (B–C$_{avg.}$ 1.69 Å, Figure 4, *vide*

supra). This B1=C2 double bond indicates strong π backdonation of the lone pair of the boron center to the π-accepting CAAC^{Me} ligand, as found in all CAAC-stabilized boryl anions.[84-86] As already observed in **3-DMAP**, one hydrogen atom has shifted from boron to the carbene carbon atom of one CAAC^{Me} ligand, which is now pyramidalized (Σ(∠C2) 330.1(9)°). Thus, the C2–B1 bond length (1.633(9) Å) is in the typical range of a boron–carbon single bond. The structure of **5** was also computed at the ωB97XD/6-31+G* level of theory by Dr. Felipe Fantuzzi. The calculated bonding parameters of **5** agree well with the experimental values (Figure 8, left). Additionally, density functional theory (DFT) calculations were carried out at the ωB97XD/6-31++G** level, revealing that the HOMO of **5** possesses π-bonding character between B1 and C1 with a nodal plane located at the C1–N2 bond region (Figure 8, right).

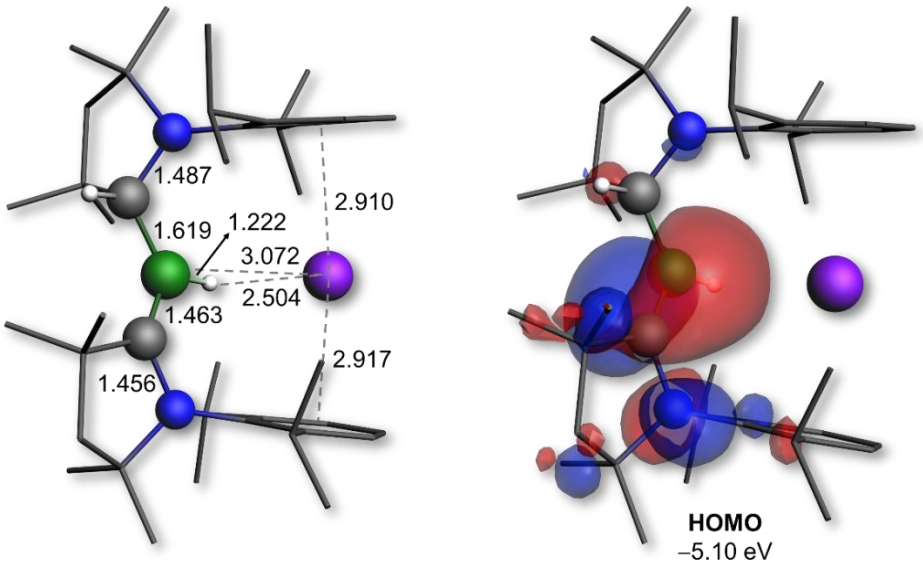

Figure 8. Left: Calculated structure of **5** at the ωB97XD/6-31+G* level of theory. Right: Plot of the HOMO of **5** (ωB97XD/6-31++G**).

Both the dissolution of **5** in THF (Scheme 30c) and the reduction of **2-CAAC^{Me}** in THF (Scheme 30b) resulted in the formation of the analogue **5-thf**, the ^{11}B NMR signal (δ_{11B} = 16.8 ppm) of which is identical to its THF-free congener. The UV-vis spectrum of **5-thf** in THF displays a broad absorption band between 450 and 650 nm (λ_{max} = 523 nm), responsible for the intense red color (see Figure 63 in the Appendix). Storing of a THF solution at –25 °C for several days provided red single crystals of **5-thf** in 55% yield. The ^{1}H NMR spectrum of isolated crystals of **5-thf** in C_6D_6 suggested the presence of three THF molecules, as already observed for other boryl anions that require additional stabilization by solvent molecules.[84-86] This was confirmed by an X-ray diffraction analysis of single crystals of **5-thf**, in which the hydride-bound potassium cation is η^6-π-stabilized now only by the Dipp substituent of the neutral CAAC^{Me} ligand (Figure 7, right). Its coordination sphere is completed by three THF molecules and an agostic interaction with one of the vicinal methyl groups (C3) of the

CAAC^{Me}H ligand. The bonding parameters of the boryl anion core vary only little from those of THF-free **5**. The major difference is the relative orientation of the pyrrolidine rings of CAAC^{Me} and CAAC^{Me}H, with Dipp moieties pointing in opposite directions.

Boryl anions are referred to as boron analogues of carbenes because of their boron-centered lone pair of electrons. The pioneering work by Yamashita, Nozaki, and co-workers on the synthesis of the first stable boryl anion in 2006 promoted these boron nucleophiles from computational curiosities,[87,88] and *in-situ* generated, highly reactive intermediates[89] to isolable compounds. Since then, boryl anions have demonstrated versatile follow-up chemistry towards a wide range of electrophiles, enabling the synthesis of otherwise inaccessible boron-containing substrates.[90] In order to verify the nucleophilicity of the novel (alkyl)hydroboryl anion **5**, a freshly prepared hexane solution of **5** was treated with MeOTf. The addition of MeOTf immediately resulted in the disappearance of the red color of **5** and the formation of a colorless precipitate (Scheme 31).

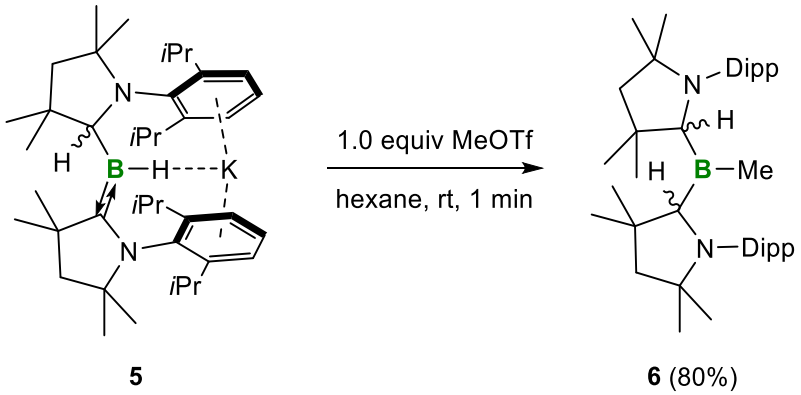

5 **6** (80%)

Scheme 31. Nucleophilic reactivity of boryl anion **5** towards MeOTf, yielding the trialkylborane **6**. Isolated yield in parentheses.

After workup, the methylated trialkylborane **6**, in which a migration of the second hydride from boron to the remaining CAAC^{Me} ligand had occurred, was isolated in 80% yield. The ^{11}B NMR spectrum of **6** displayed a very broad singlet at 93.9 ppm, typical of trialkylboranes.[91,92] The detection of one sharp ^{1}H NMR signal at 3.65 ppm, integrating for two BC*H*, suggests that there is no fluxional B-to-CAAC hydrogen shuttling in solution. While the reaction with MeOTf provided evidence for the boron-centered nucleophilicity of **5**, reactions of the boryl anion with a wide range of electrophiles including haloboranes, organohalides, heavier group 14 chlorides, as well as Zn(II), Cu(I) and Au(I) halides all resulted in the reduction of the corresponding electrophile, implying a strong reduction potential of **5**.

Even though great progress has been made in recent years, isolable boryl anions are still very rare compounds. It has become apparent, however, that boron(II) compounds such as

diborane(4) dianions can be coaxed into reacting as nucleophiles, thus mimicking the reactivity of boryl anions in the classical sense. Yamashita described the reactivity of a tetra(*o*-tolyl)diborane(4) dianion that imitates the reactivity of the respective monomeric diarylboryl anion equivalent.[93] For instance, the reaction with sulfur afforded a dianionic six-membered ring consisting of two boron and four sulfur atoms oriented in a twist-boat conformation. Inspired by these results, a benzene solution of boryl anion **5** was treated with an excess of elemental sulfur, whereupon the reaction mixture turned dark orange accompanied by the formation of a colorless precipitate (Scheme 32).

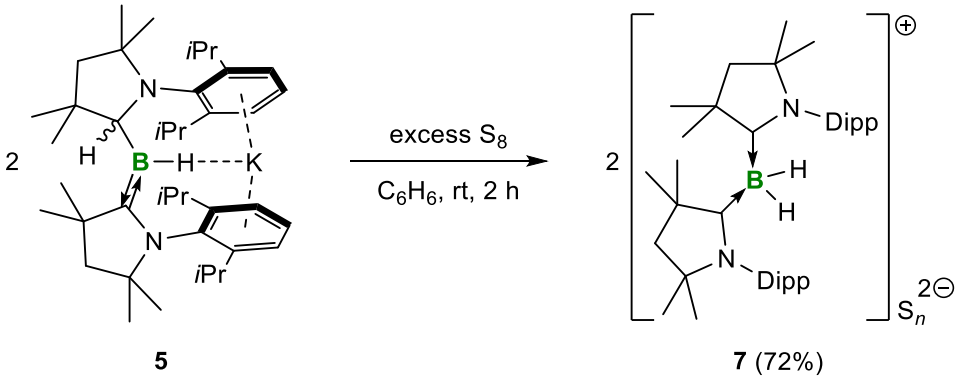

5 **7** (72%)

Scheme 32. Double oxidation of **5** with elemental sulfur back to the boronium cation **7** with a polysulfide counteranion. Isolated yield in parentheses.

After workup, **7** was isolated as an off-white solid in 72% yield. The triplet at –22.2 ppm ($^1J_{BH}$ = 84.7 Hz) in the ^{11}B NMR spectrum of **7**, as well as the set of ^{1}H NMR resonances of the CAAC^{Me} ligands indicated a double oxidation back to boronium cation [(CAAC^{Me})$_2$BH$_2^+$] (**7**), the counteranion presumably being a S_n^{2-} polysulfide. This reactivity once again highlights the pronounced reduction potential of the boryl anion **5**.

2.1.3 Synthesis of a Hydroboryl Radical

To gain further insight into the electrochemical behavior of the boronium cation **2-CAAC^{Me}** (Figure 9a) and the boryl anion **5-thf** (Figure 9c) cyclic voltammetry experiments were performed on THF solutions (0.1 M [nBu$_4$N][PF$_6$]) thereof.

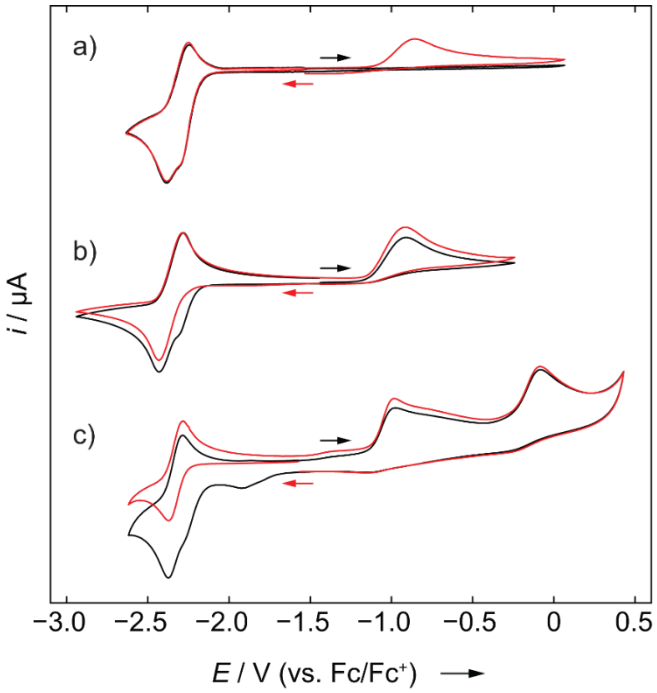

Figure 9. Cyclic voltammograms of a) **2-CAAC^{Me}**, b) the boryl radical **8** and c) the boryl anion **5-thf** in THF/0.1 M [nBu$_4$N][PF$_6$] measured at 250 mV s^{-1}. The voltammetric response for the positive (black) and negative (red) scan direction is shown for each of the compounds. Formal potentials: $E_{1/2}$ = −2.31 V (shoulder preceding the reduction: −2.28 V), E_{pa1} = ca. −0.90 V, and E_{pa2} = −0.10 V (corresponding reduction peak at −1.93 V; relative to the Fc/Fc$^+$ couple). Fc = ferrocene. Fc$^+$ = ferrocenium.

The cyclic voltammograms of **2-CAAC^{Me}** and **5-thf** were essentially identical, both showing a reversible redox event at $E_{1/2}$ = –2.31 V and an irreversible oxidation around –0.90 V (relative to the Fc/Fc$^+$ couple; Fc = ferrocene; Fc$^+$ = ferrocenium), providing further evidence that chemical one- and two-electron oxidation of **5** is indeed possible. Furthermore, a broad shoulder ($E_{1/2}$ = –2.28 V) preceding the reduction at –2.31 V in the cyclic voltammogram of **2-CAAC^{Me}** suggests that a one-electron reduction of the boronium cation to the corresponding radical species **8** should be possible (Scheme 33, *vide infra*). Unfortunately, attempts to generate **8** by direct one-electron reduction of **2-CAAC^{Me}** failed. Instead, an incomplete consumption of **2-CAAC^{Me}** was observed, providing a mixture of boryl anion **5** and radical **8**. As a result, the aim was to specifically exploit the reduction capacity of the boryl anion **5-thf**. Combining equimolar amounts of **5-thf** and **2-CAAC^{Me}** in THF instantaneously led to an intense purple solution and the precipitation of a colorless solid, presumably KOTf (Scheme 33). The ^{11}B NMR spectrum of the filtrate remained silent, indicating comproportionation to the hydroboryl

radical **8**, as suggested by the cyclic voltammetry experiments. Radical **8** is deep purple in solution and its UV-vis absorption spectrum shows a very broad absorption band between 450 and 700 nm (λ_{max} = 523 nm) in THF (see Figure 64 in the Appendix). Workup, however, provided a large crop of bright orange crystals of **8** in 89% yield. Furthermore, the cyclic voltammogram of **8** fits well in between those of the boronium cation **2-CAAC^{Me}** and the boryl anion **5-thf**, showing that both one-electron reduction and oxidation are possible (Figure 9b).

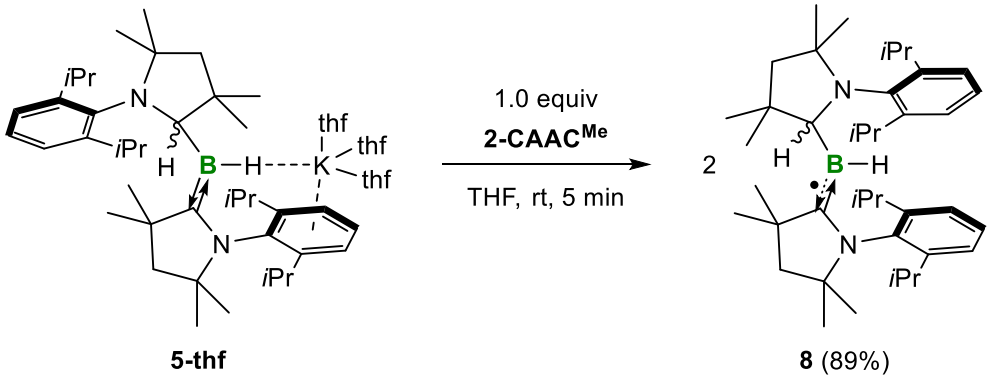

5-thf **8** (89%)

Scheme 33. Synthesis of the hydroboryl radical **8**. Isolated yield in parentheses.

An X-ray crystallographic analysis showed a structure very similar to **5** bar the potassium cation. The boron center is trigonal planar (Σ(∠B1) 359.5(6)°) and the Dipp substituents of the CAAC^{Me}H and CAAC^{Me} ligands are both oriented in the same direction (Figure 10, left).

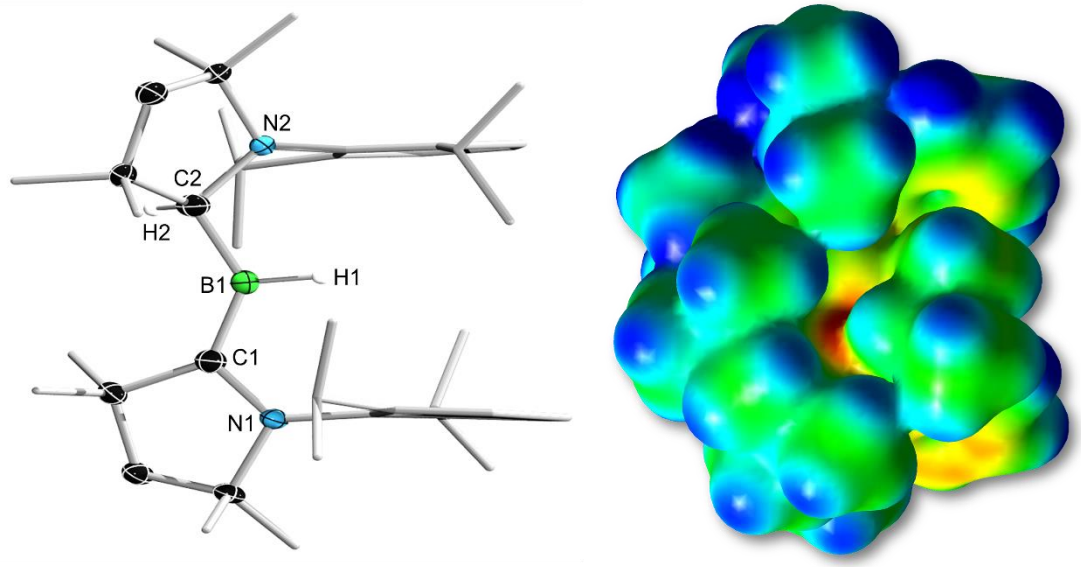

Figure 10. Left: crystallographically-derived molecular structure of **8**. Atomic displacement ellipsoids are shown at the 50% probability level. Ellipsoids of the CAAC ligand periphery and hydrogen atoms except H1 and H2 have been omitted for clarity. Selected bond lengths (Å) and angles (°): N1–C1 1.3777(15), C1–B1 1.5174(18), B1–C2 1.5817(18), C2–N2 1.4616(15), B1–H1 1.142(18), Σ(∠B1) 359.5(6), Σ(∠C1) 359.6(1). Right: electrostatic potential (ESP) map of **8** at the ωB97XD/6-31+G* level of theory. ESP charges following the notation of the solid-state structure of **8**: B1: +0.19, H1: –0.17, C1: –0.27, N1: –0.14, N2: –0.46, C2: –0.01.

Compared to the boryl anions **5** and **5-thf**, the B1–C1 (1.5174(18) Å) and C1–N1 (1.3777(15) Å) bonds at the neutral CAAC^{Me} ligand of **8** are elongated and shortened, respectively, as expected upon one-electron oxidation. The resulting partial double bonds are typical for boryl radicals stabilized by a CAAC ligand since the latter allows delocalization of the unpaired electron over the N1–C1–B1 π framework.[51-53,60,64,68,94-96]

The IR spectrum of **8** displays a B–H stretching band at 2533 cm^{-1}, which agrees with the computed (ωB97XD/6-31+G*) value of 2558 cm^{-1}. The vibrational frequency is not only ca. 200 cm^{-1} higher than that of **5**, but also 100 cm^{-1} higher than the one of Bertrand's hydroborylene **VII** ($\tilde{\nu}$(B–H) = 2455 cm^{-1}),[46] suggesting a significant strengthening of the B–H bond in the hydroboryl radical **8**. The EPR spectrum of **8** showed a broad triplet from hyperfine coupling to the ^{14}N nucleus (a(^{14}N) = 18.5 MHz) (Figure 11, black line). The simulated spectrum revealed further coupling to the quadrupolar ^{11}B nucleus (a(^{11}B) = 9.7 MHz), which is responsible for the line-broadening. The presence of two distinct couplings to the B*H* (a(^{1}H) = 13.6 MHz) and CAAC^{Me}*H* (a(^{1}H) = 4.8 MHz) nuclei suggests that the radical **8** displays no fluxional hydrogen migration between the boron and the carbene carbon atom in solution (Figure 11, red line).

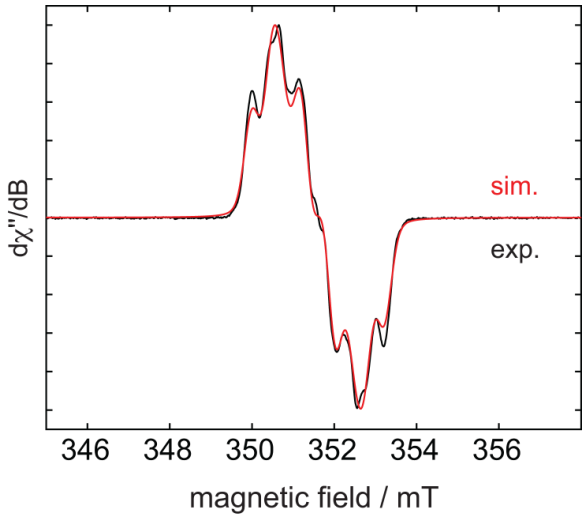

Figure 11. Experimental (black line) and simulated (red line) continuous-wave X-band EPR spectra of **8** in hexane solution at room temperature. Simulation parameters: g_{iso} = 2.0027, a(^{11}B) = 9.7 MHz (0.35 mT), a(^{14}N) = 18.5 MHz (0.66 mT), a(^{1}H) = 13.6 MHz (0.49 mT), and a(^{1}H) = 4.8 MHz (0.17 mT).

Calculations performed by Dr. Felipe Fantuzzi showed that the SOMO of **8** predominantly consists of the B1–C1 π bond with some π-antibonding character on the C1–N1 bond (Figure 12, left). The EPR spectrum, which displays a much stronger hyperfine coupling to N1 than B1, already indicated that the unpaired electron is mainly delocalized on the CAAC^{Me} ligand. This is corroborated theoretically by the computed Mulliken spin densities of 53% on C1, 21% on N1 and only 15% on B1 (Figure 12, center and right).

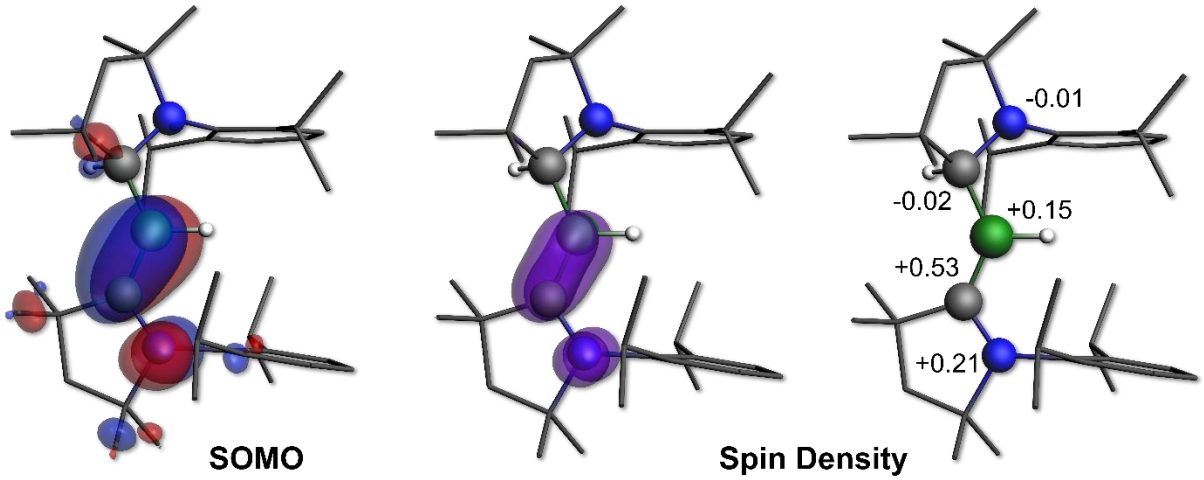

Figure 12. Left: Plot of the SOMO of **8** (surface isovalue: ± 0.03 [$e\ a_0^{-3}$]$^{1/2}$). Center: Plot of the calculated spin density of **8** (surface isovalue: 0.005 [$e\ a_0^{-3}$]). Right: Mulliken atomic spin densities.

Compound **8** represents the first neutral, structurally characterized hydroboryl radical, and is surprisingly bench-stable in the solid state. Isolated crystals of **8** proved air-stable at room temperature over a period of one week, making this species a rare example of an air-stable boron-centered radical. The only other air-stable boron-based radical reported is a permethylated icosahedral borane [*closo*-$B_{12}(CH_3)_{12}$]$^{\bullet-}$ radical anion, in which the unpaired electron is delocalized and therefore trapped within the B_{12} cage.[97] The remarkable stability of the hydroboryl radical **8** is presumably owed to a combination of the high degree of spin delocalization, the low spin density at boron and the very effective encapsulation of the B–H unit by the CAAC^{Me} and CAAC^{Me}H ligands as illustrated by the electrostatic potential map (Figure 10, right).

In summary, it was possible to extend Bertrand's substitution of the triflate moiety in CAAC-stabilized triflatoboranes to other Lewis bases than carbenes, yielding bis(base)-stabilized boronium cations. Of these, **2-CAAC^{Me}** could be selectively reduced to an (alkyl)hydroboryl anion by taking advantage of boron-to-CAAC hydride migration. This boryl anion exhibits a pronounced reduction potential, allowing for the synthesis of the corresponding neutral hydroboryl radical by one-electron oxidation of the former. The synthesis of other bis(base)-stabilized hydroborylenes according to Bertrand's synthetic route was not further investigated (see Scheme 3). Instead, the following chapters focus on the synthesis and reactivity of pseudohalide-substituted boranes and borylenes.

2.2 Synthesis and Reactivity of Isothiocyanato- and Cyanoborylenes[2]

In 2016 our group reported the reduction of the CAAC^{Me}-stabilized cyanoborane (CAAC^{Me})BBr$_2$(CN) (**XXV**) in the presence of an excess of triethylphosphine yielding the corresponding tricoordinate borylene **XXVI-PEt$_3$** (see Scheme 8). Alternatively, the related species **XXVI-IMe^{Me}** was obtained by fragmentation of the tetrameric cyanoborylene [(CAAC^{Me})B(CN)]$_4$ (**XXVII**) with the NHC IMe^{Me}.[62] It was therefore of interest to test whether the reduction of a CAAC-stabilized isothiocyanatoborane would yield a similar oligomeric, self-stabilizing [(CAAC)B(NCS)]$_n$ species, which could act as a source of dicoordinate isothiocyanatoborylenes. The following chapter includes the synthesis of CAAC-stabilized isothiocyanatoboranes and their subsequent reduction to tricoordinate isothiocyanatoborylenes. The reactivity of the latter, as well as of a related tricoordinate cyanoborylene, is explored thoroughly, and both their differences and similarities are highlighted by experimental and computational studies.

2.2.1 Synthesis of CAAC-stabilized Isothiocyanatoboranes

Curran, Lacôte and co-workers have developed a facile and versatile route to NHC-stabilized dihydroboranes, the halide, sulfonate or triflate moieties of which can be substituted by a wide range of heteroatom nucleophiles.[98] Bertrand used a similar strategy for the synthesis of (CAAC^{Cy})BH(CN)$_2$ by converting the corresponding bis(triflato)borane adduct, (CAAC^{Cy})BH(OTf)$_2$, in a double salt elimination reaction with sodium cyanide.[86] It was therefore deemed that the CAAC^{R}-stabilized triflatoboranes **1^{R}** previously presented in this work would represent suitable substrates for the introduction of the isothiocyanato moiety. To add the isothiocyanate anion [NCS$^-$] to the CAAC^{R}-stabilized borenium fragment [(CAAC^{R})BH$_2^+$], exactly one equivalent of sodium thiocyanate (NaSCN) dissolved in THF was added dropwise to a suspension of the respective triflatoborane **1^{R}** in benzene at room temperature, yielding a colorless solution in both cases (Scheme 34). After workup, the CAAC^{R}-stabilized isothiocyanatoboranes (CAAC^{R})BH$_2$(NCS) (**9^{R}**) were isolated as colorless solids in 92% (**9^{Me}**) and 89% (**9^{Cy}**) yield, respectively.

[2] The results presented herein were published in "S. Hagspiel, M. Arrowsmith, F. Fantuzzi, A. Vargas, A. Rempel, A. Hermann, T. Brückner, H. Braunschweig, Highly Colored Boron-Doped Thiazolothiazoles from the Reductive Dimerization of Boron Isothiocyanates, *Angew. Chem. Int. Ed.* **2021**, *60*, 6446–6450; *Angew. Chem.* **2021**, *133*, 6519–6524." and "S. Hagspiel, D. Elezi, M. Arrowsmith, F. Fantuzzi, A. Vargas, A. Rempel, M. Härterich, I. Krummenacher, H. Braunschweig, Reactivity of cyano- and isothiocyanatoborylenes: metal coordination, one-electron oxidation and boron-centred Brønsted basicity, *Chem. Sci.* **2021**, *12*, 7937–7942."

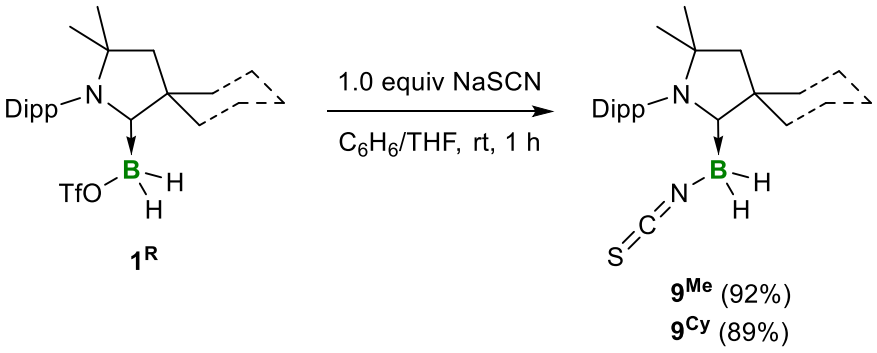

Scheme 34. Synthesis of the isothiocyanatoboranes $\mathbf{9^R}$ (R = Me, Cy). Isolated yields in parentheses.

The isothiocyanatoboranes $\mathbf{9^R}$ display a broad triplet at –20.4 ppm ($^1J_{BH}$ = 86.7 Hz, $\mathbf{9^{Me}}$) and –20.1 ppm ($^1J_{BH}$ = 87.4 Hz, $\mathbf{9^{Cy}}$) in the ^{11}B NMR spectrum, which is in agreement with the chemical shift of the NHC-analogue (IDipp)BH_2(NCS) (δ_{11B} = –23.2 ppm, broad s) reported by Curran and Lacôte,[98] indicating that the [NCS] unit is bound to boron *via* the nitrogen rather than the sulfur atom. This was further evidenced by solid-state IR spectroscopy, which revealed characteristic [BNCS] vibrational modes at 2148 and 2112 cm^{-1} ($\mathbf{9^{Me}}$) and 2154 cm^{-1} ($\mathbf{9^{Cy}}$).[98,99] The [BNCS] connectivity was confirmed unambiguously by the solid-state structures of $\mathbf{9^R}$, colorless single crystals suitable for X-ray diffraction analyses of which were obtained by vapor diffusion of hexane into saturated benzene solutions of $\mathbf{9^R}$ (Figure 13).

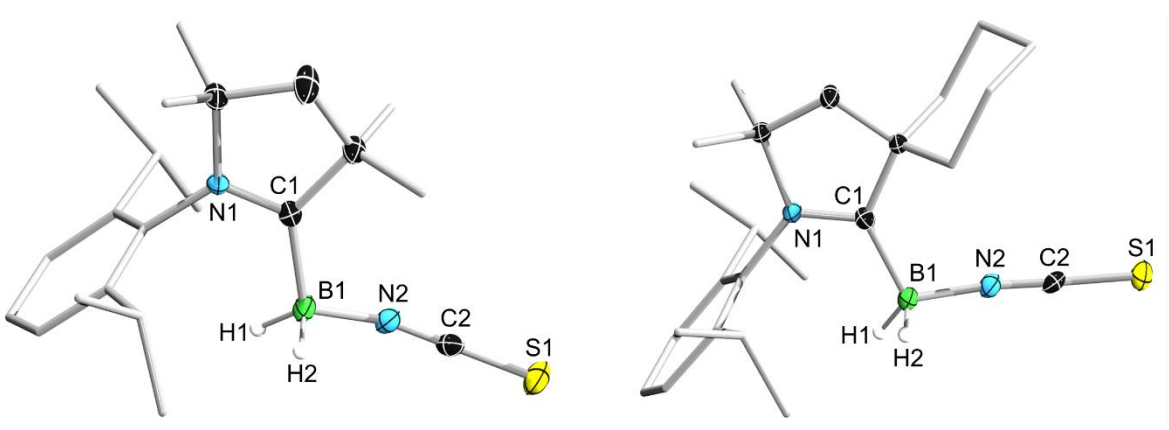

Figure 13. Crystallographically-derived molecular structures of $\mathbf{9^{Me}}$ (left) and $\mathbf{9^{Cy}}$ (right). Atomic displacement ellipsoids are shown at the 50% probability level. Ellipsoids of the CAAC ligand periphery and hydrogen atoms, except those bound to boron, have been omitted for clarity. Selected bond lengths (Å) and angles (°) for $\mathbf{9^{Me}}$: N1–C1 1.3035(19), C1–B1 1.593(2), B1–N2 1.527(2), N2–C2 1.160(2), C2–S1 1.6115(17), B1–N2–C2 168.04(18), N2–C2–S1 179.59(18); for $\mathbf{9^{Cy}}$: N1–C1 1.3053(9), C1–B1 1.598(2), B1–N2 1.533(2), N2–C2 1.159(2), C2–S1 1.6135(16), B1–N2–C2 173.85(14), N2–C2–S1 178.74(14).

In both isothiocyanatoboranes $\mathbf{9^R}$, the CAAC^R ligand acts as a pure σ donor, with C1–B1 bond lengths of 1.593(2) Å ($\mathbf{9^{Me}}$) and 1.598(2) Å ($\mathbf{9^{Cy}}$), stabilizing the vacant p orbital at the boron center. The B1–N2–C2 ($\mathbf{9^{Me}}$: 168.04(18)°; $\mathbf{9^{Cy}}$: 173.85(14)°) and the isothiocyanato moiety N2–C2–S1 ($\mathbf{9^{Me}}$: 179.59(18)°; $\mathbf{9^{Cy}}$: 178.74(14)°) each show a high degree of linearity, with characteristic N2–C2 triple (ca. 1.16 Å) and C2–S1 single (ca. 1.60 Å) bonds, as usually

observed for boron isothiocyanates.[98] While the bonding situation in **9^{R}** would thus indicate a positive charge on the nitrogen and a negative charge on the sulfur atom, the cumulenic structure with N=C and C=S double bonds, which is also preferred in the literature, will be used in the Lewis structures hereafter.

Following the synthesis of (CAAC^{Me})BBr$_2$(CN) (**XXV**) from the corresponding dihydroborane precursor established by our group,[62] the isothiocyanatoboranes **9^{R}** were converted to their corresponding dibromo analogues (CAAC^{R})BBr$_2$(NCS) (**10^{R}**). For the bromination, **9^{R}** was dissolved in DCM and a slight excess of elemental bromine was added dropwise under vigorous stirring at ambient temperature, whereupon a strong evolution of gas (HBr) was observed (Scheme 35).

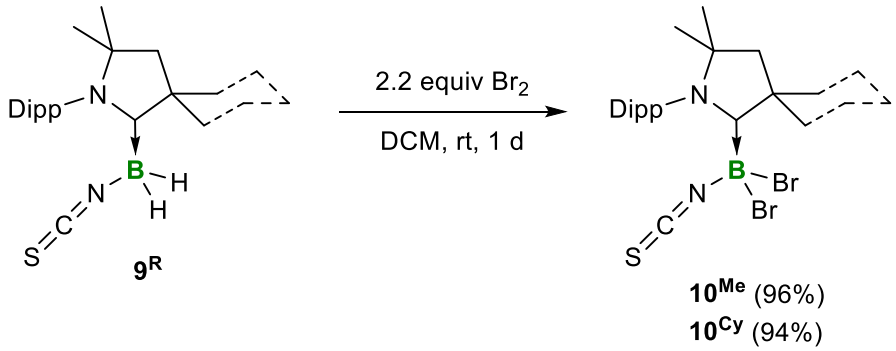

Scheme 35. Synthesis of the dibromo(isothiocyanato)boranes **10^{R}**. Isolated yields in parentheses.

The resulting amber-colored reaction mixtures were stirred overnight and subsequently worked-up analogously to the literature-known protocol for (CAAC^{Me})BBr$_2$(CN) (**XXV**).[62] The dibromo(isothiocyanato)boranes **10^{R}** were isolated as pale yellow solids in excellent yields of 96% (**10^{Me}**) and 94% (**10^{Cy}**), the ^{11}B NMR spectra of which showed a sharp singlet at –13.6 ppm (**10^{Me}**) and –13.4 ppm (**10^{Cy}**), respectively. The downfield shift of ca. 7 ppm from **9^{R}** to **10^{R}** was also observed for the analogous bromination of the cyano derivative (CAAC^{Me})BH$_2$(CN) (δ_{11B} = –33.6 ppm, t, $^{1}J_{BH}$ = 90.5 Hz) to **XXV** (δ_{11B} = –18.9 ppm, s).[62] The characteristic [BNCS] stretching bands at 2129 and 2093 cm^{-1} (**10^{Me}**) and 2143 and 2104 cm^{-1} (**10^{Cy}**) in the solid-state IR spectra vary only little from those of **9^{R}**, suggesting that the [BNCS] unit stays intact. Vapor diffusion of hexane into saturated benzene solutions of **10^{R}** yielded colorless single crystals, the X-ray diffraction analyses of which provided the final proof for the generation of the (CAAC^{R})BBr$_2$(NCS) adducts **10^{R}** (Figure 14). The bonding parameters in **10^{R}** remain essentially the same with respect to their respective dihydro precursors **9^{R}**. The C1–B1 distance of 1.691(4) Å in **10^{Cy}** is slightly longer than in **10^{Me}** (1.632(6) Å), probably due to steric repulsion between the bulky CAAC^{Cy} ligand and the bromide substituents. Both the bond lengths (B1–N2 ca. 1.50 Å; N2–C2 ca. 1.16 Å; C2–S1 ca. 1.60 Å) and angles

(B1–N2–C2 ca. 163°; N2–C2–S1 ca. 178°) of the [BNCS] unit remain in the range of respective single and triple bonds and still exhibit pronounced linearity.

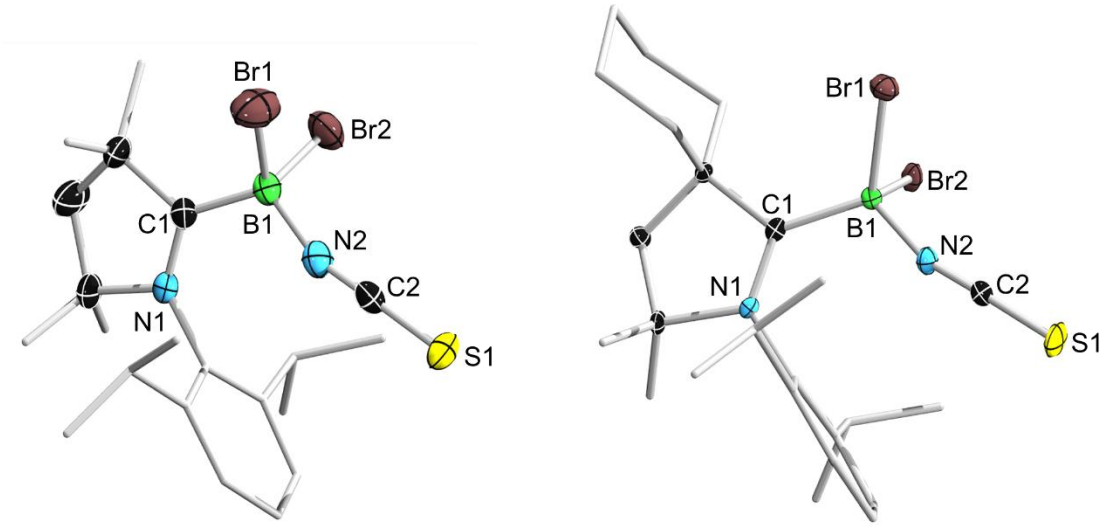

Figure 14. Crystallographically-derived molecular structures of **10^{Me}** (left) and **10^{Cy}** (right). Atomic displacement ellipsoids are shown at the 50% probability level. Ellipsoids of the CAAC ligand periphery and hydrogen atoms have been omitted for clarity. Selected bond lengths (Å) and angles (°) for **10^{Me}**: N1–C1 1.306(5), C1–B1 1.632(6), B1–N2 1.491(6), N2–C2 1.150(6), C2–S1 1.599(4), B1–N2–C2 162.0(4), N2–C2–S1 178.3(4); for **10^{Cy}**: N1–C1 1.317(3), C1–B1 1.691(4), B1–N2 1.498(4), N2–C2 1.180(3), C2–S1 1.610(3), B1–N2–C2 164.1(3), N2–C2–S1 178.7(3).

2.2.2 Synthesis of Tricoordinate Isothiocyanatoborylenes

Before carrying out the reduction of (CAAC^{R})BBr$_2$(NCS) (**10^{R}**) to potential oligomeric [(CAAC^{R})B(NCS)]$_n$ species, the initial aim was to verify the viability of transiently generated (CAAC^{R})B(NCS) borylenes. As described above, the synthesis of numerous tricoordinate borylenes was realized in particular by the reduction of CAAC-stabilized dihaloboranes in the presence of a second Lewis base.[28] Analogously, benzene solutions of **10^{R}** were added slowly to a suspension of 2.2 equivalents of KC_8 and the NHC I*i*Pr (Scheme 36).

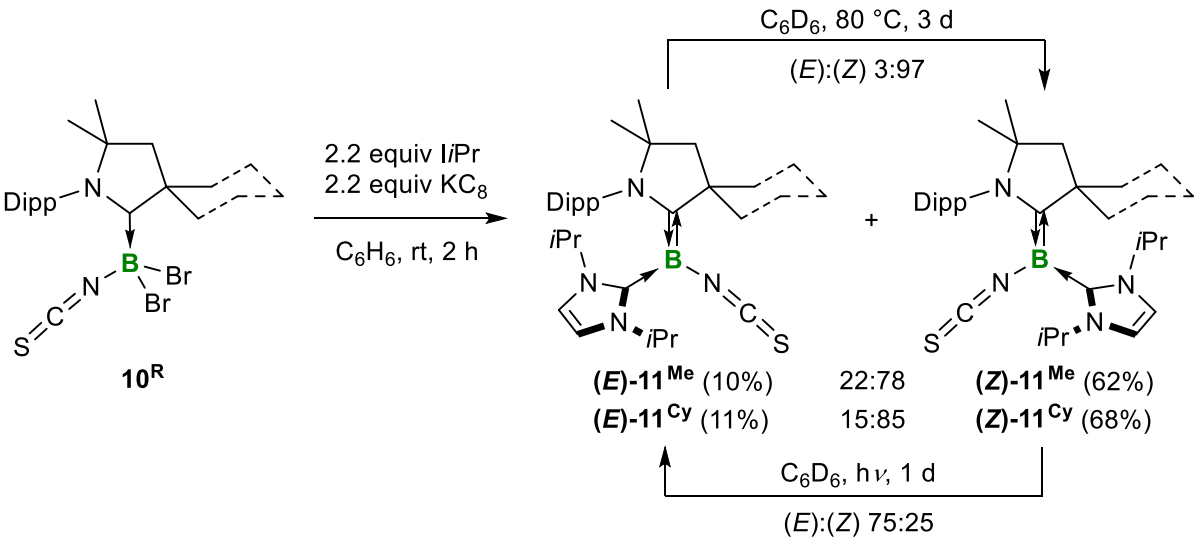

Scheme 36. Synthesis of the tricoordinate isothiocyanatoborylenes **11^{R}** and their (*E*)/(*Z*) isomerization. Isolated yields in parentheses.

After workup, fractional crystallization afforded two consecutive crops of orange crystals, which were identified by X-ray crystallographic analyses as the (*E*)- and (*Z*)-isomers of the unsymmetrical isothiocyanatoborylenes **11^{R}**. The first crop of crystals provided the (*Z*)-isomers in 62% (**(*Z*)-11^{Me}**) and 68% (**(*Z*)-11^{Cy}**) isolated yield. These showed an ^{11}B NMR resonance at –2.6 ppm (**(*Z*)-11^{Me}**) and –2.3 ppm (**(*Z*)-11^{Cy}**), respectively. The second crop yielded single crystals of the (*E*)-isomers in 11% (**(*E*)-11^{Me}**) and 10% (**(*E*)-11^{Cy}**) yield. These showed an ^{11}B NMR singlet at 3.8 ppm (**(*E*)-11^{Me}**) and 3.9 ppm (**(*E*)-11^{Cy}**). The solid-state structures of **(*Z*)-11^{Me}** and **(*E*)-11^{Cy}** display structural parameters typical of (CAAC)(NHC)-stabilized tricoordinate borylenes (Figure 15, see Figure 60 and Figure 61 in the Appendix for the solid-state structures of the isomers **(*E*)-11^{Me}** and **(*Z*)-11^{Cy}**).[46,53,62,64,65] In the (*Z*)-isomers, N1 and N2 are in a *cis*-configuration relative to the CAAC^{R}–boron bonds, which show distinct double bond character (C1–B1 ca. 1.45 Å), indicating strong π backbonding from the borylene center to the π-acidic CAAC ligand, while the pyrrolidine ring in the (*E*)-isomers is oriented so that N1 and N2 are on opposite sides of the C1=B1 double bond.

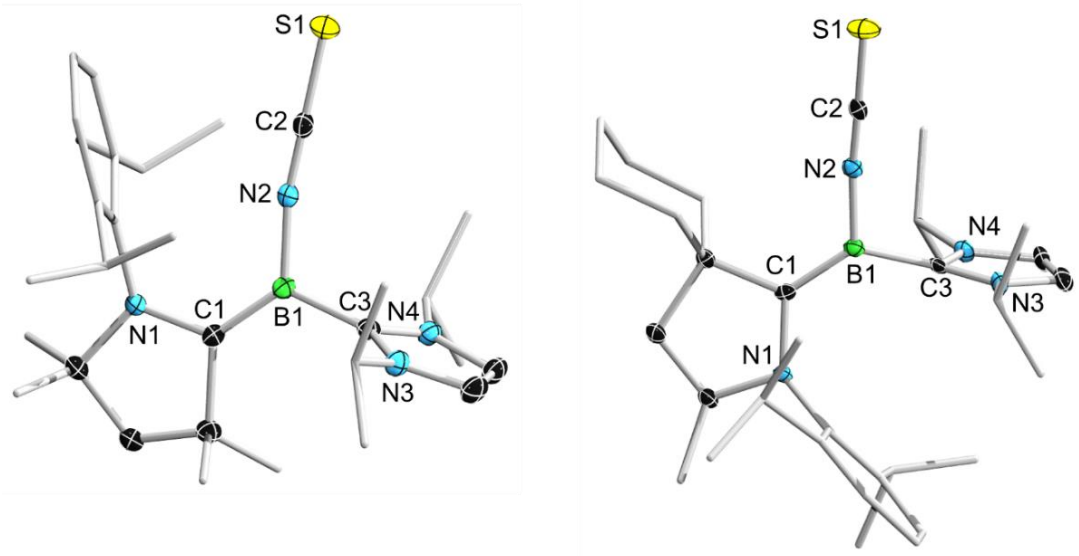

Figure 15. Crystallographically-derived molecular structures of **(*Z*)-11^{Me}** (left) and **(*E*)-11^{Cy}** (right). Atomic displacement ellipsoids are shown at the 50% probability level. Ellipsoids of the ligand peripheries and hydrogen atoms have been omitted for clarity. Selected bond lengths (Å) and angles (°) for **(*Z*)-11^{Me}**: N1–C1 1.4080(14), C1–B1 1.4591(16), B1–N2 1.4836(15), N2–C2 1.1706(15), C2–S1 1.6195(12), B1–C3 1.5885(16), C1–B1–C3 123.92(10), B1–N2–C2 169.09(11), N2–C2–S1 179.46(12); for **(*E*)-11^{Cy}**: N1–C1 1.4287(19), C1–B1 1.448(2), B1–N2 1.487(2), N2–C2 1.171(2), C2–S1 1.6119(17), B1–C3 1.589(2), C1–B1–C3 127.94(15), B1–N2–C2 171.01(16), N2–C2–S1 178.72(15).

The N2–B1–C3–N3 torsion angles of 73–85° reveal that the NHC rings are rotated almost perpendicularly to the borylene plane and coordinate as pure σ donors (B1–C3 ca. 1.59 Å). While the C2–S1 bonds (ca. 1.61 Å) remain essentially unchanged, the shortened B1–N2 (ca. 1.49 Å) and elongated N2–C2 (ca. 1.17 Å) distances suggest partial π donation from the borylene center to the NCS ligand. This is corroborated by the solid-state IR spectra of the (*Z*)-isomers of the isothiocyanatoborylenes **(*Z*)-11^{R}**, which show an identical characteristic vibrational mode for the [NCS] unit at 2101 cm^{-1}. This stretching frequency is significantly lower than the one for the adducts **9^{R}** and **10^{R}**, further evidencing the weakening of the N2–C2 bond upon π donation from the boron center to the adjacent nitrogen.

NMR-spectroscopic analyses of the crude borylene solutions prior to crystallization showed (*E*)/(*Z*) ratios of 22:78 (**11^{Me}**) and 15:85 (**11^{Cy}**). The preference for the (*Z*)-isomer is attributable to the strong steric repulsion between the bulky Dipp moiety of the CAAC^{R} ligands and the I*i*Pr ligand. The separation of the ^{11}B NMR shifts of the two isomers of ca. 5 ppm can be explained by Hirshfeld charge analysis,[100] which implies slightly negatively (ca. –0.012) and positively charged (ca. +0.003) boron atoms for **(*Z*)-11^{R}** and **(*E*)-11^{R}**, respectively. Furthermore, the different steric constraints were also apparent in the ^{1}H NMR spectra, which showed symmetrical ligand resonances for **(*Z*)-11^{R}**, indicative of free rotation about the B1–C3 bond. However, for **(*E*)-11^{R}** the ^{1}H NMR spectra showed very broad ligand resonances split into two

magnetically inequivalent sets of resonances, typical of hindered rotation. To quantify the energy barrier for the rotation around the B1–C3 bond a variable temperature ^{1}H NMR experiment was performed on a mixture of **(*Z*)-11^{Me}** and **(*E*)-11^{Me}**. Low-temperature ^{1}H NMR spectra revealed a significant sharpening of the signals for **(*E*)-11^{Me}** upon cooling to 0 °C already. At –40 °C, coalescence of the I*i*Pr resonances was observed, again followed by broadening of the resonance sets of both isomers at –80 °C. Additionally, analysis of the coalescence of various ^{1}H NMR resonances within the 25–70 °C temperature range (Table 1) provided an estimate of 15.8 kcal mol^{-1} for the Gibbs free energy of activation ($\Delta G^{\ddagger}$) of the B1–C3 bond rotation, which can be calculated using equation (1).

$$\Delta G^{\ddagger} = -RT_c \ln\left(\frac{hk_c}{k_B T_c}\right) \text{ with } k_c = \frac{\pi \Delta \nu^0}{\sqrt{2}} \qquad (1)$$

Table 1. Estimate of the Gibbs free energy of I*i*Pr rotation for **(*E*)-11^{Me}** from variable temperature ^{1}H NMR experiments.

Resonances	Shifts at rt (ppm)	Max. peak-to-peak separation $\Delta\nu^0$ (Hz)	Coalescence temperature T_c (K)	Exchange rate at coalescence k_c (s^{-1})	Gibbs free energy of activation $\Delta G^{\ddagger}$ (kJ mol^{-1})	(kcal mol^{-1})
*i*Pr-C*H*$_3$	0.33, 0.14	95	328	211	66.0	15.8
C(C*H*$_3$)$_2$	2.02, 1.93	45	313	100	64.8	15.5
NCH=CHN	6.01, 5.91	49	318	109	65.7	15.7
m-Ar-*H*	6.98, 6.73	129	338	287	67.2	16.1
				Average $\Delta G^{\ddagger}$	65.9	15.8

Furthermore, the (*E*)/(*Z*) ratio of the mixture of **11^{Me}** before and after the variable temperature NMR experiments changed, suggesting that an isomerization process between both isomers is possible. Indeed, heating of a C_6D_6 solution of isolated **(*E*)-11^{Me}** at 80 °C for three days resulted in 97% conversion to the thermodynamically preferred **(*Z*)-11^{Me}** isomer (Figure 16, left). Since the time required to reach three half-lives for this isomerization exceeded two days, no kinetic analysis was performed. Conversely, irradiation of isolated **(*Z*)-11^{Me}** under a UV lamp for one day provided a 75:25 mixture of the (*E*)- and (*Z*)-isomers. No further change of this ratio was observed over a course of ten days of irradiation (Figure 16, right).

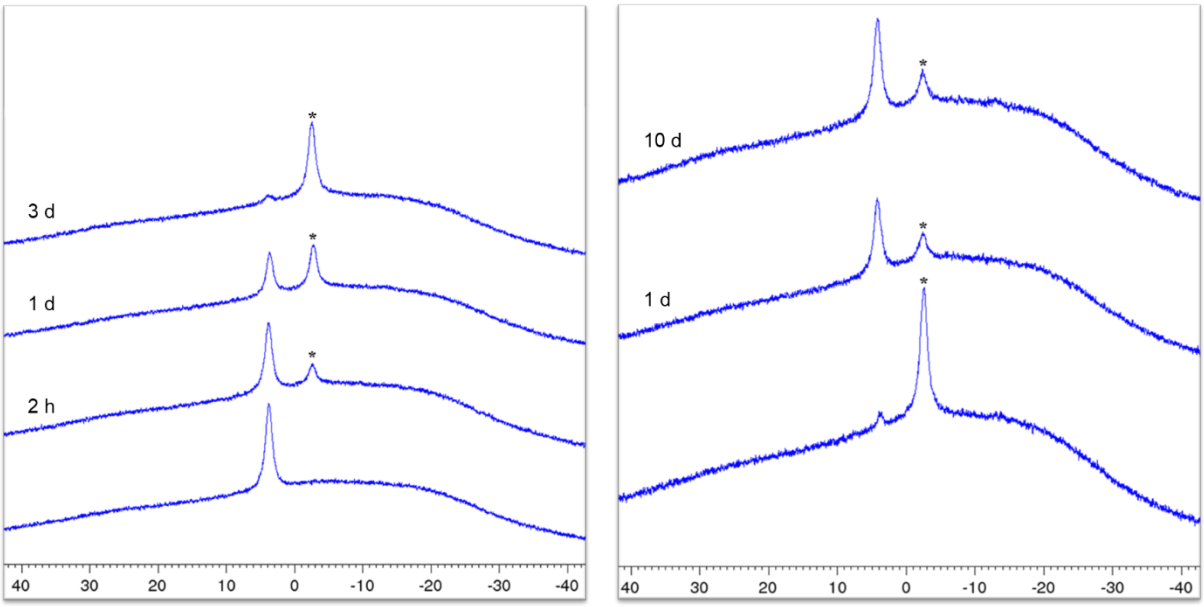

Figure 16. Left: Stack-plot of ^{11}B NMR spectra for the thermal conversion of **(*E*)-11^{Me}** to **(*Z*)-11^{Me}** (*) in C_6D_6 at 80 °C. Right: Stack-plot of ^{11}B NMR spectra of the photolytic conversion of **(*Z*)-11^{Me}** (*) to **(*E*)-11^{Me}** in C_6D_6 at room temperature.

DFT calculations at the OLYP[101-104]/TZP level performed by Dr. Alfredo Vargas at the University of Sussex, UK, further corroborated the greater thermodynamic stability of the (*Z*)-isomers of **11^{R}**, from which ΔG[**(*Z*)/(*E*)-11^{R}**] values of –6.86 kcal mol^{-1} (R = Me) and –5.01 kcal mol^{-1} (R = Cy) were obtained. It is noteworthy that the vast majority of asymmetric borylenes of the type (CAAC)(L)BR, depending on the relative sterics of L and R, are formed exclusively as a single (*Z*)- or (*E*)-isomer.[28,47,51,53,62,64,105] However, a similar thermally induced reversible isomerization has recently been observed for the first time in the (CAAC^{Me})(PMe$_3$)-stabilized borylborylene **XXXVI-PMe$_3$**, probably induced by the thermal lability of the phosphine ligand (see Scheme 17).[75] Given both the thermodynamic preference of the (*Z*)-isomer and clearer ^{1}H NMR spectrum of the CAAC^{Me} ligand compared to CAAC^{Cy}, as well as the far better isolated yield, the reactivity studies on the isothiocyanatoborylenes described in the following sections were exclusively performed with **(*Z*)-11^{Me}**.

2.2.3 Synthesis of a Tricoordinate Cyanoborylene

Previous studies in our group have already shown the viability of tricoordinate cyanoborylenes of the form (CAAC^{Me})(L)B(CN) (**XXVI-L**), which are generated either by trapping the transient (CAAC^{Me})B(CN) borylene with an additional donor ligand (L = PEt$_3$) or *via* fragmentation of the tetrameric cyanoborylene [(CAAC^{Me})B(CN)]$_4$ (**XXVII**) with a sufficiently strong and small Lewis base (L = IMe^{Me}) (see Scheme 8).[62] For better comparison of the reactivity of tricoordinate cyano- and isothiocyanatoborylenes, the tricoordinate cyanoborylene (CAAC^{Me})(I*i*Pr)B(CN) (**12**), stabilized by the NHC I*i*Pr as a second Lewis base, was

synthesized. Preliminary work has already pointed out that I*i*Pr is unable to fragment the tetramer **XXVII**, presumably due to the steric demands of the *iso*propyl substituents.[62] Therefore, trapping of the transient cyanoborylene (CAAC^{Me})B(CN) during reduction of the corresponding dibromoborane precursor **XXV** was chosen for the preparation of **12**. For this purpose, a dilute solution of (CAAC^{Me})BBr$_2$(CN) (**XXV**) in benzene was added dropwise to a suspension of 2.2 equivalents of both KC_8 and I*i*Pr under vigorous stirring (Scheme 37).

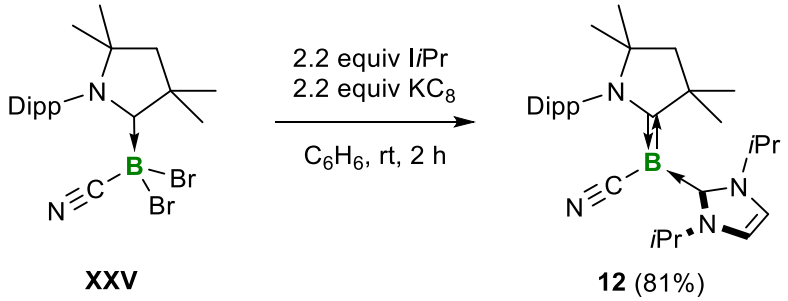

Scheme 37. Synthesis of the tricoordinate cyanoborylene **12**. Isolated yield in parentheses.

After two hours at room temperature, the resulting yellow mixture was filtered and after workup, a large crop of yellow crystals of **12** was isolated in 81% yield. The ^{11}B NMR spectrum of **12** displayed a sharp resonance at –12.1 ppm, very similar to that of the related cyanoborylene (CAAC^{Me})(IMe^{Me})B(CN) (**XXVI-IMe^{Me}**) (δ_{11B} = –11.3 ppm).[62] In contrast to the isothiocyanatoborylene **11^{Me}**, which is formed as 22:78 mixture of the (*E*)- and (*Z*)-isomers, **12** is formed as the (*Z*)-isomer only. The cyano unit and Dipp substituent of the (*Z*)-isomer are arranged on the same side with respect to the C_{CAAC}–boron double bond and no isomerization to the respective (*E*)-isomer was observed. The absolute configuration of **12** was determined *via* X-ray diffraction analysis of single crystals obtained by slow evaporation of a benzene solution (Figure 17). As already observed for the isothiocyanato analogue, the solid-state structure of **12** displays structural parameters typical of (CAAC)(NHC)-stabilized tricoordinate borylenes,[46,53,62,64,65] with a trigonal planar borylene center (Σ(∠B1) 360.0(2)°) and a short C_{CAAC}–boron bond with distinct double bond character (C1–B1 1.4630(17) Å), indicative of strong π backdonation from the electron-rich boron center to the π-acidic CAAC^{Me} ligand. The I*i*Pr ligand coordinates as pure σ donor (C3–B1 1.5918(16) Å) and is rotated perpendicularly to the borylene plane, as implied by the C1–B1–C3–N3 torsion angle of ca. 89°. The [BCN] unit shows a high degree of linearity (B1–C2–N2 171.87(13)°) and its bond lengths are in the range of single (B1–C2 1.5490(18) Å) and triple (C2–N2 1.1618(16) Å) bonds, respectively, as observed in the literature-known derivative **XXVI-IMe^{Me}**.[62]

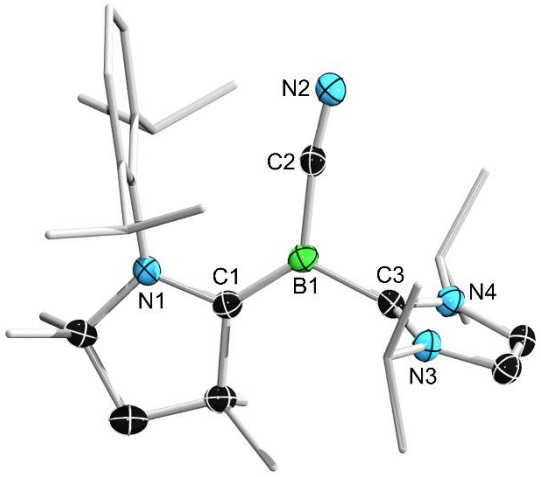

Figure 17. Crystallographically-derived molecular structure of **12**. Atomic displacement ellipsoids are shown at the 50% probability level. Ellipsoids of the ligand peripheries and hydrogen atoms have been omitted for clarity. Selected bond lengths (Å) and angles (°): N1–C1 1.4076(14), C1–B1 1.4630(17), B1–C2 1.5490(18), C2–N2 1.1618(16), B1–C3 1.5918(16), C1–B1–C3 123.12(12), B1–C2–N2 171.87(13), Σ(∠B1) 360.0(2)°.

The solid-state IR spectrum of **12** reveals one sharp vibrational mode at 2119 cm^{-1}, which fits well with the frequencies reported for the IMe^{Me}- and PEt_3-stabilized cyanoborylenes **XXVI-L**.[62] The differences in color of **(*Z*)-11^{Me}** and **12** are apparent in their UV-vis absorption spectra. While the former displays an absorption maximum at 342 nm with a broad shoulder at 390 nm, cyanoborylene **12** shows an absorption maximum at 313 nm, as well as an additional broad band at 446 nm, each accounting for the bright orange and yellow color of **(*Z*)-11^{Me}** and **12**, respectively (Figure 18).

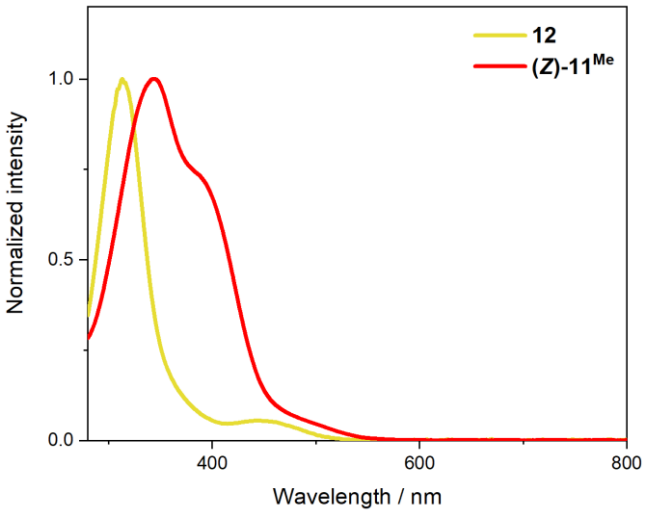

Figure 18. Overlay of the UV-vis absorption spectra of **(*Z*)-11^{Me}** (red) and **12** (yellow) in benzene at 25 °C. **(*Z*)-11^{Me}**: λ_{max} = 342 nm, λ = 390 nm (shoulder); **12**: λ_{max} = 313 nm, λ = 446 nm.

2.2.4 One-Electron Oxidation of Isothiocyanato- and Cyanoborylenes

As mentioned above, borylenes are electron-rich compounds, and in addition to their boron-centered nucleophilicity, they also exhibit pronounced reduction capacity (*vide supra*). Accordingly, Bertrand's parent borylene **VII** could be oxidized to the corresponding hydroboryl radical cation **[VII$^{\bullet+}$][GaCl$_4^-$]** with the aid of $GaCl_3$ (see Scheme 21), and Roesky and co-workers succeeded in oxidizing a doubly CAAC^{Me}-stabilized fluoroborylene to its radical cation in a similar manner (see Scheme 22).[46,65] Inspired by these results, the redox chemistry of the pseudohaloborylenes **(*Z*)-11^{Me}** and **12** was studied.

To get a first insight into the reduction behavior of **(*Z*)-11^{Me}** and **12**, cyclovoltammetric experiments were performed on the borylenes. The cyclovoltammograms in THF show a fully reversible redox event at $E_{1/2}$ = –1.06 V (**(*Z*)-11^{Me}**) and a partially reversible redox event at $E_{1/2}$ = –0.89 V (**12**) (relative to the ferrocene standard Fc/Fc$^+$), respectively, suggesting the possibility of selective chemical one-electron oxidation (Figure 19).

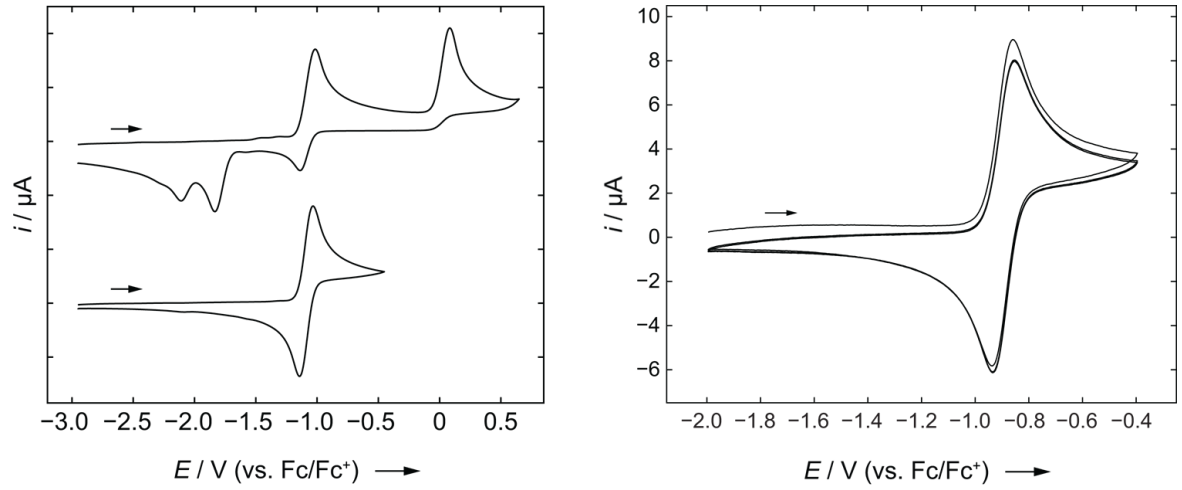

Figure 19. Left: Cyclic voltammograms of **(*Z*)-11^{Me}** in THF with [*n*Bu$_4$N][PF$_6$] (0.1 M) as supporting electrolyte (scan rate, ν = 250 mV s^{-1}, 20 ºC). The voltammogram at the bottom shows the reversibility of the first oxidation wave. Formal potentials: $E_{1/2}$ = −1.06 V, E_{pa} = ca. +0.08 V (corresponding reduction peaks at −1.83 V and −2.10 V; relative to the Fc/Fc$^+$ couple). Right: Cyclic voltammogram of **12** in THF with [*n*-Bu$_4$N][PF$_6$] (0.1 M) as supporting electrolyte (scan rate, ν = 250 mV s^{-1}, 20 ºC). Formal potential: $E_{1/2}$ = −0.89 V (relative to the Fc/Fc$^+$ couple).

Indeed, treatment of benzene solutions of **(*Z*)-11^{Me}** and **12** with exactly one equivalent of the oxidizing agent silver triflate (Ag[OTf]) afforded an immediate color change from red to yellow (**(*Z*)-11^{Me}**) or intensification of the yellow color (**12**), respectively, accompanied by the formation of a black silver precipitate (Scheme 38a). The ^{11}B NMR spectra of the respective filtrates remained silent, indicating the formation of a paramagnetic species. After workup, the boryl radical cations **[(*Z*)-11$^{Me\bullet+}$][OTf$^-$]** and **[12$^{\bullet+}$][OTf$^-$]** were obtained as yellow solids in 81% and 85% yield, respectively. As indicated by the cyclovoltammetry experiments of

(*Z*)-11^{Me} and **12**, the one-electron oxidation of the borylenes to the corresponding radical cations proved to be fully reversible chemically. The reductions of the radical cations with a slight excess of KC_8 in benzene cleanly afforded the isothiocyanato- and cyanoborylene, respectively, in essentially quantitative yields (Scheme 38b).

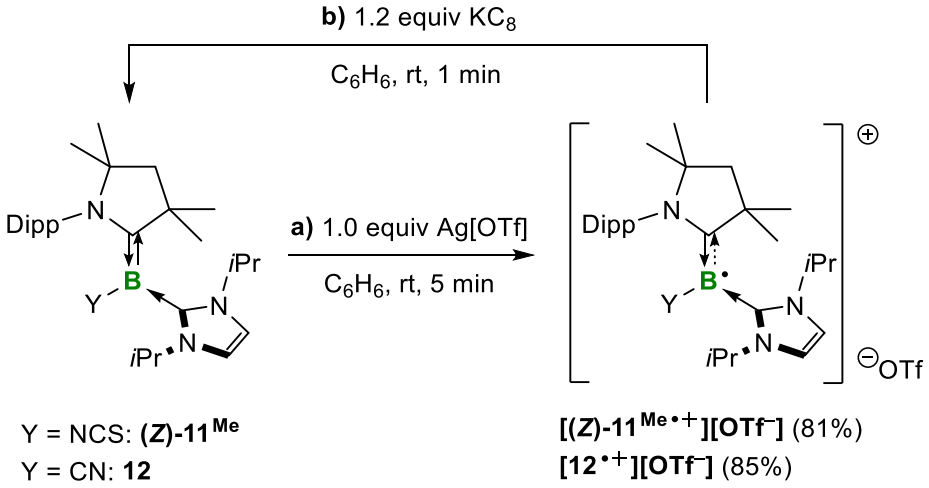

Scheme 38. Reversible chemical one-electron oxidation of **(*Z*)-11^{Me}** and **12** to the boryl radical cations **[(*Z*)-11$^{Me•+}$][OTf$^-$]** and **[12$^{•+}$][OTf$^-$]**. Isolated yields in parentheses.

The EPR spectra of both pseudohaloboryl radical cations show significant differences in terms of their hyperfine coupling (Figure 20). While the EPR spectrum of **[(*Z*)-11$^{Me•+}$][OTf$^-$]** displays a broad resonance (peak-to-peak linewidth 1.9 mT) at g_{iso} = 2.003 with no observable coupling to adjacent nuclei, the EPR spectrum of **[12$^{•+}$][OTf$^-$]** shows a multiplet at g_{iso} = 2.0025 with hyperfine coupling to the boron ($a(^{10,11}B)$ = 9.0 MHz), as well as the nitrogen nuclei of the CAAC^{Me} ligand ($a(^{14}N)$ = 21.7 MHz) and the cyano substituent ($a(^{14}N)$ = 18.0 MHz). This is in good agreement with other CAAC-stabilized boryl radicals and radical cations, which usually show distinct coupling to the pyrrolidine ring of the CAAC ligand due to pronounced delocalization of electron density from boron to the latter.[46,64,65]

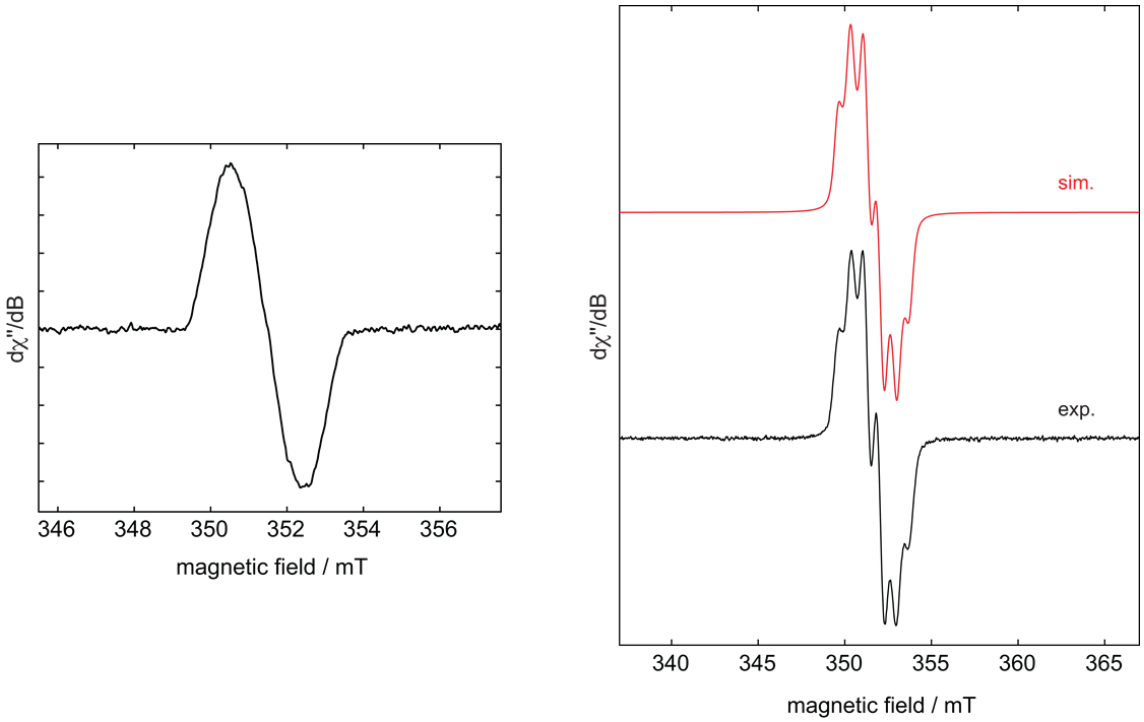

Figure 20. Left: Experimental continuous-wave X-band EPR spectrum of **[(*Z*)-11$^{Me•+}$][OTf$^-$]** in benzene solution at room temperature. The isotropic g value is g_{iso} = 2.003 and the peak-to-peak linewidth is 1.9 mT. Right: Experimental (black line) and simulated (red line) continuous-wave X-band EPR spectra of **[12$^{•+}$][OTf$^-$]** in benzene solution at room temperature. Best-fit simulation parameters: g_{iso} = 2.0025, a(^{10,11}B) = 9.0 MHz, a(^{14}N) = 21.7 MHz, and a(^{14}N) = 18.0 MHz.

Slow evaporation of benzene solutions afforded yellow single crystals of **[(*Z*)-11$^{Me•+}$][OTf$^-$]** and **[12$^{•+}$][OTf$^-$]** suitable for X-ray diffraction analyses (Figure 21). Both boryl radical cations retain the (*Z*)-configuration of the C_{CAAC}–boron bond, which is slightly elongated (C1–B1 ca. 1.46 Å) to a partial double bond, as expected upon one-electron oxidation.[46,65] The low-valent boron centers remain trigonal planar (Σ(∠B1) ca. 360°) and are stabilized each by the I*i*Pr ligand acting as pure σ donor (B1–C3 ca. 1.59 Å). Neither the bonding parameters of the cyano nor of the isothiocyanato moieties, change significantly upon oxidation of the borylenes. Both structures still show pronounced linearity of the respective pseudohalo substituent as well as carbon–nitrogen triple and nitrogen–sulfur single bonds. However, while the NCS substituent shows a noticeable increase of π interaction from the nitrogen atom to the vicinal borylene center (B1–N2 1.454(2) Å; **(*Z*)-11^{Me}**: B1–N2 1.4836(15) Å), the respective B1–C2 distance of 1.548(7) Å in **[12$^{•+}$][OTf$^-$]** suggests no enhanced stabilization from the cyano group in comparison to precursor **12** (B1–C2 1.5490(18) Å). The stronger π donation of the isothiocyanato moiety compared to the cyano substituent was further evidenced by the solid-state IR spectra of the boryl radical cations, in which the characteristic vibrational mode of the isothiocyanato group ($\tilde{\nu}$(NCS) = 2056 cm^{-1}) is observed at lower wavenumbers with respect to the borylene precursor ($\tilde{\nu}$(NCS) = 2101 cm^{-1}). In contrast, the wavenumber of the CN stretching

mode at 2145 cm^{-1} in **[12$^{\bullet+}$][OTf$^-$]** is shifted ca. 26 cm^{-1} higher compared to the one in **12** ($\tilde{\nu}$(CN) = 2119 cm^{-1}) indicating a strengthening of the C≡N triple bond upon oxidation of the cyanoborylene.

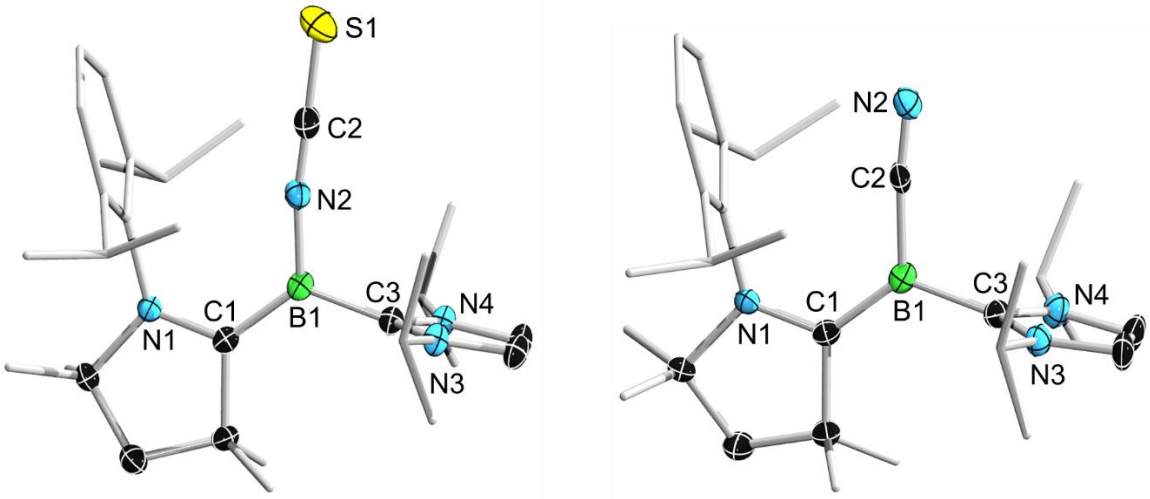

Figure 21. Crystallographically-derived molecular structures of **[(*Z*)-11$^{Me\bullet+}$][OTf$^-$]** (left) and **[12$^{\bullet+}$][OTf$^-$]** (right). Thermal ellipsoids are shown at the 50% probability level. Ellipsoids of the ligand peripheries, the triflate anion and hydrogen atoms omitted for clarity. Selected bond lengths (Å) and angles (°) for **[(*Z*)-11$^{Me\bullet+}$][OTf$^-$]**: N1–C1 1.342(2), C1–B1 1.510(2), B1–N2 1.454(2), N2– C2 1.170(2), C2–S1 1.5835(18), B1–C3 1.590(2), B1–N2–C2 169.90(16), N2–C2–S1 179.00(16). For **[12$^{\bullet+}$][OTf$^-$]**: N1–C1 1.335(6), C1–B1 1.510(7), B1–C2 1.548(7), C2–N2 1.146(6), B1–C3 1.590(7), B1–N2–C2 172.9(5).

The pronounced electron delocalization across the CAAC^{Me} ligand and the respective pseudohalide substituent was further corroborated quantumchemically by calculations of the spin density obtained from the multipole-derived charges up to quadruple expansion (MDC-q) at the OLYP/TZ2P level of theory (Figure 22**,** calculations performed by Dr. Felipe Fantuzzi).

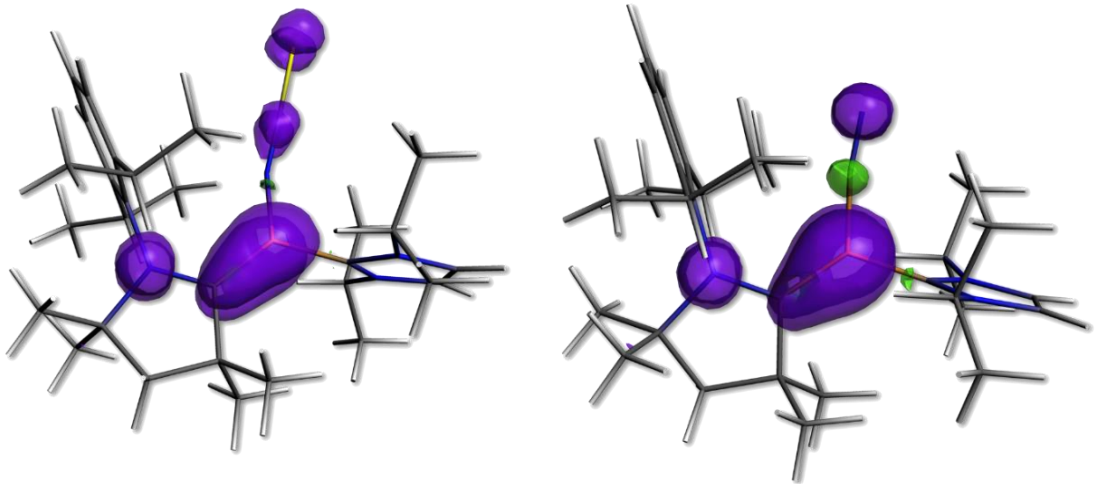

Figure 22. Spin density plots of **[(*Z*)-11$^{Me\bullet+}$][OTf$^-$]** (left) and **[12$^{\bullet+}$][OTf$^-$]** (right) obtained from the multipole-derived charges up to quadruple expansion (MDC-q) at the OLYP/TZ2P level of theory. Selected spin densities (values following the notation of the solid-state structures of **[(*Z*)-11$^{Me\bullet+}$][OTf$^-$]** and **[12$^{\bullet+}$][OTf$^-$]**) for **[(*Z*)-11$^{Me\bullet+}$][OTf$^-$]**: N1: 0.220; C1: 0.179; B1: 0.295; N2: 0.013; C21: 0.058; S1: 0.103; for **[12$^{\bullet+}$][OTf$^-$]**: N1: 0.219; C1: 0.125; B1: 0.388; C21: 0.009; N2: 0.134.

The spin density in both radical cations is delocalized over the [N1–C1–B1–Y] π framework (Y = NCS, CN), with the highest contribution at boron. In contrast to Bertrand's hydroboryl radical cations (spin density at boron = 0.50),[46,47] the boron spin density of the pseudohaloboryl radical cations is noticeably lower (Y = NCS: 0.295; Y = CN: 0.388), which is presumably owed to the additional delocalization of the spin density over the isothiocyanato and cyano substituents, respectively.

As mentioned above, the oxidation of the pseudohaloborylenes resulted in a color change from red to yellow (**[(*Z*)-11$^{Me•+}$][OTf$^-$]**) or the intensification of the yellow color (**[12$^{•+}$][OTf$^-$]**), respectively. This observation was further investigated by UV-vis absorption spectroscopy performed on benzene solutions of the radical cations (Figure 23).

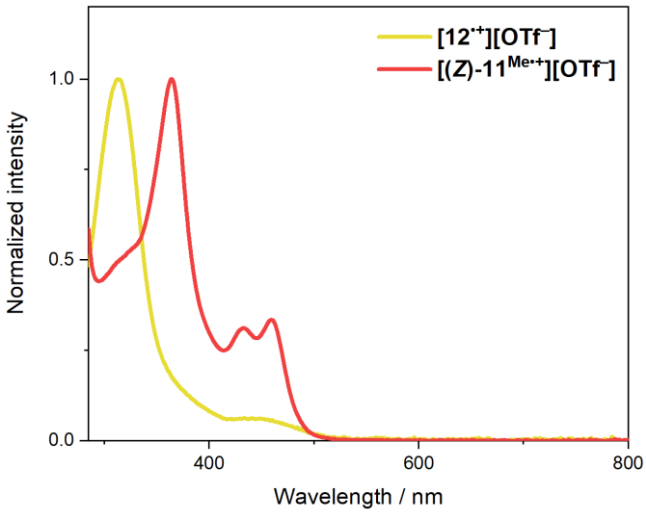

Figure 23. Overlay of UV-vis absorption spectra of **[(*Z*)-11$^{Me•+}$][OTf$^-$]** (red) and **[(*Z*)-12$^{•+}$][OTf$^-$]** (yellow) in benzene at 25 °C. **[(*Z*)-11$^{Me•+}$][OTf$^-$]**: λ = 318 nm (shoulder), λ_{max} = 364 nm, λ = 433 nm, λ = 460 nm; **[12$^{•+}$][OTf$^-$]**: λ_{max} = 313 nm, λ = 452 nm.

While the absorption spectrum of the cyano derivative (λ_{max} = 313 nm, λ = 452 nm) essentially does not change with respect to the cyanoborylene precursor **12**, the absorption maximum of the isothiocyanatoboryl radical cation exhibits a slight hypsochromic shift of ca. 20 nm to λ_{max} = 364 nm, concomitant with the occurrence of two new absorption bands at 433 and 460 nm, collectively accounting for the intense yellow color of **[(*Z*)-11$^{Me•+}$][OTf$^-$]**.

2.2.5 Coordination Chemistry of Isothiocyanato- and Cyanoborylenes

After the demonstrated reversible one-electron oxidation of the tricoordinate borylenes **(*Z*)-11^{Me}** and **12** to the corresponding radical cations, the next focus of this work was to determine to which extent these electron-rich borylenes exhibit boron-centered nucleophilicity. The solid-state structures of **(*Z*)-11^{Me}** and **12** already indicated that the electron density of the borylene lone pair is predominantly delocalized across the CAAC^{Me}–boron double bond, with the I*i*Pr ligand being rotated perpendicularly to the borylene plane and serving as σ donor only (*vide supra*). Accordingly, the HOMOs of the pseudohaloborylenes **(*Z*)-11^{Me}** (–2.727 eV) and **12** (–2.917 eV) are composed of strong π contributions in the CAAC^{Me}–boron bonding region, with negligible involvement of the carbene carbon atom of the NHC ligands (Figure 24).

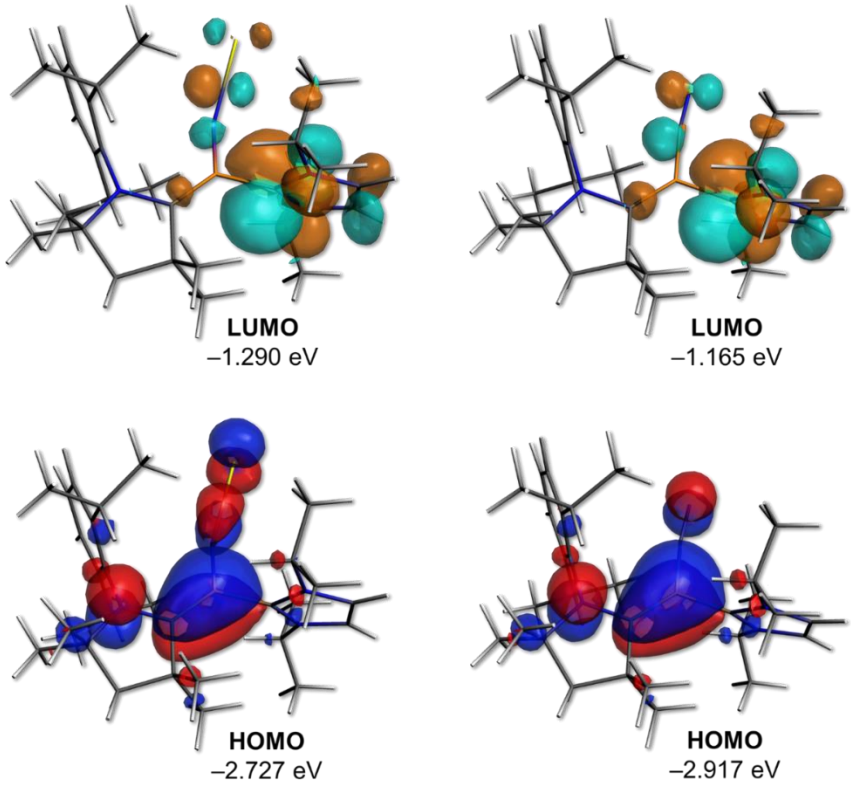

Figure 24. Canonical Kohn–Sham molecular orbitals of **(*Z*)-11^{Me}** (left) and **12** (right) at the OLYP/TZ2P level of theory. Selected Hirshfeld atomic charges (values following the notation of the solid-state structures of **(*Z*)-11^{Me}** and **12**) for **(*Z*)-11^{Me}**: N1: –0.061; C1: –0.068; B1: –0.012; N2: –0.142; C2: +0.035; S1: –0.210; C3: +0.072; for **12**: N1: –0.055; C1: –0.050; B1: –0.064; C2: –0.032; N2: –0.282; C3: +0.076.

However, both borylenes display distinct contribution of the respective pseudohalide substituent, suggesting that the electron density of the HOMO is also partially localized on the terminal sulfur and nitrogen atom, respectively. The LUMOs of **(*Z*)-11^{Me}** (–1.290 eV) and **12** (–1.165 eV) mainly feature the vacant p orbitals of the NHC ligands (Figure 24). The less negative Hirshfeld charge at boron for **(*Z*)-11^{Me}** (–0.012) and **12** (–0.064), respectively, suggests that the latter is more electron-rich than the isothiocyanato congener, which is in

agreement with the relative ^{11}B NMR shifts of the two borylenes (**(*Z*)-11^{Me}**: δ_{11B} = –2.6 ppm; **12**: δ_{11B} = –12.1 ppm). Consequently, cyanoborylene **12** should exhibit an enhanced boron-centered nucleophilicity compared to **(*Z*)-11^{Me}**.

The boron-centered nucleophilicity attributed to borylenes was demonstrated by Kinjo and co-workers, who showed that the bis(oxazol-2-ylidene)-stabilized phenylborylene **XVI** can coordinate as a neutral η^1-σ-donor to chromium(0) and group 9 precursors (see Scheme 24 and Scheme 25),[48,78] as well as Lewis acidic $GaCl_3$.[46,78,106] Similarly, our group has reported boron-centered adduct formation between a bis(isonitrile)-stabilized durylborylene and $GaCl_3$, whereas the hard Lewis acid $AlCl_3$ coordinates at the isonitrile nitrogen (see Scheme 26).[79] Inspired by these results, the reactivity of the tricoordinate pseudohaloborylenes **(*Z*)-11^{Me}** and **12** towards group 6 carbonyl complexes was investigated. For this purpose, THF solutions of the group 6 carbonyl precursors [M(CO)$_6$] (M = Cr, Mo, W) were irradiated for three hours at room temperature to generate the corresponding complexes [M(CO)$_5$(thf)] *in situ*. Subsequently, the isothiocyanatoborylene **(*Z*)-11^{Me}** was added to each mixture, resulting in an instant intensification of the solution color (Scheme 39, left).

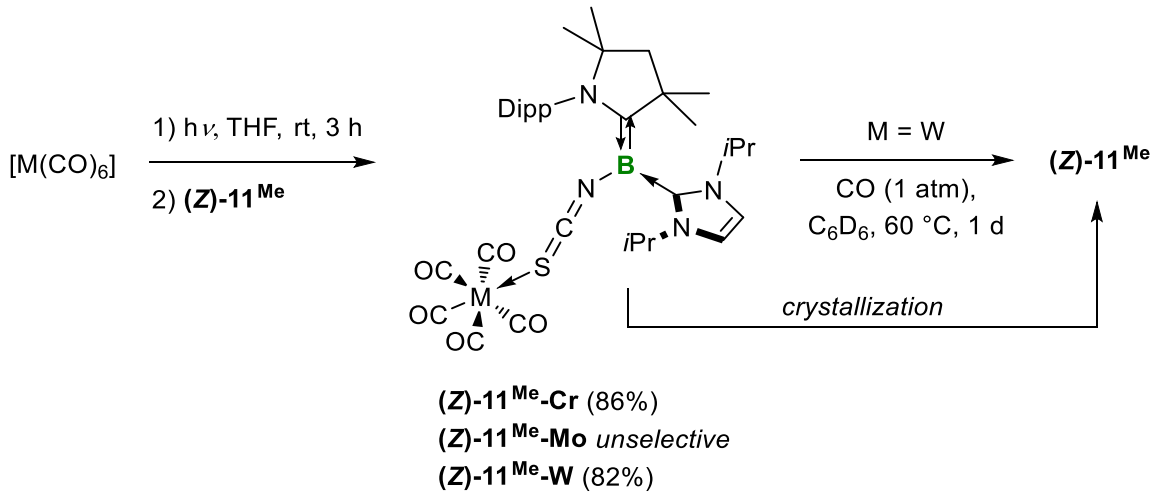

Scheme 39. Reversible adduct formation between **(*Z*)-11^{Me}** and group 6 hexacarbonyls. Isolated yields in parentheses.

The ^{11}B NMR spectrum of the reaction mixtures of **(*Z*)-11^{Me}-Cr** (δ_{11B} = –3.8 ppm) and **(*Z*)-11^{Me}-W** (δ_{11B} = –3.9 ppm), respectively, showed one resonance only shifted ca. 1 ppm upfield from the **(*Z*)-11^{Me}** borylene precursor, thus indicating that the boron centers remain tricoordinate and the borylene-metal complexes retain the (*Z*)-configuration of the CAAC–boron double bond. Significant changes of the ^{1}H NMR resonances of the CAAC^{Me} and I*i*Pr ligands suggested the formation of adducts by metal coordination to the terminal sulfur donors of **(*Z*)-11^{Me}**. This was further evidenced by the ^{13}C{^{1}H} NMR spectra of **(*Z*)-11^{Me}-M**, which revealed two characteristic resonances for the respective [M(CO)$_5$] carbonyl fragment at

ca. 220 and 215 ppm each, as reported for [M(CO)$_5$(L)] group 6 complexes.[43,48,107] In contrast, all attempts to synthesize the analogous complex **(*Z*)-11^{Me}-Mo** only led to intractable mixtures of unidentifiable products. After workup, complexes **(*Z*)-11^{Me}-Cr** and **(*Z*)-11^{Me}-W** were isolated as red-brown solids in 86% and 82% yield, respectively. The UV-vis absorption spectra of **(*Z*)-11^{Me}-M** were essentially identical, displaying a very broad absorption maximum at 365 nm (M = Cr) and 367 nm (M = W), with secondary absorptions in the 450 to 600 nm region, collectively accounting for the red-brown color of the borylene-metal complexes (Figure 25).

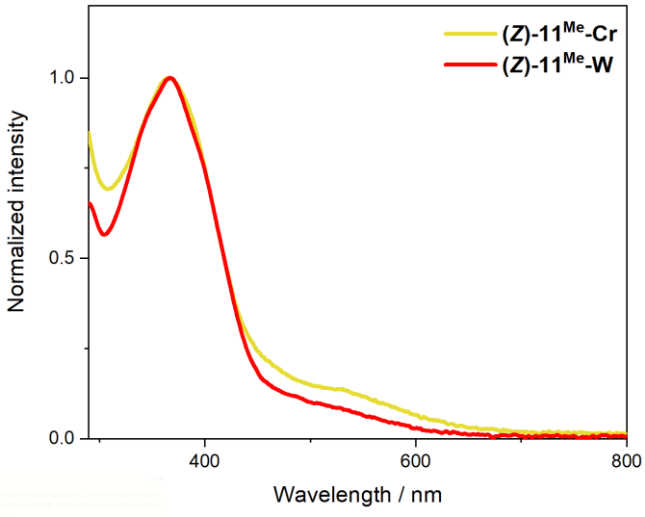

Figure 25. Overlay of UV-vis absorption spectra of **(*Z*)-11^{Me}-Cr** (yellow) and **(*Z*)-11^{Me}-W** (red) in benzene at 25 °C. **(*Z*)-11^{Me}-Cr**: λ_{max} = 365 nm; **(*Z*)-11^{Me}-W**: λ_{max} = 367 nm.

The solid-state IR spectra of **(*Z*)-11^{Me}-Cr** ($\tilde{\nu}$(CO) = 2057, 1968, 1932, 1903 cm^{-1}) and **(*Z*)-11^{Me}-W** ($\tilde{\nu}$(CO) = 2066, 1972, 1911, 1880 cm^{-1}) each showed four CO stretching bands, confirming again that one CO ligand had indeed been replaced, and exposed further that the [NCS] unit in **(*Z*)-11^{Me}-M** (M = Cr: $\tilde{\nu}$(NCS) = 2108 cm^{-1}; M = W: $\tilde{\nu}$(NCS) = 2106 cm^{-1}) stays intact. A comparison of the CO vibrational frequencies of Kinjo's phenylborylene-chromium complex **XVI-Cr** ($\tilde{\nu}$(CO) = 2016, 1977, 1933, 1892 cm^{-1})[48] and the isothiocyanatoborylene-metal complexes **(*Z*)-11^{Me}-M** discloses that **XVI** binds significantly stronger to the respective transition-metal centers, thus yielding slightly blue-shifted vibrational modes. Although **(*Z*)-11^{Me}-M** could be isolated as powders by removal of the reaction solvent *in vacuo*, all attempts to obtain single crystals of **(*Z*)-11^{Me}-M** resulted in quantitative recovery of the starting borylene **(*Z*)-11^{Me}**, indicating a very weak S→M interaction. Furthermore, heating of a C_6D_6 solution of **(*Z*)-11^{Me}-W** under an atmosphere of CO led to quantitative liberation of the borylene **(*Z*)-11^{Me}** and full recovery of [W(CO)$_6$] after one day (Scheme 39, right). A literature search showed that there have been no other group 6 M^0 complexes with RN=C=S donor ligands reported, presumably due to the weak interaction between sulfur and the respective transition-metal center.

Similarly, the addition of the tricoordinate cyanoborylene **12** to irradiated THF solutions of the [M(CO)$_6$] (M = Cr, Mo, W) precursors immediately resulted in an intensification of the yellow color (Scheme 40). After workup, the cyanoborylene-metal complexes **12-M** were obtained as yellow solids in 91% (M = Cr), 89% (M = Mo) and 87% (M = W) yield, respectively.

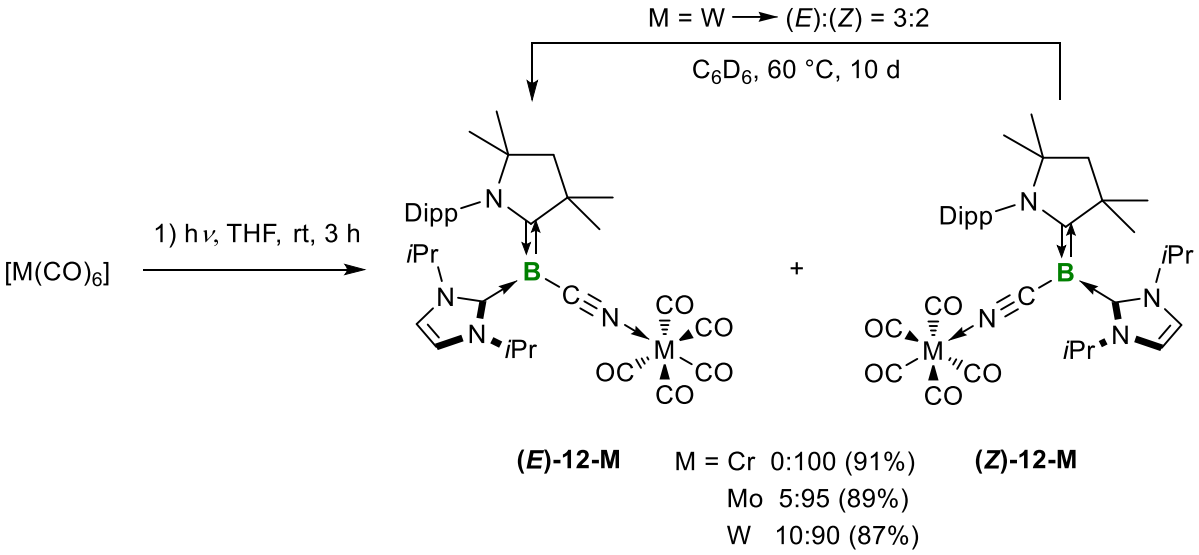

Scheme 40. Adduct formation between **12** and group 6 hexacarbonyls. Isolated yields in parentheses.

As already observed for the isothiocyanato derivatives, the ^{11}B NMR spectra of the reaction mixtures of **12-M** (M = Cr, Mo, W) showed one slightly upfield-shifted resonances (δ_{11B} = –13.2 to –13.8 ppm) compared to the precursor **12** (δ_{11B} = –12.1 ppm). While the ^{11}B NMR spectrum of **12-Cr** showed only the (*Z*)-isomer, **12-Mo** and **12-W** were formed as a mixture of the (*E*)- and (*Z*)-isomers in 5:95 and 10:90 ratio, respectively. The ^{11}B NMR shift of the respective (*E*)-isomer (δ_{11B} = –8.4 ppm) is shifted ca. 5 ppm downfield, as is the resonance of the isothiocyanatoborylene **(*E*)-11^{Me}** with respect to its (*Z*)-isomer (*vide supra*). Additionally, while **(*Z*)-12-Cr** and **(*Z*)-12-Mo** did not isomerize at higher temperatures, prolonged heating of a C_6D_6 solution of the isolated 10:90 mixture of **(*E*)/(*Z*)-12-W** at 60 °C afforded a 3:2 (*E*)/(*Z*) mixture, evidencing that the (*Z*)-isomer is the kinetic and the (*E*)-isomer the thermodynamic product. As observed for the isothiocyanatoborylene precursor **(*E*)-11^{Me}**, the ^{1}H and ^{13}C{^{1}H} NMR resonances of the CAAC^{Me} and I*i*Pr ligands of **(*E*)-12-W** were very broad, again indicative of hindered rotation around the B–C_{NHC} bond due to steric constraints. In contrast, the respective NMR spectra of **(*Z*)-12-W** displayed symmetrical ligand resonances suggesting free rotation at room temperature. Whereas **(*Z*)-12-Mo** could be isolated cleanly by fractional crystallization, the slow and partial isomerization of **(*Z*)-12-W** to **(*E*)-12-W** in solution even at room temperature prevented the clean isolation of either isomer. The UV-vis absorption spectra of the cyanoborylene-metal complexes **12-M** recorded in benzene each displayed one very

broad absorption maximum at 340 nm (M = Cr), 345 nm (M = Mo) and 354 nm (M = W), respectively, accounting for the intense yellow-brown color of the complexes (Figure 26). These absorption bands are shifted ca. 25–40 nm hypsochromically compared to cyanoborylene **12**, as also observed for the isothiocyanatoborylene **(*Z*)-11^{Me}** upon metal complexation.

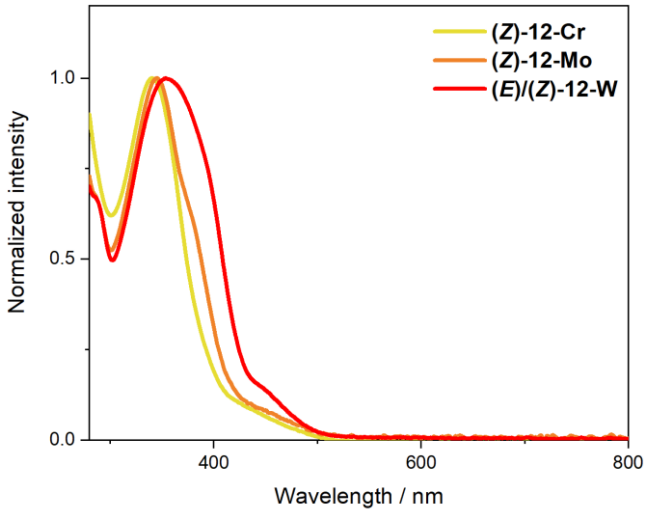

Figure 26. Overlay of UV-vis absorption spectra of **(*Z*)-12-Cr** (yellow), **(*Z*)-12-Mo** (orange) and **(*E*)/(*Z*)-12-W** (red) in benzene at 25 °C. **(*Z*)-12-Cr**: λ_{max} = 340 nm; **(*Z*)-12-Mo**: λ_{max} = 345 nm; **(*E*)/(*Z*)-12-W**: λ_{max} = 354 nm.

The solid-state IR spectra of the isolated cyanoborylene metal complexes **(*Z*)-12-M** revealed vibrational modes at 2134 cm^{-1} (M = Cr), 2126 cm^{-1} (M = Mo) and in the 2067–1858 cm^{-1} region that agree with the expected values for the C≡N and CO ligands, respectively. The solid-state IR spectrum of the (*E*)/(*Z*) mixture of **(*E*)/(*Z*)-12-W** also showed four stretching bands in the 2066–1856 cm^{-1} region, as well as two sharp vibrational bands at 2143 and 2121 cm^{-1} for the cyano group of each isomer. Generous washing of the original 10:90 (*E*)/(*Z*) mixture of **12-W** with a mixture of hexane and THF and subsequent drying *in vacuo* afforded a few milligrams of pure **(*Z*)-12-W**, enabling the assignment of $\tilde{\nu}$(CN) = 2143 cm^{-1} to the (*Z*)-isomer. While the vibrational frequencies of the pseudohaloborylene-metal complexes **(*Z*)-11^{Me}-M** and **12-M** are essentially identical, the N→M interaction in **12-M** proved much stronger, as neither prolonged heating at elevated temperatures under a CO atmosphere (1 atm), nor removal of the solvent *in vacuo* regenerated the cyanoborylene **12**, as observed for **(*Z*)-11^{Me}-M**. Consequently, single crystals of **12-M** could be obtained by vapor diffusion of hexane into saturated benzene solutions (M = Cr, Mo) or by slow evaporation of a saturated benzene solution (M = W), respectively. X-ray diffraction analyses performed on yellow single crystals of **12-M** verified that adduct formation occurred through the cyano nitrogen atom rather than the electron-rich boron center, and furthermore confirmed the configuration of the CAAC^{Me}–boron double bond in **(*Z*)-12-Cr**, **(*Z*)-12-Mo** and **(*E*)-12-W** (Figure 27). The bond lengths and angles in the

borylene moiety of these complexes do not differ significantly from those in **12**, with trigonal planar boron centers, short C1–B1 (ca. 1.46 Å) bonds with double bond character and a B1–C3 distance of ca. 1.58 Å, indicating that the I*i*Pr ligand acts as a pure σ donor. The N2–M bond lengths (N2–Cr1 2.0614(17), N2–Mo1 2.200(3), N2–W1 2.163(3) Å) are typical for nitrile–carbonyl complexes of the chromium triade.[108,109]

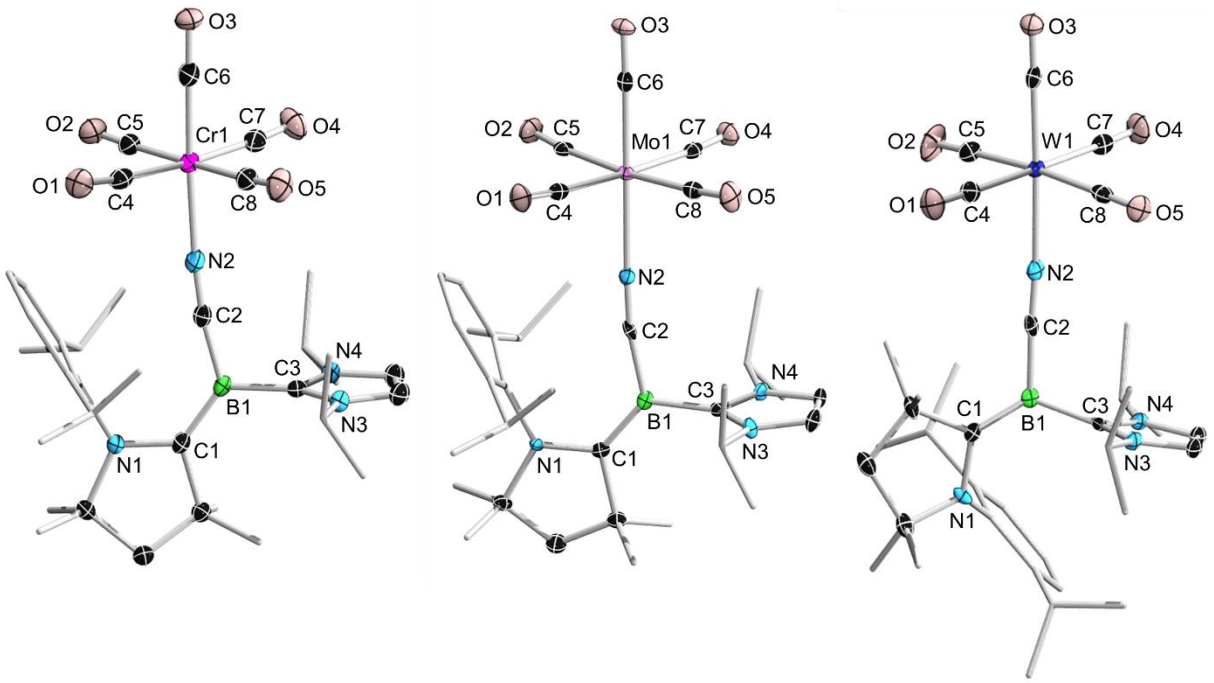

Figure 27. Crystallographically-derived molecular structures of **(*Z*)-12-Cr**, **(*Z*)-12-Mo** and **(*E*)-12-W** (from left to right). Thermal ellipsoids are shown at the 50% probability level. Ellipsoids on the ligand peripheries and hydrogen atoms omitted for clarity. Selected bond lengths (Å) for **(*Z*)-12-Cr**: N1–C1 1.399(2), C1–B1 1.456(3), B1–C2 1.542(3), C2–N2 1.158(2), B1–C3 1.588(3), N2–Cr1 2.0614(17), Cr1–C6 1.842(2), C6–O3 1.154(2). For **(*Z*)-12-Mo**: N1–C1 1.382(5), C1–B1 1.468(5), B1–C2 1.544(5), C2–N2 1.157(4), B1–C3 1.573(6), N2–Mo1 2.200(3), Mo1–C6 1.961(3), C6–O3 1.166(4). For **(*E*)-12-W**: N1–C1 1.408(5), C1–B1 1.436(6), B1–C2 1.541(6), C2–N2 1.156(5), B1–C3 1.596(5), N2–W1 2.163(3), W1–C6 1.978(4), C6–O3 1.154(5).

At first sight the preferred coordination of the [M(CO)$_5$] fragment to the isothiocyanato and cyano substituents of **(*Z*)-11^{Me}** and **12**, respectively, rather than at the borylene centers, seems mostly due to the excessive steric congestion of the latter by the CAAC^{Me} and I*i*Pr ligands. A comparison with the ^{11}B NMR shift of Kinjo's phenylborylene **XVI** (δ_{11B} = –1.1 ppm),[48] which coordinates to transition metals as a boron-centered donor,[48,78] indeed suggests that the borylene center in **(*Z*)-11^{Me}** (δ_{11B} = –2.6 ppm) should be similarly nucleophilic to **XVI**, while that of **12** (δ_{11B} = –12.1 ppm) should be even more nucleophilic. However, the calculated Hirshfeld charges of the terminal cyano nitrogen (–0.282) and isothiocyanato sulfur atoms (–0.210) in **12** and **(*Z*)-11^{Me}**, respectively, are significantly more negative than those of the boron atoms (**12**: –0.064; **(*Z*)-11^{Me}**: –0.012), which further favors coordination at the respective pseudohalide substituent (see legend of Figure 24).

2.2.6 Boron-Centered Brønsted Basicity of Isothiocyanato- and Cyanoborylenes

While the activation of H_2 by dicoordinate neutral and cationic borylenes is known,[63,68] and insertions of transient dicoordinate borylenes into intramolecular C–H and C–C σ bonds have been observed,[38,70,71,73] examples of σ bond activation by tricoordinate borylenes remain limited to the protonation of the boron center by strong Brønsted acids. Accordingly, tricoordinate borylenes, such as Bertrand's bis(CAAC^{Cy})-stabilized parent borylene **VII** or Kinjo's phenylborylene **XVI** can be protonated by HOTf ($pK_a^{(DMSO)}$ = –14.3),[110] yielding the corresponding boronium cations **XLVI** and **[XVI-Me$^+$][OTf$^-$]** (see Scheme 19 and Scheme 20).[46,48] Following this, the ability of the pseudohaloborylenes **(*Z*)-11^{Me}** and **12** to react as Brønsted bases was investigated. For this purpose, the much weaker acid thiophenol ($pK_a^{(DMSO)}$ = 10.3)[111] was used instead of HOTf in the hope of determining the pK_a of these borylenes. The reaction mixture of **(*Z*)-11^{Me}** with 1.2 equivalents of thiophenol in C_6D_6 at room temperature rapidly turned from intense orange to colorless and resulted in a 2:3 mixture of the hydroboronium species **13^{NCS}** (δ_{11B} = –18.9 ppm) and the thiolatoborane **14^{NCS}** (δ_{11B} = –6.0 ppm) (Scheme 41a).

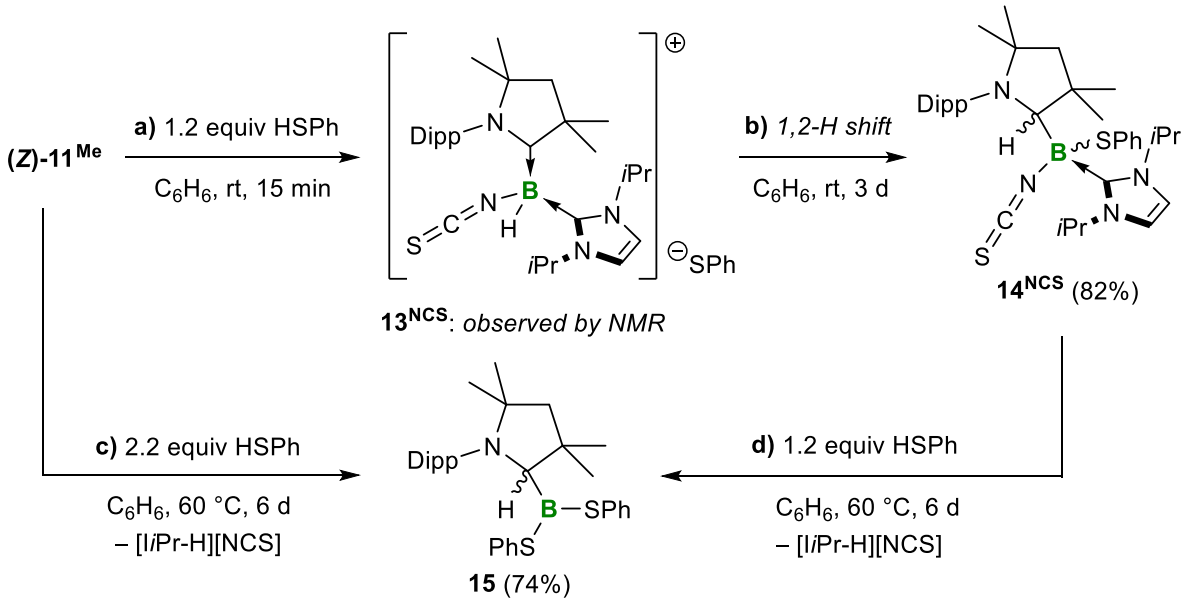

Scheme 41. Reversible protonation of **(*Z*)-11^{Me}** with thiophenol. Isolated yields in parentheses.

The $^1H\{^{11}B\}$ NMR spectrum of the product mixture showed a broad B*H* resonance at 3.76 ppm for **13^{NCS}** and a singlet at 3.70 ppm in the ^1H NMR spectrum for **14^{NCS}**, characteristic of a protonated carbene carbon atom of the CAAC^{Me} ligand.[74] Over the course of three days at room temperature in solution **13^{NCS}** converted entirely to **14^{NCS}**, allowing the isolation of the latter (Scheme 41b). After workup, the thiolatoborane **14^{NCS}** was obtained as an 85:15 mixture of diastereomers in 82% yield. Colorless single crystals of the (*R*,*R*)/(*S*,*S*) diastereomer of **14^{NCS}**

suitable for X-ray diffraction analysis were obtained by vapor diffusion of hexane into a saturated benzene solution (Figure 28).

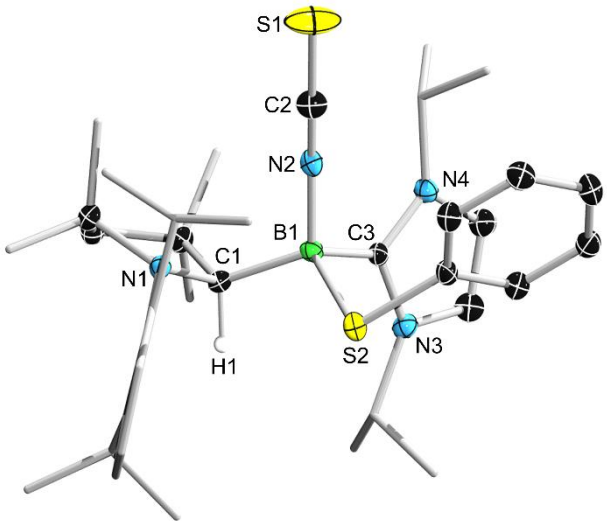

Figure 28. Crystallographically-derived molecular structure of **14**^{NCS}. Thermal ellipsoids are shown at the 50% probability level. Ellipsoids on the ligand peripheries and hydrogen atoms omitted for clarity, except for the proton bound to C1. Selected bond lengths (Å) and angles (°): N1–C1 1.507(3), C1–B1 1.643(4), B1–C3 1.661(4), B1–N2 1.515(3), N2–C2 1.156(3), C2–S1 1.603(3), B1–S2 1.968(3), B1–N2–C2 167.3(2), N2–C2–S1 178.0(2), Σ(∠C1) 335.6(2).

The solid-state structure authenticated **14**^{NCS} as the product of the formal 1,2-addition of the H–S bond to the C_{CAAC}–B double bond. The protonation of the former carbene carbon results in its pyramidalization (Σ(∠C1) 335.6(2)°), thus the CAAC^{Me}H moiety represents an anionic substituent (C1–B1 1.643(4) Å). Both the B1–N2 (1.515(3) Å) and the B1–S2 (1.968(3) Å) distances are in the range typical for the respective boron–element single bonds. Consequently, neither the isothiocyanato nor the thiophenolate substituent indicate any stabilizing π donation to the p orbital at the boron center, which is electronically saturated by the σ-donating I*i*Pr ligand (B1–C3 1.661(4) Å).

The conversion of **13**^{NCS} to **14**^{NCS} proceeds *via* a hydride shift from boron to the adjacent carbene carbon of the CAAC^{Me} ligand, typical for CAAC-stabilized hydroboranes and hydroboronium species, as already discussed above.[74] The hydride migration is followed by nucleophilic attack of the thiophenolate anion PhS^- at the tricoordinate cationic boron center. This clean conversion can be monitored *in situ* by ^{11}B NMR-spectroscopy of the reaction mixture (Figure 29).

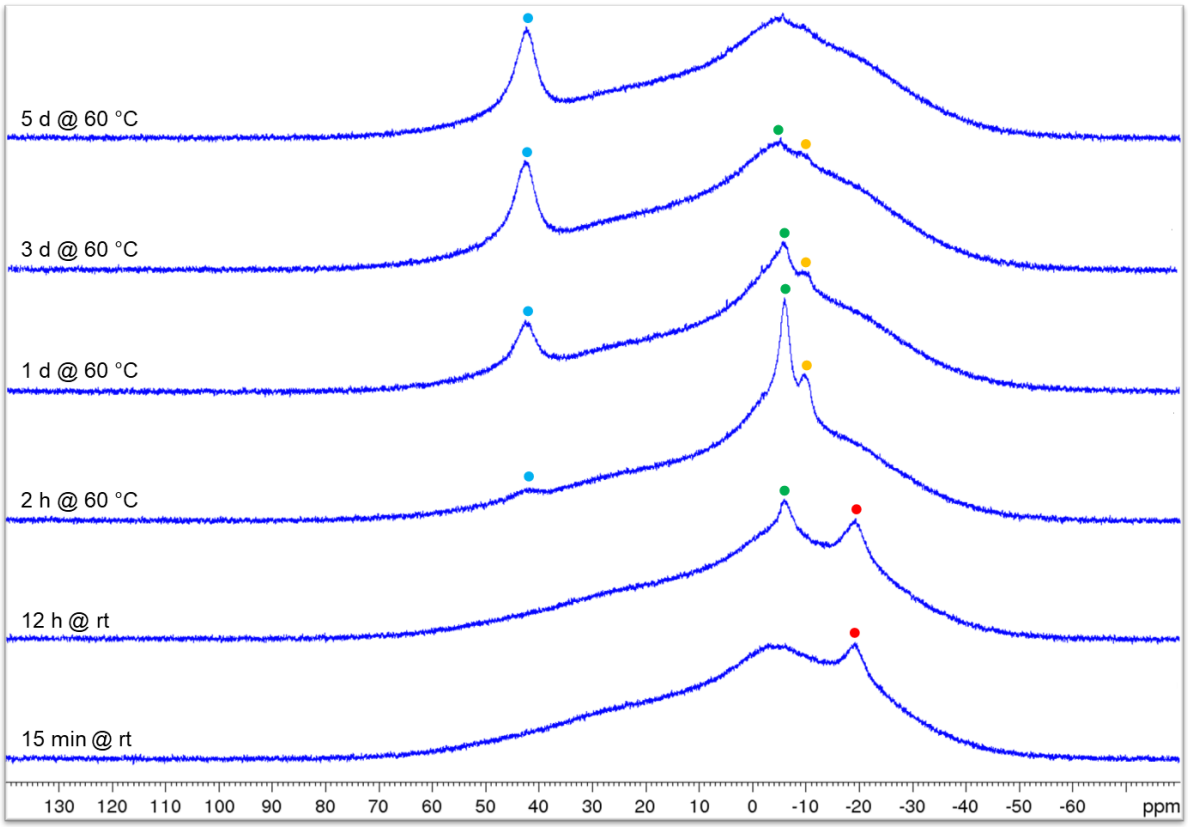

Figure 29. Stack-plot of ^{11}B NMR spectra of the conversion of **(*Z*)-11^{Me}** to **15** (•) *via* **13^{NCS}** (•) and **14^{NCS}** (major diastereomer •, minor diastereomer •) in C_6D_6.

Treatment of **(*Z*)-11^{Me}** with an excess of thiophenol at room temperature resulted in the quantitative generation of **13^{NCS}** (•), which slowly converts to **14^{NCS}** (•) over a course of twelve hours. The conversion of **13^{NCS}** to **14^{NCS}** can be accelerated by heating the mixture to 60 °C, yielding both diastereomers of **14^{NCS}** (• and •), as well as a new species, compound **15** (•), with an ^{11}B NMR resonance at 42.6 ppm. Prolonged heating of the reaction mixture at 60 °C afforded full conversion of **14^{NCS}** to **15** (Scheme 41c). Alternatively, the reaction of isolated **14^{NCS}** with 1.2 equivalents of thiophenol at 60 °C also yielded the tricoordinate dithiolatoborane **15**, in which both the isothiocyanate substituent and the I*i*Pr ligand are formally replaced by two thiophenolate moieties (Scheme 41d). In addition, the imidazolium salt [I*i*Pr-H][NCS] is formed as a byproduct, as determined by ^{1}H NMR spectroscopy. After workup, the dithiolatoborane **15** was isolated as a colorless solid in 74% yield. The ^{1}H NMR spectrum of **15** showed a singlet at 2.91 ppm, characteristic for the proton of the CAAC^{Me}H substituent. The resonances of the latter are further split into two magnetically inequivalent sets, as usually observed for species containing protonated CAAC ligands.[74]

In contrast, the analogous reaction of the cyanoborylene **12** with 1.2 equivalents of thiophenol led to partial fading of the yellow color of the solution. After 15 minutes at room temperature the ^{1}H and ^{11}B NMR spectra showed ca. 85% conversion of **12** to the corresponding

hydroboronium salt **13**^{CN}, while no further conversion of **13**^{CN} to the **14**^{CN} analogue of **14**^{NCS} was observed (Scheme 42a).

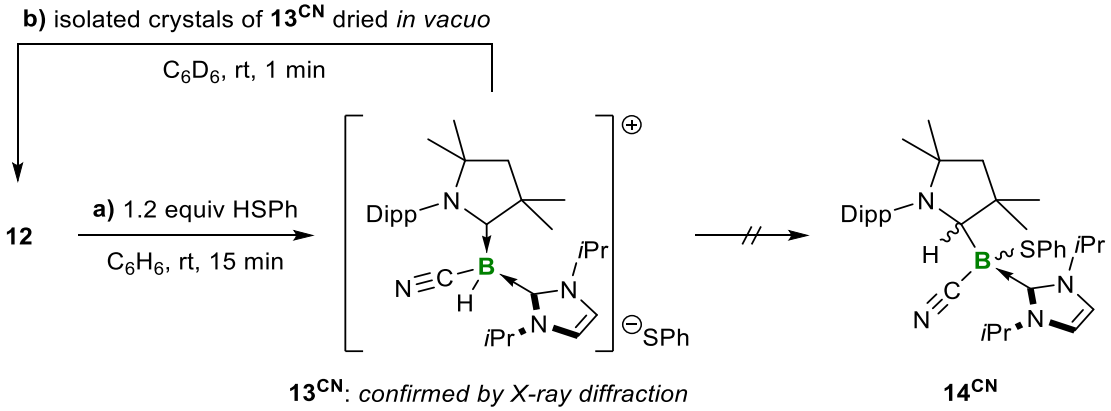

Scheme 42. Reversible protonation of **(*Z*)-11**^{Me} with thiophenol.

Since the ratio of the mixture did not change over the course of one day at room temperature, various attempts to isolate **13**^{CN} were made. Prolonged heating of the reaction mixture at 80 °C did not lead to full conversion of **12** to **13**^{CN}, but afforded a 65:35 ratio of **12** and **13**^{CN}, suggesting an equilibrium between the cyanoborylene and its protonated congener. Upon cooling, a few colorless single crystals of **13**^{CN} suitable for X-ray diffraction analysis were obtained (Figure 30).

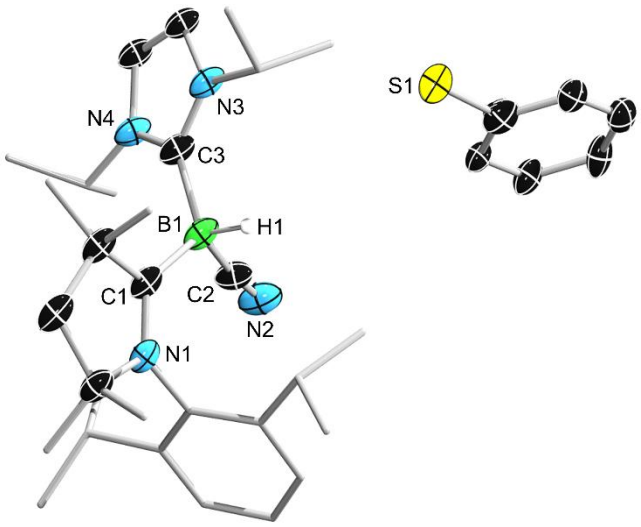

Figure 30. Crystallographically-derived molecular structure of **13**^{CN}. Thermal ellipsoids are shown at the 50% probability level. Ellipsoids on the ligand peripheries and hydrogen atoms omitted for clarity, except for the boron-bound hydride. Selected bond lengths (Å) and angles (°): N1–C1 1.2990(19), C1–B1 1.622(2), B1–C2 1.591(2), C2–N2 1.148(2), B1–C3 1.627(2), B1–C2–N2 173.11(16).

In contrast to **14**^{NCS}, in which the hydride migrated from boron to carbon, the hydride in **13**^{CN} is still bound to the cationic boron center. The (cyano)hydroboronium cation is stabilized by the carbene ligands, both acting as pure σ donors (C1–B1 1.622(2) Å, B1–C3 1.627(2) Å), as previously observed for several similar dihydroboronium species (*vide supra*).

When the solvent of the reaction mixture was removed *in vacuo* and the resulting yellow solid dried *in vacuo* at 60 °C for four hours, **12** was recovered in essentially quantitative yield, further confirming the reversibility of its protonation (Scheme 42b). In a further attempt, the initial reaction mixture was left undisturbed overnight, yielding colorless crystals of **13^{CN}**, the supernatant of which was decanted. The isolated crystals of **13^{CN}** were washed with hexane, left to dry in the glovebox at atmospheric pressure for one hour and redissolved in C_6D_6, which yielded a solution of **12** with only a small amount of thiophenol, the rest having evaporated. These additional observations all confirm the reversibility of the protonation of the cyanoborylene **12** even in the solid state. To monitor the equilibrium between the cyanoborylene **12** and the boronium species **13^{CN}**, variable temperature ^{1}H and ^{11}B NMR experiments were performed. A d_8-toluene solution of **12** was treated with an excess of thiophenol, whereupon the yellow color vanished and **13^{CN}** precipitated as a colorless solid. Heating of this suspension showed that the concentration of **12** and thiophenol in solution increased steadily from 25 to 100 °C. However, the lack of solubility of the boronium salt **13^{CN}** in suitable NMR solvents prevented a quantitative analysis of the acid-base equilibrium. Given these difficulties in assessing the relative Brønsted basicity of **(*Z*)-11^{Me}** and **12** experimentally, gas-phase proton affinity (PA) calculations were performed by Dr. Felipe Fantuzzi. The computed gas-phase PA for the thiophenolate anion (339.4 kcal mol^{-1}) agrees well with the experimental value of 349.0±2 kcal mol^{-1}.[112] The PAs calculated for **(*Z*)-11^{Me}** (268.3 kcal mol^{-1}) and **12** (267.9 kcal mol^{-1}), respectively, are identical within the error of the calculation. At first sight, these results seem in contradiction with the experimental observations of irreversible protonation for **(*Z*)-11^{Me}** and reversible protonation for **12**. However, the former is only rendered irreversible by the subsequent boron-to-CAAC hydrogen shuttling and nucleophilic attack of the thiophenolate anion at boron. The higher proton affinity of the thiophenolate anion confirms its stronger basicity compared to that of **(*Z*)-11^{Me}** and **12**, as indicated by the reversibility of the protonation of **12** by thiophenol. Additionally, the calculated gas-phase proton affinities of **(*Z*)-11^{Me}** and **12** are comparable to those of the superbases CsOH (267 kcal mol^{-1})[113] and the unsaturated NHCs 1,3-dialkyl/diarylimidazol-2-ylidenes (262–275 kcal mol^{-1}).[114]

2.3 Synthesis and Reactivity of Boron-doped Thiazolothiazoles[3]

The reduction of base-stabilized dihaloboranes often results in inter- and intramolecular insertion reactions of the transiently generated dicoordinate borylenes into C–H or C–C bonds.[70,72,73,115] Alternatively, the latter can be trapped by suitable Lewis bases and consequently isolated as tricoordinate borylenes.[28,53,64] A special case is certainly the reduction of the CAAC^{Me}-stabilized dibromo(cyano)borane **XXV**, the corresponding transient dicoordinate cyanoborylene of which stabilizes itself in the absence of a second donor ligand by forming the tetrameric cyanoborylene **XXVII**.[62] As described previously, the trapping of the transient isothiocyanatoborylene by the NHC I*i*Pr, yielding (CAAC^{R})(I*i*Pr)B(NCS) (**11^{R}**), already demonstrated the viability of tricoordinate isothiocyanatoborylenes. Accordingly, the focus of the work reported in the following chapter was to investigate whether the reduction of the related CAAC^{R}-stabilized isothiocyanatoboranes **10^{R}** in the absence of an additional Lewis base would yield similar oligomeric, self-stabilizing [(CAAC^{R})B(NCS)]$_n$ species.

2.3.1 Synthesis of Boron-doped Thiazolothiazoles

Analogously to the reduction of the CAAC^{Me}-stabilized dibromo(cyano)borane **XXV** to the self-stabilizing cyanoborylene **XXVII**, the isothiocyanatoboranes (CAAC^{R})BBr$_2$(NCS) (**10^{R}**) were reduced with 2.2 equivalents of KC_8 in the absence of a second Lewis base (Scheme 43).

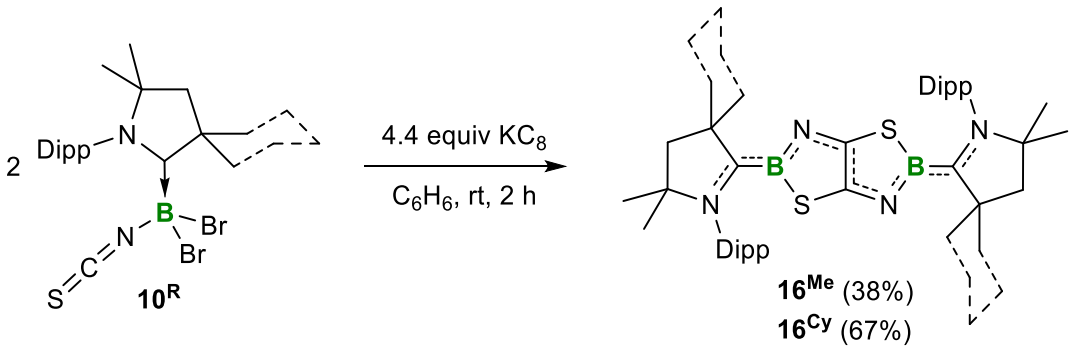

Scheme 43. Reductive cyclization of **10^{R}** in the absence of a Lewis base, yielding the B,N,S-heteroaromatics **16^{R}**. Isolated yields in parentheses.

Immediately after the addition of benzene to the solid reactants, the resulting suspensions turned deep blue and were stirred for two hours at room temperature. After workup, dark blue crystals of the bis(CAAC^{R})-stabilized thiazaborolo[5,4-*d*]thiazaboroles (TzbTzb) **16^{Me}** and **16^{Cy}** were isolated in 38% and 67% yield, respectively. The low crystalline yield of **16^{Me}** is due to its much

[3] The results presented herein were partly published in "S. Hagspiel, M. Arrowsmith, F. Fantuzzi, A. Vargas, A. Rempel, A. Hermann, T. Brückner, H. Braunschweig, Highly Colored Boron-Doped Thiazolothiazoles from the Reductive Dimerization of Boron Isothiocyanates, *Angew. Chem. Int. Ed.* **2021**, *60*, 6446–6450; *Angew. Chem.* **2021**, *133*, 6519–6524."

higher solubility compared to the cyclohexyl derivative, which partly crystallizes out of the reaction mixture already. Both B,N,S-heterocycles **16^{R}** show a broad ^{11}B NMR signal around 32 ppm, as well as one symmetrical set of CAAC^{R} ligand resonances in the ^{1}H NMR spectrum. X-ray diffraction analyses of **16^{R}** revealed fully planar, centrosymmetric structures with a central TzbTzb unit, formally resulting from the dimerization of two dicoordinate (CAAC^{R})B(NCS) borylenes through S→B adduct formation and C–C coupling at the C2 position. In cooperation with Dr. Felipe Fantuzzi, plausible mechanistic pathways for the reductive cyclization of **10^{Me}** were investigated using DFT calculations (Figure 31).

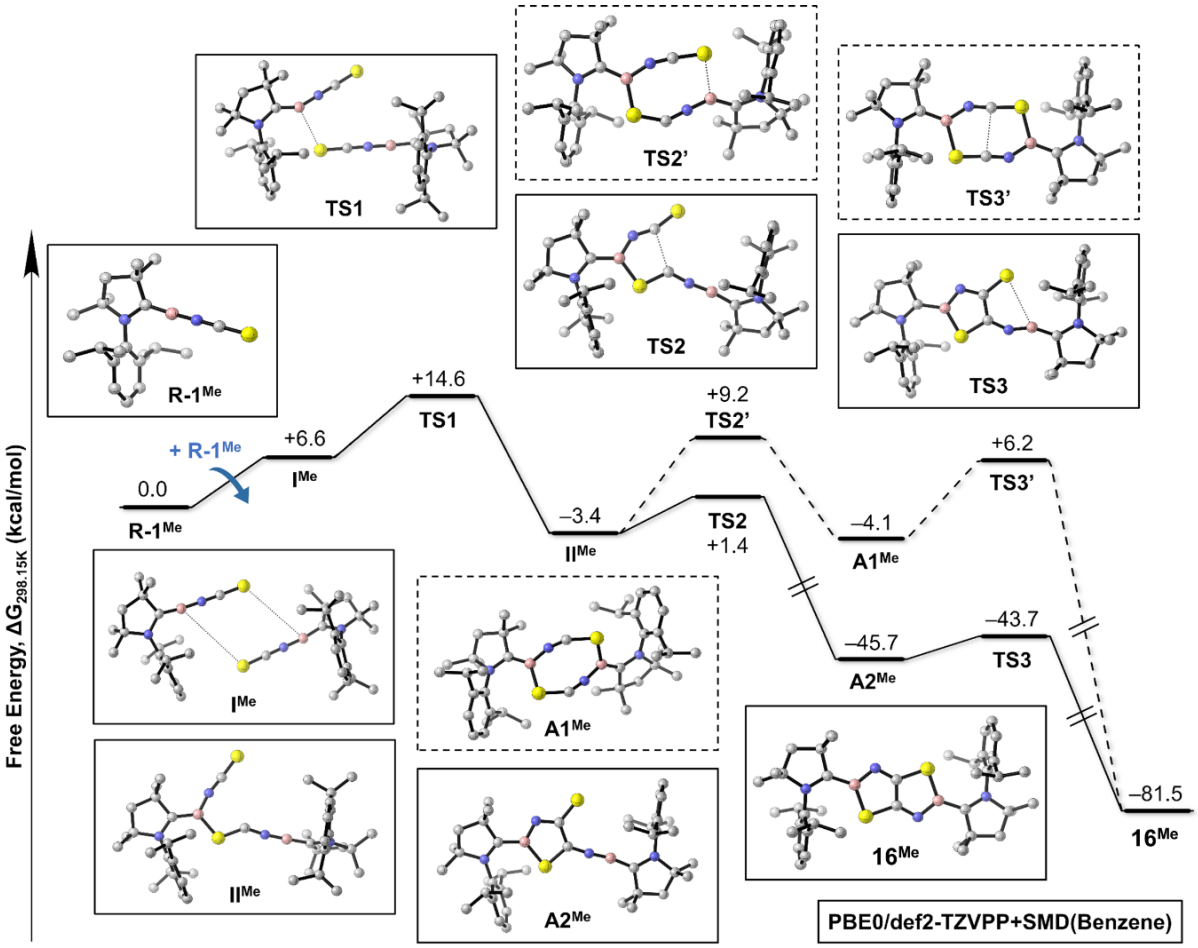

Figure 31. Free energy landscape of path 1 (dashed lines) and path 2 (solid lines) for the formation of **16^{Me}** at the PBE0/def2-TZVPP level of theory.

Starting with the dicoordinate isothiocyanatoborylene **R-1^{Me}**, the first step is the approach of two **R-1^{Me}** borylene units forming **I^{Me}**. Subsequently, an S→B adduct formation to compound **II^{Me}** takes place *via* **TS1** with an energy barrier of 14.6 kcal mol^{-1}. From there, two competitive reaction pathways are possible. In path 1 (dashed lines), a second S→B adduct formation *via* **TS2'** with a barrier of 9.2 kcal mol^{-1} leads to the eight-membered ring **A1^{Me}**. A C–C coupling step from **A1^{Me}** then leads to the B,N,S-heterocycle **16^{Me}**, the formation of which is exergonic by a total of –81.5 kcal mol^{-1} and with a barrier (**TS3'**) of 10.3 kcal mol^{-1} from **A1^{Me}**.

Alternatively, the second viable pathway (path 2, solid lines) proceeds *via* an early C–C coupling (**TS2** 1.4 kcal mol^{-1}), leading to the stable intermediate **A2^{Me}**. The second S→B adduct formation is followed by the generation of **16^{Me}** *via* **TS3**. The corresponding energy barriers of **TS2** and **TS3** are lower than those of path 1, thus implying that both mechanistic pathways are viable, with a preference for path 2. These results indicate that C–C coupling can also occur immediately after the first S→B adduct formation. Conversely, direct C–C coupling from two isolated dicoordinate borylenes (**R-1^{Me}**) *via* path 3 (Figure 32), leading to intermediate **III^{Me}**, is inaccessible, as the corresponding transition state **TS4** has a barrier of 31.9 kcal mol^{-1}. Additionally, the formation of the B,N,S-heterocycle **16^{Me}** through a concerted transition state also seems unlikely, as all attempts to optimize such a transition state directly converged to **TS1**.

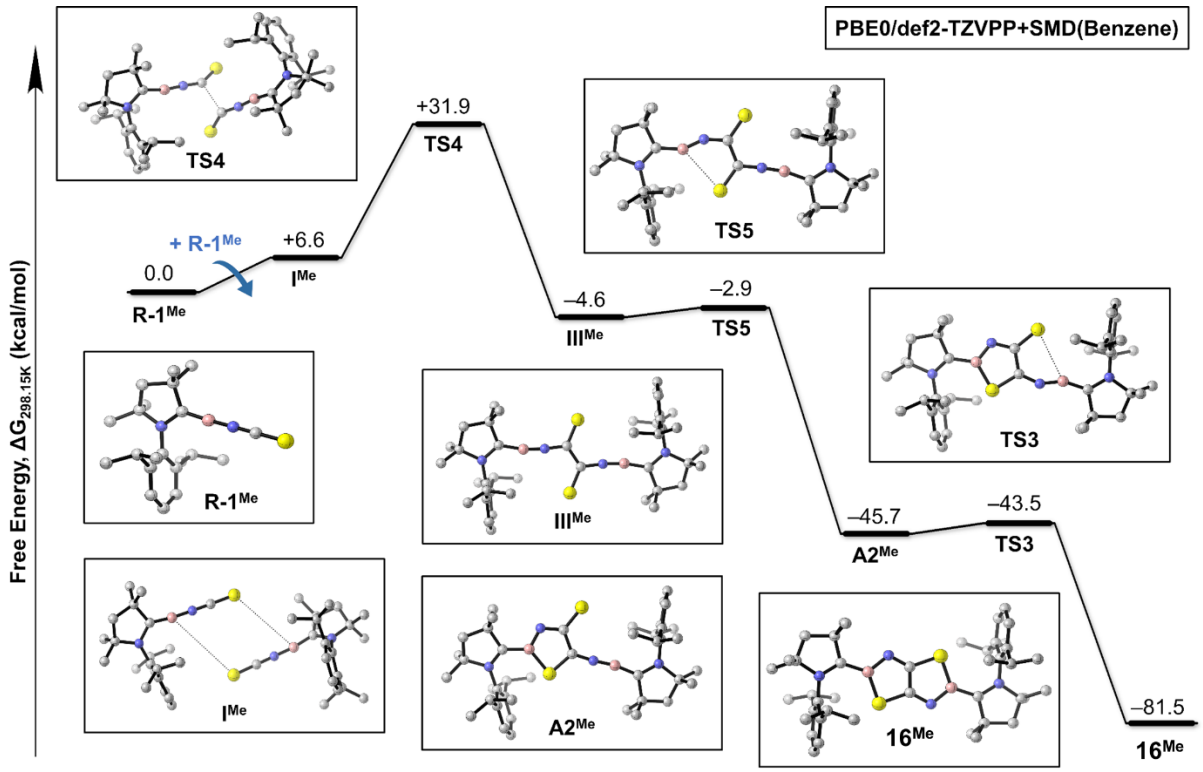

Figure 32. Free energy landscape of path 3 for the formation of **16^{Me}** at the PBE0/def2-TZVPP level of theory.

X-ray crystallographic analyses performed on single crystals of **16^{R}** showed that the solid state structures of the B,N,S-heterocycles are comparable to their carbon analogues, thiazolo[5,4-*d*]thiazoles (TzTz) (Figure 33, see Figure 62 in the Appendix for molecular structure of **16^{Cy}**).[116] The incorporation of the boron atoms in the TzbTzb unit results in shortening of the C–N bonds and lengthening of the endocyclic C–C bond by less than 3%, while the C–S bonds remain unaffected.[116] A pronounced degree of π electron delocalization over the entire $(NCBNC)_2$ framework is indicated by the average N1–C1 (1.33 Å), C1–B1

(1.54 Å), B1–N2 (1.42 Å), N2–C2 (1.33 Å), and C2–C2' (1.42 Å) bond lengths, that are all within the range of partial double bonds. In contrast, the B1–S1' distance of ca. 1.86 Å is relatively long for a boron–sulfur single bond, as a comparison with $B(SPh)_3$ (B–S 1.81 Å) shows,[117] implying that the sulfur atoms essentially do not participate in the delocalized π system of **16^{R}**.

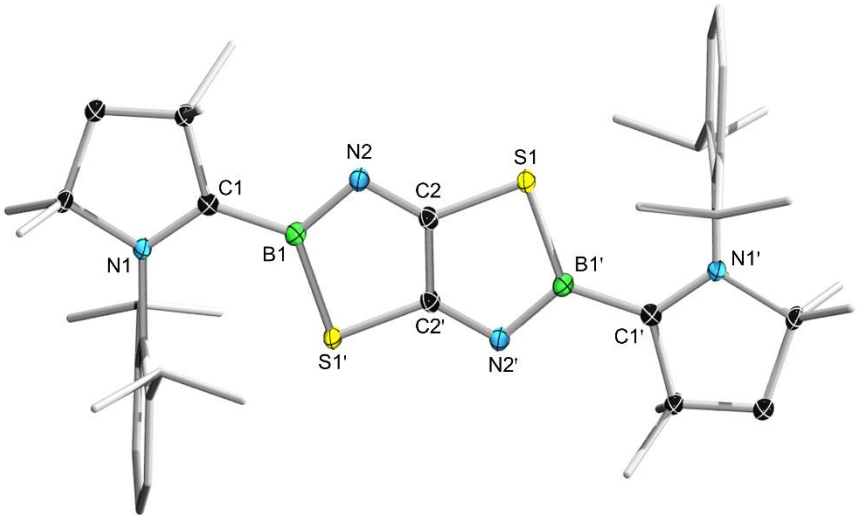

Figure 33. Crystallographically-derived molecular structure of **16^{Me}**. Thermal ellipsoids drawn at 50% probability level. Ellipsoids on the ligand peripheries and hydrogen atoms have been omitted for clarity. Selected bond lengths (Å) and angles (°): N1–C1 1.3281(15), C1–B1 1.5442(17), B1–N2 1.4187(16), N2–C2 1.3328(15), C2–C2' 1.421(2), C2–S1 1.7515 (12), B1–S1' 1.8691(14), C1–B1–N2 127.1(1), B1–N2–C2 109.4(1), B1–S1'–C2' 88.55(6), S1–B1–N2 111.8(1), S1–C2–C2' 109.6(1), N2–C2–S1 129.7(1).

To further investigate the role of π delocalization, the electronic structures of **16^{Me}** and other related sulfur-containing heterocycles were analyzed computationally by Dr. Felipe Fantuzzi. Particularly, the TzTz analogue of **16^{Me}**, 2,5-bis(2,2,4,4-tetramethyl-3,4-dihydro-2*H*-pyrrol-5-yl)thiazolo-[5,4-*d*]thiazole **LI**, and its dicationic *N*-arylated derivative **[LII]$^{2+}$** were investigated theoretically, the latter being isoelectronic to **16^{Me}**. In contrast to **LI**, the HOMO of **16^{Me}** is π-delocalized over the entire $(NCBNC)_2$ scaffold with the exclusion of the sulfur atoms (Figure 34). The LUMO of **16^{Me}**, in turn, is mainly localized in the CAAC–boron bond region, while that of **LI** exhibits slightly larger contributions of the endocyclic N–C bond and the sulfur atoms, respectively.

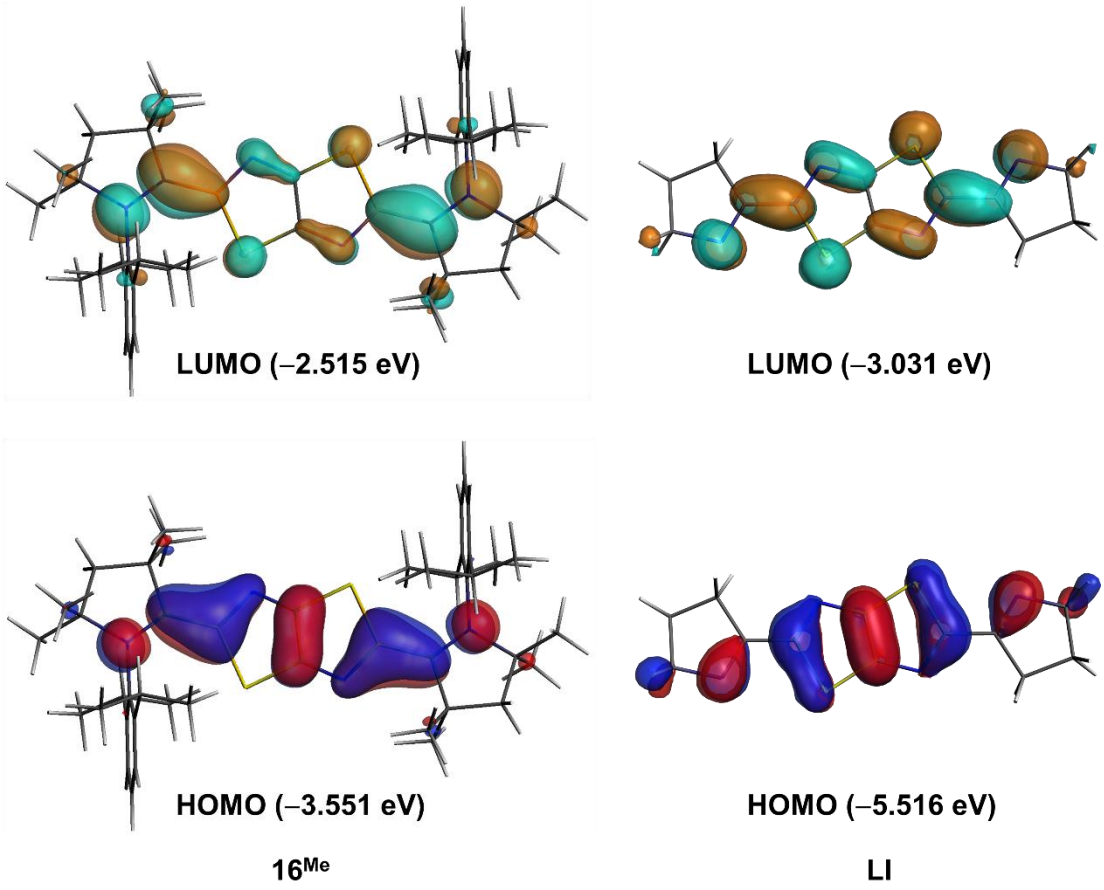

Figure 34. Plots of HOMO and LUMO of **16^{Me}** (left) and **LI** (right) at the OLYP/TZP level of theory.

Moreover, the analysis of the fully delocalized π orbital of **16^{Me}** and **[LII]$^{2+}$** shows that the delocalization is affected by the presence of the boron atoms due to the decrease in energy match between the participating 2p orbitals,[118] and becomes less prominent in **16^{Me}** (Figure 35). The thiazole rings of the carbon analogue consequently possess a higher degree of aromaticity compared to the CAAC^{R}-stabilized BNC_2S cycles in **16^{R}**.[119]

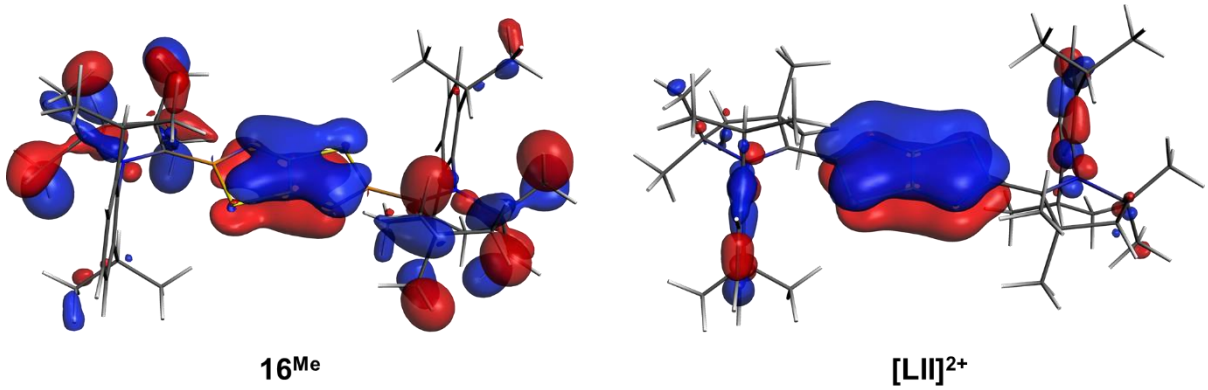

Figure 35. Low-energy fully delocalized π orbital of **16^{Me}** and **[LII]$^{2+}$**.

In order to describe the aromaticity of **16^{Me}** in more detail, calculations using the anisotropy of the induced current density (ACID) method were performed,[120,121] revealing the presence of a diatropic, clockwise π electron circulation along the bicyclic central unit of **16^{Me}**, typical of aromatic compounds (Figure 36).

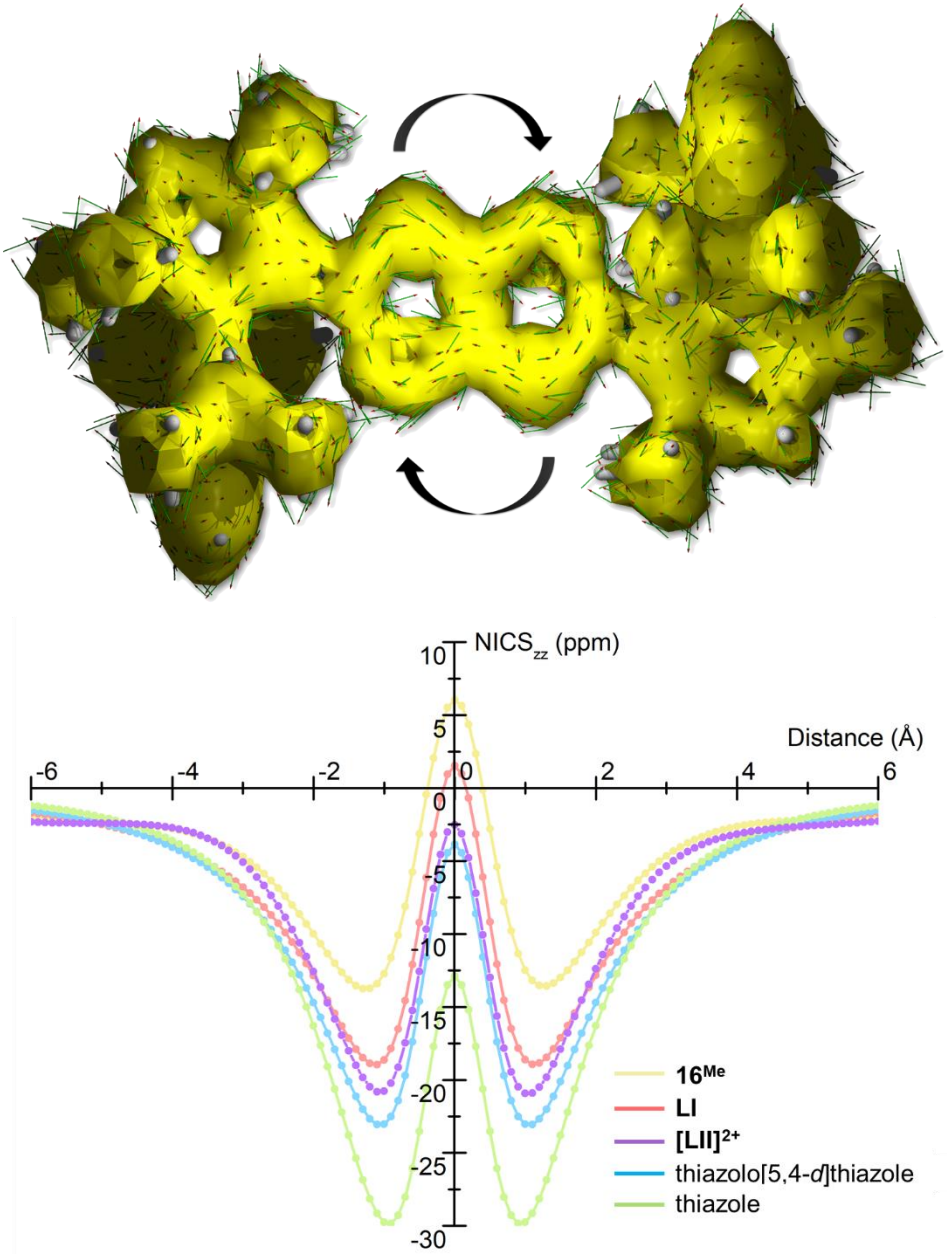

Figure 36. ACID plot of **16^{Me}** (isosurface: 0.025) (top) and NICS$_{zz}$-scans of **16^{Me}**, **LI**, **[LII]$^{2+}$** and other S,N-heterocycles for comparison (bottom).

The attribution of a weak but distinct aromatic character for **16^{Me}** is also supported by the computed nucleus-independent chemical shifts (NICS).[122,123] The values of NICS(0) (–6.3), NICS(1) (–7.0) and the zz tensor component at 1 Å above the ring, NICS$_{zz}$(1) (–12.6), respectively, are less negative for the B,N,S-heteroarene **16^{Me}** than those of comparable heteroaromatics (Table 2).

Table 2. NICS(0), NICS(1), $NICS_{zz}(0)$ and $NICS_{zz}(1)$ values for **16^{Me}**, **LI**, **[LII]$^{2+}$**, thiazolo[5,4-*d*]thiazole and thiazole at the B3LYP/6-311++G** level of theory from structures optimized at the OLYP/TZP level.

	NICS(0) (ppm)	NICS(1) (ppm)	$NICS_{zz}(0)$ (ppm)	$NICS_{zz}(1)$ (ppm)
16^{Me}	–6.3	–7.0	6.0	–12.5
LI	–9.6	–8.6	1.5	–18.6
[LII]$^{2+}$	–11.3	–10.1	–2.5	–20.9
thiazolo[5,4-*d*] thiazole	–10.9	–9.5	–3.9	–23.0
thiazole	–13.1	–11.3	–12.9	–29.8

In addition to the aromaticity, the intense color of the B,N,S-heterocycles **16^{R}** was also compared with the negligible coloration of their carbon analogues. While the latter, in particular ArTzTzAr (Ar = phenyl, thienyl, thiazenyl, pyridyl), are generally colorless to yellow,[124-126] **16^{Me}** and **16^{Cy}** absorb around 675 nm, accounting for their intense blue color (**16^{Me}**: ε = 66200 M^{-1} cm^{-1}; **16^{Me}**: ε = 83300 M^{-1} cm^{-1}), with secondary absorption maxima around 628 and 453 nm (Figure 37, top).

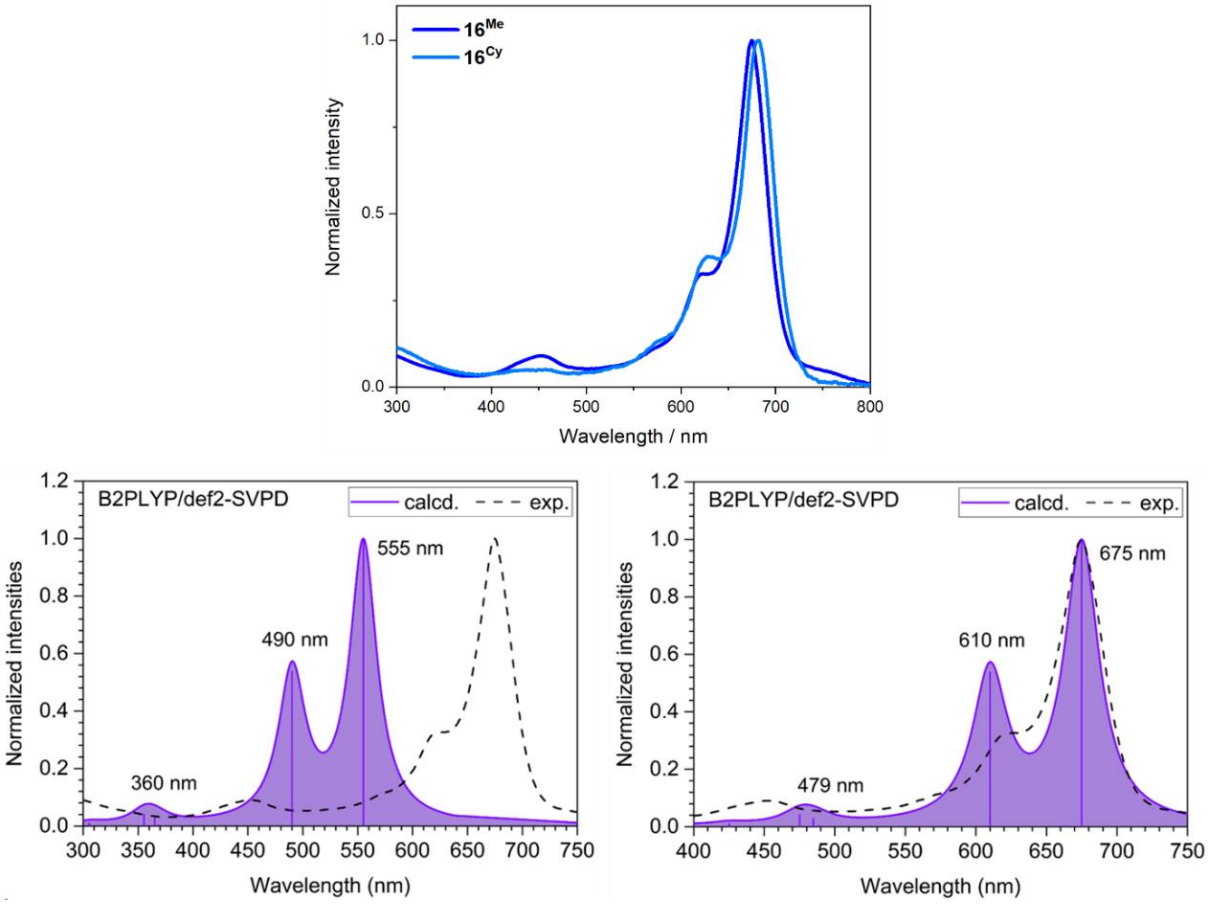

Figure 37. Top: Overlay of UV-vis absorption spectra of **16^{Me}** (dark blue) and **16^{Cy}** (light blue) in DCM at 25 °C. **16^{Me}**: λ = 453 nm, λ = 630 nm, λ_{max} = 680 nm; **16^{Cy}**: λ = 455 nm, λ = 632 nm, λ_{max} = 680 nm. Bottom: Comparison between the TDDFT spectra at the B2PLYP/def2-SVPD level of theory without (left) and with linear correction (120 nm) (right). Dashed curves represent the experimental UV-vis spectrum.

TDDFT calculations using the double-hybrid functional B2PLYP with the def2-SVPD basis set show that the absorptions around 675 and 628 nm are the π→π* transitions HOMO→LUMO (93%) and HOMO–1→LUMO (93%), respectively (Figure 37, bottom). The spectrum on the left displays the absorption bands qualitatively correct, but the wavelengths are shifted as often observed in TDDFT calculations. The figure on the right shows the absorption spectrum corrected by a linear shift of 120 nm, which agrees well with the experimentally obtained data. Two states contribute to the band around 453 nm, one of which (S_7) results from the charge transfer excitation from HOMO–1 to LUMO+4 (88%), while the second (S_9) is related to a n→π* transition consisting of HOMO–7→LUMO (44%) and HOMO–2→LUMO+1 (41%) excitations (see Table 3 for selected transitions). Furthermore, the replacement of the two endocyclic carbon atoms in **LI** with electron-deficient boron atoms leads to a significant reduction of the HOMO–LUMO gap of **16^{Me}** (**LI**: –2.485 eV; **16^{Me}**: –1.036 eV), explaining the pronounced red-shift of its lowest-energy absorption band.

Table 3. TDDFT results for **16^{Me}** at the B2PLYP/def2-SVPD level of theory.

State	Wavelength (nm)		f_{osc}	Excitation
	without correction	corrected (120 nm)		
S_1	555.2	675.0	0.2622	HOMO→LUMO (93%)
S_2	490.2	610.0	0.1411	HOMO–1→LUMO (93%)
S_3	542.7	662.5	0.0008	HOMO–2→LUMO (93%)
S_4	443.9	563.7	0.0000	HOMO→LUMO+1 (93%)
S_5	368.9	488.7	0.0010	HOMO→LUMO+2 (92%)
S_6	372.7	492.5	0.0000	HOMO→LUMO+3 (95%)
S_7	355.3	475.1	0.0110	HOMO→LUMO+4 (88%)
S_8	354.8	474.6	0.0000	HOMO→LUMO+5 (91%)
S_9	365.1	484.9	0.0073	HOMO–7→LUMO (44%) HOMO–2→LUMO+1 (41%)

As the HOMO of **16^{Me}** is π-delocalized across the entire $(NCBNC)_2$ scaffold with the exclusion of the sulfur atoms, the focus was on finding out whether the reactive sites of the B,N,S-heterocycle are predominantly located at the CAAC-stabilized B=N units or the endocyclic partial C=C double bond. Due to the above-mentioned low isolated yield of **16^{Me}**, reactivity studies on the B,N,S-heteroaromatics were exclusively carried out with the cyclohexyl derivative **16^{Cy}** and will be discussed in the following section.

2.3.2 Coordination and Protonation of the B,N,S-heteroaromatics

The highly electron-deficient thiazolo[5,4-*d*]thiazole (TzTz) building block has generated increasing interest in materials chemistry for its tunable optoelectronic properties.[127-129] Due to their light-harvesting properties, TzTz-based materials find various applications in solar cells,[130-132] as photocatalysts[133,134] and as chemosensors.[135-138] The mode of detection in these sensing applications are varied, ranging from fluorescence quenching through coordination,[135] non-coordinative electron transfer[138] or radical cation formation,[139] to fluorescence enhancement.[137] Furthermore, the Lewis-basic nature of the thiazole nitrogen atom can also be utilized, as its protonation significantly shifts both the absorption and emission wavelengths of TzTz-based compounds.[140,141] Inspired by these interesting optoelectronic properties and potential applications of TzTz-containing materials, the aim of the following section was to investigate whether the boron-doped TzTz analogue, the thiazaborolo[5,4-*d*]thiazaborole **16^{Cy}**, shows similar properties and reactivity.

Initially, the coordination ability of **16^{Cy}** was investigated, as computational analyses revealed that the HOMO is delocalized across the entire $(NCBNC)_2$ scaffold (*vide supra*). Previous studies have shown that copper(I) species both yield complexes with various boron compounds,[142] N-heterocycles,[143] as well as carbon–carbon multiple bonds.[144,145] Consequently, tetrameric $[Cu(C_6F_5)]_4$ was chosen as substrate to explore the coordination ability of **16^{Cy}**. Treatment of **16^{Cy}** with 0.55 equivalents of $[Cu(C_6F_5)]_4$ resulted in an immediate color change from blue to purple (Scheme 44).

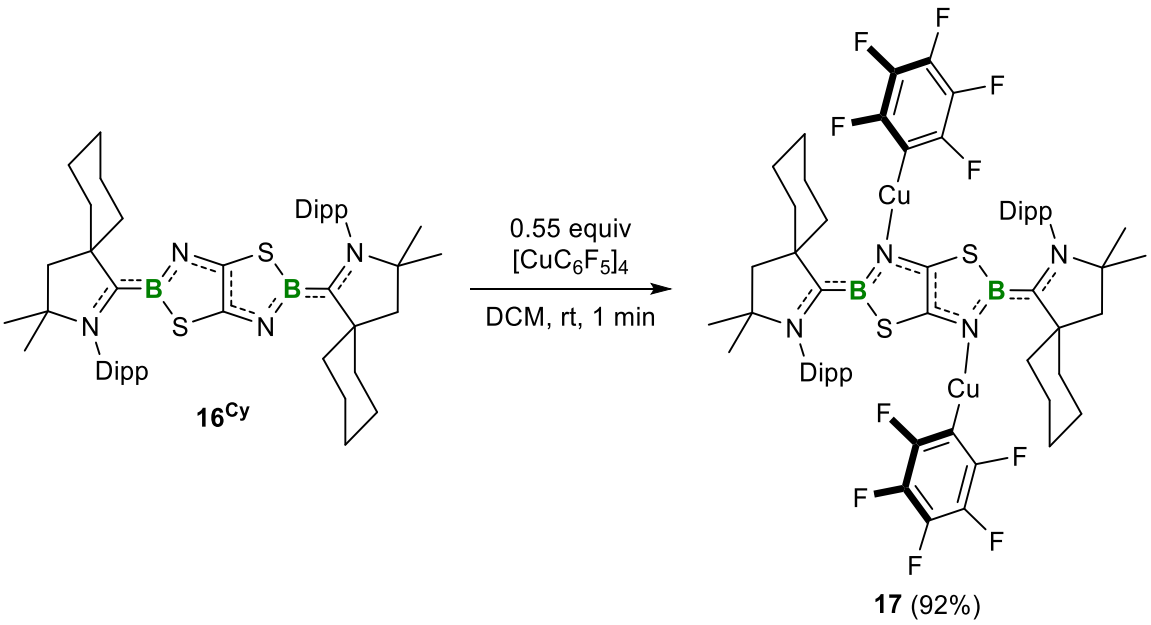

Scheme 44. Coordination of $Cu(C_6F_5)$ to **16^{Cy}**, yielding **17**. Isolated yield in parentheses.

The ^{11}B NMR spectrum of the reaction mixture remained essentially unchanged (δ_{11B} = 33.0 ppm; **16^{Cy}**: δ_{11B} = 32.5 ppm), suggesting the presence of a symmetrical structure in which the boron atoms do not participate in the coordination. The ^{19}F NMR spectrum showed three higher order multiplets at –111.2, –116.5 and –164.4 ppm, upfield-shifted compared to [Cu(C$_6$F$_5$)]$_4$ (δ_{19F} = –107.2, –153.4, –162.3 ppm),[146] implying fragmentation and coordination of the latter to **16^{Cy}**. Slow evaporation of a DCM solution afforded deep blue single crystals of **17** in 92% yield. An X-ray diffraction analysis revealed that coordination of Cu(C$_6$F$_5$) takes place at both endocyclic nitrogen atoms N2/N2' (Figure 38).

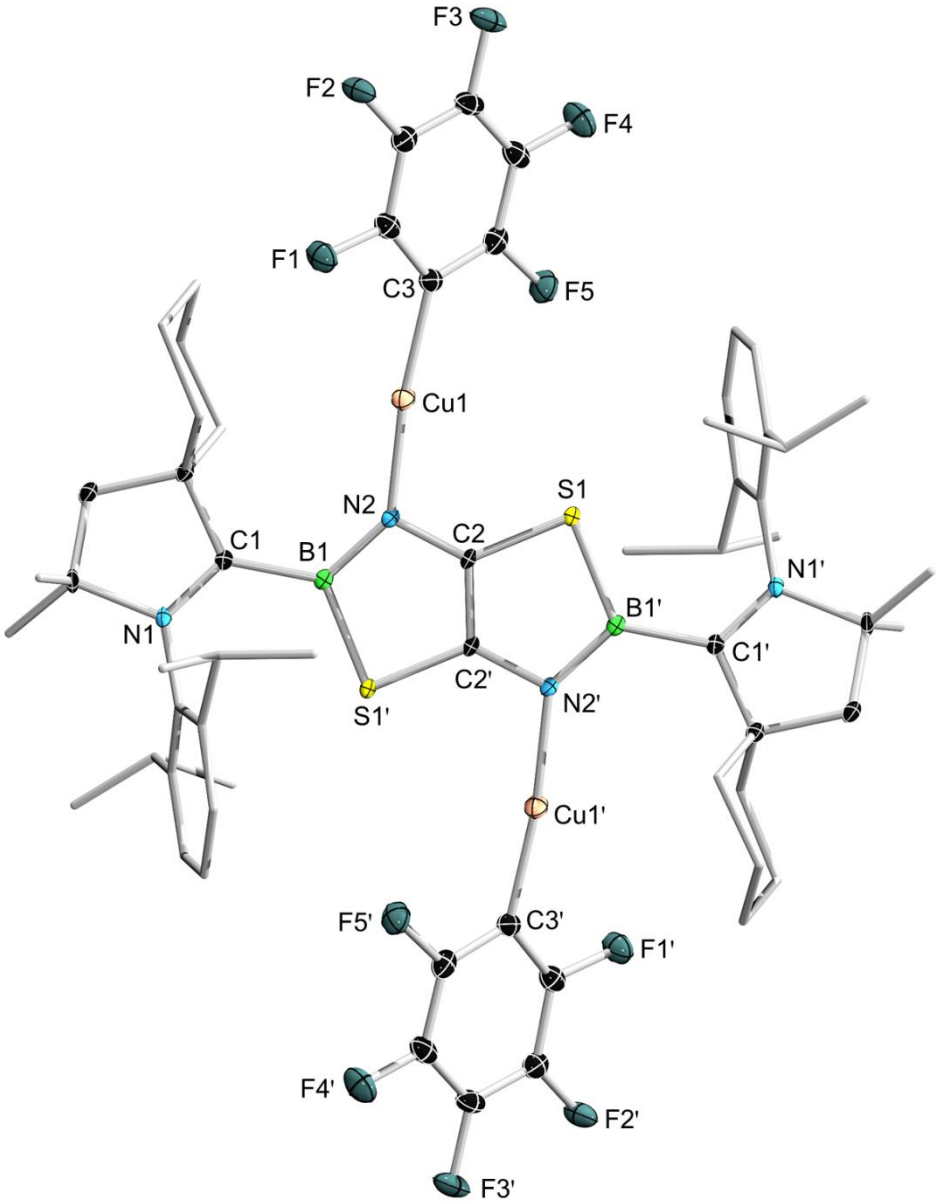

Figure 38. Crystallographically-derived molecular structure of **17**. Thermal ellipsoids are shown at the 50% probability level. Ellipsoids on the ligand peripheries and hydrogen atoms have been omitted for clarity. Selected bond lengths (Å) and angles (°): N1–C1 1.316(2), C1–B1 1.577(3), B1–N2 1.422(3), N2–C2 1.377(2), C2–C2' 1.377(4), C2–S1 1.7371 (19), B1–S1' 1.851(2), N2–Cu1 1.9115(16), Cu1–C3 1.916(2), N2–Cu1–C3 173.1(1), N1–C1–B1–N2 163.33(18).

The dicoordinate copper atoms display a nearly linear coordination geometry (N2–Cu1–C3 173.1(1)°), in which the Cu1–C3 bond length of 1.916(1) Å is considerably shorter than those found for the tetranuclear species $[Cu(C_6F_5)]_4$ (1.962(2)–2.007(2) Å),[146] which shows bridging rather than terminal aryl moieties. The N2–Cu1 distance of 1.9115(16) Å is comparable to those in related *N*-oxazolinyl or *N*-pyridinyl copper complexes.[147,148] In comparison to **16^{Cy}**, the C1–B1 (1.577(3) Å) and N2–C2 (1.377(2) Å) distances are lengthened by 2–3%, whereas the N1–C1 (1.316(2) Å) and C2–C2' (1.377(4) Å) distances are shortened by 1–3%, indicating a lower degree of π delocalization in **17**. The UV-vis absorption spectrum of **17** in DCM displays two maxima of almost equal intensity at 573 and 621 nm accounting for the deep purple color, significantly blue-shifted compared to the B,N,S-heterocyclic precursor **16^{Cy}** (Figure 39).

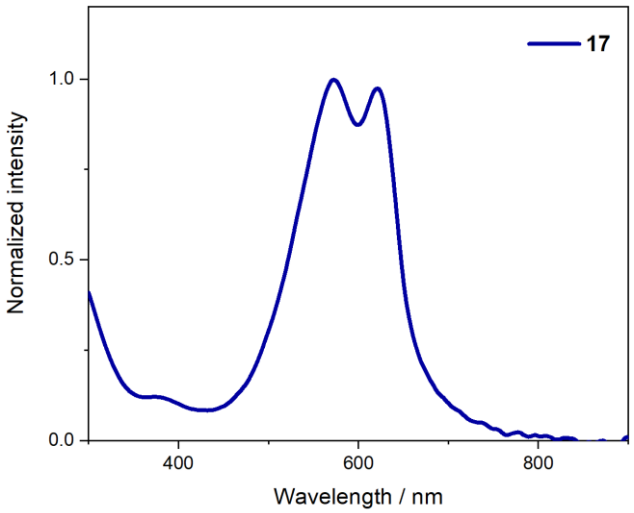

Figure 39. UV-vis absorption spectrum of **17** in DCM at 25 °C. **17**: λ_{max} = 573 nm; λ = 621 nm.

Given the nucleophilic nature of the endocyclic nitrogen atoms N2/N2' in **16^{Cy}**, the next consideration was that their protonation could lead to interesting changes in the optoelectronic properties of **16^{Cy}**. Indeed, treatment of **16^{Cy}** with 2.0 equivalents of HCl·toluene (0.10 M) resulted in an instant color change from blue to red (Scheme 45a). After workup, **18-Cl** was isolated as an intensely red solid in 86% yield, the ^{11}B NMR signal (δ_{11B} = 32.8 ppm) of which did not vary significantly from **16^{Cy}**, suggesting protonation of the nitrogen atoms rather than the tricoordinate boron centers. The ^{1}H NMR spectrum of **18-Cl** showed one symmetrical set of CAAC^{Cy} resonances as well as a broad, highly deshielded 2*H* singlet at 13.00 ppm, confirming the protonation of N2/N2' and indicating a very electron-poor TzbTzb heterocycle.

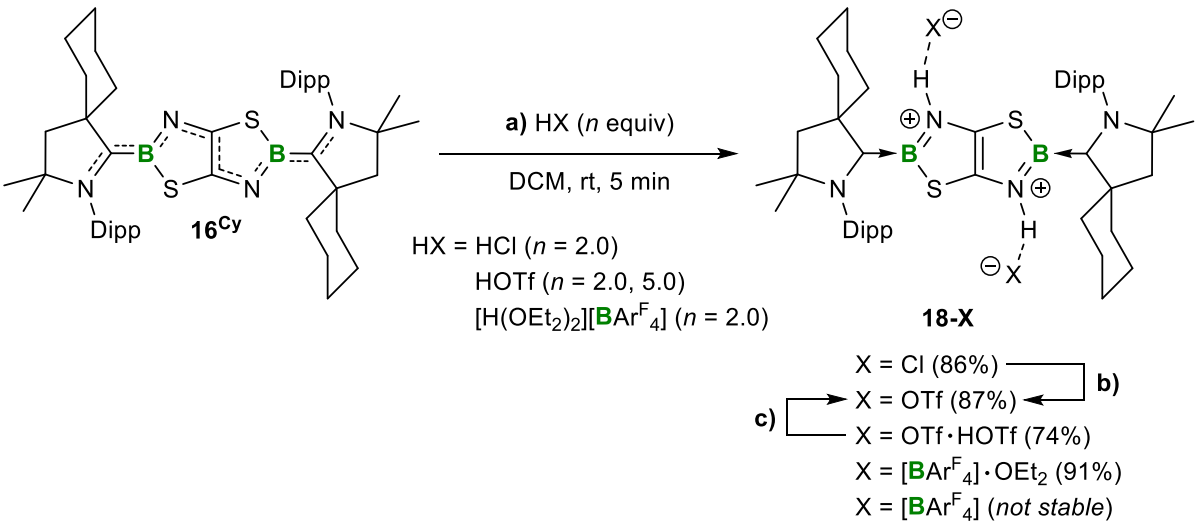

Scheme 45. a) Double protonation of **16^{Cy}** with selected Brønsted acids to the dications **18-X**. **b)** Ag[OTf] (2.0 equiv), CD_2Cl_2, rt, 1 min; **c) 16^{Cy}** (1.0 equiv), CD_2Cl_2, rt, 1 min. Isolated yields in parentheses.

Vapor diffusion of hexane into a saturated DCM solution afforded red single crystals of **18-Cl** suitable for X-ray crystallographic analysis (Figure 40, see Table 4 for selected bonding parameters). The solid-state structure of **18-Cl** revealed pronounced hydrogen bonding between the chloride counteranion and the nitrogen-bound protons (H2···Cl1 2.28(2) Å), thus explaining the high downfield shift of the ^{1}H NMR N*H* resonances.

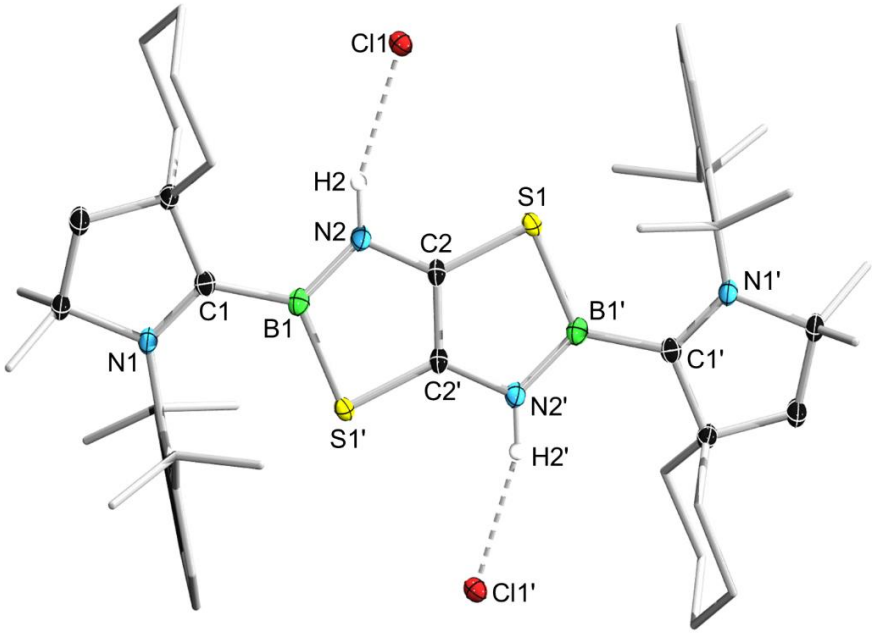

Figure 40. Crystallographically-derived molecular structure of **18-Cl**. Thermal ellipsoids are shown at the 50% probability level. Ellipsoids on the ligand periphery and hydrogen atoms, except those bound to nitrogen, have been omitted for clarity. See Table 4 for selected bond lengths and angles.

To investigate the influence of the counteranion both on the colorimetric properties and the N*H* chemical shift of the resulting dicationic species, **16^{Cy}** was then treated with the Brønsted acid HOTf. The reaction of **16^{Cy}** with 2.0 equivalents of HOTf immediately resulted in an orange

solution (Scheme 45a). Slow evaporation of the solvent under atmospheric pressure afforded a large crop of orange crystals of **18-OTf** in 87% isolated yield (Figure 41).

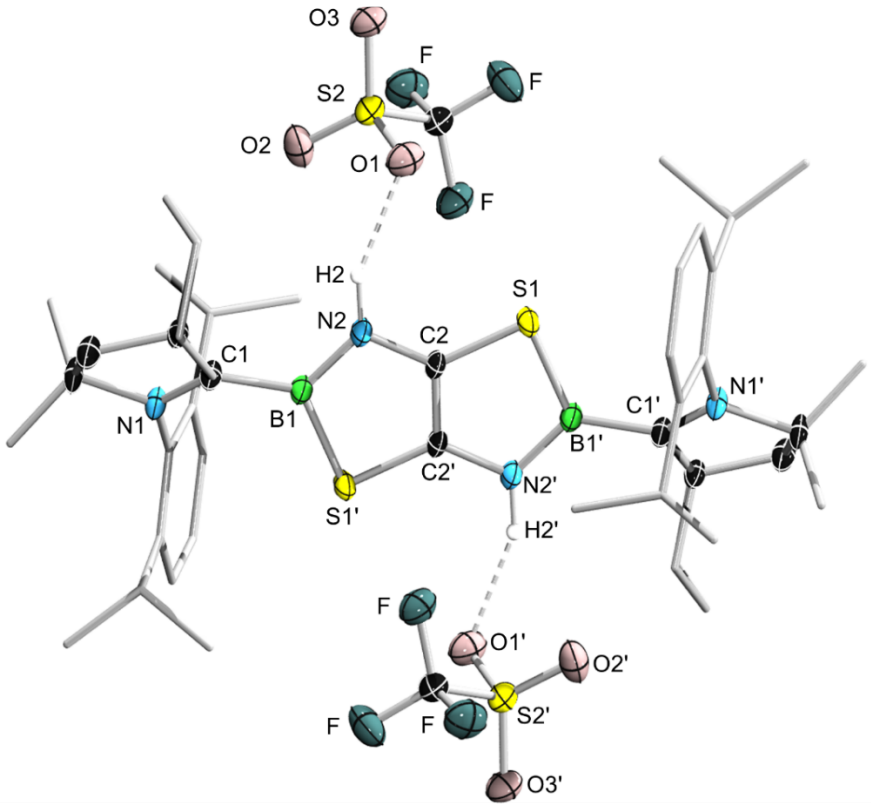

Figure 41. Crystallographically-derived molecular structure of **18-OTf**. Thermal ellipsoids are shown at the 50% probability level. Ellipsoids on the ligand periphery and hydrogen atoms, except those bound to nitrogen, have been omitted for clarity. See Table 4 for selected bond lengths and angles.

Like that of **18-Cl**, the solid-state structure of **18-OTf** shows hydrogen bonding between one oxygen atom of OTf^- and the nitrogen-bound protons (H2···O1 2.03(3) Å). It is worth mentioning that, while the addition of a large excess of HOTf to $\mathbf{16^{Cy}}$ resulted in protonation of the $CAAC^{Cy}$ ligands and decomposition of the B,N,S-heterocycle $\mathbf{16^{Cy}}$, the use of 5.0 equivalents of triflic acid led to the formation of a HOTf adduct of **18-OTf**, **18-OTf·HOTf**, in which the additional HOTf molecules interact with the OTf^- anions *via* O–H···O hydrogen bonding (Scheme 45a). Orange single crystals of **18-OTf·HOTf** were obtained *via* slow evaporation of the reaction mixture in 74% yield (Figure 42). Furthermore, the equimolar reaction of $\mathbf{16^{Cy}}$ with **18-OTf·HOTf** resulted in the selective formation of **18-OTf** (Scheme 45c), which can alternatively be obtained by salt metathesis of **18-Cl** with Ag[OTf] (Scheme 45b). While the ^{11}B NMR shifts of **18-OTf** (δ_{11B} = 33.1 ppm) and **18-OTf·HOTf** (δ_{11B} = 33.5 ppm) differ only slightly from that of **18-Cl**, the ^{1}H NMR resonances of the N*H* protons at 10.50 and 9.20 ppm, respectively, are upfield-shifted by 2.5 and 3.8 ppm compared to **18-Cl**, implying a gradual increase in the electron density of the B,N,S-heterocycle (Figure 45).

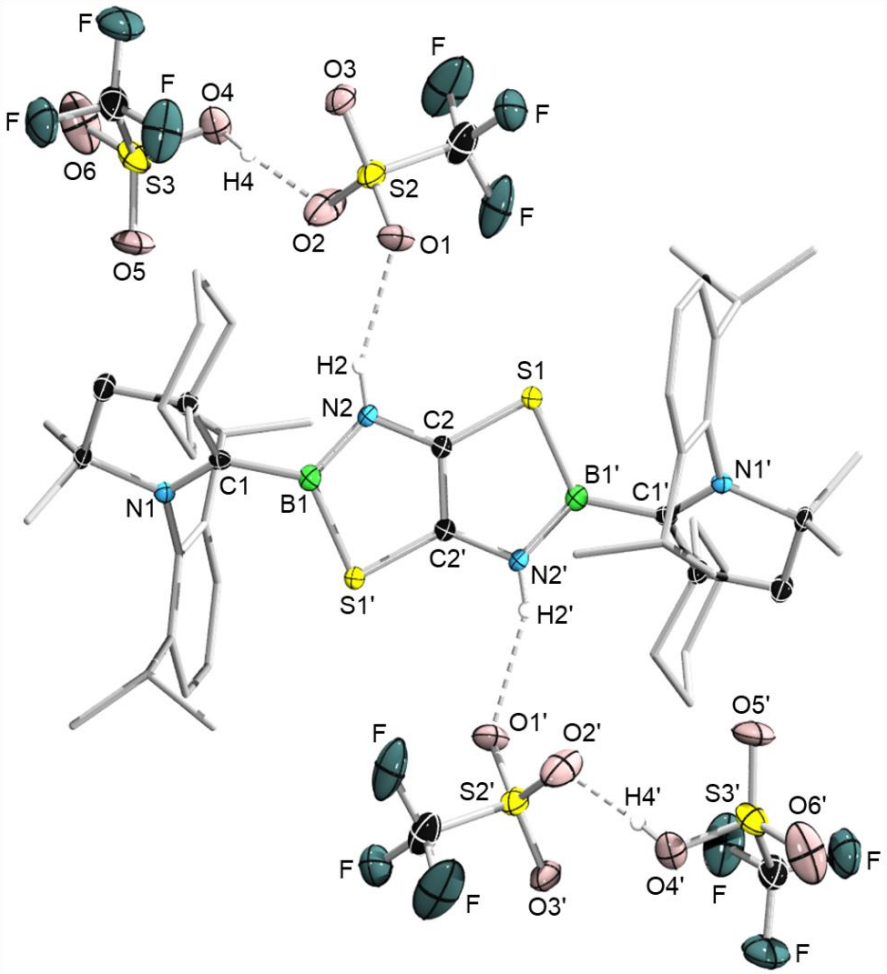

Figure 42. Crystallographically-derived molecular structure of **18-OTf·HOTf**. Thermal ellipsoids are shown at the 50% probability level. Ellipsoids on the ligand periphery and hydrogen atoms, except those bound to nitrogen and H4/H4', have been omitted for clarity. See Table 4 for selected bond lengths and angles.

To further investigate the effect of the anion coordination strength observed for **18-X** (X = Cl, OTf, OTf·HOTf), **16^{Cy}** was finally protonated with Brookhart's acid, $[H(OEt_2)_2][BAr^F{}_4]$ ($BAr^F{}_4$ = B(3,5-$(CF_3)_2C_6H_3)_4$). Upon addition of 2.0 equivalents of $[H(OEt_2)_2][BAr^F{}_4]$, the color of the reaction mixture instantaneously changed from blue to yellow (Scheme 45a). As expected, the resulting ^{11}B NMR spectrum showed two signals, one broad resonance for the endocyclic boron atoms (δ_{11B} = 33.7 ppm) and one sharp singlet at –6.6 ppm for the $[BAr^F{}_4^-]$ counteranions. Slow evaporation of the solvent under atmospheric pressure afforded bright yellow crystals of **18-$[BAr^F{}_4]$·Et$_2$O** in 91% isolated yield suitable for X-ray diffraction analysis. The solid-state structure showed that the N*H* protons in this case are hydrogen-bonded to the two diethyl ether molecules generated by the $[H(OEt_2)_2^+]$ cation, rather than to the $[BAr^F{}_4^-]$ anion (Figure 43). Again, the ^{1}H NMR N*H* resonance at 6.89 ppm is shifted another 2.3 ppm upfield from **18-OTf·HOTf**, as expected from the weaker N–H···O interaction.

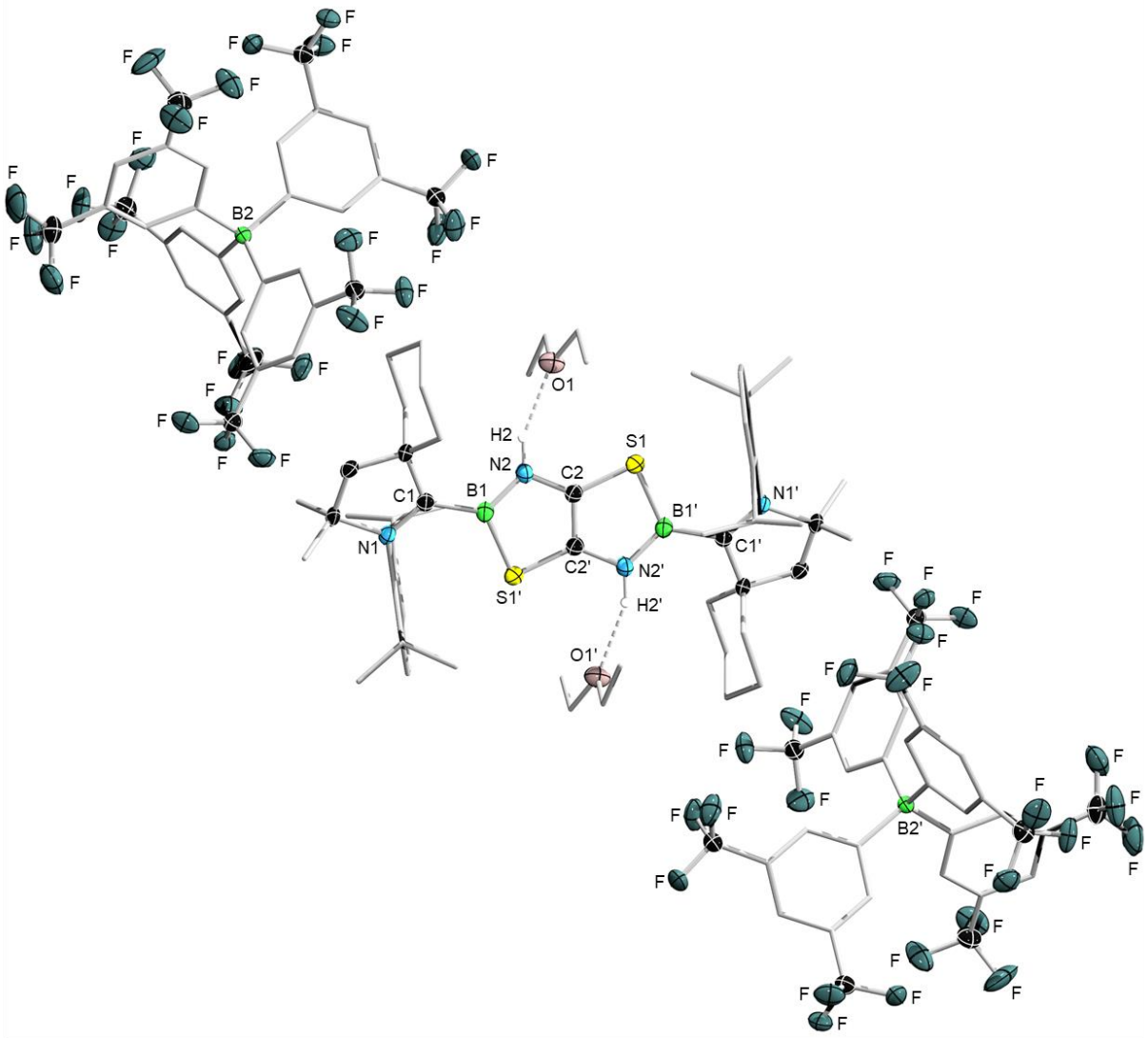

Figure 43. Crystallographically-derived molecular structure of **18-[BAr$^{F}_{4}$]·Et$_2$O**. Thermal ellipsoids are shown at the 50% probability level. Ellipsoids on the ligand periphery and hydrogen atoms, except those bound to nitrogen, have been omitted for clarity. See Table 4 for selected bond lengths and angles.

Removal of the solvent *in vacuo* and redissolving of ether-free **18-[BAr$^{F}_{4}$]** in CD_2Cl_2 led to partial decomposition of the dication. Slow evaporation of this solution afforded ether-free, yellow crystals of **18-[BAr$^{F}_{4}$]**, which displays N–H···F hydrogen bonding to a CF_3 group of the [BAr$^{F}_{4}$$^{-}$] anion in the solid state (Figure 44). The ^{1}H NMR N*H* resonance at 6.84 ppm is similar to that of **18-[BAr$^{F}_{4}$]·Et$_2$O**, suggesting that the N–H···OEt$_2$ and N–H ···F$_3$C hydrogen bonds are of similar strength.

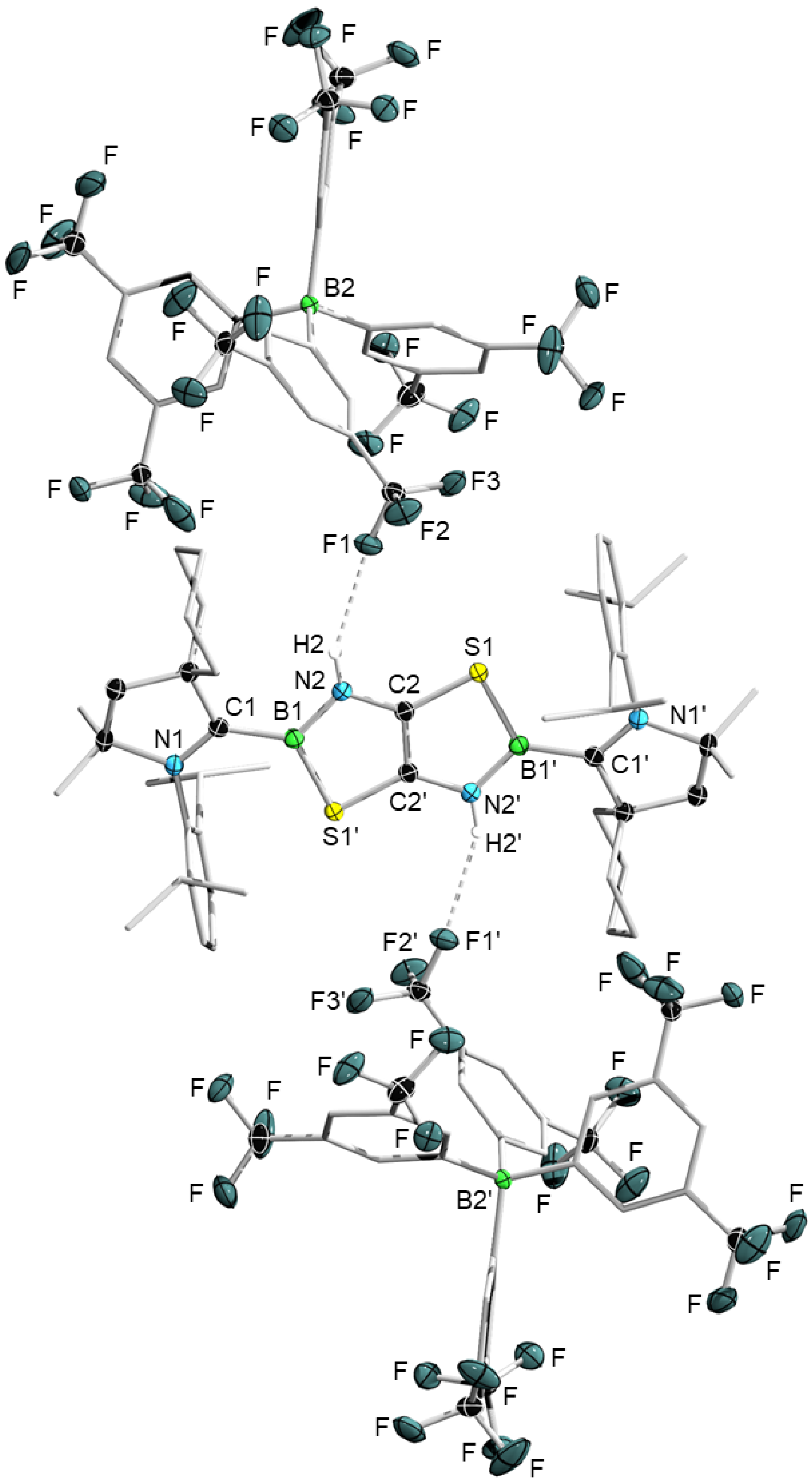

Figure 44. Crystallographically-derived molecular structure of **18-[BAr^{F}$_4$]**. Thermal ellipsoids are shown at the 50% probability level. Ellipsoids on the ligand periphery and hydrogen atoms, except those bound to nitrogen, have been omitted for clarity. See Table 4 for selected bond lengths and angles.

The solid-state IR spectra of the dications **18-X** showed a broad N–H stretching band in the 3000–3400 cm^{-1} region, which is shifted to higher wavenumbers in the order of X = Cl < OTf < OTf·HOTf < [BAr^F_4], indicating a gradual strengthening of the N–H bond, concomitant with weakening of the respective H···X hydrogen bond. This correlates well with the trend observed in the ^{1}H NMR shifts of the N*H* protons (Figure 45).

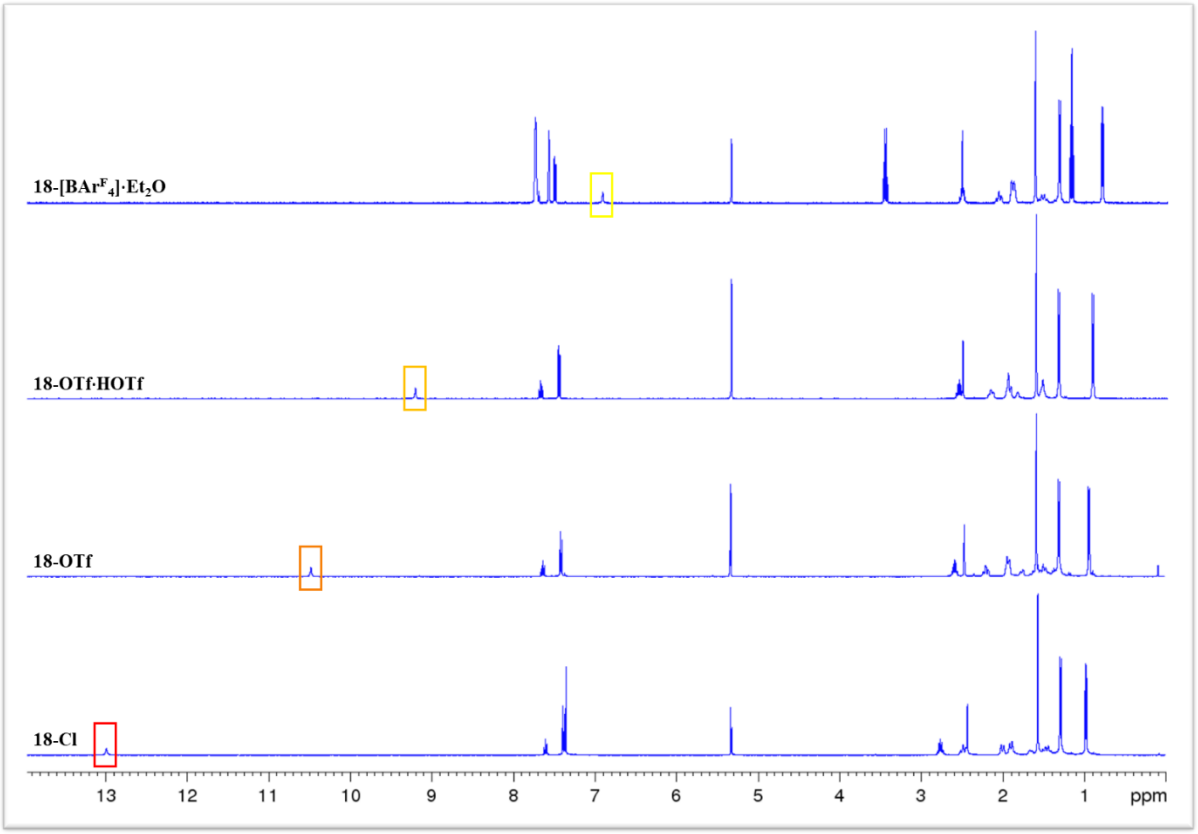

Figure 45. Stack-plot of ^{1}H NMR spectra of **18-Cl**, **18-OTf**, **18-OTf·HOTf** and **18-[BAr^F_4]·Et$_2$O** in CD_2Cl_2 showing the gradual upfield shift of the framed N*H* resonance. The contours of the boxes represent the color of the respective dication.

The crystallographically-derived solid-state structures of **18-X** were all centrosymmetric and display hydrogen bonding of the diprotonated B,N,S-heterocyclic core and either the two counterions (X = Cl, OTf, OTf·HOTf, [BAr^F_4]) or the solvent (X = [BAr^F_4]·Et_2O). The bond lengths in the π-delocalized $(NCBNC)_2$ scaffold change significantly upon protonation of the endocyclic nitrogen atoms N2/N2' (see Table 4). The C1–B1 (avg. 1.58 Å) and N1–C1 (avg. 1.30 Å) bond lengths increase and decrease, respectively, compared to those in **16^{Cy}** and are thus indicative of a purely σ-donating interaction between the CAAC^{Cy} ligands and the TzbTzb unit. While the B1–N2 (avg. 1.41 Å) distance remains essentially unchanged, the N2–C2 (avg. 1.38 Å) bond is slightly lengthened and the B1–S1 (avg. 1.82 Å) and C2–C2' (avg. 1.34 Å) bonds are shortened, the latter now being a double bond. As a consequence, the π delocalization is disrupted, as observed in the copper complex **17**. Similar changes in the endocyclic bond

lengths were observed upon protonation of a related TzTz compound with trifluoroacetic acid.[149] In the neutral B,N,S-heterocycle **16^{Cy}** the CAAC^{Cy} ligands are oriented so that the π overlap between the N2–C1 and the TzbTzb unit is maximized, as shown by the N1–C1–B1–N2 torsion angle of 170.13(16)° tending towards 180°. In contrast, the degree of rotation of the CAAC^{Cy} ligands away from coplanarity in **18-X** increases, as seen in the N1–C1–B1–N2 torsion angle decreasing from 170.98(17)° to 137.7(2)° in the order of X = Cl > [BAr$^{F}_4$] > [BAr$^{F}_4$]·Et$_2$O > OTf > OTf·HOTf. The pronounced rotation of the CAAC^{Cy} ligands in the triflate derivatives confirms the absence of boron-to-CAAC π backbonding. However, the lack of steric or electronic trend in the variation of the N1–C1–B1–N2 torsion angle implies that this may simply be a crystal packing effect in the solid state rather than an electronic effect.

Table 4. Selected bond lengths (Å) and angles (°) for the crystallographically-derived molecular structures of **16^{Cy}**, **17** and **18-X**.

	16^{Cy}	**17**	**18-Cl**	**18-OTf**	**18-OTf·HOTf**	**18-[BAr$^{F}_4$]·Et$_2$O**	**18-[BAr$^{F}_4$]**
N1–C1	1.325(2)	1.316(2)	1.305(3)	1.301(3)	1.299(2)	1.296(3)	1.300(2)
C1–B1	1.543(2)	1.577(3)	1.581(3)	1.578(3)	1.576(3)	1.579(4)	1.569(2)
B1–N2	1.419(2)	1.422(3)	1.415(3)	1.417(4)	1.410(3)	1.407(4)	1.417(2)
N2–C2	1.332(2)	1.377(2)	1.377(2)	1.386(3)	1.381(3)	1.380(3)	1.376(2)
C2–C2'	1.421(3)	1.377(4)	1.366(4)	1.347(5)	1.353(4)	1.358(5)	1.358(3)
C2'–S1	1.7481(16)	1.7371(19)	1.7324(18)	1.736(3)	1.735(2)	1.726(3)	1.7298(16)
B1–S1	1.8598(18)	1.851(2)	1.838(2)	1.817(3)	1.821(3)	1.809(3)	1.8251(19)
N2–H2[a]	–	–	0.88(2)	0.94(4)	0.82(2)	0.92(3)	0.86(2)
H2···Y	–	–	2.28(2)[b]	2.03(3)[c]	2.16(2)[c]	2.05(3)[c]	2.33(3)[d]
N1–C1–B1–N2	170.13(16)	163.33(18)	170.98(17)	147.6(3)	137.7(2)	163.3(3)	166.16(16)

[a] The N-bound hydrogen atoms were detected in the inverse Fourier map and freely refined. [b] Y = Cl1. [c] Y = O1. [d] Y = F1.

To gain further insight into the different coloration of the dications **18-X**, UV-vis absorption and emission spectra were recorded. The UV-vis spectra of DCM solutions of **18-X** each display one structured absorption band with a maximum between 450–493 nm, gradually bathochromatically shifted in the order of X = Cl > OTf ≥ OTf·HOTf > [BAr$^{F}_4$]·Et$_2$O (Figure 46, Table 5). **18-Cl** and **18-[BAr$^{F}_4$]·Et$_2$O** show a second absorption maximum of slightly lower intensity, which is red-shifted by 20 nm for **18-Cl** and blue-shifted by 20 nm for **18-[BAr$^{F}_4$]·Et$_2$O** (see photographs of solutions of **18-X** in Figure 46). Unfortunately, the ether-free dication **18-[BAr$^{F}_4$]** was not sufficiently stable in solution to acquire photospectroscopic data.

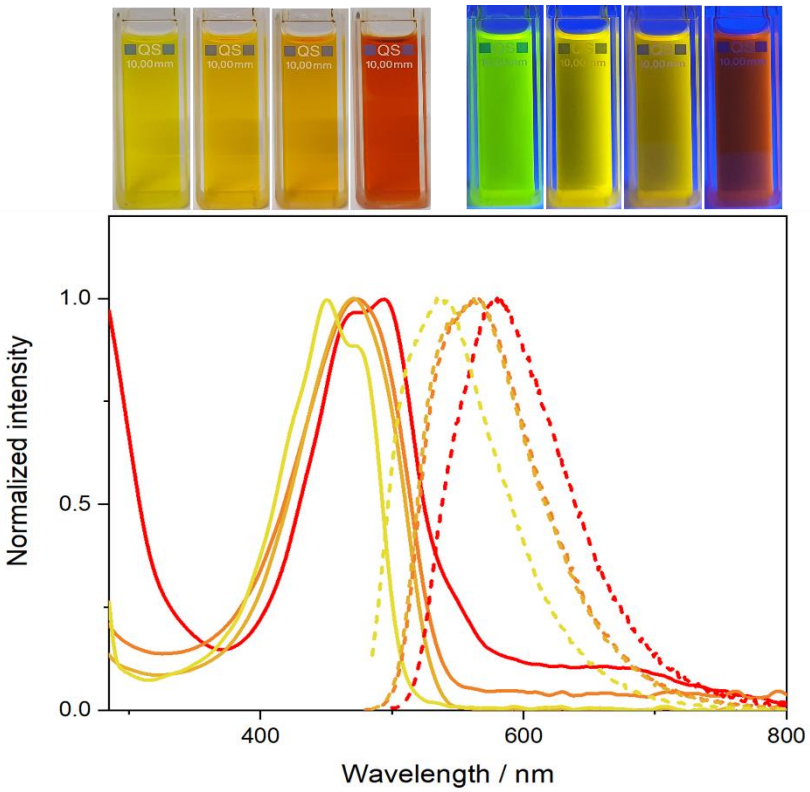

Figure 46. Top: photographs of solutions of **18-[BAr$^{F}_{4}$]·Et$_2$O**, **18-OTf·HOTf**, **18-OTf** and **18-Cl** (from left to right) under ambient light and UV irradiation at 254 and 366 nm. Bottom: UV-vis absorption (solid lines) and fluorescence (dashed lines) of **18-X** with X = Cl (red), OTf (dark orange), OTf·HOTf (light orange), and [BAr$^{F}_{4}$]·Et$_2$O (yellow) in DCM at 25 °C. See Table 5 for absorption and emission maxima.

Solutions of **18-X** were brightly fluorescent under UV irradiation, with emission colors ranging from red for **18-Cl** *via* yellow for **18-OTf** and **18-OTf·HOTf** to green for **18-[BAr$^{F}_{4}$]·Et$_2$O** (see photographs of irradiated solutions of **18-X** in Figure 46). In order to investigate the emissive properties of the diprotonated species **18-X** in detail, fluorescence spectra were recorded in cooperation with the group of Prof. Holger Helten at the University of Würzburg, Germany. The fluorescence spectra of **18-X** displayed an unstructured emission band, gradually hypsochromically shifted in the same sequence as the absorption spectra, from 580 nm for **18-Cl** to 539 nm for **18-[BAr$^{F}_{4}$]·Et$_2$O** (Table 5). This blue-shift reflects the gradual decrease in the electron-accepting strength of the diprotonated TzbTzb core, as seen with the upfield shift of the ^{1}H NMR resonances of the N*H* protons (Figure 45, *vide supra*). The dicationic species of a comparable TzTz compound showed a similar conjugate base-dependence, the absorption and emission maxima of which were red-shifted by 27 nm upon switching from HCl to trifluoroacetic acid as the proton source.[149] The authors claimed that this observation reflects an increase in the electron-accepting nature of the TzTz core as π overlap with peripheral triarylamino groups decreases due to steric constraints imposed by the hydrogen-bonded counteranion. In the present case, the comparison of the solid-state structures of **18-X** excludes

steric effects, thus the modulation of the naked-eye and fluorescence colors must be entirely dependent on the electron-withdrawing effect of the hydrogen-bonded counteranions or diethyl ether, respectively. The dications **18-X** show moderate quantum efficiencies, with Φ_{fl} values of 23% for **18-OTf**, 27% for **18-OTf·HOTf** and 33% for **18-[BAr$^F_4$]·Et$_2$O**. Due to partial decomposition of **18-Cl** during the measurement, no quantum yield for the chloride derivative was determined (Table 5).

Table 5. Photophysical data for **16^{Cy}**, **17**, **18-X** and **19-X** in DCM.

Compound	λ_{abs} (nm)	Secondary maxima (nm)[b]	λ_{em} (nm)[c]	Φ_{fl}[d]
16^{Cy}	680	628, 453	–	–
17	573, 621[a]	–	–	–
18-Cl	493	470	580	n.d.
18-OTf	474	–	566	0.23
18-OTf·HOTf	471	–	562	0.27
18-[BAr$^F_4$]·Et$_2$O	450	473	539	0.33
19-Cl	700, 762[a]	497, 458, 369	–	–
19-OTf	688	762, 484	–	–
19-[BAr$^F_4$]·Et$_2$O	637	513, 484, 780	–	–

[a] Maxima of equal intensity. [b] In order of decreasing intensity. [c] Excited at the wavelength of the respective absorption maximum. [d] Fluorescence quantum yield determined absolutely with an integrating sphere.

Given the strong influence of the twofold protonation of **16^{Cy}** on the color of the resulting dications **18-X**, the next consideration was whether the selective single protonation of **16^{Cy}** would yield compounds with intermediate optoelectronic properties. Therefore, **16^{Cy}** was treated with equimolar amounts of HCl, HOTf and [H(OEt$_2$)$_2$][BAr$^F_4$], yielding the desired monoprotonated species **19-X** (Scheme 46a).

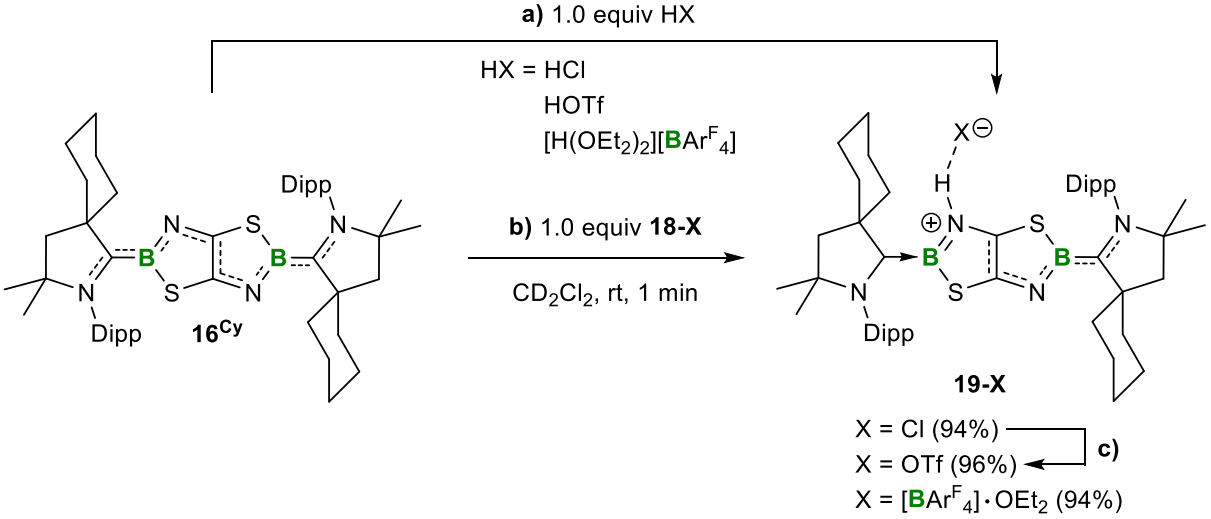

Scheme 46. a) Monoprotonation of **16^{Cy}** with selected Brønsted acids. **b)** Comproportionation of **16^{Cy}** and **18-X** to monocations **19-X**. **c)** Ag[OTf] (1.0 equiv), CD_2Cl_2, rt, 1 min. Isolated yields in parentheses.

However, the difficulty of getting the stoichiometry exactly right at such small reactions scales (ca. 10–20 mg of **16^{Cy}**) resulted in the formation of small amounts of diprotonated **18-X**, which prevented the clean isolation of the monocations **19-X** from this reaction route. In contrast, the comproportionation of **16^{Cy}** and dicationic **18-X** in CD_2Cl_2 afforded intense blue solutions of the desired monocations **19-X** in analytically pure quality (Scheme 46b). Alternatively, **19-OTf** could be synthesized *via* salt metathesis of **19-Cl** with one equivalent of Ag[OTf], yielding a blue solution of **19-OTf** after filtration of the colorless precipitate (AgCl) (Scheme 46c). Since the difference between the two boron nuclei of the neutral and the dicationic species proved to be very small already, only one broad resonance was detected in the ^{11}B NMR spectrum of **19-Cl** (δ_{11B} = 32.0 ppm). In contrast, the ^{11}B NMR spectra show two overlapping resonances for **19-OTf** (δ_{11B} = 32.5 and 31.5 ppm) and **19-[BAr$^F_4$]·Et$_2$O** (δ_{11B} = 32.2 and 31.2 ppm), respectively, for the two slightly different boron environments of the protonated and the neutral Tzb moieties. The ^{1}H and ^{13}C{^{1}H} NMR spectra of **19-X** displayed two sets of magnetically inequivalent and partly broadened CAAC^{Cy} ligand resonances. The ^{1}H NMR spectrum of **19-Cl** and **19-OTf** showed a N*H* proton resonance, integrating for 1*H*, which is shifted ca. 3.5 ppm upfield from the corresponding dicationic species **18-Cl** and **18-OTf** to 9.42 and 7.13 ppm, respectively, as expected for the more electron-rich monocationic B,N,S-heterocycle. The N*H* resonance of **19-[BAr$^F_4$]·Et$_2$O** and **18-[BAr$^F_4$]·Et$_2$O**, in turn, both appear at ca. 6.9 ppm, which indicates that the N–H···OEt$_2$ hydrogen bond has little influence on the electron density of the heterocyclic core in solution. Consequently, the mono- and dicationic TzbTzb core in these salts may be considered "naked". While both the dications **18-X** and monocations **19-X** proved stable in the solid state under inert atmosphere over several months, the low stability of the latter in solution over longer periods of time, even at –30 °C, precluded the isolation of single crystals of **19-X** suitable for X-ray diffraction experiments.

The stability of the monocations **19-X** in solution, however, was sufficient to investigate their photophysical properties. Unlike their dicationic congeners **18-X**, the monoprotonated species **19-X** exhibit no fluorescence up to the near-IR region. Their UV-vis absorption spectra recorded in DCM display a complex set of structured absorption bands (Figure 47, Table 5). The major absorption maxima in the 640–780 nm region correspond to the neutral Tzb moiety in analogy to **16^{Cy}** (λ_{max} = 680 nm), whereas the minor ones in the 450–520 nm region are similar to the diprotonated species **18-X** (λ = 450–490 nm). As observed for **18-X**, the absorption maximum is hypsochromically shifted upon moving to less strongly coordinating counteranions X.

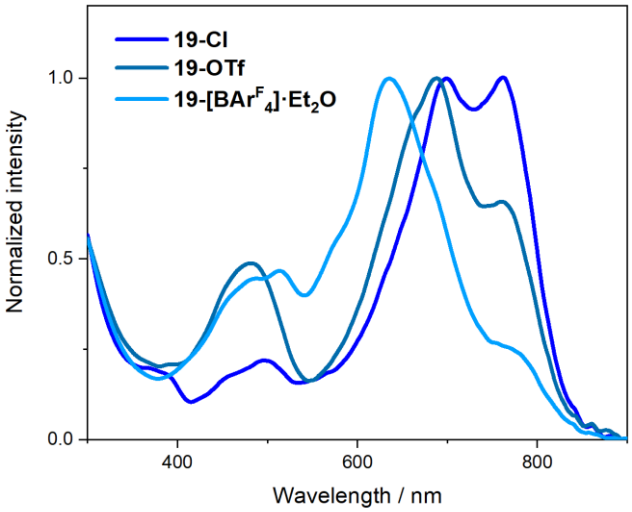

Figure 47. Overlay of UV-vis absorption spectra of **19-X** with X = Cl (dark blue), OTf (petrol blue), and [BAr$^F_4$]·Et$_2$O (light blue) in DCM at 25 °C. See Table 5 for absorption maxima.

2.3.3 Hydroboration of the B,N,S-heteroaromatics

After the successful protonation of the thiazaborolo[5,4-*d*]thiazaborole **16^{Cy}**, the next step was to investigate whether **16^{Cy}** also reacts with other element–H bonds. For this purpose, hydroboranes were initially chosen, as they display strongly polarized hydridic B–H bonds. The B,N,S-heterocycle **16^{Cy}** was at first treated with 2.5 equivalents of catecholborane (HBCat) in DCM, whereupon the intense blue color immediately vanished, accompanied by precipitation of a colorless solid (Scheme 47).

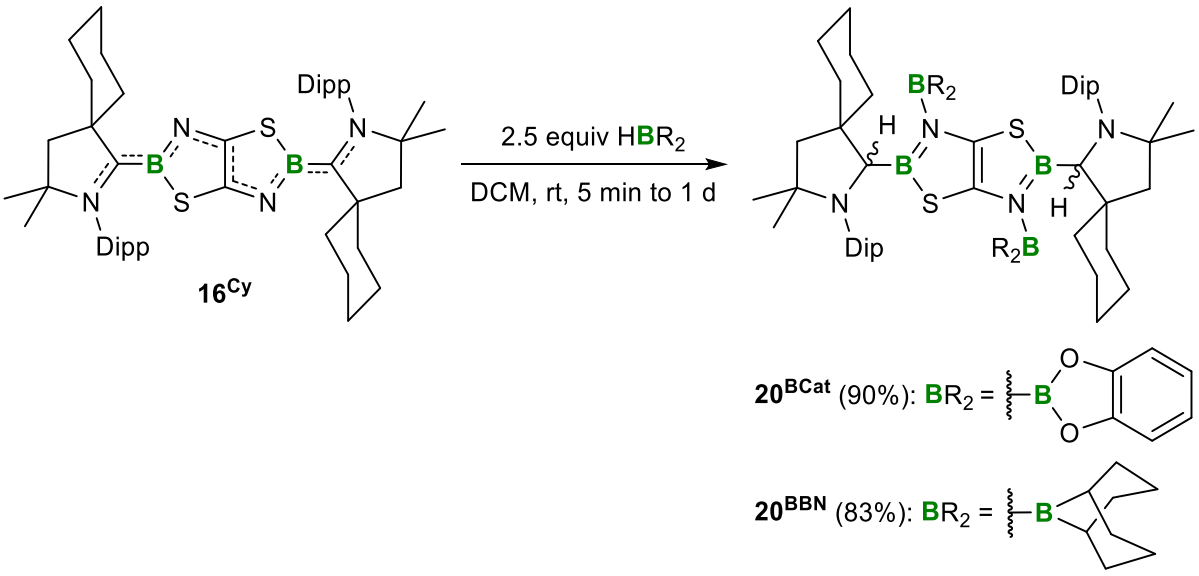

Scheme 47. Hydroboration of **16^{Cy}**, yielding **20^{BCat}** and **20^{BBN}**. Isolated yields in parentheses.

The ^{11}B NMR spectrum of the reaction mixture displayed two new resonances at 52.2 and 26.1 ppm, the latter of which was tentatively assigned to the [BCat] unit bound to the

heterocyclic core.[150] The very broad singlet at 52.2 ppm suggested the presence of a symmetric environment of both endocyclic boron atoms and further implied a tricoordinate boron environment. Consequently, the singlet in the ^{1}H NMR spectrum at 5.01 ppm, integrating for 2*H*, was assigned to protons bound to the former carbene carbon atoms. Further evidence for the protonation of the latter was provided by the CAAC^{Cy} ligand resonances, which were split into two magnetically inequivalent sets.[74] After workup, the product **20^{BCat}** was isolated as an off-white solid in 90% yield. Vapor diffusion of hexane into a saturated DCM solution afforded colorless single crystals of **20^{BCat}** (Figure 48).

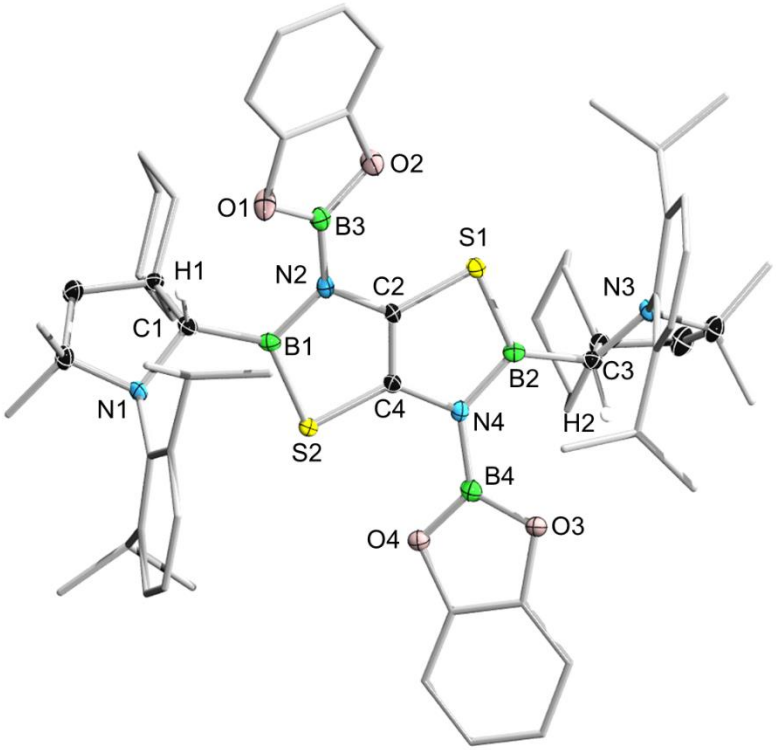

Figure 48. Crystallographically-derived molecular structure of **20^{BCat}**. Thermal ellipsoids are shown at the 50% probability level. Ellipsoids on the ligand periphery and hydrogen atoms, except H1 and H2, have been omitted for clarity. Selected bond lengths (Å) and angles (°): N1–C1 1.480(3), C1–B1 1.565(3), B1–N2 1.451(3), N2–B3 1.433(3), N2–C2 1.419(3), C2–C4 1.332(3), C4–S2 1.749(2), S2–B1 1.819(2), Σ(∠C1) 333.4(3).

X-ray crystallographic analysis authenticated **20^{BCat}** as the formal 1,3-hydroboration product, in which two equivalents of HBcat have been added to the endocyclic partial B=N double bonds in **16^{Cy}**, followed by a hydrogen shuttling from the boron center to the adjacent carbene carbon atom of each CAAC^{Cy} ligand, resulting in a pyramidalization of the latter (Σ(∠C1) 333.4(3)°). Thus, the C1–B1 distance between the anionic CAAC^{Cy}H substituent and the boron center increases from 1.543(2) Å in **16^{Cy}** to 1.565(3) Å in **20^{BCat}**, being relatively short with respect to other CAACH–boron bond lengths.[74] The former π delocalization across the central $(NCBNC)_2$ scaffold is hampered, as indicated by the B1–N2 (1.451(3) Å) and C2–C4 (1.332(3) Å) bonds showing distinct double bond character. The significantly shortened B1–S2

distance of 1.819(2) Å compared to 1.8598(18) Å in **16^{Cy}** suggests partial stabilization of the vacant p orbitals of the endocyclic boron centers by the adjacent sulfur atoms. Furthermore, both the B1–N2 (1.451(3) Å) and N2–B3 (1.433(2) Å) bond lengths imply a much stronger donation of the nitrogen-centered lone pair to the endocyclic boron atom than to the catecholboryl moiety, which is partly stabilized by the neighboring oxygen atoms. Since HBCat added cleanly to the B,N,S-heterocycle **16^{Cy}**, the possibility of extending this formal 1,3-hydroboration reaction to other sterically more demanding and less or more reactive hydroboranes was explored. The borane 9-borabicyclo[3.3.1]nonane (9-BBN) is considerably more bulky and usually forms a stable dimer in non-coordinating solvents.[151] Treatment of a DCM solution of **16^{Cy}** with 2.5 equivalents of 9-BBN resulted in a greyish solution over a course of one day at ambient temperature (Scheme 47). The ^{11}B NMR spectrum of the mixture showed two broad resonances at 66.0 and 52.2 ppm, indicating the formation of a hydroboration product similar to **20^{BCat}**. After addition of pentane, slow evaporation of this mixture provided a large crop of colorless single crystals of **20^{BBN}** in 83% yield suitable for X-ray diffraction analysis (Figure 49).

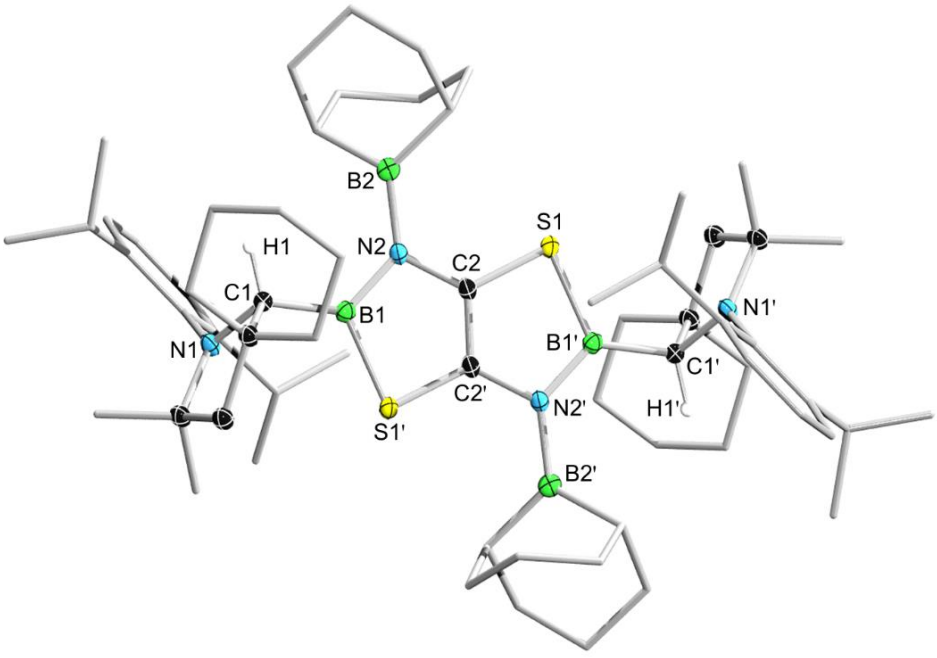

Figure 49. Crystallographically-derived molecular structure of **20^{BBN}**. Thermal ellipsoids are shown at the 50% probability level. Ellipsoids on the ligand periphery and hydrogen atoms except, H1 and H1', have been omitted for clarity. Selected bond lengths (Å) and angles (°): N1–C1 1.4895(17), C1–B1 1.600(2), B1–N2 1. 1.4483(19), N2–B2 1.4583(19), N2–C2 1.4201(17), C2–C2' 1.334(3), C4–S2 1.7484(15), S1'–B1 1.8340(16), Σ(∠C1) 329.2(2).

The solid-state structure of **20^{BBN}** confirms that indeed a formal 1,3-hydroboration reaction analogue to **20^{BCat}** has occurred, resulting in protonation of the former CAAC^{Cy} ligands at the C1 position (Σ(∠C1) 329.2(2)°). The C1–B1 (1.600(2) Å) bond length is elongated upon loss

of the strong π acceptor properties of the carbene ligand and is in the range typical of boron–carbon single bonds. Both the internal C2=C2' double bond (1.334(3) Å) and the B1–N2 distance of 1.4483(19) Å are essentially identical to those of **20^{BCat}**. However, the slightly longer N2–B2 (1.4583(19) Å) and B1–S1' (1.8340(16) Å) bond lengths in **20^{BBN}** compared to **20^{BCat}** indicate a less effective π donation from the nitrogen and sulfur atoms to the boron centers B2 and B1, respectively. This effect may be due to crystal packing effects in the solid state, since the dialkyl fragment in **20^{BBN}** is not as electron-donating as the oxygens in **20^{BCat}**.

Contrary to the highly selective hydroboration of **16^{Cy}** with HBCat and 9-BBN, the analogous reaction with $BH_3{\cdot}SMe_2$ only led to an intractable mixture of unidentifiable products. Additionally, all attempts to perform other hydroelementation reactions with primary and secondary silanes, amines and phosphines failed, as no conversion could be observed, either at ambient or at elevated temperatures. Previously in this work, the reaction of the tricoordinate pseudohaloborylenes **(*Z*)-11^{Me}** and **12** with thiophenol was described (*vide supra*). Inspired by these results, a DCM solution of **16^{Cy}** was treated with 2.2 equivalents of thiophenol, resulting in a color change from blue to deep red within one hour at room temperature (Scheme 48).

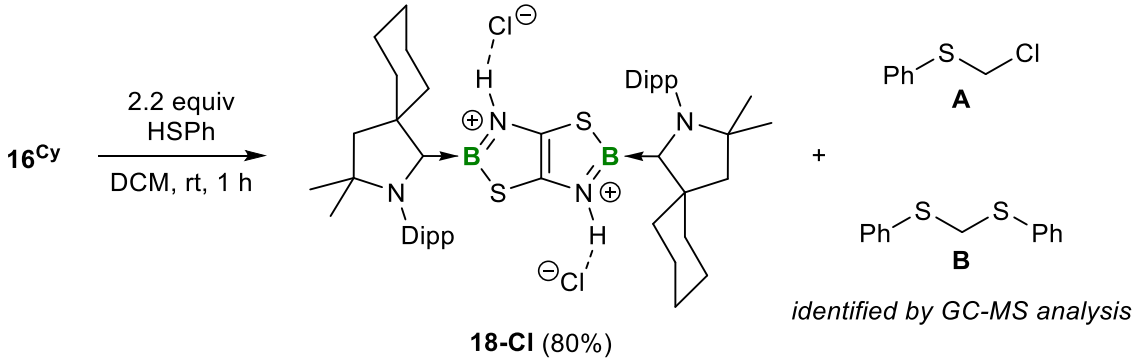

Scheme 48. Protonation of **16^{Cy}** with thiophenol, yielding the dication **18-Cl**. Isolated yield in parentheses.

Addition of pentane to the reaction mixture induced precipitation of an intensely red solid, which was isolated in 80% yield. The ^{11}B NMR chemical shift (δ_{11B} = 32.8 ppm) of the isolated product did not vary significantly from that of the starting material **16^{Cy}**, suggesting that both the boron centers and the carbene carbon atoms of the CAAC^{Cy} ligands remain tricoordinate. The ^{1}H NMR spectrum revealed the presence of a symmetrical set of ligand resonances, however, no signals for the expected protons of thiophenol could be detected in the aromatic region. Furthermore, a broad singlet at 13.0 ppm, integrating for two protons with respect to two CAAC^{Cy} ligands, was observed, suggesting the formation of the dication **18-Cl**, in which both endocyclic nitrogen atoms are protonated and two chloride counterions are present. The dication **18-Cl** had also been obtained by protonation of the B,N,S-heterocycle **16^{Cy}** with

2.0 equivalents of HCl·toluene, as described in the previous section (*vide supra*). According to literature-known protocols, thiophenol likely undergoes nucleophilic substitution reactions with DCM in the presence of a Brønsted base or catalyst,[152-155] respectively, yielding the thioethers (chloromethyl)(phenyl)sulfane (**A**) and bis(phenylthio)methane (**B**). The filtrate of the reaction mixture was subjected to a GC-MS analysis, which indeed corroborated the generation of **A** (158 *m/z*) and **B** (232 *m/z*) in a ratio of 3:70, thus explaining the formation of the diprotonated species **18-Cl**. The B,N,S-heterocycle $\mathbf{16^{Cy}}$ is apparently a sufficiently strong Brønsted base to deprotonate thiophenol, which subsequently reacts with the solvent DCM in the manner described. All attempts to replace DCM by other common solvents only led to a complex mixture of products, none of which could be assigned to either a thiophenolate analogue of the diprotonated TzbTzb compounds **18-X**, or any hydrothiolation product.

2.4 Attempts to Synthesize other Pseudohalide-substituted Boron Species

Motivated by the results obtained with cyano- and isothiocyanato-substituted boranes and borylenes (*vide supra*), another aim of this work was to introduce other pseudohalide substituents, such as isocyano (NC), isocyanato (NCO) and azido (N_3) groups. Herein, particular interest was placed on the synthesis of CAAC-stabilized pseudohaloboranes of the form ($CAAC^{Me}$)BH_2Y (Y = NC, NCO, N_3), which were subsequently to be converted to the corresponding dihaloboranes ($CAAC^{Me}$)BBr_2Y and ultimately reduced to the respective pseudohaloborylenes.

2.4.1 Attempted Syntheses of ($CAAC^{Me}$)BH_2Y (Y = NC, NCO, N_3)

As preliminary work by Curran and Lacôte,[98] Bertrand,[86] and our group has shown, the triflatoboranes ($CAAC^{R}$)BH_2(OTf) **1^{R}** are ideally suited for the replacement of the triflate group with a variety of pseudohalide substituents. The isocyanate anion [NCO^-] represents the lighter homologue of isothiocyanate [NCS^-] and thus exhibits a similar ambiphilic character. Consequently, the potential reduction of ($CAAC^{R}$)BBr_2(NCO) in the absence or presence of a stabilizing Lewis base could lead to NCO analogues of the heterocycles **16^{R}** or the tricoordinate borylenes **11^{R}**, respectively. Furthermore, the incorporation of an azido moiety [N_3^-] could open up interesting follow-up chemistry of the resulting CAAC-stabilized azidoboranes, potentially allowing for various post-synthetic transformations through 1,3-dipolar cycloaddition and nitrene insertion reactions.[156-158] The generation of the corresponding azidoborylenes, either transient, self-stabilizing or stabilized by another donor ligand could enable the construction of novel B,N-doped materials. Following the protocol of Curran and Lacôte and the syntheses of the isothiocyanatoboranes **9^{R}** presented above,[98] the reactions of **1^{Me}** with several cyanate and azide sources were carried out (Scheme 49).

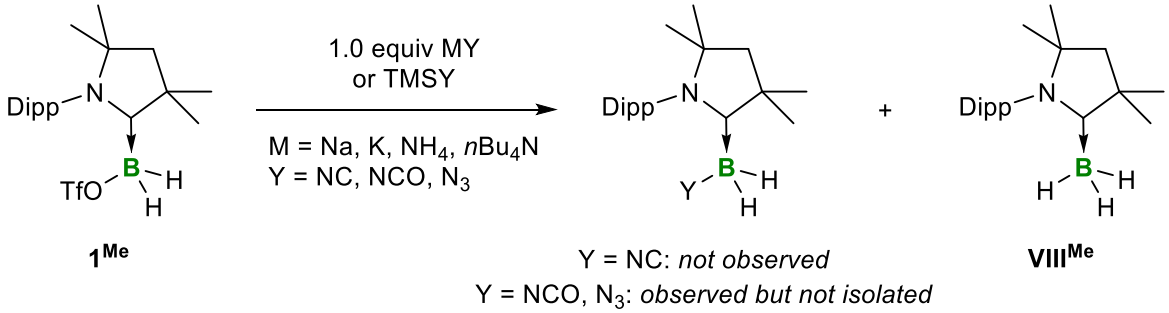

Scheme 49. Attempted syntheses of pseudohaloboranes ($CAAC^{Me}$)BH_2Y (Y = NC, NCO, N_3). TMS = trimethylsilyl.

In contrast to sodium thiocyanate, potassium cyanate has a much poorer solubility in common, polar solvents, which is why the salt could only be added to **1^{Me}** in form of a suspension in THF.

After complete addition, the mixture was stirred for one day at room temperature. In contrast to the synthesis of **9^{R}**, no clear solution was formed, but the reaction mixture remained a colorless suspension. The ^{11}B NMR spectrum of the reaction mixture, however, showed the formation of new boron species with resonances at –20.4 ppm (t, $^{1}J_{BH}$ = 97.2 Hz) and –32.3 ppm (q, $^{1}J_{BH}$ = 87.4 Hz) in a ratio of ca. 85:15, next to unreacted **1^{Me}** (ca. 40%). While the quartet could be assigned to (CAAC^{Me})BH$_3$ (**VIII^{Me}**),[74] the former was tentatively assigned to the desired product (CAAC^{Me})BH$_2$(NCO), as its chemical shift and coupling constant are similar to those of the NCS analogues **9^{R}**. Additional stirring at room temperature resulted in further conversion of **1^{Me}** to (CAAC^{Me})BH$_2$(NCO) and **VIII^{Me}**. Unfortunately, all attempts to separate the desired product (CAAC^{Me})BH$_2$(NCO) from (CAAC^{Me})BH$_3$ (**VIII^{Me}**) *via* extraction, fractional crystallization or sublimation failed due to essentially identical solubility of both compounds and decomposition of (CAAC^{Me})BH$_2$(NCO) at elevated temperatures *in vacuo*. Similarly, the triflatoborane **1^{Me}** was combined with a suspension of exactly one equivalent of sodium azide in THF (Scheme 49). Regardless of the reaction time, a product mixture of a new boron species and **VIII^{Me}** was obtained, in addition to unreacted **1^{Me}**. The new species was tentatively assigned as the desired azidoborane, (CAAC^{Me})BH$_2$(N$_3$), on the basis of its triplet in the ^{11}B NMR spectrum at –13.8 ppm (t, $^{1}J_{BH}$ = 99.0 Hz), which is similar to that of analogous NHC-stabilized azidoboranes.[98,159] In repeated attempts, however, the ratio of (CAAC^{Me})BH$_2$(N$_3$) and **VIII^{Me}** varied from 9:1 to 2:3, thus precluding the isolation of the desired product (CAAC^{Me})BH$_2$(N$_3$) in pure form due to its similar solubility to **VIII^{Me}**. Moreover, (CAAC^{Me})BH$_2$(N$_3$) tended to decompose to unidentifiable product mixtures during workup. As a result of the poor solubility of the alkali metal salts of cyanate and azide in THF, their ammonium and tetrabutyl ammonium salts were also tested. Although these showed significantly better solubility, all of these approaches also resulted in the formation of a product mixture of the respective (CAAC^{Me})BH$_2$Y (Y = NCO, N$_3$) and **VIII^{Me}**. Similar results were obtained when a crown ether (15-crown-5 for Na; 18-crown-6 for K) or cryptand ([2.2.1]cryptand for Na) was added to the reaction mixture to aid solubility of the alkali metal salts by complexation of the cation. When attempting to replace THF with the more polar solvent DMSO, which was also used by Curran and Lacôte for the synthesis of the corresponding NHC-borane adducts,[98] the ^{11}B NMR spectrum only showed the formation of two new boron species with broad resonances at –11.1 and 2.4 ppm, which were assigned to the compounds [(CAAC^{Me})(DMSO)BH$_2$]OTf and [(CAAC^{Me}H)(DMSO)$_2$BH]OTf, respectively, which are analogues of the boronium cations **2-L** and **3-L** (L = DMAP, Pyr) described in the first chapter (*vide supra*). Apparently, DMSO is sufficiently nucleophilic to

induce both the replacement of the triflate substituent in **1^{Me}** and a 1,2-hydride migration from boron to the adjacent carbene carbon atom. The possibility of eliminating bromotrimethylsilane (TMSBr) instead of salt elimination reactions was subsequently investigated. With the corresponding substrates TMSNCO and $TMSN_3$, however, no conversion was observed either at ambient or at elevated temperatures. Overall, the synthesis of NHC-stabilized pseudohaloboranes established by Curran and Lacôte was not transferable to the analogous CAAC adducts,[98] or only to a small extent. In addition to a partly unselective formation of the desired products ($CAAC^{Me}$)BH_2Y (Y = NCO, N_3), their workup and isolation, in particular, were problematic, which is why these routes were abandoned. The separation of ($CAAC^{Me}$)BH_3 (**VIII^{Me}**) is essential as the bromination of a product mixture would yield ($CAAC^{Me}$)BBr_3 (**VI^{Me}**) next to the desired ($CAAC^{Me}$)BBr_2Y. The subsequent reduction of this mixture would likely result in the formation of undesirable byproducts due to the contamination with **VI^{Me}**.

In addition to isocyanate and azide moieties, the introduction of an isocyano (NC) substituent at CAAC-stabilized boranes might also provide interesting follow-up chemistry. The reduction of ($CAAC^{Me}$)BBr_2(NC) in the presence of a second Lewis base L, for instance, could lead to the corresponding tricoordinate isocyanoborylenes ($CAAC^{Me}$)(L)B(NC). The reduction in the absence of a donor ligand, in turn, could potentially afford the tetrameric isocyanoborylene [($CAAC^{Me}$)B(NC)]$_4$.[62] The literature-known complex Na[$Cr(CO)_5$(CN)] has proven a suitable substrate for the addition of a [$Cr(CO)_5$(CN)] fragment to transition metals *via* salt elimination.[160,161] Accordingly, one equivalent of a THF solution of Na[$Cr(CO)_5$(CN)] was added dropwise to a solution of the triflatoborane **1^{Me}** in benzene (Scheme 50).

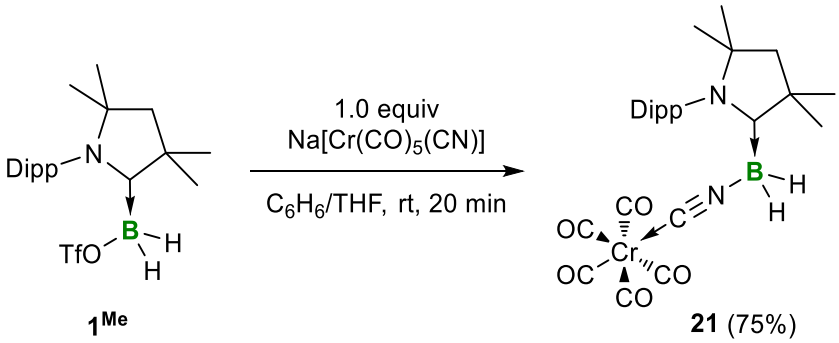

Scheme 50. Synthesis of the $CAAC^{Me}$-stabilized isocyanoborane chromium complex **21^{Me}**. Isolated yield in parentheses.

The resulting pale yellow solution was stirred for 20 minutes at room temperature prior to evaporation of the solvent. After workup, slow evaporation of a dichloromethane solution afforded a large crop of colorless single crystals of [($CAAC^{Me}$)BH_2(NC($Cr(CO)_5$)] (**21**) in 75% yield. Complex **21** displays a broad triplet at –21.6 ppm in the ^{11}B NMR spectrum, which agrees well with the chemical shift observed for similar carbene-stabilized boranes with [BNC]

connectivity.[98,162] The solid-state IR spectrum of **21** provided further evidence for the successful formation of the complex, showing both characteristic B–H stretching modes at 2431 and 2333 cm^{-1} and a sharp vibrational mode at 2165 cm^{-1} for the [NC] moiety, as well as a set of IR bands for the CO ligands at 2066, 2003 and 1895 cm^{-1}, typical for such metal carbonyl complexes.[163] Additionally, X-ray diffraction analysis performed on single crystals of **21** unambiguously confirmed that the [(CAAC^{Me})BH_2(NC)] unit is indeed bound to the chromium pentacarbonyl fragment (Figure 50). The C2–Cr1 (2.0298(15) Å) and B1–N2 (1.5391(19) Å) distances are within the range of the respective single bonds, while the N2–C2 (1.1518(19) Å) distance exhibits triple bond character. The CAAC^{Me} ligand stabilizes the boron center as pure σ donor, as indicated by the C1–B1 and N1–C1 bond lengths of 1.609(2) Å and 1.2991(18) Å, respectively.

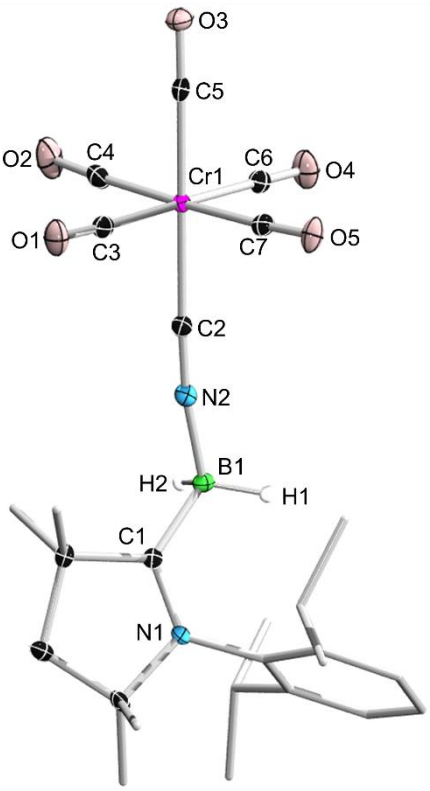

Figure 50. Crystallographically-derived molecular structure of **21**. Thermal ellipsoids are shown at the 50% probability level. Ellipsoids on the CAAC ligand periphery and hydrogen atoms, except those bound to boron, omitted for clarity. Selected bond lengths (Å) and angles (°): N1–C1 1.2991(18), C1–B1 1.609(2), B1–N2 1.5391(19), N2–C2 1.1518(19), C2–Cr1 2.0298(15), Cr1–C6 1.8662(15), C6–O3 1.1475(18), B1–N2–C2 170.91(14); N2–C2–Cr1 176.25(12).

As complex **21** exhibits the desired [(CAAC^{Me})BH_2(NC)] connectivity, the next target was the cleavage of the metal carbonyl fragment [$Cr(CO)_5$] to obtain the CAAC^{Me}-stabilized isocyanoborane. Therefore, several attempts were made to cleave the carbon–chromium bond (Scheme 51).

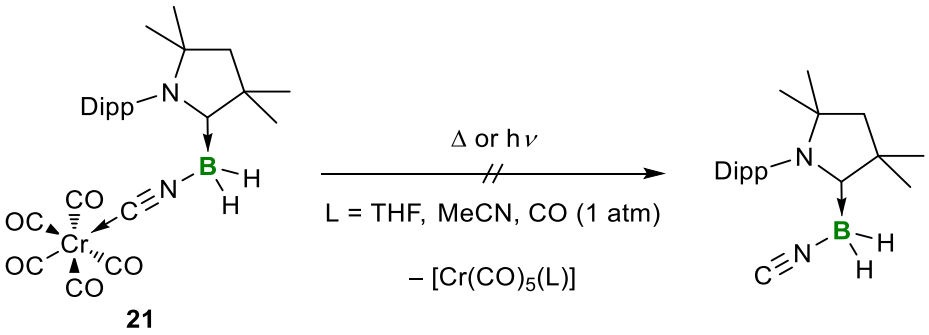

Scheme 51. Attempts to liberate the chromium pentacarbonyl fragment from **21** to obtain free (CAAC^{Me})BH$_2$(NC).

Neither prolonged heating nor photolysis of solutions of **21** in coordinating solvents such as THF and acetonitrile (MeCN) resulted in the elimination of the respective [Cr(CO)$_5$(L)] (L = THF, MeCN) complex. Dissolving of **21** in MeCN, in turn, led to the formation of a new boron species that was tentatively assigned to [(CAAC^{Me}H)BH(NC(Cr(CO)$_5$)(NCMe)] based on its broad doublet at –13.1 ppm ($^1J_{BH}$ = 112 Hz) in the ^{11}B NMR spectrum. Moreover, heating of a solution of complex **21** under an atmosphere of carbon monoxide showed no signs of conversion to the desired product (CAAC^{Me})BH$_2$(NC) even after two weeks at 80 °C. Stronger σ donor ligands were not tested as these would also likely induce a 1,2-hydride migration from boron to the adjacent carbene carbon atom instead of the cleavage of the metal carbonyl fragment. In conclusion, all attempts to gain access to other pseudohaloboranes of the form (CAAC^{Me})BH$_2$Y (Y = NCO, N$_3$, NC) *via* the triflatoborane **1^{Me}** were thus far unsuccessful.

2.4.2 Synthesis of a Tricoordinate Bromoborylene

Since the aforementioned reactions of triflatoborane **1^{Me}** did not provide access to NC-, NCO- and N$_3$-functionalized CAAC^{Me}-borane adducts, attempts were made to carry out salt elimination reactions directly on an already existing haloborylene. As described above, the first metal-free parent borylene (CAAC^{Cy})$_2$BH (**VII**) was synthesized by reduction of (CAAC^{Cy})BBr$_3$ (**VI^{Cy}**) with an excess of KC$_8$ (see Scheme 2). While the mechanism of the formation of **VII** has not been fully elucidated to date, the replacement of the bromide by the hydride substituent is attributed to intermolecular radical hydrogen abstraction.[46] To circumvent this problem, our group established the synthesis of analogous chloroborylenes (CAAC^{Me})(L)BCl **XXXI-L** (see Scheme 10).[64] On the one hand the reduction of (CAAC^{Me})BCl$_3$ (**XXX**) in the presence of a Lewis base L (L = CAAC^{Me}, NHCs, phosphines) enables steric and electronic tuning of the resulting haloborylenes, on the other hand it is significantly more selective and leads to high isolated yields, presumably due to the less reactive B–Cl bond compared to B–Br. Roesky and co-workers used an analogous approach for the

synthesis of a bis(CAAC^{Me})-stabilized fluoroborylene (CAAC^{Me})$_2$BF (**XXXIII**) *via* reduction of (CAAC^{Me})BF$_3$ (**XXXII**) in the presence of CAAC^{Me} (see Scheme 11).[65]

Using these selective synthetic routes to haloborylenes and the related tricoordinate pseudohaloborylenes (*vide supra*) as models, a diluted benzene solution of (CAAC^{Me})BBr$_3$ (**VI^{Me}**) was added dropwise to a suspension of 2.2 equivalents of both KC$_8$ and the Lewis base I*i*Pr (Scheme 52).

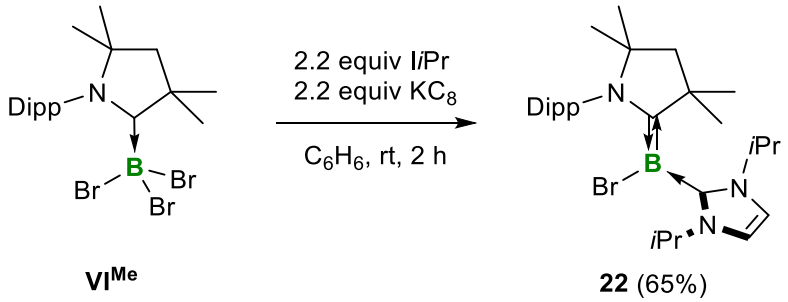

VI^{Me} **22** (65%)

Scheme 52. Synthesis of bromoborylene **22**. Isolated yield in parentheses.

The resulting intensely red suspension was stirred for two hours at room temperature prior to filtration. After solvent removal and extraction with pentane, slow crystallization at –30 °C afforded a crop of red single crystals of (CAAC^{Me})(I*i*Pr)BBr (**22**) in 65% yield. The bromoborylene **22** displays an ^{11}B NMR resonance at 0.7 ppm, comparable with those reported for its closest relatives, the chloroborylenes (CAAC^{Me})(IMe)BCl (**XXXI-IMe**) (δ_{11B} = 8.4 ppm) and (CAAC^{Me})(IMe^{Me})BCl (**XXXI-IMe^{Me}**) (δ_{11B} = 5.5 ppm),[64] the parent borylene (CAAC^{Me})(IMe^{Me})BH (δ_{11B} = 2.9 ppm),[105] as well as the tricoordinate pseudohaloborylenes **(*Z*)-11^{Me}** (δ_{11B} = –2.6 ppm) and **12** (δ_{11B} = –12.1 ppm) discussed above. The ^{1}H NMR spectrum shows one symmetrical set of ligand resonances as already observed for **(*Z*)-11^{Me}** and **12**, indicating the formation of the (*Z*)-isomer of **22** only. However, prolonged heating of a C$_6$D$_6$ solution at 60 °C selectively led to the formation of new ligand resonances split into two magnetically inequivalent sets, concomitant with the appearance of a new resonance at 8.8 ppm in the ^{11}B NMR spectrum, both suggesting the possibility of a (*Z*)- to (*E*)-isomerization of **22**, as already observed for the cyanoborylene-tungsten complex **12-W**. X-ray crystallographic analysis of red single crystals of **22** confirmed the (*Z*)-configuration of the bromoborylene **22** (Figure 51).

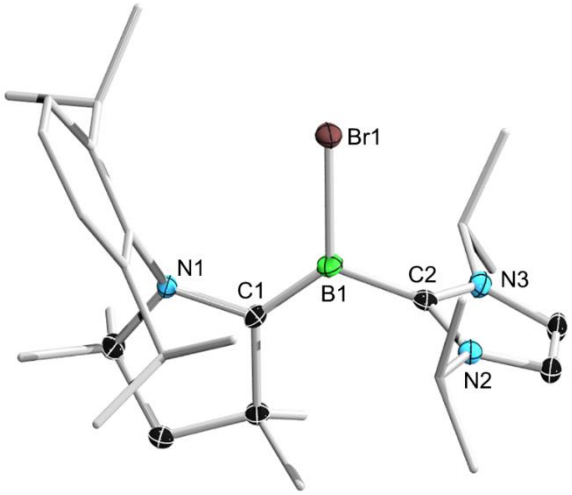

Figure 51. Crystallographically-derived molecular structure of **22**. Atomic displacement ellipsoids are shown at the 50% probability level. Ellipsoids of the ligand peripheries and hydrogen atoms have been omitted for clarity. Selected bond lengths (Å) and angles (°): N1–C1 1.443(2), C1–B1 1.434(3), B1–C2 1.581(3), B1–Br1 2.0195(19), C1–B1–C2 125.24(15), Σ(∠B1) 359.9(2)°.

The solid-state structure of **22** displays bonding parameters typical of tricoordinate borylenes,[46,47,62,64] with a trigonal planar boron center (Σ(∠B1) 359.9(2)°) and a short CAAC^{Me}–boron bond (C1–B1 1.434(3) Å) with double bond character, suggesting strong π backdonation from the electron-rich borylene center to the π-acidic CAAC^{Me} ligand. The I*i*Pr ligand is almost perpendicular to the CAAC^{Me}–B–Br plane (torsion angle C1–B1–C2–N3 84.3(2)°), stabilizing the boron center as pure σ donor (B1–C2 1.581(3) Å). The B1–Br1 distance of 2.0195(19) Å is in the range of boron–bromine single bonds and fits well into the series of rising boron–halide bond lengths with respect to the other reported CAAC-supported haloborylenes (B–F 1.3999(15) Å; B–Cl ca. 1.85 Å).[64,65] Furthermore, the B1–Br1 distance is slightly longer than that of the only other bromoborylene **XXIX** reported (B–Br 1.989(6) Å).[63] The UV-vis absorption spectrum of a benzene solution of the bromoborylene **22** exhibits a major broad absorption band at 499 nm, with a shoulder at 365 nm, collectively accounting for the intense red color (see Figure 65 in the Appendix). This coloration is comparable to both the (CAAC^{Me})(NHC)-stabilized chloroborylenes reported by our group and the above-described isothiocyanatoborylene **(*Z*)-11^{Me}** (*vide supra*).[64]

Metal-free chloro- and fluoroborylenes remain scarce and are essentially limited to the examples mentioned above. Moreover, there is only one other literature-known bromoborylene, **XXIX**, reported by Xie and co-workers in 2017.[63] This tricoordinate bromoborylene **XXIX**, which at the same time is the first and only reported silylene-stabilized borylene, has shown its ability to undergo halide abstraction reactions, forming an unprecedented tricoordinate borylene cation.[63] In light of this, the (CAAC^{Me})(I*i*Pr)-stabilized bromoborylene **22** was tested in

substitution reactions by elimination of an alkali metal bromide salt or bromotrimethylsilane (TMSBr). Bromoborylene **22** and various pseudohalide sources were therefore combined and their reaction mixtures monitored *in situ* by ^{11}B NMR spectroscopy (Scheme 53).

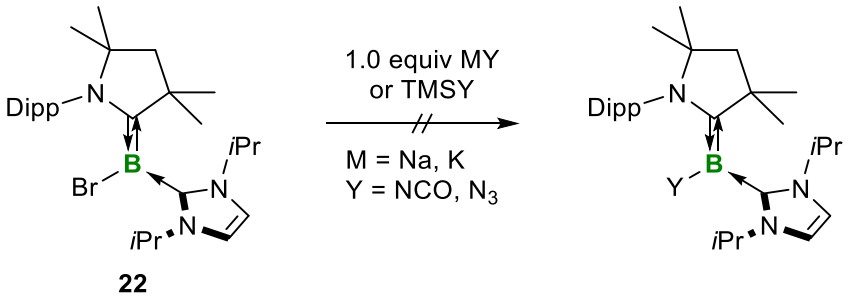

22

Scheme 53. Attempted syntheses of isocyanato- and azidoborylenes by bromide-pseudohalide exchange at **22.**

Treatment of **22** with an excess of (trimethylsilyl)isocyanate (TMSNCO) and -azide ($TMSN_3$) in C_6D_6, respectively, did not show any consumption of the starting bromoborylene **22**, either at ambient or at elevated temperatures. The elimination of TMSBr is apparently an insufficient driving force to favor the formation of the respective borylenes (CAAC^{Me})(I*i*Pr)BY (Y = NCO, N_3). In contrast, the salt elimination of alkali metal bromides is usually a powerful method to introduce nucleophiles, thus potentially allowing the generation of the desired products. The reactions of **22** with equimolar amounts of KOCN and NaN_3, however, only resulted in intractable mixtures of unidentifiable products. Consequently, the synthesis of pseudohaloborylenes with isocyanato and azido functionalities, which are structurally and electronically comparable to the aforementioned isothiocyanato- and cyanoborylenes **11^{R}** and **12**, remained unsuccessful in the course of this work.

2.5 Synthesis and Reactivity of CAAC-stabilized Boraphosphaketenes[4]

The 2-phosphaethynolate anion [PCO⁻] is the heavier homologue of the cyanate ion [NCO⁻] and is therefore isoelectronic to the latter. While both species generally exhibit similar reactivity, that of the [PCO⁻] anion is largely dominated by the relatively weak P–CO bond and the tendency of P–C multiple bonds to oligomerize, unlike the cyanate anion.[164] The first rational synthesis of a [PCO⁻] salt as well as its structural authentication was provided by Becker and co-workers in 1992.[165] However, it was a series of syntheses of Na[OCP] salts published by Grützmacher and Benkő that allowed the access of a nucleophilic [PCO⁻] unit and its incorporation into both transition-metal and main-group systems.[164,166] Grützmacher and Goicoechea have introduced the [PCO] moiety into main-group species, but so far only a handful of boron-functionalized examples are known. Depending on the connectivity of the [BOCP] and [BPCO] fragments, these species are referred to as boraphosphaethynolates and boraphosphaketenes, respectively. Both isomers have already shown interesting reactivity patterns, including acting as synthetic equivalents of phosphinidenes by exchange of CO at the [BPCO] unit by CN*t*Bu,[167] decarbonylation and formal phosphinidene dimerization,[167] and intramolecular phosphinidene insertion of a [PCO]-substituted borafluorene.[168]

2.5.1 Synthesis of Adducts of the Parent Boraphosphaketene and their Dimers

As shown in previous chapters, the CAAC^R-stabilized triflatoboranes (CAAC^R)BH$_2$(OTf) (**1^R**) were found to be excellent substrates for the nucleophilic substitution of the isothiocyanate anion (*vide supra*). Accordingly, dilute THF solutions of the sodium phosphaethynolate salt (Na[OCP]) were added dropwise to benzene solutions of **1^R** at ambient temperature (Scheme 54).

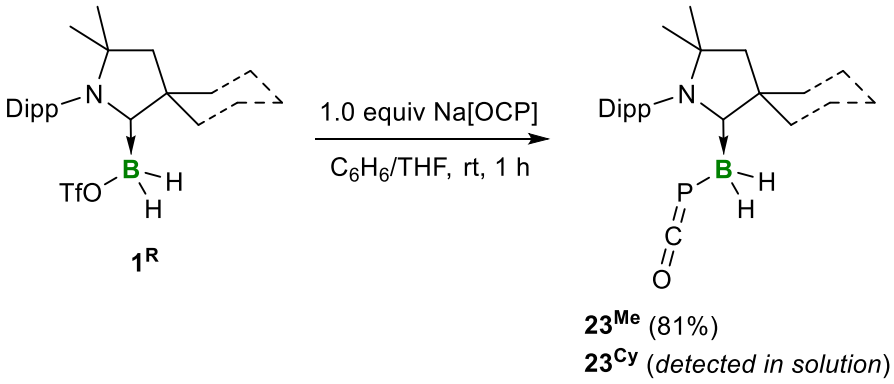

23^{Me} (81%)
23^{Cy} (*detected in solution*)

Scheme 54. Synthesis of the CAAC^R-stabilized parent boraphosphaketenes **23^R**. Isolated yields in parentheses.

[4] The results presented herein were published in "S. Hagspiel, F. Fantuzzi, R. D. Dewhurst, A. Gärtner, F. Lindl, A. Lamprecht, H. Braunschweig, Adducts of the Parent Boraphosphaketene H$_2$BPCO and their Decarbonylative Insertion Chemistry, *Angew. Chem. Int. Ed.* **2021**, *60*, 24, 13666–13670; *Angew. Chem.* **2021**, *133*, 13780–13784."

The resulting yellow solutions were stirred for one hour at room temperature, after which time high conversion to species with high-field shifted ^{31}P NMR resonances at –336.6 ppm (**23^{Me}**) and –339.2 ppm (**23^{Cy}**) were observed, which were assigned to the CAAC^{R}-stabilized parent boraphosphaketenes, (CAAC^{R})BH$_2$(PCO) (**23^{R}**). After workup, boraphosphaketene **23^{Me}** was isolated as a yellow solid in 81% yield and stored at –30 °C under the exclusion of light as phosphaketenes generally tend to decompose under ambient temperature and light.[164,166] Like its isothiocyanato analogue (CAAC^{Me})BH$_2$(NCS) (**9^{Me}**) (δ_{11B} = –20.4 ppm), **23^{Me}** shows a broad ^{11}B NMR triplet at –27.3 ppm ($^{1}J_{BH}$ = 101 Hz). The ^{31}P NMR resonance at –336.6 ppm is close to that reported by Goicoechea and co-workers for a boraphosphaethynolate (*i.e.* BOCP; δ_{31P} = –285.9 ppm),[169] as well as a crystallographically characterized boraphosphaketene reported by Wilson and Gilliard (BPCO; δ_{31P} = –289.7 ppm).[168] A strong metal-carbonyl-like band observed at 1899 cm^{-1} in the IR spectrum of **23^{Me}**, however, suggested that the isolated product is actually the boraphosphaketene isomer. While Wilson and Gilliard did not report an IR spectrum of their compound, such a band is absent in the IR spectrum of Goicoechea's boraphosphaethynolate.[169] The doublet in the ^{13}C{^{1}H} NMR spectrum of **23^{Me}** for the P-bound carbon nucleus further evidenced the [BPCO] connectivity, with its chemical shift and coupling constant (δ_{13C} = 192.8 ppm, $^{1}J_{PC}$ = 44.4 Hz) resembling that of Gilliard's and Wilson's boraphosphaketene (δ_{13C} = 192.0 ppm, $^{1}J_{PC}$ = 80.4 Hz) rather than that of Goicoechea's boraphosphaethynolate (δ_{13C} = 140.2 ppm, $^{1}J_{PC}$ = 17.6 Hz). DFT calculations performed on **23^{Me}** provided further evidence for the [BPCO] motif, with computed chemical shifts at δ_{11B} = –32, δ_{31P} = –338 and δ_{13C} = 202 ppm, and a vibrational CO frequency at 1950 cm^{-1} (Figure 52). The calculated chemical shifts of the [BOCP] isomer are respectively δ_{11B} = –6, δ_{31P} = –320 and δ_{13C} = 166 ppm, while the IR vibrational band was predicted at 1697 cm^{-1}.

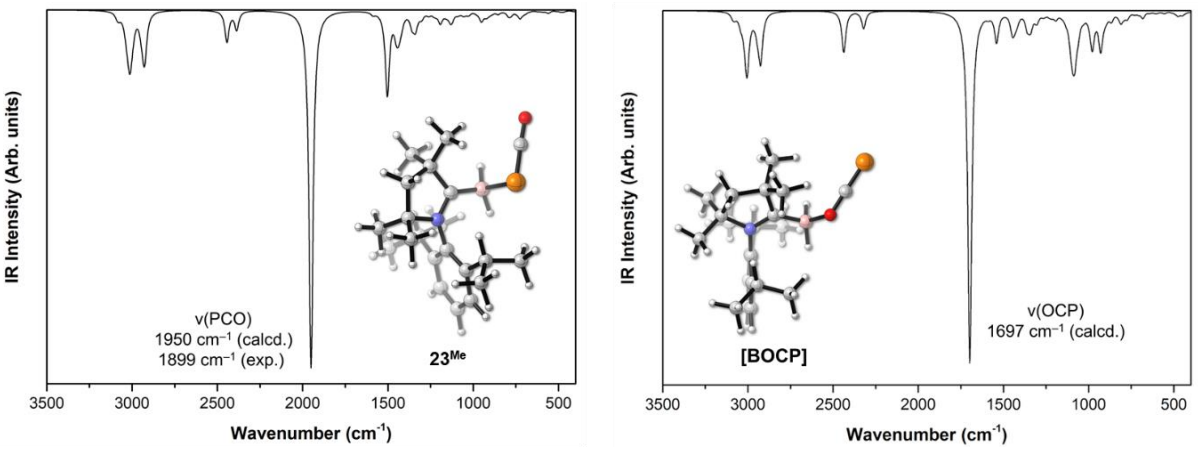

Figure 52. Computed IR spectra of **23^{Me}** (left) and the [BOCP] isomer of **23^{Me}** (right) at the PBE0-D3(BJ)/6-31+G** level of theory. A scaling factor of 0.955 was used.

Subsequent to the successful binding of the [PCO⁻] moiety to the [(CAAC^{Me})BH$_2^+$] fragment, attempts were made to convert (CAAC^{Me})BH$_2$(PCO) (**23^{Me}**) to the corresponding dibrominated compound. The desired adduct, (CAAC^{Me})BBr$_2$(PCO), could potentially provide access to phosphaketenyl-substituted borylenes, which themselves would represent interesting building blocks as highly reactive heteroallenic species. Following the syntheses of the dibrominated cyano- and isothiocyanatoboranes **XXV** and **10^{R}**, boraphosphaketene **23^{Me}** was dissolved in DCM and 2.2 equivalents of elemental bromine were added dropwise to the reaction mixture at room temperature, whereupon a strong evolution of gas was observed (Scheme 55).

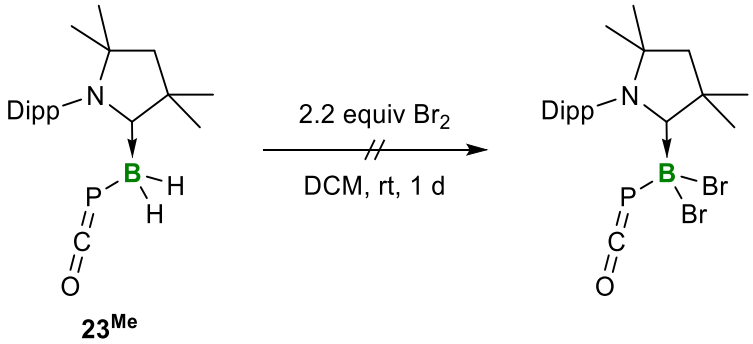

23^{Me}

Scheme 55. Attempted bromination of the boraphosphaketenes **23^{Me}**.

The resulting amber-colored solution was stirred overnight at ambient temperature, the solvent subsequently removed *in vacuo* and the resulting yellow solid washed with pentane. The ^{11}B and ^{1}H NMR spectra of a C_6D_6 solution of the isolated solid revealed the generation of (CAAC^{Me})BBr$_3$ (**VI^{Me}**), suggesting the selective cleavage of the boron–phosphorus bond of the [BPCO] fragment in **23^{Me}**. The [PCO] unit could have potentially been removed from the reaction mixture in the form of HPCO, which may have been formed by protonation of the former with HBr, generated by the bromination of **23^{Me}**. Metastable solutions of HPCO could recently be obtained by Goicoechea and co-workers by protonation of the Na[OCP] salt with stearic acid, however, rapid decomposition of the compound was observed above –50 °C.[170] Even when using alternative bromination reagents, no selective synthesis of the desired (CAAC^{Me})BBr$_2$(PCO) could be achieved in the course of this work. Consequently, further studies focused on the reactivity of the parent boraphosphaketene **23^{Me}**.

Both boraphosphaketenes **23^{Me}** and **23^{Cy}** were found to be unstable in solution, converting over time to the dimeric compounds **24^{R}** (Scheme 56). While **23^{Me}** could be isolated and stored, as mentioned above, all attempts to isolate **23^{Cy}** as a solid sample only led to the isolation of the conversion product **24^{Cy}**. The latter was obtained in 84% yield by drying, washing and recrystallizing a mixture of **1^{Cy}** and Na[OCP]. Compound **24^{Me}**, in turn, was obtained in 73% yield by storing a toluene solution of **23^{Me}** for two weeks at –30 °C (Scheme 56).

The cycloaddition products showed ^{31}P NMR-spectroscopic resonances at ca. 125 ppm. Upon conversion of **23^{R}**, the corresponding ^{11}B NMR signal shifts slightly to lower fields, concomitant with a broadening of the former triplet to a singlet resonance at –24.1 ppm (**24^{Me}**) and –23.8 ppm (**24^{Cy}**).

23^{Me} (*isolated as a solid*)
23^{Cy} (*detected in solution*)

24^{Me} (73%)
24^{Cy} (84%)

Scheme 56. Dimerization of the boraphosphaketenes **23^{R}** to the *cyclo*-C_2P_2 species **24^{R}**. Isolated yields in parentheses.

X-ray diffraction analyses authenticated compounds **24^{R}** as the *cyclo*-C_2P_2 dimers of the monomeric boraphosphaketenes **23^{R}** (Figure 53). The C_2P_2 cores of **24^{R}** are essentially isostructural with that of the dimeric organophosphaketene, [OCP(*p*-$C_6H_4OMe)_3]_2$, from Benkő and Grützmacher,[171] featuring phosphorus–carbon (P1–C2 ca. 1.85 Å) single bonds and carbonyl (C2–O1 ca. 1.20 Å) double bonds. Only the pyramidalization at the phosphorus atoms differs slightly (**24^{Me}**: Σ(∠P1) 299.2°; **24^{Cy}**: Σ(∠P1) 306.0°; [OCP(*p*-$C_6H_4OMe)_3]_2$: Σ(∠P1) 308.3°), with the highest degree of pyramidalization being observed in the least sterically hindered derivative **24^{Me}**. Unsurprisingly, the dimerization of **24^{R}** also results in the disappearance of the characteristic vibrational band of the [PCO] moiety. The solid-state IR spectra of the *cyclo*-C_2P_2 dimers exhibit characteristic CO stretching bands at 1613 cm^{-1} (**24^{Me}**) and 1606 cm^{-1} (**24^{Cy}**), respectively. The dimerization of **24^{R}** through their P=C bonds forming cycles with [BPCO] connectivity, further confirms the boraphosphaketene structure of **24^{R}**.

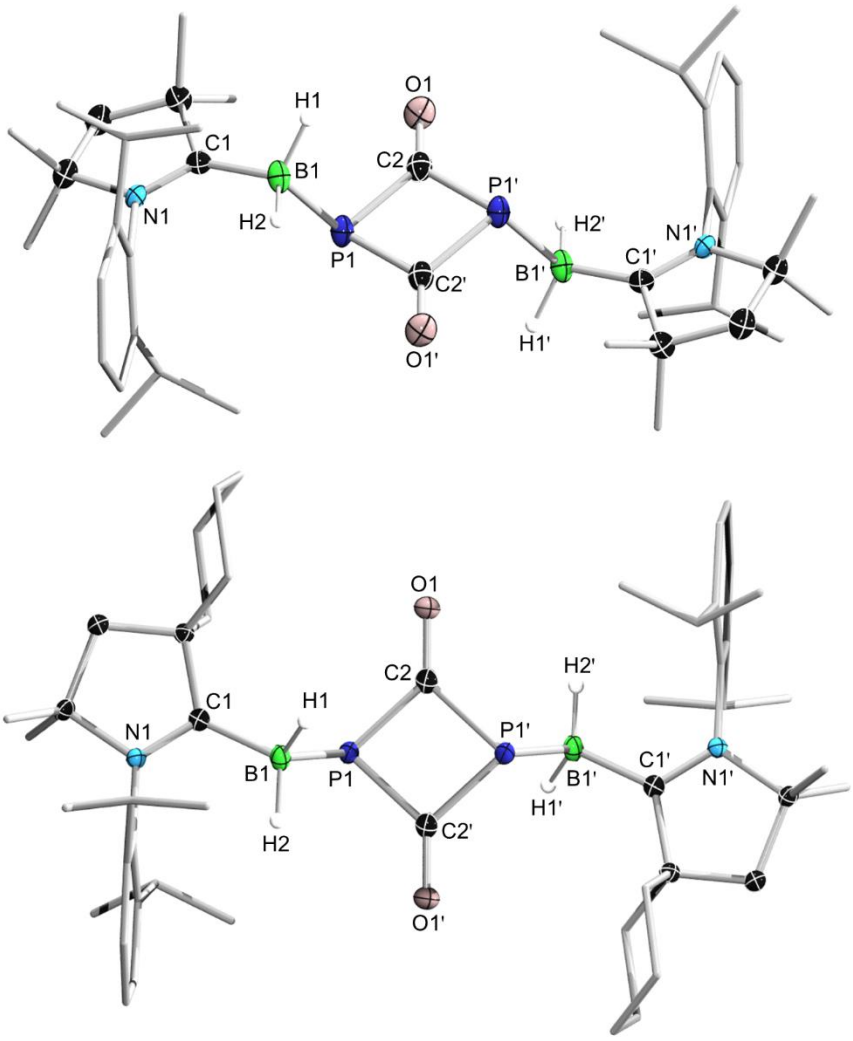

Figure 53. Crystallographically-derived molecular structures of **24^{Me}** (top) and **24^{Cy}** (bottom). Thermal ellipsoids are shown at the 50% probability level. Ellipsoids on the ligand peripheries and hydrogen atoms, except those attached to boron, omitted for clarity. Selected bond lengths (Å) and angles (°) for **24^{Me}**: N1–C1 1.300(11), C1–B1 1.559(6), B1–P1 2.0113(15), P1–C2 1.8652(13), P1–C2' 1.8561(13), C2–O1 1.2048(16), ΣP1 299.18(11); for **24^{Cy}**: N1–C1 1.303(2), C1–B1 1.604(2), B1–P1 1.9856(18), P1–C2 1.8514(16), P1–C2' 1.8463(17), C2–O1 1.2189(19), Σ(∠P1) 306.04(13).

Having the new boraphosphaketene **24^{Me}** in hand as a stable, isolated solid, its phosphinidene-generating abilities were investigated subsequently. Unfortunately, photolysis of **24^{Me}** only led to an intractable mixture of unidentifiable compounds. The decarbonylative insertion chemistry of **24^{Me}**, however, showed much more promising results, which will be discussed in the following section.

2.5.2 Synthesis of 1,2-Phosphaborinines

In 2015 Martin and co-workers reported the synthesis of the first 1,2-phosphaborinines by formal insertion of a phosphinidene derived from *cyclo*-[P_5Ph_5] into boroles.[172] Inspired by these results, the phosphinidene-like reactivity of the CAAC^{Me}-stabilized boraphosphaketene **23^{Me}** towards a range of boroles [RBC_4Ph_4] (R = Ph, 2-thienyl (Tn), Mes (Mes = 2,4,6-trimethylphenyl)) was investigated. These (hetero)arene-substituted boroles have already shown their ability to undergo a wide variety of insertion reactions and were therefore also chosen as promising substrates.[172-176] Upon addition of **23^{Me}** to benzene solutions of the boroles [RBC_4Ph_4], the intense coloration of the reaction mixture changed from deep blue and purple, respectively, to bright yellow over a course of five (R = Ph, 2-thienyl) to thirty (R = Mes) minutes, accompanied by the evolution of gas (Scheme 57).

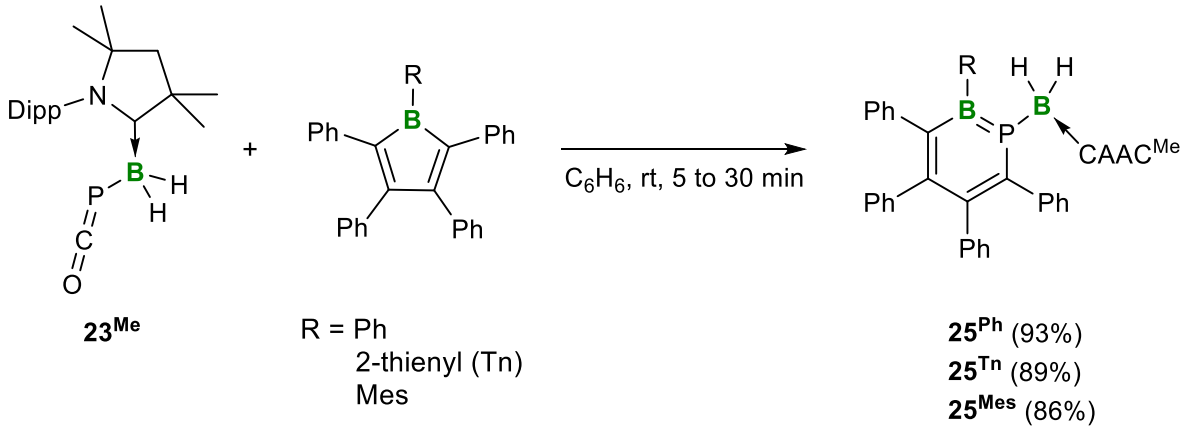

Scheme 57. Decarbonylative insertion of **23^{Me}** into boroles, yielding 1,2-phosphaborinines **25^{R}**. Isolated yields in parentheses. Mes = 2,4,6-trimethylphenyl.

Based on ^{11}B and ^{31}P NMR-spectroscopic data each reaction mixture showed the clean formation of a new product, proposed to be the expected 1,2-phosphaborinine **25^{R}**. All three of these B,P-isosteres of benzene show relatively similar ^{11}B (**25^{Ph}**: δ_{11B} = 42.8; **25^{Tn}**: δ_{11B} = 39.7; **25^{Mes}**: δ_{11B} = 45.7 ppm) and ^{31}P (**25^{Ph}**: δ_{31P} = 81.0; **25^{Tn}**: δ_{31P} = 80.4; **25^{Mes}**: δ_{31P} = 72.1 ppm) NMR resonances of their endocyclic heteronuclei, these data being in line with those of the only other known phosphaborinines reported by Martin (δ_{11B} = 38.4, 38.9 ppm; δ_{31P} = 77.6, 76.9 ppm).[172] The corresponding resonances of the exocyclic boron nuclei (**25^{Ph}**: δ_{11B} = –28.0; **25^{Tn}**: δ_{11B} = –27.9; **25^{Mes}**: δ_{11B} = –28.1 ppm) are essentially identical to each other, since they are less influenced by the varying R group. Moreover, the chemical shift of the [(CAAC^{Me})BH_2] unit in **25^{R}** does not change significantly compared to that of the carbene-stabilized boraphosphaketene **23^{Me}**. The 1,2-phosphaborinines can be isolated as yellow solids in 93% (**25^{Ph}**), 89% (**25^{Tn}**) and 86% (**25^{Mes}**) yield, respectively. The UV-vis absorption spectra of **25^{R}** recorded in benzene at room temperature exhibit one absorption band at 361 nm (**25^{Ph}**), 367 nm

(**25**^{Tn}) and 364 nm (**25**^{Mes}), respectively, accounting for their yellow color, while the 2-thienyl congener **25**^{Tn} shows an additional absorption shoulder at 320 nm (Figure 54).

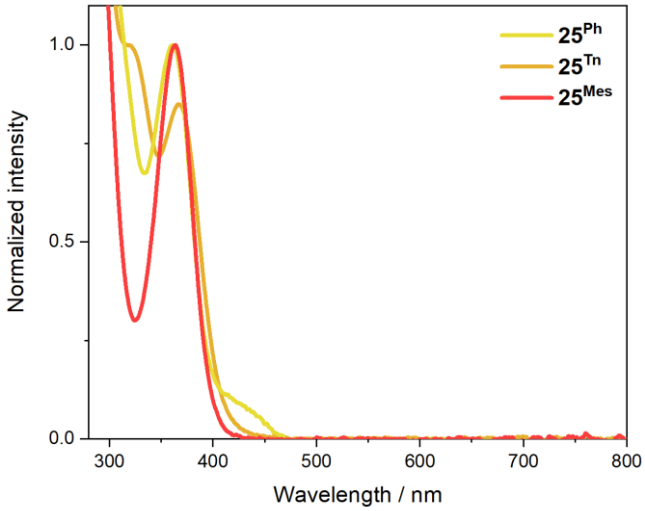

Figure 54. Overlay of UV-vis absorption spectra of **25**^{Ph} (yellow), **25**^{Tn} (orange) and **25**^{Mes} (red) in benzene at 25 °C. **25**^{Ph}: λ_{max} = 361 nm; **25**^{Tn}: λ_{max} = 320 nm (shoulder), λ = 367 nm; **25**^{Mes}: λ_{max} = 364 nm.

It is noteworthy that the room temperature reaction of the *cyclo*-P_2C_2 dimer **24**^{Me} with pentaphenylborole did not lead to the phosphaborinine **25**^{Ph}, suggesting the irreversibility of the dimerization process of **23**^{R} to **24**^{R}. Slow evaporation of a concentrated benzene solution afforded yellow single crystals of **25**^{Ph} suitable for X-ray crystallographic analysis (Figure 55).

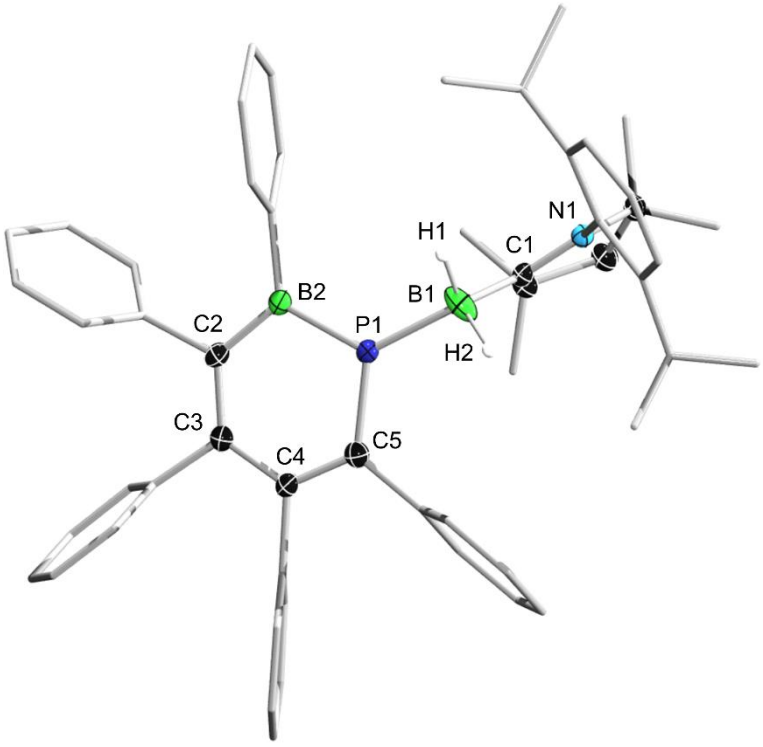

Figure 55. Crystallographically-derived molecular structure of **25**^{Ph}. Thermal ellipsoids are shown at the 50% probability level. Ellipsoids of peripheral groups and hydrogen atoms except those attached to boron have been omitted for clarity. Selected bond lengths (Å): N1–C1 1.3079(18), C1–B1 1.603(2), B1–P1 1.9568(18).

While a disorder present in the central C_4BP ring of the solid-state structure of **25^{Ph}** prevented detailed analysis of the endocyclic bonding parameters, the data unambiguously confirmed the identity of the 1,2-phosphaborinine **25^{Ph}**. The central ring in **25^{Ph}** displays a planar C_4BP unit with five phenyl groups oriented in a propeller-like fashion, as frequently observed for their lighter homologs, 1,2-azaborinines.[177] The P1–B1 bond (1.9558(18) Å) of the BH_2 substituent, stabilized by a pure σ-donating CAAC^{Me} ligand (C1–B1 1.603(2) Å), is in the typical range of a P–B single bond.

DFT calculations were performed by Dr. Felipe Fantuzzi in order to investigate both the electronic and the aromatic nature of the 1,2-phosphaborinine **25^{Ph}** computationally. While the HOMO of **25^{Ph}** is π-delocalized through the central C_4BP ring and exhibits π-bonding character in the boron–phosphorus region, the LUMO is mainly composed of the C–N π* orbital at the CAAC^{Me} ligand (Figure 56).

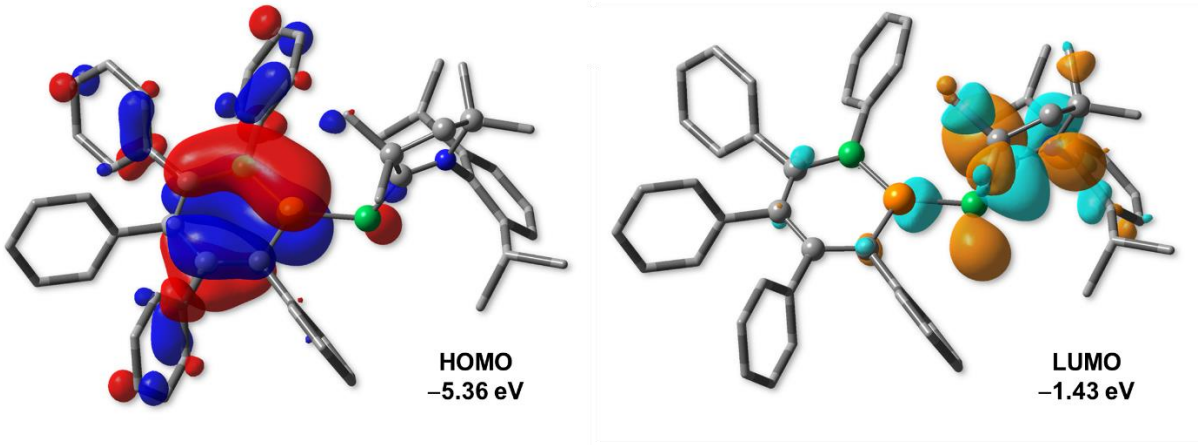

Figure 56. Canonical Kohn-Sham molecular orbitals of **25^{Ph}** at the PBE0-D3 (BJ)/6-31+G** level.

The high kinetic stability of the phosphaborinine is corroborated theoretically by a large HOMO–LUMO gap of ca. 4 eV. The ACID plot displays a clockwise, diatropic ring current flow in the central phosphaborinine core, indicating the aromatic character of the system (Figure 57, top). The aromaticity is further validated by the computed NICS values. The scan of the $NICS_{zz}$ component at points along the axis perpendicular to the ring plane above and below the ring show a similar curve for **25^{Ph}**, the parent 1,2-azaborinine C_4H_6BN and benzene (Figure 57, bottom).

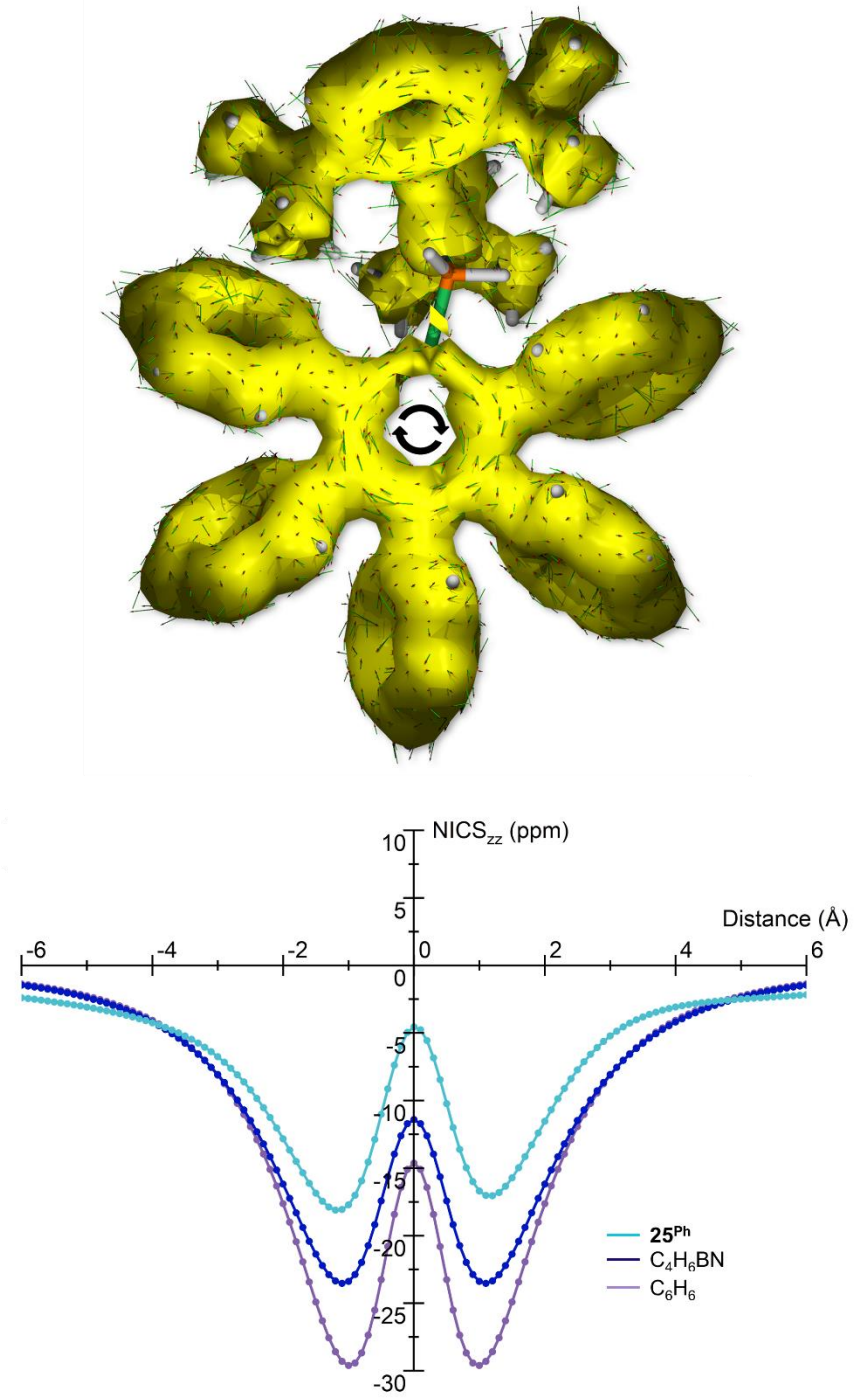

Figure 57. Calculated ACID plot (isovalue: 0.025) of **25^{Ph}** (top) and NICS$_{zz}$ scan curves of C_6H_6, C_4H_6BN and **25^{Ph}** at the PBE0-D3 (BJ)/6-311++G** level (bottom).

All three NICS$_{zz}$ scans display a minimum value in the negative NICS$_{zz}$ region. The calculated NICS(0) and NICS$_{zz}$(1) values for **25^{Ph}** are –5.48 and –16.70 ppm, respectively, and thereby less negative than those obtained for C_4H_6BN (NICS(0) = –6.81 ppm; NICS$_{zz}$(1) = –22.45 ppm) and benzene (NICS(0) = –8.24 ppm; NICS$_{zz}$(1) = –29.62 ppm). Additionally, the computed values of **25^{Ph}** are similar to those of Martin's 1,2-phosphaborinine systems.[172] Consequently, both the planarity of the central C_4BP ring and the calculated ACID and NICS plot ascribe a moderate aromatic character to **25^{Ph}**.

2.5.3 Coordination of a 1,2-Phosphaborinine to Group 6 Metal Complexes

As aromatic system with six delocalized π electrons, the 1,2-phosphaborinine **25^{Ph}** should be able to coordinate to transition metals and form piano stool complexes. In order to demonstrate the aromaticity of the 1,2-phosphaborinine core and the associated coordination ability, **25^{Ph}** was treated with group 6 complexes [M(CO)$_3$(NCMe)$_3$] (M = Cr, Mo, W). The 1,2-phosphaborinine **25^{Ph}** and the respective tris(acetonitrile) tricarbonyl metal complexes were combined in THF and the reaction mixtures were monitored *in situ* by ^{11}B and ^{31}P NMR spectroscopy. While full consumption of **25^{Ph}** was observed after stirring for two days and overnight at room temperature for the chromium and the molybdenum derivatives, respectively, the analogous reaction with [W(CO)$_3$(NCMe)$_3$] required heating at 60 °C for two days for quantitative conversion of **25^{Ph}** (Scheme 58).

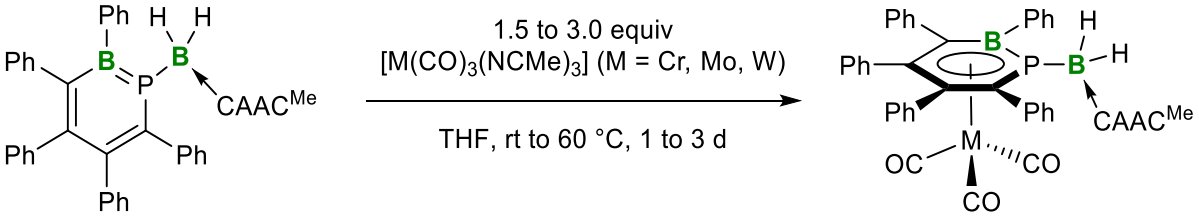

25^{Ph}

25^{Ph}-Cr (91%)
25^{Ph}-Mo (94%)
25^{Ph}-W (83%)

Scheme 58. Synthesis of π complexes of **25^{Ph}** with group 6 transition metals, yielding **25^{Ph}-M**. Isolated yields in parentheses.

After workup, the half-sandwich complexes **25^{Ph}-M** were isolated as yellow solids in 91% (M = Cr), 94% (M = Mo) and 83% (M = W) yield. The ^{11}B NMR resonances of the endocyclic boron nuclei were shifted ca. 16 ppm upfield (**25^{Ph}-Cr**: δ_{11B} = 27.5; **25^{Ph}-Mo**: δ_{11B} = 27.1; **25^{Ph}-W**: δ_{11B} = 25.2 ppm) from that of the precursor **25^{Ph}**, which is in agreement with the reported upfield shift of a 1,2-thiaborinine upon coordination to [Cr(CO)$_3$].[178] The ^{1}H NMR spectra of **25^{Ph}-M** suggested steric constraints of the CAAC^{Me} ligand periphery as the resonances split into two magnetically inequivalent sets, typical of hindered rotation. However, the detection of only one ^{13}C{^{1}H} NMR shift at 234.7 (**25^{Ph}-Cr**), 223.7 (**25^{Ph}-Mo**) and 213.8 ppm (**25^{Ph}-W**), respectively, for the three CO ligands indicated rapid rotation about the C$_4$BP ring on the NMR timescale. Furthermore, the significant upfield shift of the ^{31}P NMR resonance (**25^{Ph}-Cr**: δ_{31P} = –12.6; **25^{Ph}-Mo**: δ_{31P} = –4.59; **25^{Ph}-W**: δ_{31P} = –21.3 ppm) implied that the coordination of the central C$_4$BP ring to the metal center involves the phosphorus atom.

The UV-vis absorption spectra of the phosphaborinine-metal complexes **25^{Ph}-M** in benzene each display an absorption maximum at 346 nm (**25^{Ph}-Cr**), 347 nm with a shoulder at 405 nm (**25^{Ph}-Mo**), and 342 nm (**25^{Ph}-W**), respectively, which is in line with their intense yellow coloration (Figure 58).

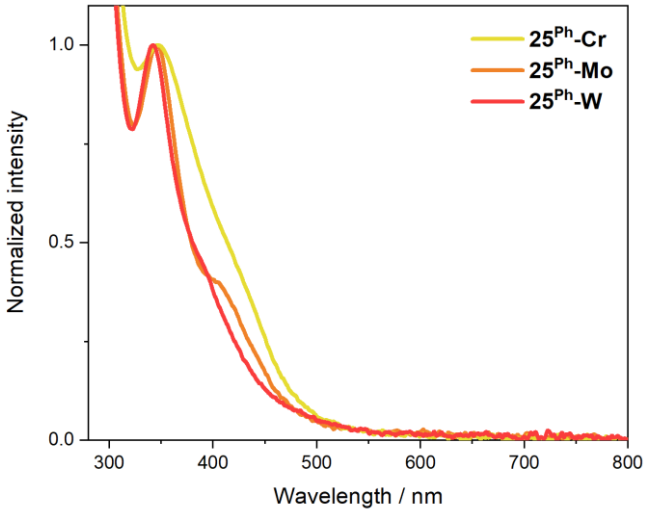

Figure 58. Overlay of UV-vis absorption spectra of **25^{Ph}-Cr** (yellow), **25^{Ph}-Mo** (orange) and **25^{Ph}-W** (red) in benzene at 25 °C. **25^{Ph}-Cr**: λ_{max} = 346 nm; **25^{Ph}-Mo**: λ_{max} = 347 nm, λ = 405 nm (shoulder); **25^{Ph}-W**: λ_{max} = 342 nm.

Slow evaporation of a saturated benzene solution afforded yellow single crystals of **25^{Ph}-Cr** suitable for X-ray crystallographic analysis (Figure 59). The solid-state structure of **25^{Ph}-Cr** confirmed the η^6 coordination of the C_4BP core with a centroid···Cr1 distance of 1.709 Å between the planar 1,2-phosphaborinine ring and the chromium center. The phosphorus atom shows some small degree of pyramidalization (Σ(∠P1) 354.8(2)°), consequently the exocyclic BH_2 unit is slightly bent towards the chromium center.

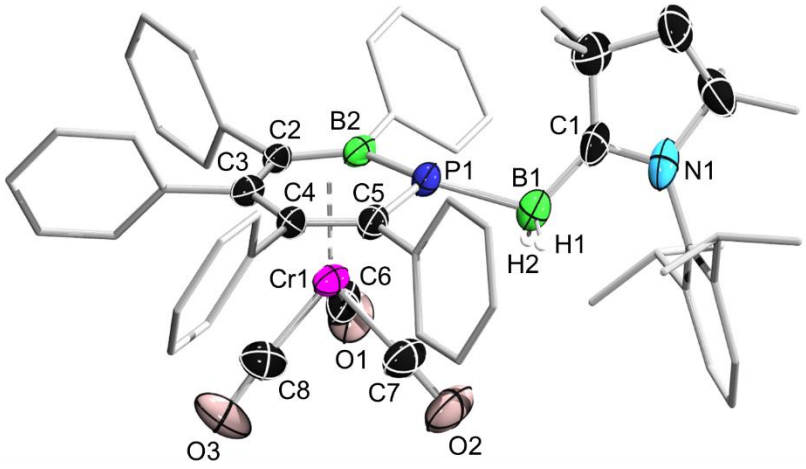

Figure 59. Crystallographically-derived molecular structure of **25^{Ph}-Cr**. Thermal ellipsoids are shown at the 50% probability level. Ellipsoids of peripheral groups and hydrogen atoms, except those attached to boron, have been omitted for clarity. Selected bond lengths (Å) and angles (°): N1–C1 1.311(5), C1–B1 1.567(7), B1–P1 1.985(5), P1–B2 1.832(4), B2–C2 1.504(5), C2–C3 1.417 (5), C3–C4 1.449(4), C4–C5 1.447(5), C5–P1 1.780(4), Centroid···Cr1 1.709, Cr1–C_{avg} 1.831, C_{avg}–O_{avg} 1.172, Σ(∠P1) 354.8(2), ΣB2 359.8(6), B2–P1–C5 106.84(17).

It is worth mentioning that the outstanding ligand properties of the C_4BP unit apparently compensate the steric repulsion of the bulky phenyl substituents, which has often prevented the coordination of similar perarylated (hetero)arenes to transition metals.[178,179] In order to further quantify the ligand strength of the 1,2-phosphaborinine **25^{Ph}**, solid-state IR spectra of complexes **25^{Ph}-M** were recorded, revealing sets of CO vibrational bands (**25^{Ph}-Cr**: $\tilde{\nu}$(CO) = 1936, 1872, 1880 cm^{-1}; **25^{Ph}-Mo**: $\tilde{\nu}$(CO) = 1943, 1855 cm^{-1}; **25^{Ph}-W**: $\tilde{\nu}$(CO) = 1936, 1870, 1845 cm^{-1}) with significantly lower frequencies than those of the 1,2-azaborinine chromium complex ($\tilde{\nu}$(CO) = 1979, 1916, 1900 cm^{-1}) reported by Ashe.[180] Furthermore, the C–O stretching frequencies of **25^{Ph}-M** are even lower than those of Martin's thiaborinine–$Cr(CO)_3$ complex ($\tilde{\nu}$(CO) = 1964, 1908, 1873 cm^{-1}),[178] which is indicative of much stronger backdonation from the 1,2-phosphaborinine-metal fragment into the π* orbitals of the CO ligands. The remarkable ability of the C_4BP core in **25^{Ph}** to coordinate in a η^6 fashion was also corroborated experimentally by heating C_6H_6 solutions of **25^{Ph}-M** to 80 °C over a course of one week. In contrast to Martin's thiaborinine–$Cr(CO)_3$ complex,[178] no signs of decomposition were observed.

The excellent stability of the phosphaborinine-metal complexes **25^{Ph}-M**, as well as the benzene analogue [(η^6-C_6H_6)$Cr(CO)_3$] for comparison, were further investigated theoretically by computational methods. The complexation energies of **25^{Ph}** with the respective [$M(CO)_3$] fragment (M = Cr, Mo, W) is described by the total energy Δ*E*, which is composed of strain (ΔE_{strain}) and interaction (ΔE_{int}) contributions (Equation 2).

$$\Delta E = \Delta E_{strain} + \Delta E_{int} \qquad (2)$$

The computed ΔE_{int} value of –73.3 kcal mol^{-1} for [(η^6-C_6H_6)$Cr(CO)_3$] is slightly reduced by a small ΔE_{strain} contribution of +3.8 kcal mol^{-1}, which is mainly caused by structural distortions of the benzene ligand. Thus, the resulting complexation energy is –69.5 kcal mol^{-1}, which is in good agreement with previously reported values.[181,182] For the phosphaborinine-metal complexes ΔE_{strain} reaches values up to +15.7 kcal mol^{-1}. However, strong ΔE_{int} contributions compensate not only the repulsive effects, but also dictate the more stabilizing role of the C_4BP core in **25^{Ph}** with respect to benzene. Consequently, the computed complexation energies of the **25^{Ph}-M** systems, being –85.6 kcal mol^{-1} (**25^{Ph}-Cr**), –82.2 kcal mol^{-1} (**25^{Ph}-Mo**) and –98.8 kcal mol^{-1} (**25^{Ph}-W**), respectively, are significantly larger than that of the benzene congener.

III Summary

The first part of this thesis deals with the synthesis of the boronium cations **2-L** (L = CAAC^{Me}, IMe^{Me}, PMe$_3$, DMAP, Pyr) by the displacement of the triflate group of **1^{Me}** by various Lewis bases (Scheme 59a). The addition of two equivalents of pyridine and DMAP to **1^{Me}** further induced a boron-to-CAAC hydrogen shuttling, forming the bis(Lewis-base) adducts **3-L** (L = DMAP, Pyr) (Scheme 59b).

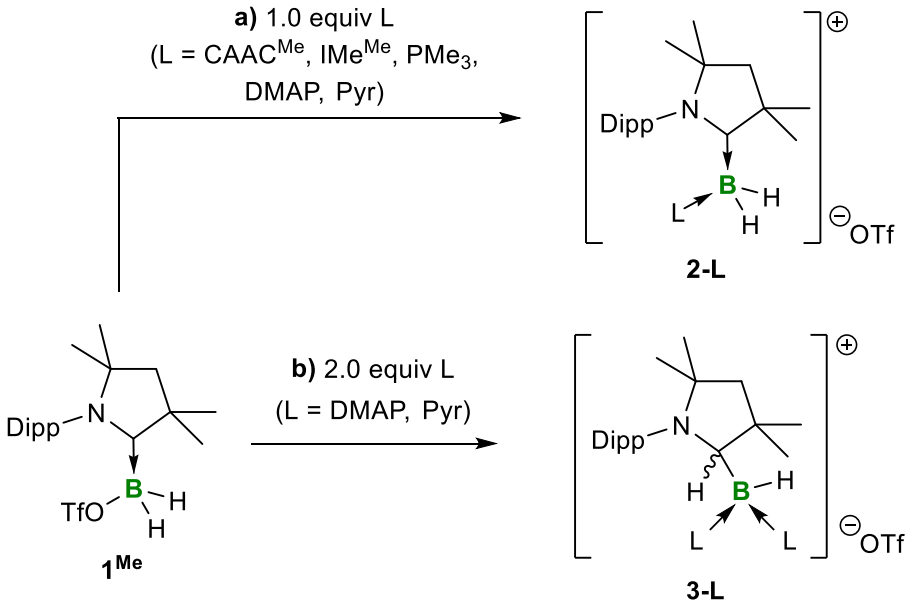

Scheme 59. Synthesis of the base-stabilized boronium cations **2-L** and **3-L**.

While attempts to reduce **2-L** and **3-L** under various conditions all resulted in unselective reactions, the twofold reduction of **2-CAAC^{Me}** cleanly yielded, depending on the solvent used, the (alkyl)hydroboryl anions **5** and **5-thf**, by 1,2-migration of a hydride from boron to the adjacent carbene carbon atom of one CAAC^{Me} ligand (Scheme 60a-c). X-ray crystallographic analyses of **5** and **5-thf** revealed monomeric structures, in which the potassium cation bound to the B*H* hydride is stabilized through η^6 π interactions with two (**5**) or one Dipp substituents and additional THF molecules (**5-thf**). The boryl anions **5** and **5-thf** have shown to predominantly react as one-electron reducing agent. Thus, the comproportionation of equimolar amounts of **2-CAAC^{Me}** and **5-thf** afforded the neutral hydroboryl radical **8**, isolated crystals of which proved air-stable, owing to the unique stereoelectronic properties of the two encapsulating CAAC^{Me} ligands (Scheme 60d).

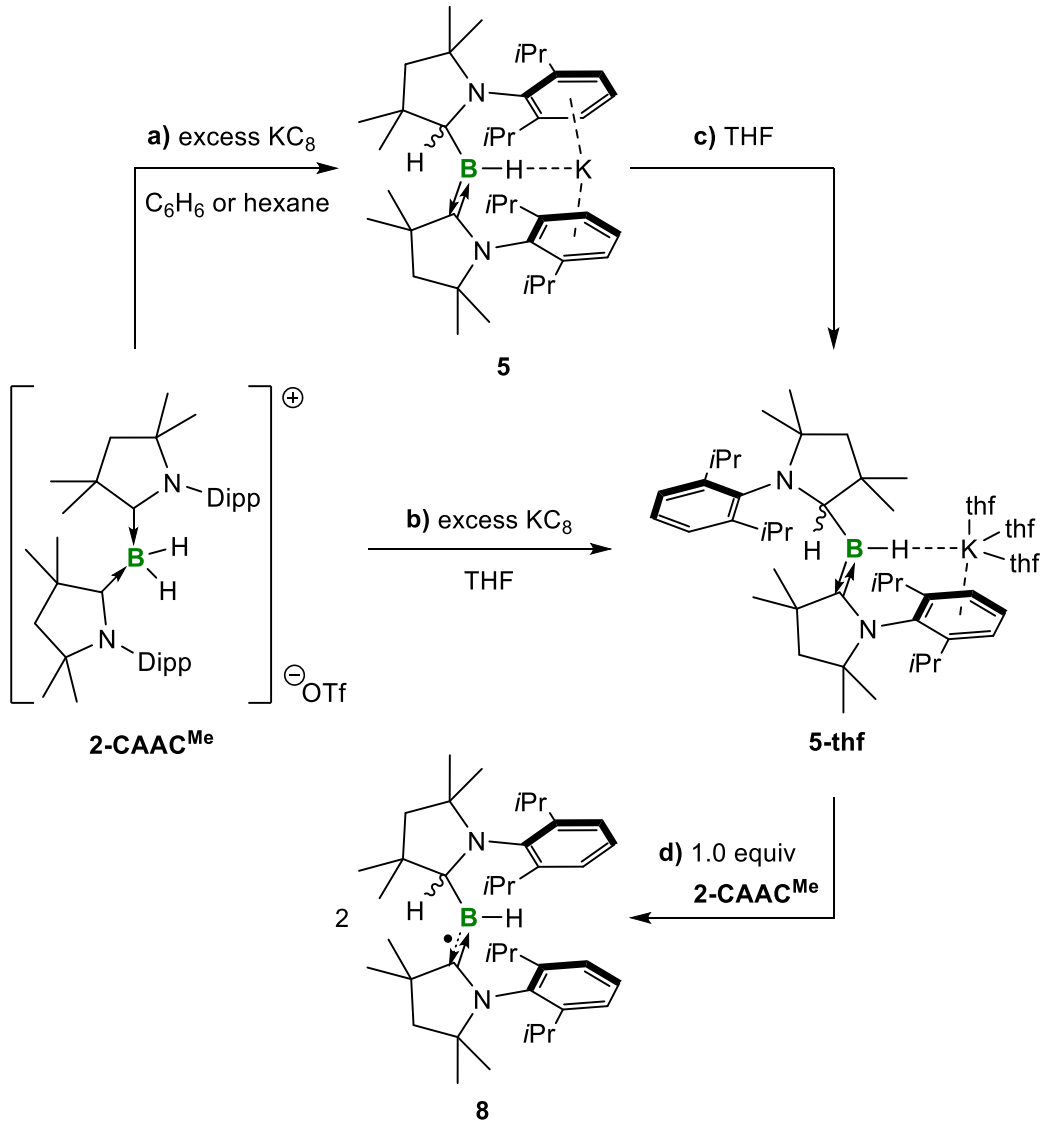

Scheme 60. Reduction of boronium cation **2-CAAC^{Me}** to the boryl anions **5** (**a**) and **5-thf** (**b** + **c**), and subsequent comproportionation to the hydroboryl radical **8** (**d**).

The reaction of **5** with elemental sulfur led to double oxidation back to the boronium cation [(CAAC^{Me})$_2$BH$_2^+$] (**7**), the counteranion presumably being a S_n^{2-} polysulfide, highlighting the reversibility of the 1,2-hydrogen shift. The boron-centered nucleophilicity of the boryl anion **5** was demonstrated by its reactivity towards MeOTf, resulting in the isolation of the methylated trialkylborane **6** by migration of the second hydride to the remaining CAAC^{Me} ligand.

The next chapter focuses on the synthesis and reactivity of tricoordinate isothiocyanato- und cyanoborylenes of the form (CAAC^R)(I*i*Pr)BY (R = Me, Cy; Y = NCS, CN). The CAAC^R-stabilized isothiocyanatoboranes **9^R** were obtained *via* salt elimination of NaSCN with the respective triflatoborane precursors **1^R** and subsequent bromination, generating the corresponding (CAAC^R)BBr$_2$(NCS) adducts **10^R**. The twofold reduction of **10^R** and of the literature-known cyano derivative **XXV** with KC$_8$ in the presence of the NHC I*i*Pr resulted in

the formation of the unsymmetrical doubly Lewis-base-stabilized pseudohaloborylenes **11^{R}** (Y = NCS) and **12** (Y = CN), respectively (Scheme 61).

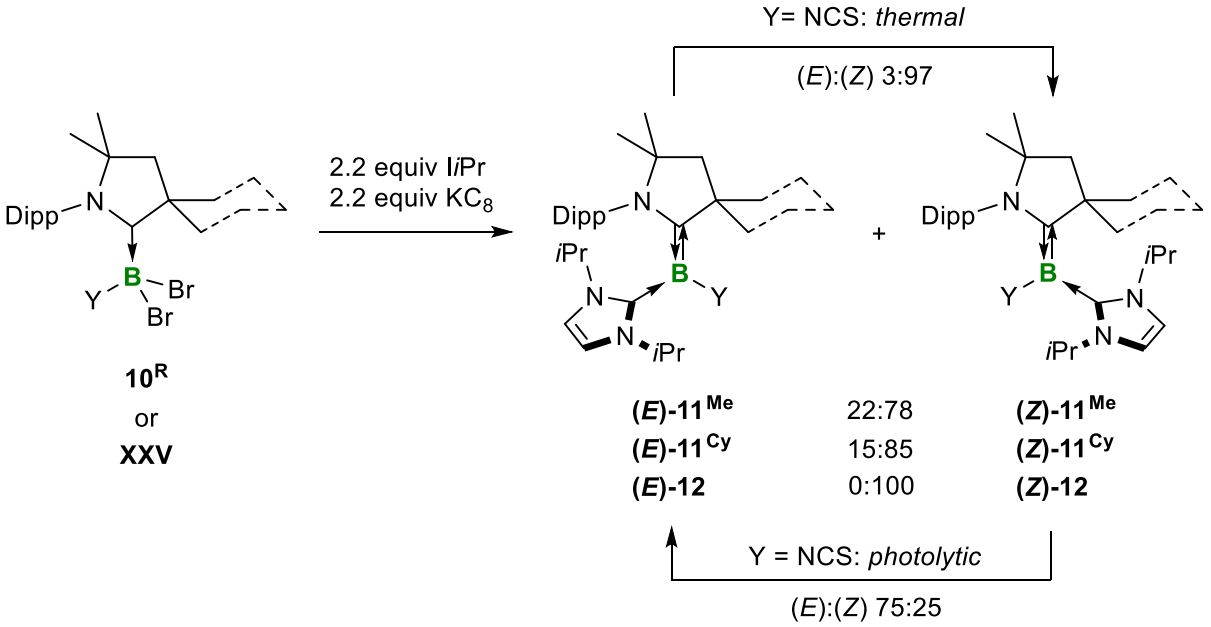

Scheme 61. Synthesis and isomerization of the isothiocyanato- and cyanoborylenes **11^{R}** and **12**.

While the cyanoborylene **12** was exclusively obtained as the (*Z*)-isomer, the isothiocyanatoborylenes **(*E*)/(*Z*)-11^{R}** were formed as a mixture of (*E*)/(*Z*)-isomers, which could not only be separated by fractional crystallization but also partially converted into each other under thermal ((*E*)→(*Z*)) and photolytic ((*Z*)→(*E*)) conditions. The cyclovoltammograms of **(*Z*)-11^{Me}** and **12** suggested that selective (reversible) one-electron oxidation of the borylenes is possible. Indeed, the room temperature reactions of **(*Z*)-11^{Me}** and **12** with exactly one equivalent of Ag[OTf] afforded the corresponding pseudohaloboryl radical cations **[(*Z*)-11$^{Me\bullet+}$][OTf^{-}]** and **[12$^{\bullet+}$][OTf^{-}]** (Scheme 62a). The oxidation proved to be fully reversible upon addition of KC_8, quantitatively regenerating the borylenes **(*Z*)-11^{Me}** and **12** (Scheme 62b).

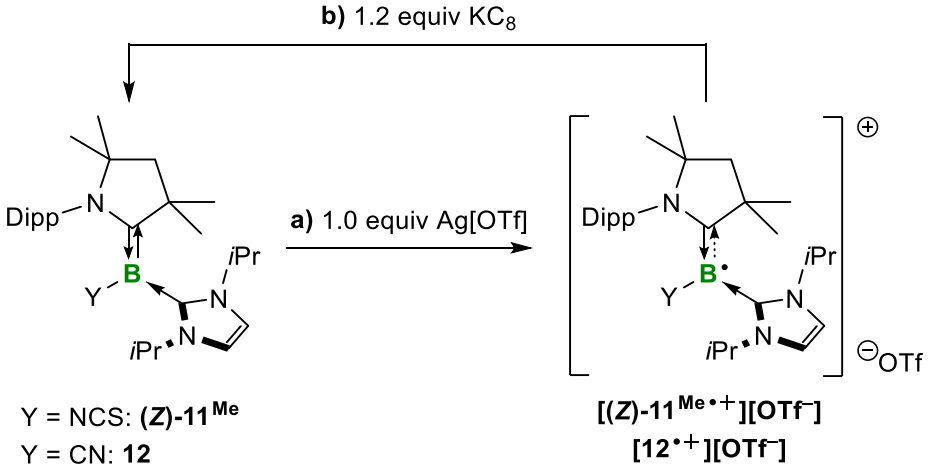

Scheme 62. Reversible chemical one-electron oxidation of the pseudohaloborylenes **(*Z*)-11^{Me}** and **12** to the corresponding boryl radical cations **[(*Z*)-11$^{Me\bullet+}$][OTf^{-}]** and **[12$^{\bullet+}$][OTf^{-}]**.

Computational analyses performed by Dr. Felipe Fantuzzi revealed that the HOMO of the tricoordinate pseudohaloborylenes **(*Z*)-11^{Me}** and **12** is delocalized over the [(N–C)$_{CAAC}$–B–Y] framework, with a major π-bonding contribution at the C$_{CAAC}$–B bond. While the borylene center bears a slightly negative partial charge, the main negative charge is located at the terminal sulfur and nitrogen atoms of the isothiocyanato and cyano substituent, respectively. As a consequence, **(*Z*)-11^{Me}** and **12** act as neutral sulfur-/nitrogen- rather than boron-centered donor ligands towards group 6 carbonyls, as reactions with [M(CO)$_5$(thf)] (M = Cr, Mo, W) provided the corresponding transition-metal borylene complexes **11^{Me}-M** and **12-M** (Scheme 63).

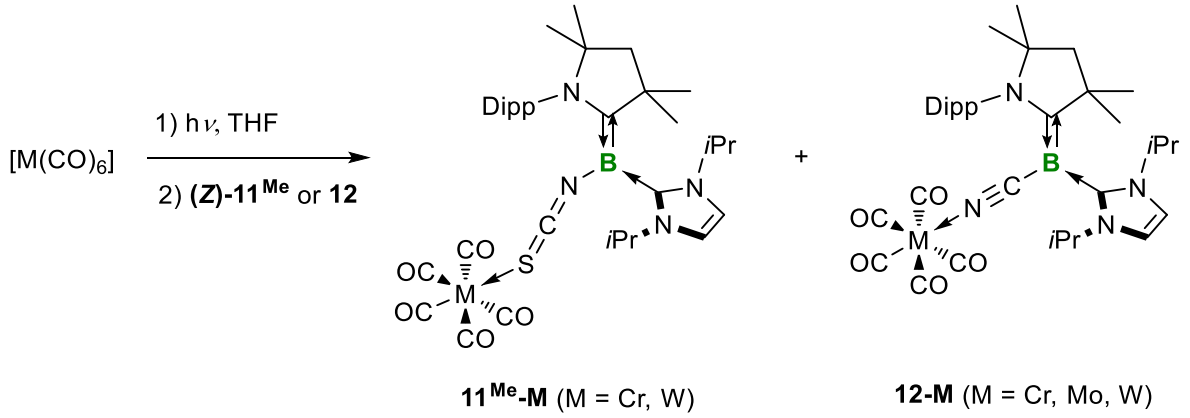

Scheme 63. Adduct formation between the pseudohaloborylenes **(*Z*)-11^{Me}** and **12** and group 6 hexacarbonyls, yielding **11^{Me}-M** and **12-M**.

The boron-centered nucleophilicity of the borylenes **(*Z*)-11^{Me}** and **12** was demonstrated by their protonation with relatively weakly acidic thiophenol. The protonation of **(*Z*)-11^{Me}** at boron is driven by a B-to-C$_{CAAC}$ hydrogen shuttling and the irreversible nucleophilic attack of the thiophenolate anion at the boron center, yielding compound **14^{NCS}** (Scheme 64a,b). Further treatment of either **(*Z*)-11^{Me}** or **14^{NCS}** with an excess of thiophenol at 60 °C selectively afforded the dithiolatoborane **15** alongside the imidazolium salt [I*i*Pr-H][NCS] as a byproduct (Scheme 64c,d). The reaction of the cyanoborylene **12** with thiophenol, in turn, yielded the protonated boronium species **13^{CN}**, the formation of which proved to be fully reversible, even in the solid state (Scheme 64a,e). Calculations revealed that both pseudohaloborylenes have in fact similar proton affinities (ca. 268 kcal mol^{-1}), of the same order as the inorganic superbase CsOH or unsaturated NHCs.

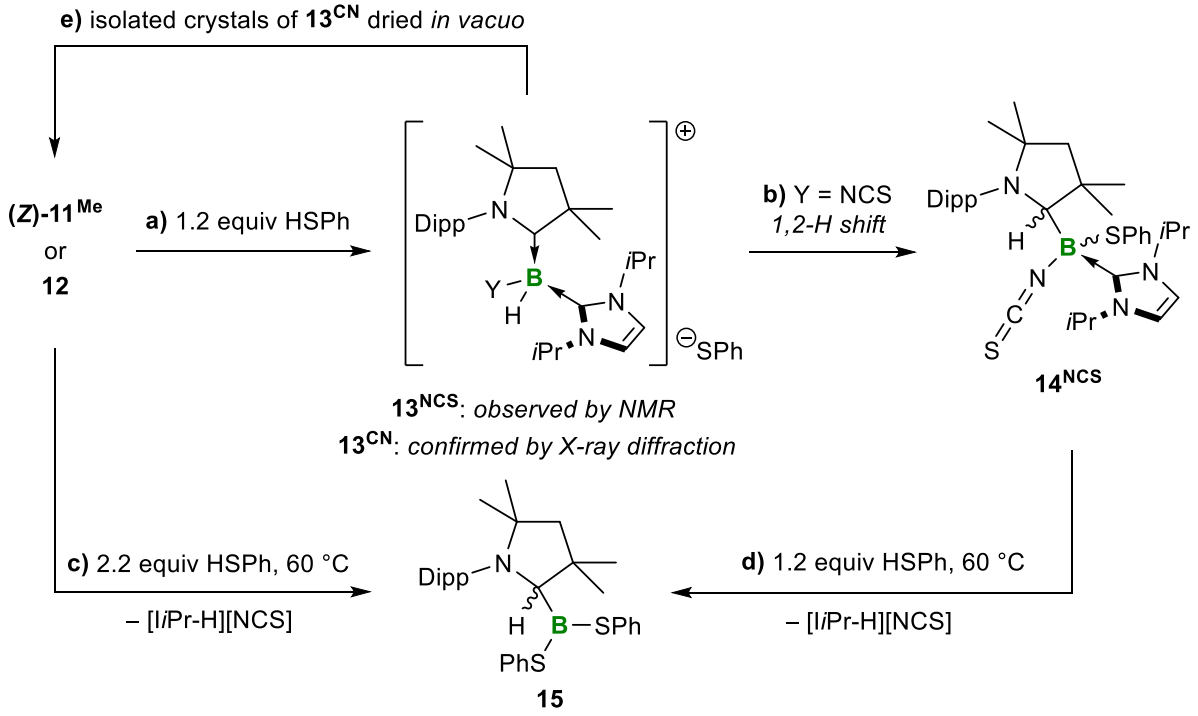

Scheme 64. Irreversible and reversible protonation of **(*Z*)-11^{Me}** and **12**, respectively, with thiophenol.

In the third chapter of this work the reduction of the (CAAC^{R})BBr$_2$(NCS) precursors **10^{R}** in the absence of a second stabilizing Lewis base is described. The reaction of **10^{R}** with KC_8 yielded the CAAC^{R}-stabilized, fused [1,3,2]thiazaborolo[5,4-*d*]-[1,3,2]thiazaboroles **16^{R}** through the reductive dimerization and C–C coupling of transient isothiocyanatoborylenes (Scheme 65). DFT calculations showed that the HOMO of **16^{Me}** is delocalized across the entire (NCBNC)$_2$ scaffold with the exclusion of the sulfur atoms. As a result, a weak but distinct aromatic character can be attributed to these deep blue-colored B,N,S-heterocycles **16^{R}** on the basis of the computed ACID and their NICS values.

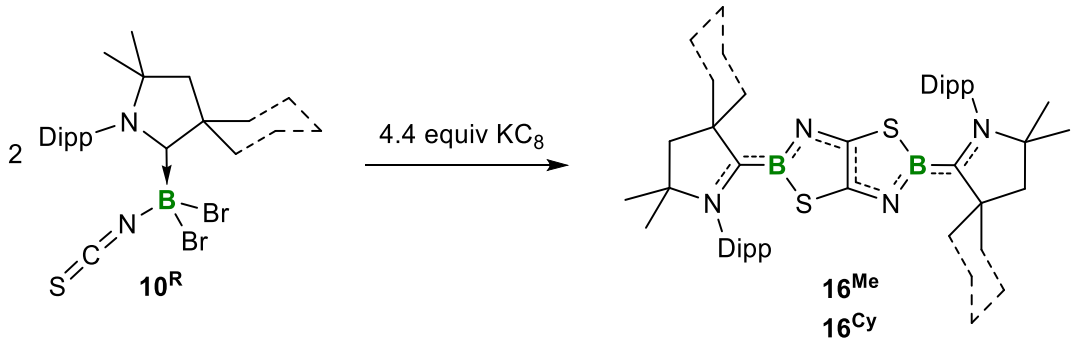

Scheme 65. Reductive cyclization of **16^{R}** in the absence of a Lewis base.

Subsequently, the coordination properties and reactivity of **16^{Cy}** towards Brønsted acids was investigated. By treatment of **16^{Cy}** with [Cu(C$_6$F$_5$)]$_4$ the purple complex **17** was obtained, in which the endocyclic nitrogen atoms coordinate to one copper fragment each (Scheme 66a). Given the *N*-centered nucleophilic nature in **16^{Cy}** and the associated color change upon its

coordination, the next consideration was that the protonation of the endocyclic nitrogen atoms could lead to interesting changes in the optoelectronic properties of **16^{Cy}**. Indeed, the twofold protonation of **16^{Cy}** with various Brønsted acids resulted in the formation of the dicationic species **18-X** (Scheme 66b).

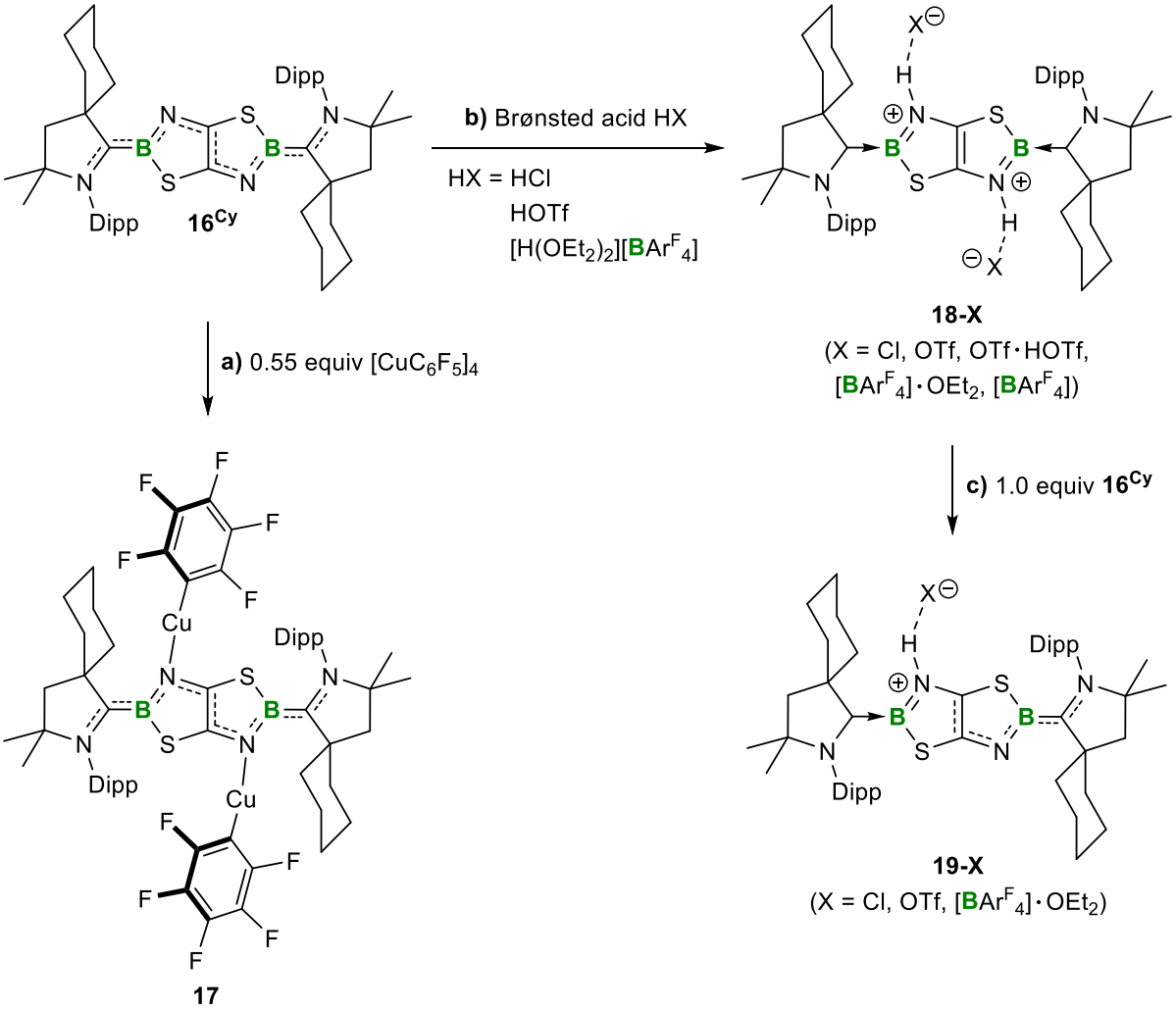

Scheme 66. a) Coordination of Cu(C_6F_5) to **16^{Cy}**. Double (**b**) and single (**c**) protonation of **16^{Cy}** with selected Brønsted acids.

Depending on the strength of the X···H hydrogen bonding, the visible and fluorescence colors of **18-X** varied from red (X = Cl) *via* orange (X = OTf, OTf·HOTf) to yellow ([BAr^F_4]·Et_2O, [BAr^F_4]). The comproportionation of the neutral B,N,S-heterocycle **16^{Cy}** and diprotonated **18-X** selectively provided the corresponding monocations **19-X**, which exhibit intermediate photophysical properties (Scheme 66c).

After the successful protonation of the thiazaborolo[5,4-*d*]thiazaborole **16^{Cy}**, the next step was to investigate whether **16^{Cy}** also reacts with other E–H bonds. While all attempts to perform hydroelementation reactions with primary and secondary silanes, amines and phosphines failed, the hydroboranes HBCat and 9-BBN were found to add cleanly to the B=N double bonds in

16^{Cy}, concomitant with a 1,2-hydride migration from boron to the carbene carbon atom, yielding the hydroboration products **20**^{BCat} and **20**^{BBN} (Scheme 67).

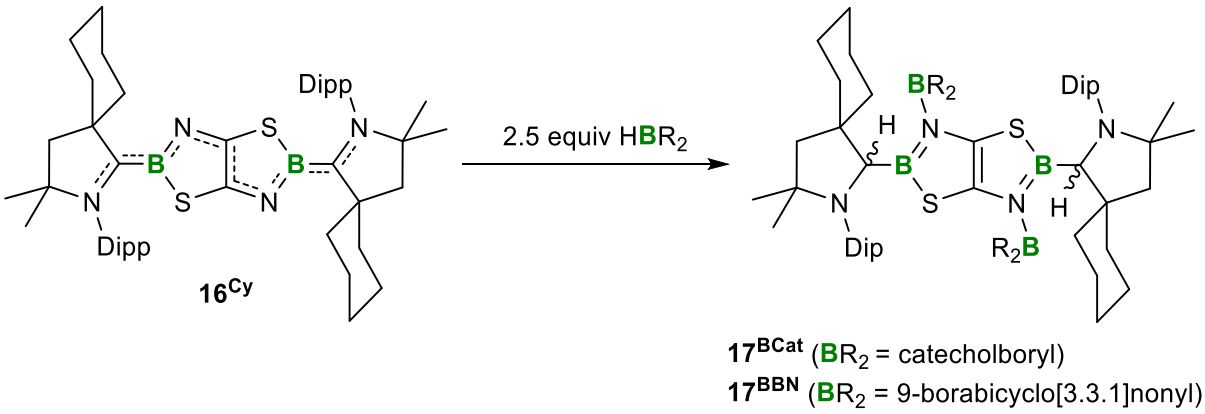

Scheme 67. Formal 1,3-hydroboration of the B,N,S-heterocycle **16**^{Cy}, yielding **20**^{BCat} and **20**^{BBN}.

Motivated by the results obtained with cyano- and isothiocyanato-substituted boranes and borylenes, another aim of this work was to introduce other pseudohalide substituents. Therefore, the triflatoborane **1**^{Me} was treated with several isocyanide, cyanate and azide sources, attempting the generation of (CAAC^{Me})BH$_2$Y (Y = NC, NCO, N$_3$). In addition to a partly unselective formation of the desired products (CAAC^{Me})BH$_2$Y, their workup and isolation, in particular, were problematic, which is why these routes were not investigated further. While the desired [(CAAC^{Me})BH$_2$(NC)] connectivity could be obtained by the reaction of **1**^{Me} with Na[Cr(CO)$_5$(CN)], yielding the chromium borane adduct **21**, subsequent cleavage of the metal carbonyl fragment from **21** failed. In another attempt to obtain the desired pseudohaloborylenes, salt elimination reactions were attempted on a haloborylene precursor. The reduction of (CAAC^{Me})BBr$_3$ (**VI**^{Me}) in the presence of I*i*Pr afforded bromoborylene **22** (Scheme 68a). Subsequent treatment of **22** with several pseudohalide sources either did not show any consumption of the starting borylene **22** or resulted in intractable mixtures of unidentifiable products (Scheme 68b). The synthesis of pseudohaloborylenes with isocyanato and azido functionalities, respectively, thus remained unsuccessful in the course of this work.

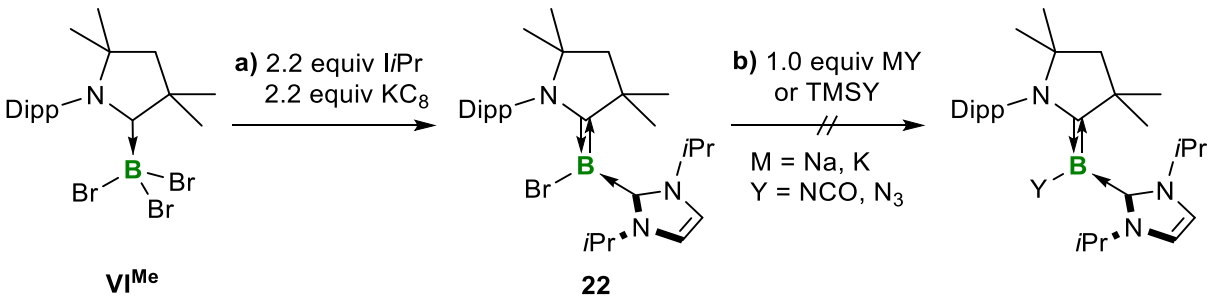

Scheme 68. a) Synthesis of the tricoordinate bromoborylene **22**. **b)** Attempts to synthesize isocyanato- and azidoborylenes by bromide-pseudohalide exchange at **22**.

Finally, in the last chapter of this work the synthesis and reactivity of $CAAC^R$ adducts of the parent boraphosphaketene is described. Bonding of the 2-phosphaethynolate anion to boron was achieved by nucleophilic substitution at the triflatoboranes **1^R** with Na[OCP] (Scheme 69).

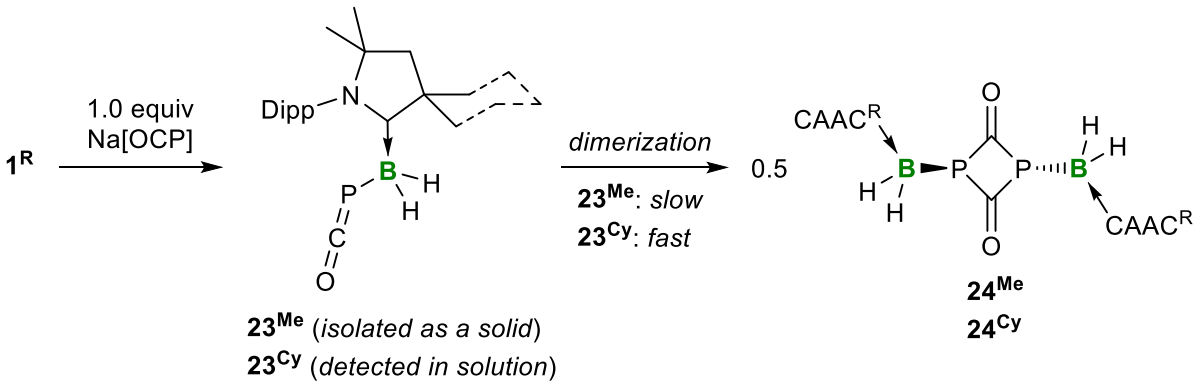

Scheme 69. Synthesis of the $CAAC^R$-stabilized boraphosphaketenes **23^R** and their dimers **24^R**. Isolated yields in parentheses.

The resulting boraphosphaketenes **23^R** were found to be unstable in solution, converting over time to their *cyclo*-C_2P_2 dimers **24^R**. However, monomeric **23^{Me}** could be isolated and stored as solid, allowing for the exploration of its phosphinidene-generating abilities. Combining **23^{Me}** with a range of boroles [RBC_4Ph_4] (R = Ph, 2-thienyl (Tn), Mes) at room temperature formally led to the decarbonylative insertion of the phosphinidene [($CAAC^{Me}$)BH_2P] into the borole ring and isolation of the 1,2-phosphaborinines **25^R** (R = Ph, Tn, Mes) (Scheme 70).

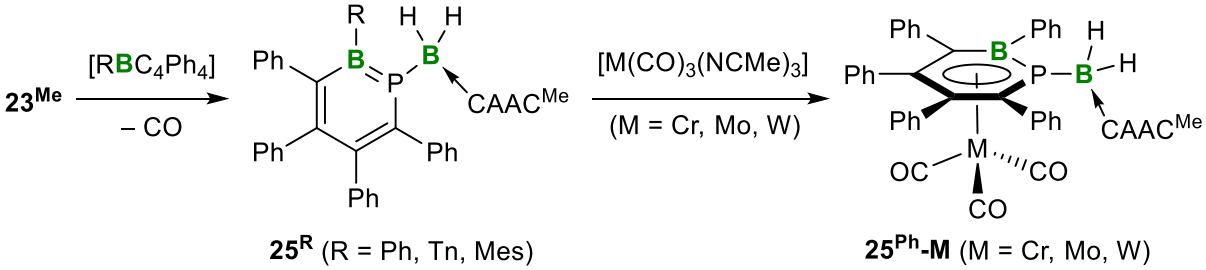

Scheme 70. Synthesis of the 1,2-phosphaborinines **25^R** and π complexes of **25^{Ph}** with group 6 transition metals, yielding **25^{Ph}-M**.

These B,P-isosteres of benzene show a moderate degree of aromaticity as indicated by the computed ACID and the NICS values of **25^{Ph}**. Accordingly, the 1,2-phosphaborinine **25^{Ph}** is capable of coordinating to group 6 tricarbonyl complexes in a η^6 fashion, forming the half-sandwich complexes **25^{Ph}-M** (M = Cr, Mo, W). Solid-state IR spectroscopy performed on the π complexes **25^{Ph}-M** and DFT calculations on **25^{Ph}** revealed that these B,P-heteroaromatics are significantly stronger donor ligands than their lighter 1,2-azaborinine homologues.

IV Zusammenfassung

Der erste Teil dieser Arbeit beschäftigt sich mit der Synthese der Boroniumkationen **2-L** (L = CAAC^{Me}, IMe^{Me}, PMe$_3$, DMAP, Pyr) mittels Verdrängung der Triflatgruppe von **1^{Me}** durch verschiedene Lewis-Basen (Schema 1a). Die Zugabe von zwei Äquivalenten von Pyridin oder DMAP zu **1^{Me}** induzierte darüber hinaus eine Bor-zu-CAAC-Wasserstoffwanderung unter Ausbildung der zweifachen Lewis-Basen-Addukte **3-L** (L = DMAP, Pyr) (Schema 1b).

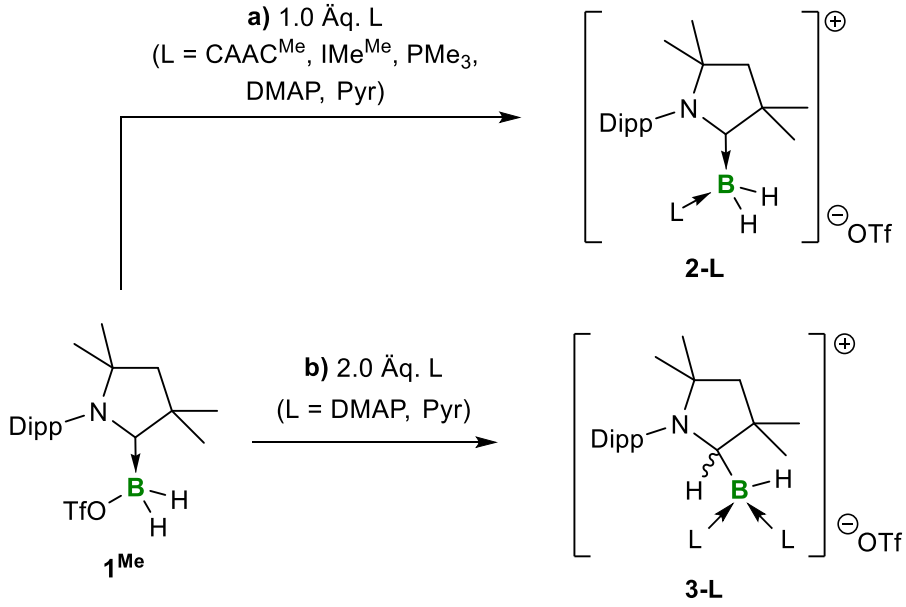

Schema 1. Synthese der Basen-stabilisierten Boroniumkationen **2-L** und **3-L**.

Während alle Versuche, **2-L** und **3-L** unter verschiedensten Bedingungen zu reduzieren in unselektiven Reaktionen resultierten, lieferte die zweifache Reduktion von **2-CAAC^{Me}** in Abhängigkeit des verwendeten Lösungsmittels die (Alkyl)hydroborylanionen **5** und **5-thf**, deren Bildung über eine 1,2-Wanderung eines Hydrids vom Boratom zum benachbarten Carbenkohlenstoffatom des CAAC^{Me}-Liganden verläuft (Schema 2a-c). Röntgenstruktur-analysen an **5** und **5-thf** offenbarten jeweils eine monomere Struktur, in denen das an das B*H*-Hydrid gebundene Kaliumkation mittels η^6-π-Wechselwirkungen mit zwei (**5**) oder einem Dipp-Substituenten sowie zusätzlichen THF-Molekülen (**5-thf**) stabilisiert wird. Die Borylanionen **5** und **5-thf** zeigten, dass diese vorrangig als ein-Elektronenreduktionsmittel reagieren. Dementsprechend ergab die Komproportionierung äquimolarer Mengen von **2-CAAC^{Me}** und **5-thf** das neutrale Hydroborylradikal **8**, wobei sich isolierte Kristalle der Verbindung aufgrund der einzigartigen stereoelektronischen Eigenschaften der beiden einkapselnden CAAC^{Me}-Liganden als luftstabil erwiesen (Schema 2d).

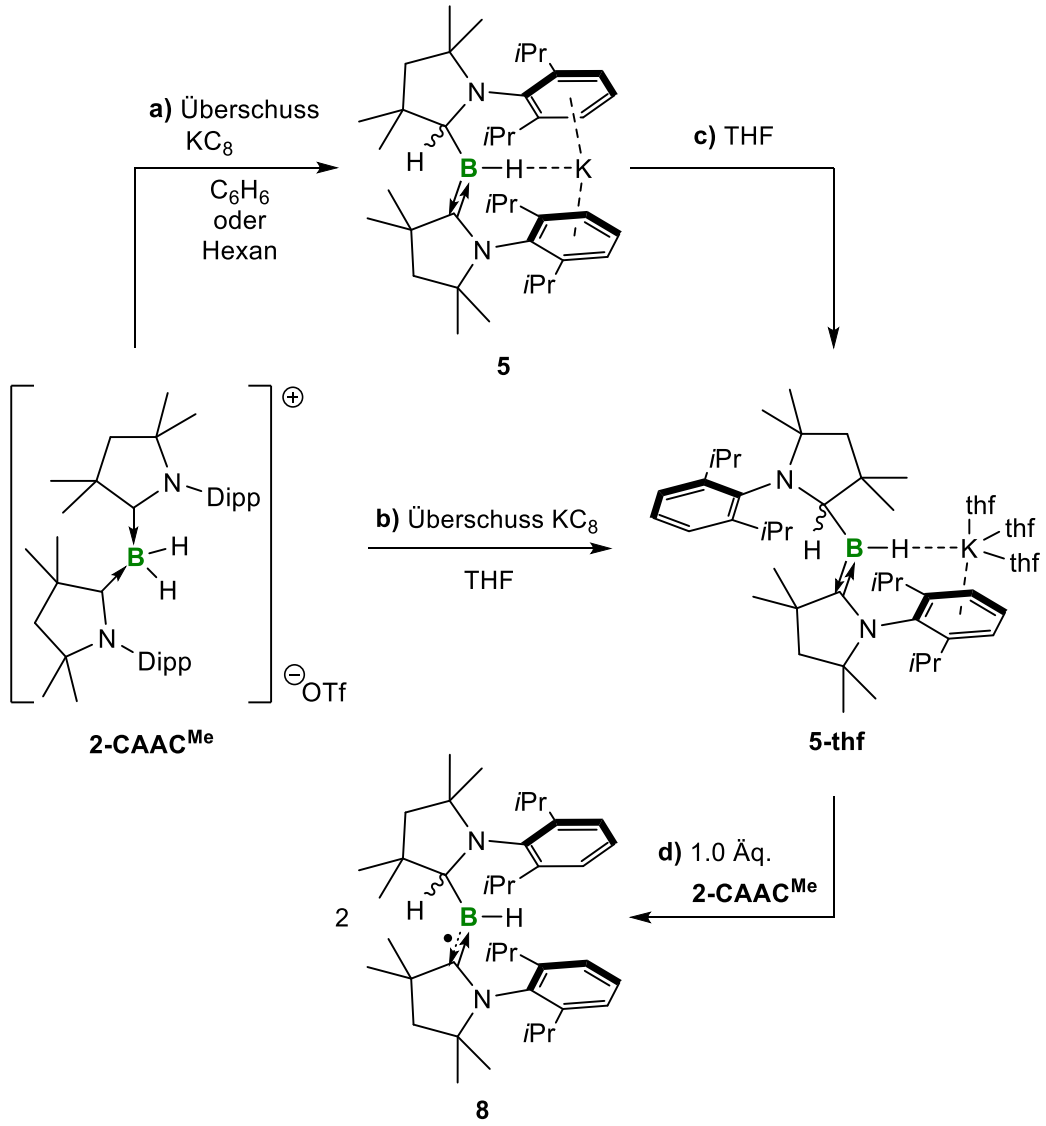

Schema 2. Reduktion des Boroniumkations **2-CAAC^{Me}** zu den Borylanionen **5** (**a**) und **5-thf** (**b** + **c**) sowie die anschließende Komproportionierung zum Hydroborylradikal **8** (**d**).

Die Reaktion von **5** mit elementarem Schwefel führte zur doppelten Oxidation zurück zum Boroniumkation [(CAAC^{Me})$_2$BH$_2^+$] (**7**), dessen Gegenion vermutlich ein S_n^{2-}-Polysulfid darstellt, was die Reversibilität der 1,2-Wasserstoffwanderung hervorhebt. Die Bor-zentrierte Nucleophilie des Borylanions **5** wurde mit dessen Reaktivität gegenüber MeOTf demonstriert, wobei hier durch Wanderung des zweiten Hydrids zum verbleibenden CAAC^{Me}-Liganden das methylierte Trialkylboran **6** isoliert werden konnte.

Das nächste Kapitel fokussiert sich auf die Synthese und Reaktivität dreifach koordinierter Isothiocyanato- und Cyanoborylene der Form (CAAC^R)(I*i*Pr)BY (R = Me, Cy; Y = NCS, CN). Die CAAC^R-stabilisierten Isothiocyanatoborane **9^R** wurden mithilfe einer Salzeliminierung aus NaSCN und den Triflatoboranvorläufern **1^R** sowie deren anschließender Bromierung zu den

entsprechenden Addukten (CAAC^{R})BBr$_2$(NCS) (**10^{R}**) erhalten. Die zweifache Reduktion von **10^{R}** und des literaturbekannten Cyanoderivats **XXV** mit KC_8 in Gegenwart des NHCs I*i*Pr resultierte in der Bildung der unsymmetrischen zweifach Lewis-Basen-stabilisierten Pseudohalogenborylene **11^{R}** (Y = NCS) beziehungsweise **12** (Y = CN) (Schema 3).

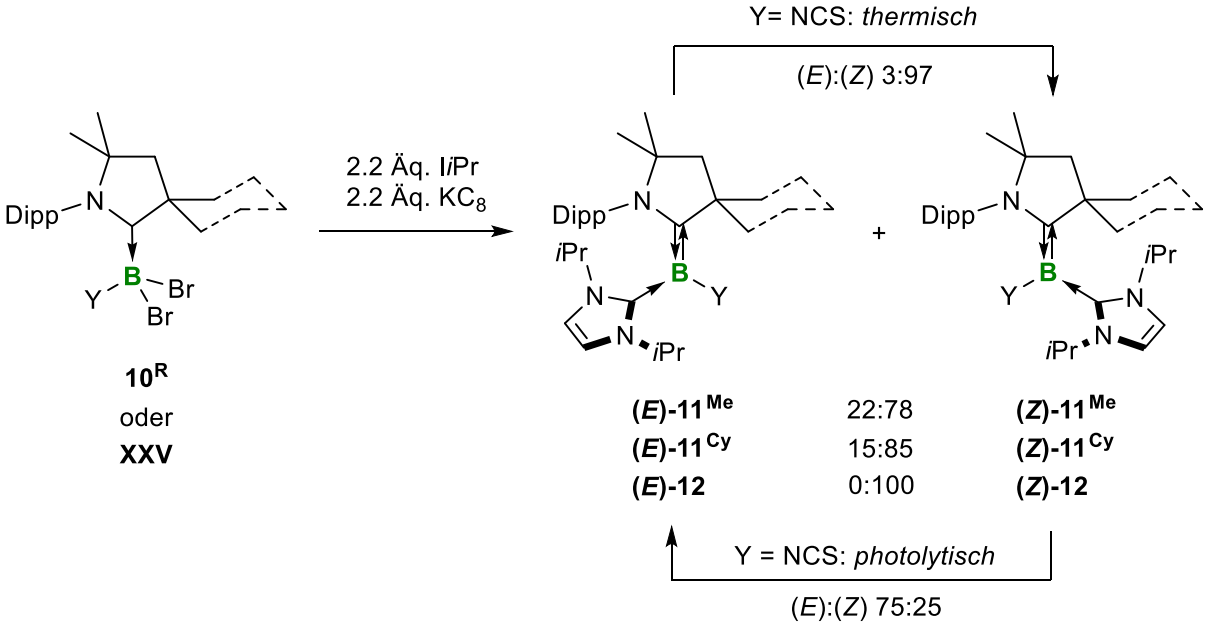

Schema 3. Synthese und Isomerisierung der Isothiocyanato- und Cyanoborylene **11^{R}** und **12**.

Während das Cyanoborylen **12** ausschließlich als (*Z*)-Isomer erhalten wurde, bildeten sich die Isothiocyanatoborylene **(*E*)/(*Z*)-11^{R}** als Gemisch von (*E*)/(*Z*)-Isomeren, welche nicht nur mittels fraktionierter Kristallisation getrennt, sondern unter thermischen ((*E*)→(*Z*)) und photolytischen ((*Z*)→(*E*)) Bedingungen auch partiell ineinander überführt werden konnten. Die Cyclovoltammogramme von **(*Z*)-11^{Me}** und **12** deuteten darauf hin, dass eine selektive (reversible) ein-Elektronenoxidation der Borylene möglich ist. Tatsächlich lieferten die Reaktionen von **(*Z*)-11^{Me}** and **12** mit genau einem Äquivalent Ag[OTf] bei Raumtemperatur die entsprechenden Pseudohalogenborylradikalkationen **[(*Z*)-11$^{Me\bullet+}$][OTf^{-}]** und **[12$^{\bullet+}$][OTf^{-}]** (Schema 4a). Die Oxidation erwies sich durch die Zugabe von KC_8 als vollständig reversibel, wobei quantitativ die Borylene **(*Z*)-11^{Me}** und **12** zurückerhalten wurden (Schema 4b).

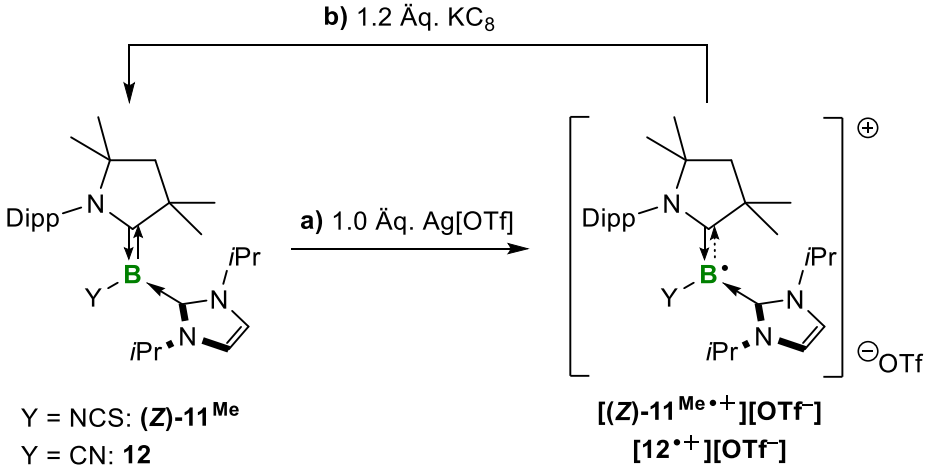

Schema 4. Reversible chemische Ein-Elektronenoxidation der Pseudohalogenborylene **(*Z*)-11^{Me}** und **12** zu den entsprechenden Borylradikalkationen **[(*Z*)-11$^{Me•+}$][OTf$^–$]** und **[12$^{•+}$][OTf$^–$]**.

Von Dr. Felipe Fantuzzi durchgeführte theoretische Rechnungen zeigten, dass das HOMO der dreifach koordinierten Pseudohalogenborylene **(*Z*)-11^{Me}** und **12** mit einem großen Beitrag der C_{CAAC}–B-Bindung über das [(N–C)$_{CAAC}$–B–Y]-Gerüst delokalisiert ist. Obwohl das Borylenzentrum eine geringfügig negative Partialladung trägt, ist der Hauptteil der negativen Ladung an den terminalen Schwefel- und Stickstoffatomen des Isothiocyanato- beziehungsweise Cyanosubstituenten lokalisiert. Folglich reagieren **(*Z*)-11^{Me}** und **12** vorrangig als neutrale Schwefel-/Stickstoff-zentrierte und nicht als Bor-zentrierte Donorliganden gegenüber Gruppe 6 Carbonylen, da Reaktionen mit [M(CO)$_5$(thf)] (M = Cr, Mo, W) die entsprechenden Übergangsmetall-Borylenkomplexe **11^{Me}-M** und **12-M** lieferten (Schema 5).

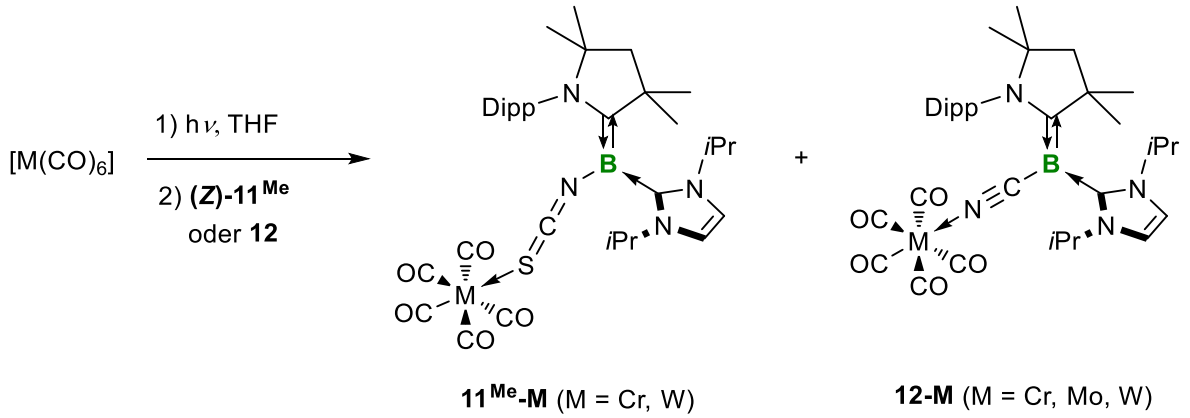

Schema 5. Adduktbildung zwischen den Pseudohalogenborylenen **(*Z*)-11^{Me}** und **12** und Gruppe 6 Hexacarbonylen zu **11^{Me}-M** und **12-M**.

Die Bor-zentrierte Nucleophilie der Borylene **(*Z*)-11^{Me}** und **12** wurde mithilfe ihrer Protonierung durch relativ schwach acides Thiophenol demonstriert. Die Protonierung von **(*Z*)-11^{Me}** am Boratom wird durch eine B-zu-C_{CAAC}-Wasserstoffwanderung und den irreversiblen nucleophilen Angriff des Thiophenolatanions am Borzentrum vorangetrieben, was

zu Verbindung **14**^{NCS} führt (Schema 6a,b). Die weitere Umsetzung von **(*Z*)-11**^{Me} oder **14**^{NCS} mit einem Überschuss an Thiophenol bei 60 °C lieferte neben dem Imidazoliumsalz [I*i*Pr-H][NCS] als Nebenprodukt selektiv das Dithiolatoboran **15** (Schema 6c,d). Im Gegensatz dazu führte die Reaktion des Cyanoborylens **12** mit Thiophenol zur protonierten Boroniumspezies **13**^{CN}, dessen Bildung sich sogar im Festkörper als vollständig reversibel erwies (Schema 6a,e). Rechnungen zufolge haben beide Pseudohalogenborylene tatsächlich ähnliche Protonaffinitäten (ca. 268 kcal mol^{-1}), die in der gleichen Größenordnung wie die der anorganischen Superbase CsOH und ungesättigter NHCs liegen.

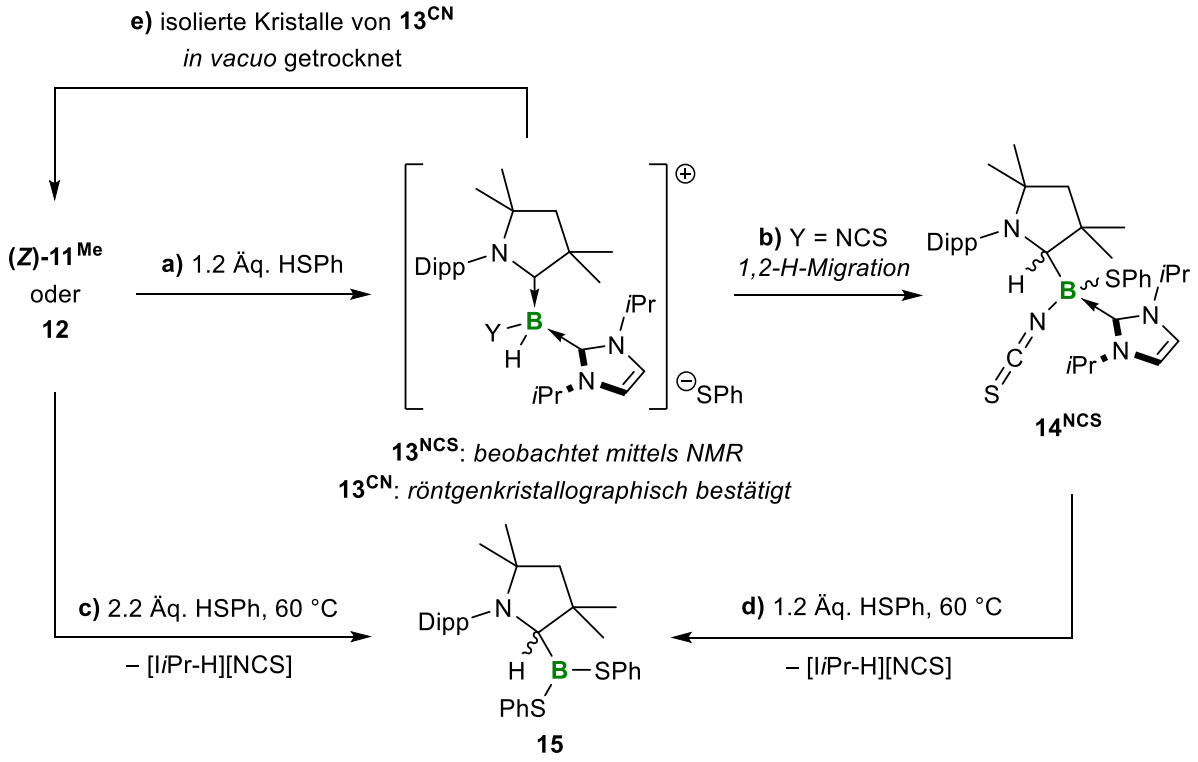

Schema 6. Irreversible und reversible Protonierung von **(*Z*)-11**^{Me} beziehungsweise **12** mit Thiophenol.

Im dritten Kapitel dieser Arbeit ist die Reduktion der (CAAC^{R})BBr$_2$(NCS) Vorstufen **10**^{R} in Abwesenheit einer zweiten stabilisierenden Lewis-Base beschrieben. Die Reaktion von **10**^{R} mit KC_8 lieferte die CAAC^{R}-stabilisierten, fusionierten [1,3,2]Thiazaborolo[5,4-*d*]-[1,3,2]thiazaborole **16**^{R} mittels reduktiver Dimerisierung und C–C-Knüpfung von transienten Isothiocyanatoborylenen (Schema 7). DFT-Rechnungen zeigten, dass das HOMO von **16**^{Me} über das gesamte $(NCBNC)_2$-Gerüst unter Ausschluss der Schwefelatome delokalisiert ist. Als Konsequenz kann den tiefblau gefärbten B,N,S-Heterocyclen **16**^{R} auf Basis der berechneten Anisotropie der induzierten Stromdichte (ACID) und der Kern-unabhängigen chemischen Verschiebungen (NICS) ein schwacher, aber ausgeprägter aromatischer Charakter zugeschrieben werden.

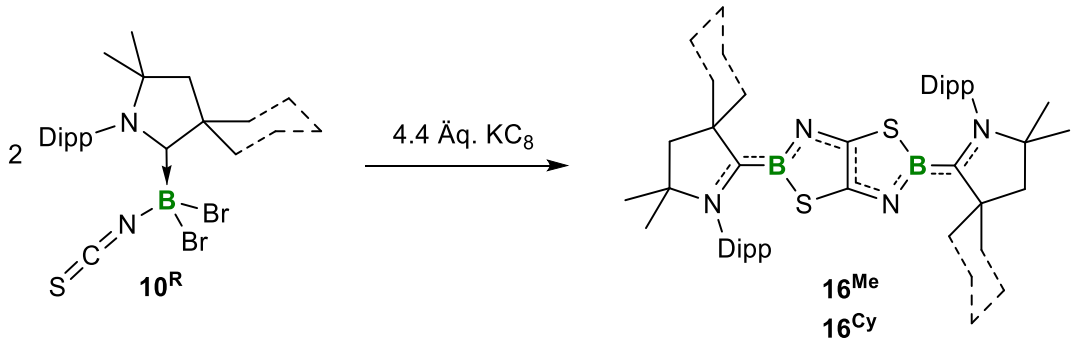

Schema 7. Reduktive Cyclisierung von **16^{R}** in Abwesenheit einer Lewis-Base.

Im Anschluss wurde das Koordinationsvermögen sowie die Reaktivität des B,N,S-Heteroaromaten **16^{Cy}** gegenüber Brønsted-Säuren untersucht. Bei der Umsetzung von **16^{Cy}** mit $[Cu(C_6F_5)]_4$ wurde der violette Komplex **17** erhalten, in dem die endocyclischen Stickstoffatome jeweils an ein Kupferfragment koordinieren (Schema 8a).

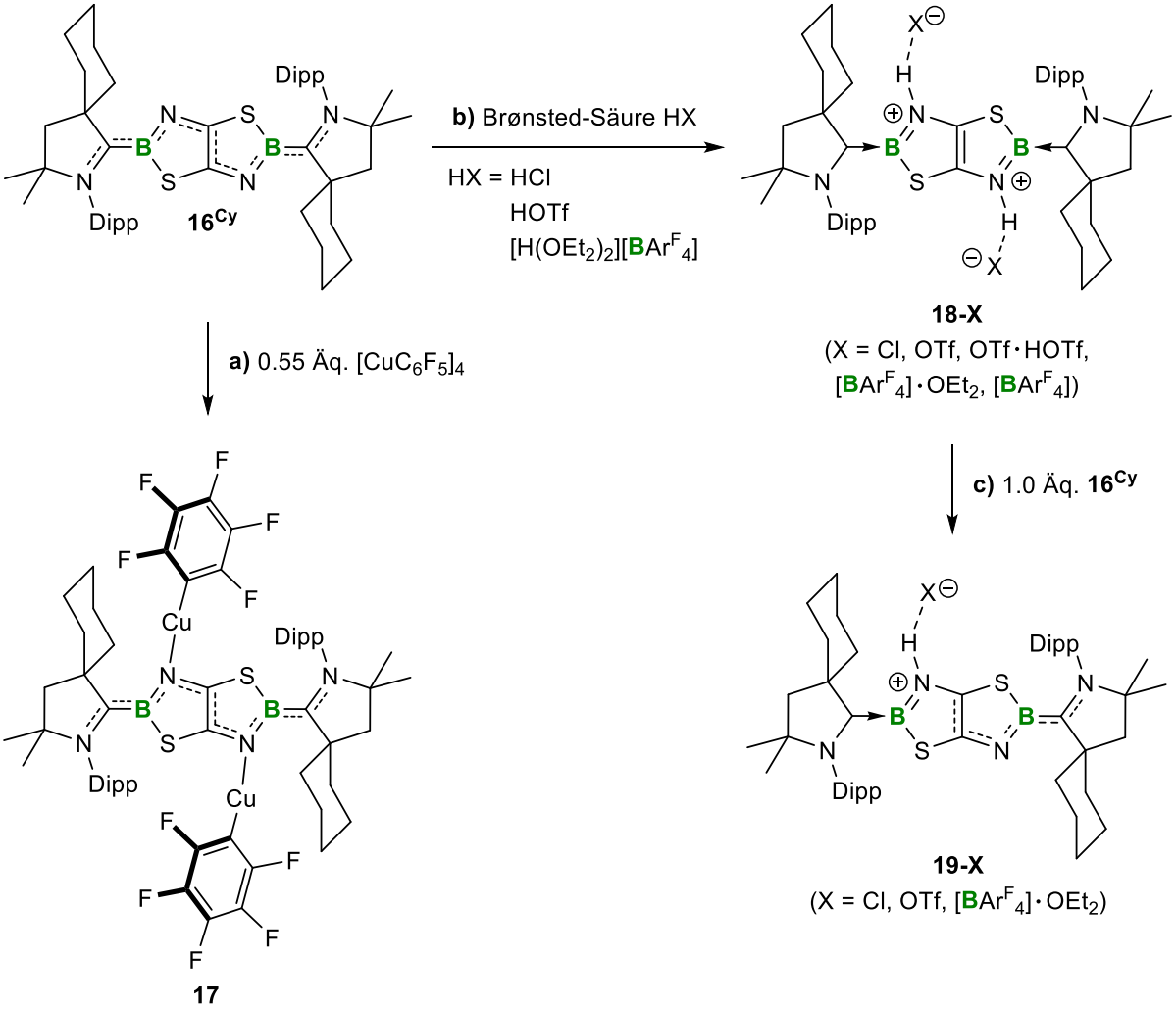

Schema 8. a) Koordination von $Cu(C_6F_5)$ an **16^{Cy}**. Doppelte (**b**) und einfache (**c**) Protonierung von **16^{Cy}** mit ausgewählten Brønsted-Säuren.

Aufgrund der *N*-zentrierten nucleophilen Natur von **16^{Cy}** und der mit der Koordination verbundenen Farbänderung war die nächste Überlegung, dass die Protonierung der endocyclischen Stickstoffatome zu interessanten Änderungen der optoelektronischen Eigenschaften von **16^{Cy}** führten könnten. Tatsächlich resultierte die zweifache Protonierung von **16^{Cy}** mit verschiedenen Brønsted-Säuren in der Bildung der dikationischen Spezies **18-X** (Schema 8b). In Abhängigkeit der Stärke der X···H-Wasserstoffbrückenbindung variierten die beobachtbare Farbe sowie die Farbe der Fluoreszenz von **18-X** von rot (X = Cl) über orange (X = OTf, OTf·HOTf) nach gelb ([BAr$^F_4$]·Et$_2$O, [BAr$^F_4$]). Darüber hinaus lieferte die Komproportionierung des neutralen B,N,S-Heterocyclus **16^{Cy}** mit den diprotonierten Vertretern **18-X** selektiv die entsprechenden Monokationen **19-X**, welche intermediäre photophysikalische Eigenschaften aufweisen (Schema 8c).

Nach der erfolgreichen Protonierung des Thiazaborolo[5,4-*d*]thiazaborols **16^{Cy}** war der nächste Schritt zu untersuchen, inwiefern **16^{Cy}** auch mit anderen E–H-Bindungen reagiert. Während alle Versuche, Hydroelementierungen mit primären und sekundären Silanen, Aminen und Phosphanen durchzuführen, scheiterten, konnte gezeigt werden, dass die Hydroborane HBcat und 9-BBN selektiv an die B=N-Doppelbindung in **16^{Cy}** addieren. Eine 1,2-Migration des Hydrids vom Borzentrum auf das Carbenkohlenstoffatom liefert anschließend die 1,3-Hydroborierungsprodukte **20^{BCat}** und **20^{BBN}** (Schema 9).

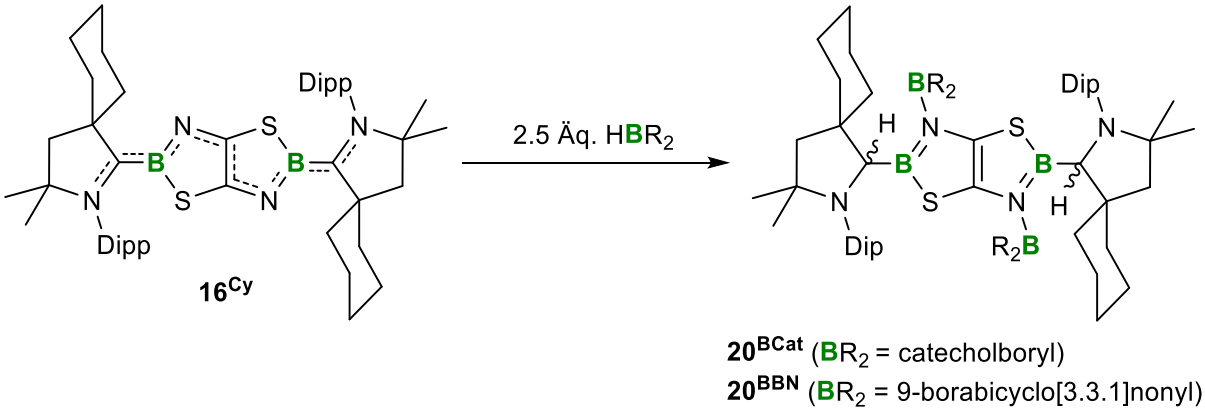

Schema 9. Formale 1,3-Hydroborierung des B,N,S-Heterocyclus **16^{Cy}** zu **20^{BCat}** und **20^{BBN}**.

Motiviert von den mit Cyano- und Isothiocyanato-substituierten Boranen und Borylenen erhaltenen Ergebnissen war ein weiteres Ziel dieser Arbeit, andere Pseudohalogenidsubstituenten einzuführen. Dafür wurde das CAAC^{Me}-stabilisierte Triflatoboran **1^{Me}** mit verschiedenen Isocyanid-, Cyanat- und Azidquellen umgesetzt, um (CAAC^{Me})BH$_2$Y (Y = NC, NCO, N$_3$) zu erhalten. Zusätzlich zu einer zum Teil unselektiven Bildung der erwünschten Produkte (CAAC^{Me})BH$_2$Y erwiesen sich die Aufarbeitung und insbesondere deren Isolierung als problematisch, weshalb diese Syntheserouten nicht

weiterverfolgt wurden. Während die Synthese der gewünschten [(CAAC^{Me})BH$_2$(NC)]-Konnektivität durch die Reaktion von **1^{Me}** mit Na[Cr(CO)$_5$(CN)] hin zum Chrom-Boranaddukt **21** erzielt werden konnte, scheiterten die Versuche, das Metallcarbonylfragment [Cr(CO)$_5$] von **21** abzuspalten, um das CAAC^{Me}-stabilisierte Isocyanoboran zu erhalten. Folglich wurde versucht, Salzeliminierungen direkt an einem bereits bestehenden Halogenborylen durchzuführen, um die erwünschten Pseudohalogenborylene darzustellen. Die Reduktion von (CAAC^{Me})BBr$_3$ (**VI^{Me}**) in Gegenwart von I*i*Pr lieferte das dreifach koordinierte Bromborylen **22** (Schema 10a). Die anschließenden Umsetzungen von **22** mit diversen Pseudohalogenidquellen zeigten entweder keinen Verbrauch des Startmaterials **22** oder resultierten in Gemischen nicht identifizierbarer Produkte (Schema 10b). Die Synthese von Pseudohalogenborylenen mit Isocyanato- beziehungsweise Azidofunktionalitäten blieben im Rahmen dieser Arbeit demnach erfolglos.

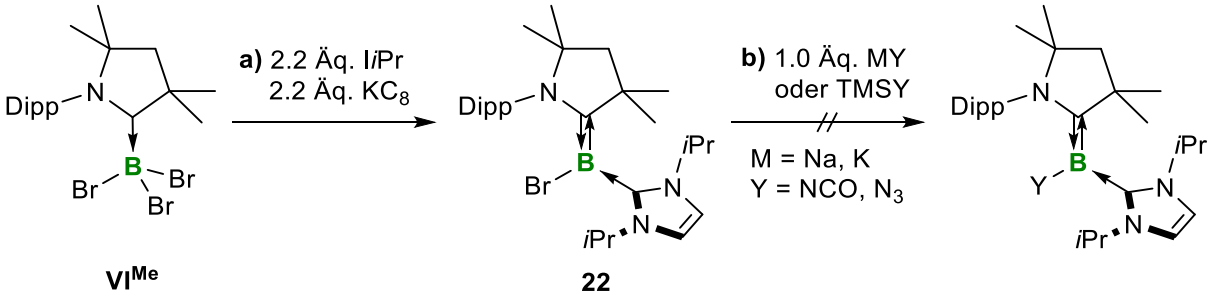

VI^{Me} **22**

Schema 10. a) Synthese des dreifach koordinierten Bromborylens **22**. **b)** Versuche, Isocyanato- und Azidoborylene mittels eines Bromid-Pseudohalogenidaustauschs an **22** darzustellen.

Schließlich wird im letzten Kapitel dieser Arbeit die Synthese und Reaktivität von CAAC^{R}-Addukten des Stammboraphosphaketens beschrieben. Die Anknüpfung des 2-Phosphaethinolatanions an Bor wurde mithilfe einer nucleophilen Substitutionsreaktion des Triflatoborans **1^{R}** mit Na[OCP] erreicht (Schema 11).

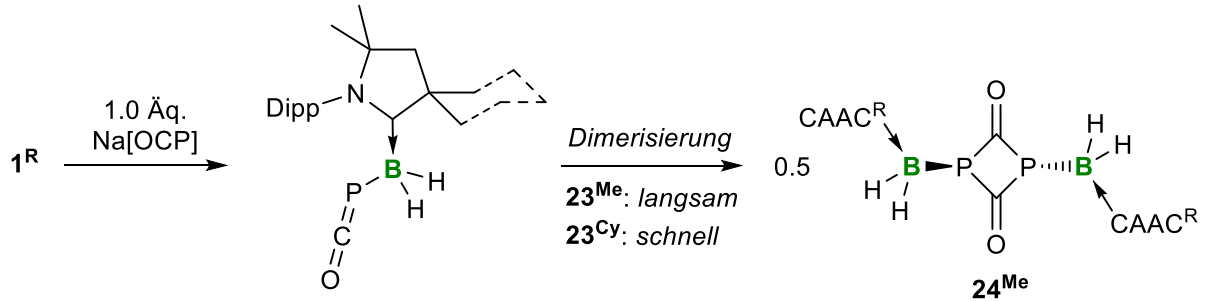

23^{Me} (*als Feststoff isoliert*)
23^{Cy} (*in Lösung detektiert*)

Schema 11. Synthese der CAAC^{R}-stabilisierten Boraphosphaketene **23^{R}** und deren Dimere **24^{R}**.

Die resultierenden CAAC^{R}-stabilisierten Boraphosphaketene **23^{R}** erwiesen sich in Lösung als instabil und wandelten sich mit der Zeit in ihre *cyclo*-C$_2$P$_2$-Dimere **24^{R}** um. Dennoch konnte

monomeres **23^{Me}** isoliert und als Feststoff gelagert werden, was die Untersuchung von dessen Phosphiniden-generierenden Fähigkeit ermöglichte. Die Vereinigung des Boraphosphaketens **23^{Me}** mit einer Reihe an Borolen [RBC$_4$Ph$_4$] (R = Ph, 2-Thienyl (Tn), Mes) führte bei Raumtemperatur formal zur decarbonylierenden Insertion des Phosphinidens [(CAAC^{Me})BH$_2$P] in the Borolring und zur Isolierung der 1,2-Phosphaborinine **25^{R}** (R = Ph, Tn, Mes) (Schema 12).

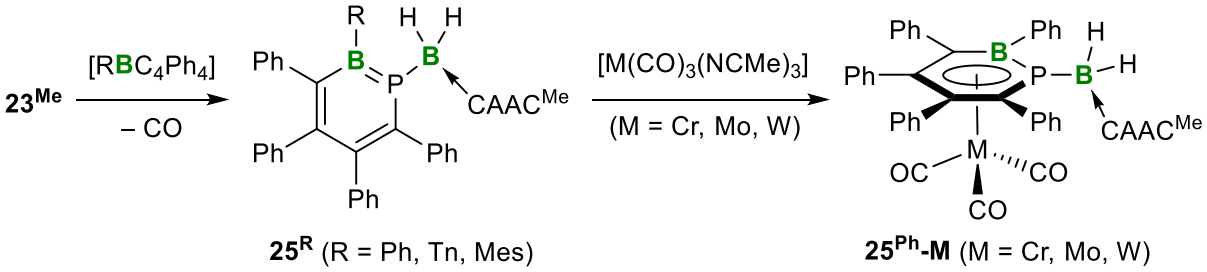

Schema 12. Synthese der 1,2-Phosphaborinine **25^{R}** und der π-Komplexe von **25^{Ph}** mit Gruppe 6 Übergangsmetallen, Verbindungen **25^{Ph}-M**.

Diese B,P-Isostere des Benzols zeigen einen moderaten Grad an Aromatizität, was durch deren berechnete Anisotropie der induzierten Stromdichte und den Kern-unabhängigen chemischen Verschiebungen angedeutet wird. Dementsprechend ist das 1,2-Phosphaborinin **25^{Ph}** in der Lage, in einer η^6-Koordination an Tricarbonylkomplexe der Gruppe 6 zu binden, und die entsprechenden Halbsandwichkomplexe **25^{Ph}-M** (M = Cr, Mo, W) zu bilden. An den π-Komplexen **25^{Ph}-M** aufgenommene Festkörper-IR-Spektren und an **25^{Ph}** durchgeführte DFT-Rechnungen offenbarten, dass diese B,P-Heteroaromaten signifikant stärkere Donorliganden als ihre leichteren Homologe, 1,2-Azaborinine, darstellen.

V Experimental

5.1. General Considerations

All manipulations were performed either under an atmosphere of dry argon (Argon 5.0) or *in vacuo* using standard Schlenk line or glovebox techniques. The solvents used were dried over suitable drying agents (*n*-pentane and *n*-hexane over NaK alloys, benzene and toluene over sodium, diethyl ether and tetrahydrofuran over Na/benzophenone or K/benzophenone, dichloromethane and chloroform over P_2O_5), distilled under an argon atmosphere and stored over molecular sieves. Deuterated solvents were dried over 4 Å or 3 Å molecular sieves and degassed by three freeze-pump-thaw cycles prior to use.

5.1.1 Analytical methods

Unless otherwise stated, **NMR spectra** were acquired either on a Bruker Avance 500 or a Bruker Avance 400 NMR spectrometer. Chemical shifts (δ) are listed in ppm and internally referenced to the carbon nuclei ($^{13}C\{^1H\}$) or residual protons (^1H) of the solvent. Heteronuclei NMR spectra are referenced to external standards (^{11}B: $BF_3{\cdot}OEt_2$, ^{19}F: $CFCl_3$, ^{31}P: 85% H_3PO_4). Furthermore, the signals were assigned using standard 2D NMR experiments.

EPR measurements at X-band (9.85 GHz) were carried out at room temperature using a Bruker ELEXSYS E580 CW EPR spectrometer. CW EPR spectra were measured using 1 mW microwave power and 0.5 G field modulation at 100 kHz, with a conversion time of 20 ms. The spectral simulations were performed using MATLAB 8.6 and the EasySpin 5.2.25 toolbox.

FT-IR spectra (solid-state) were recorded on a Bruker FT-IR spectrometer ALPHA II.

UV-vis spectra were measured on a METTLER TOLEDO UV-vis-Excellence UV5 spectrophotometer inside a glovebox.

Emission spectra were recorded using an Edinburgh Instruments FLSP920 spectrometer equipped with a double monochromator for both excitation and emission, operating in right-angle geometry mode, and all spectra were fully corrected for the spectral response of the instrument. Fluorescence quantum yields were measured using a calibrated integrating sphere from Edinburgh Instruments combined with the FLSP920 spectrometer described above.

Photochemical experiments were performed using a LOT-Quantum Design GmbH mercury-xenon vapor lamp (I = 19 A, U = 26 V).

Cyclic voltammetry experiments were performed using a Gamry Instruments Reference 600 potentiostat. A standard three-electrode cell configuration was employed using a platinum disk working electrode, a platinum wire counter electrode, and a silver wire, separated by a Vycor tip, serving as the reference electrode. Formal redox potentials are referenced to the ferrocene/ferrocenium ($[Cp_2Fe]^{+/0}$) redox couple by using decamethylferrocene ($[Cp^*_2Fe]$; $E_{1/2} = -0.427$ V in THF) as an internal standard. Tetra-(*n*-butyl)ammonium hexafluorophosphate ($[nBu_4N][PF_6]$) was employed as the supporting electrolyte. Compensation for resistive losses (*iR* drop) was employed for all measurements.

GCMS data were recorded on an Agilent 7890A gas chromatograph (column: HP-5MS 5% phenyl methyl siloxane, 27 m, Ø 0.25 mm, film: 0.25 µm; injector: 250 °C; oven: 40 °C (8 min), 20 °C to 280 °C (5 min); He (1.5 mL min^{-1}) equipped with an Agilent 5975C mass detector with triple-axis detector and FID detector in EI mode.

Elemental analyses (C, H, N, S) were performed on an Elementar vario MICRO cube elemental analyzer.

The **high-resolution mass** (**HRMS**) spectrometry was determined with an Exactive Plus HRMS device with an Orbitrap detector from Thermo-Scientific using the ionization method specified.

The **crystal data** were collected on a Bruker X8-APEX II diffractometer with a CCD area detector and multi-layer mirror monochromated Mo_{Ka} radiation, on a Bruker D8 Quest diffractometer with a CMOS area detector and multi-layer mirror monochromated Mo_{Ka} radiation, or on a XtaLAB Synergy, Dualflex diffractometer with a HyPix area detector and multi-layer mirror monochromated Cu_{Ka} radiation. The structures were solved using intrinsic phasing method,[183] refined with the ShelXL program[184] and expanded using Fourier techniques. All non-hydrogen atoms were refined anisotropically. Hydrogen atoms were included in structure factors calculations. Hydrogen atoms were assigned to idealized geometric positions or, if possible, found directly. The crystallographic data used in the publications were deposited with the Cambridge Crystallographic Data Center (CCDC) and are available at https://www.ccdc.cam.ac.uk/structures. The images of the solid state structures were created with the software Pov-Ray. Relevant data and parameters as well as the CCDC numbers of the published compounds may be found in the Appendix.

5.1.2 Starting Materials

The following compounds were synthesized using literature procedures:

$CAAC^{Me}$,[20] $CAAC^{Cy}$,[20] $(CAAC^{Me})BH_3$ (**VIII**^{Me}),[74] $(CAAC^{Cy})BH_3$ (**VIII**^{Cy}),[185] $(CAAC^{Me})BBr_3$ (**VI**^{Me}),[84] $(CAAC^{Me})BH_2(CAAC^{Me}H)$,[74] $(CAAC^{Me})BBr_2(CN)$ (**XXV**),[62] I*i*Pr,[186] KC_8,[187] $Na[Cr(CO)_5(CN)]$.[161]

The following compounds and reagents were used from the stock of the group or provided by its staff:

MeOTf, IMe^{Me},[188] PMe_3, pyridine, DMAP, 4,4'-bipyridine, S_8, NaSCN, Br_2, $[Cr(CO)_6]$, $[Mo(CO)_6]$, $[W(CO)_6]$, AgOTf, thiophenol, HBCat, 9-BBN, $[CuC_6F_5]_4$, HCl·toluene (0.01 M), HOTf, Brookhart's acid,[189] $Na(OCP)\cdot(dioxane)_{2.5}$,[171] 1,2,3,4,5-pentaphenylborole,[190] 1-(thien-2-yl)-2,3,4,5-tetraphenylborole,[191] 1-mesityl-2,3,4,5-tetraphenylborole,[192] $[Cr(CO)_3(MeCN)_3]$,[193] $[Mo(CO)_3(MeCN)_3]$,[193] $[W(CO)_3(MeCN)_3]$.[193]

5.1.3 Overview of Numbered Compounds

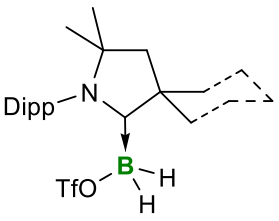

CAAC^{Me} (**1^{Me}**)
CAAC^{Cy} (**1^{Cy}**)

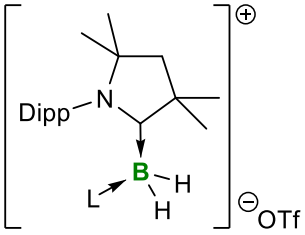

L = CAAC^{Me} (**2-CAAC^{Me}**)
IMe^{Me} (**2-IMe^{Me}**)
PMe_3 (**2-PMe_3**)
DMAP (**2-DMAP**)
pyridine (**2-Pyr**)

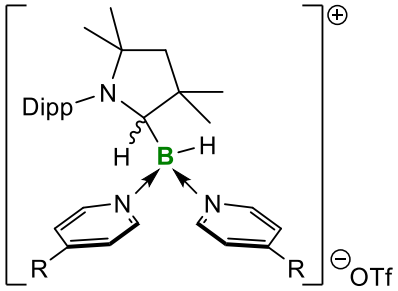

R = NMe_2 (**3-DMAP**)
H (**3-Pyr**)

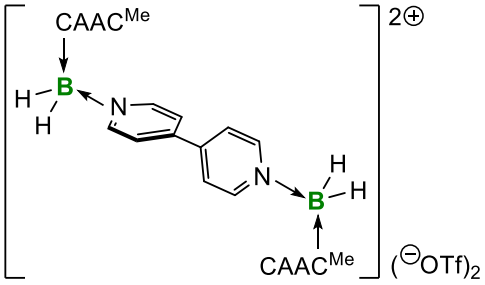

4-Bipy

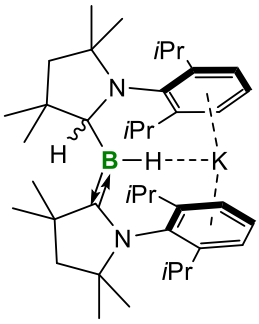

5

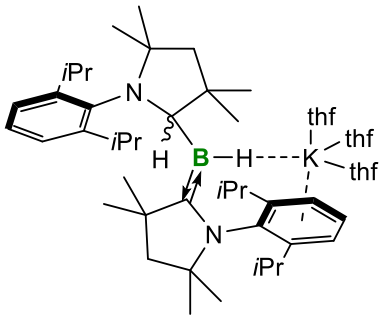

5-thf

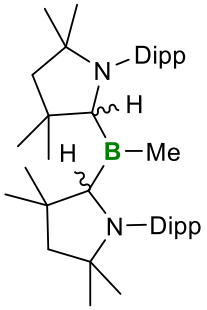

6

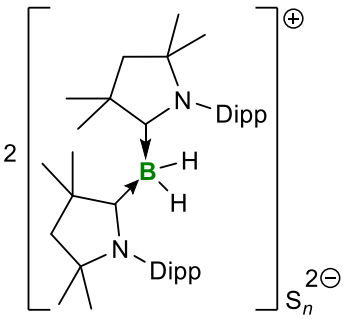

7

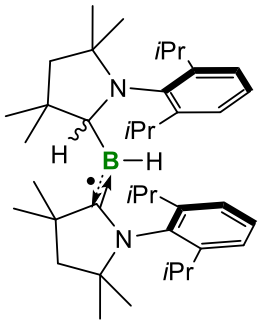

8

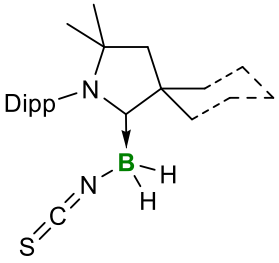

CAAC^{Me} (**9^{Me}**)
CAAC^{Cy} (**9^{Cy}**)

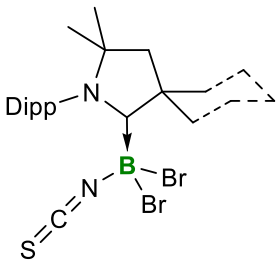

CAAC^{Me} (**10^{Me}**)
CAAC^{Cy} (**10^{Cy}**)

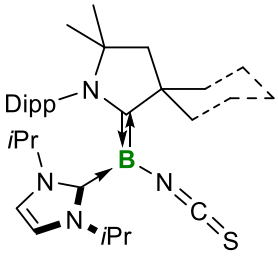

CAAC^{Me} ((***E***)-**11^{Me}**)
CAAC^{Cy} ((***E***)-**11^{Cy}**)

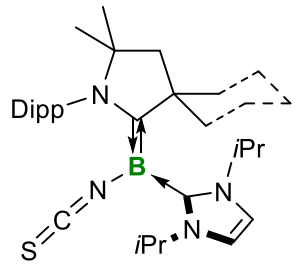

CAAC^{Me} (**(*Z*)-11^{Me}**)
CAAC^{Cy} (**(*Z*)-11^{Cy}**)

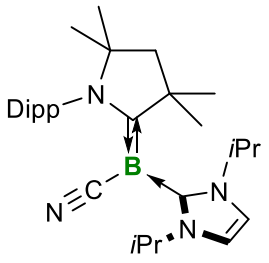

12

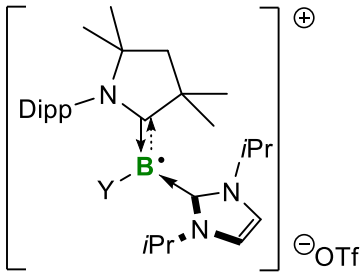

Y = NCS (**[(*Z*)-11$^{Me\bullet+}$][OTf^{-}]**)
CN (**[12$^{\bullet+}$][OTf^{-}]**)

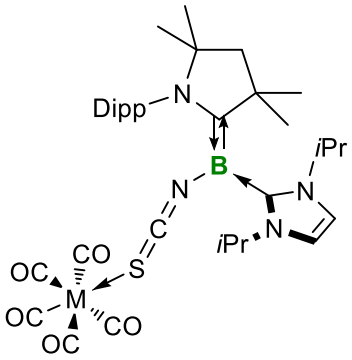

M = Cr (**(*Z*)-11^{Me}-Cr**)
W (**(*Z*)-11^{Me}-W**)

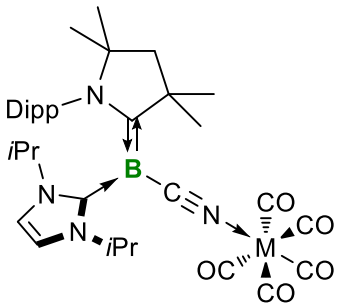

M = W (**(*E*)-12-W**)

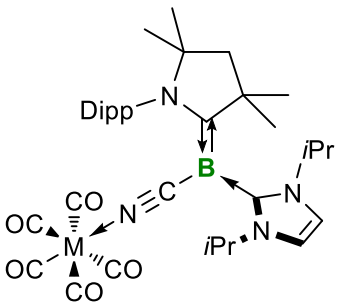

M = Cr (**(*Z*)-12-Cr**)
Mo (**(*Z*)-12-Mo**)
W (**(*Z*)-12-W**)

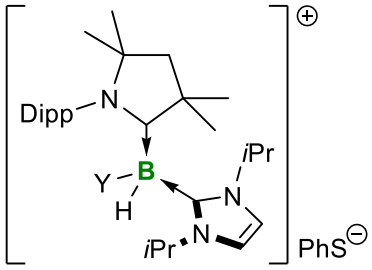

Y = NCS (**13^{NCS}**)
CN (**13^{CN}**)

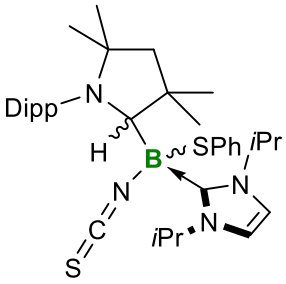

14^{NCS}

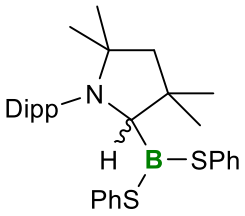

15

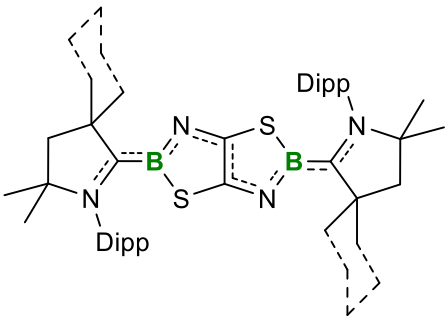

CAAC^{Me} (**16^{Me}**)
CAAC^{Cy} (**16^{Cy}**)

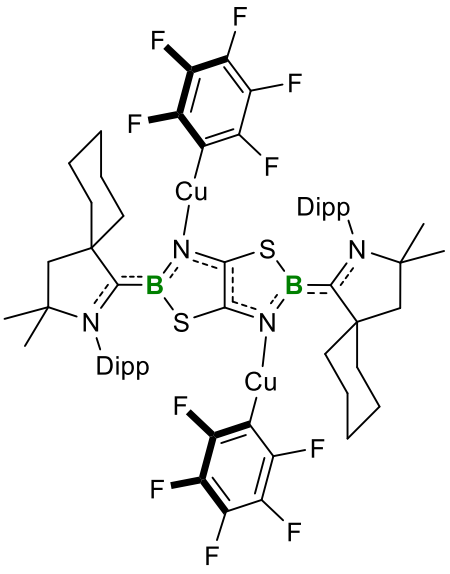

17

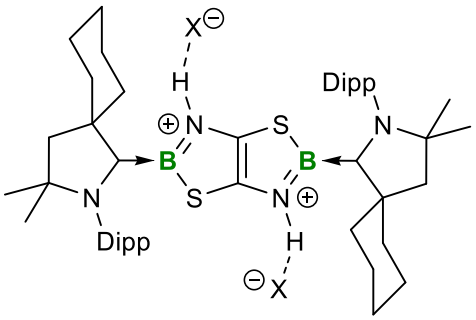

X = Cl (**18-Cl**)
OTf (**18-OTf**)
OTf·HOTf (**18-OTf·HOTf**)
[**B**Ar$^F_4$]·OEt$_2$ (**18-[BAr$^F_4$]·OEt$_2$**)
[**B**Ar$^F_4$] (**18-[BAr$^F_4$]**)

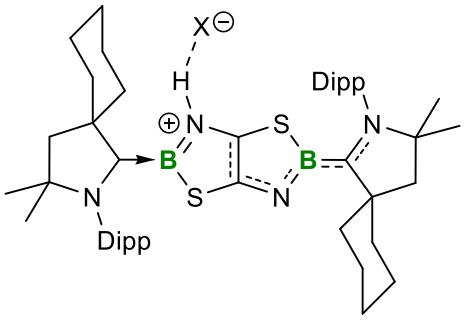

X = Cl (**19-Cl**)
OTf (**19-OTf**)
[**B**Ar$^F_4$]·OEt$_2$ (**19-[BAr$^F_4$]·OEt$_2$**)

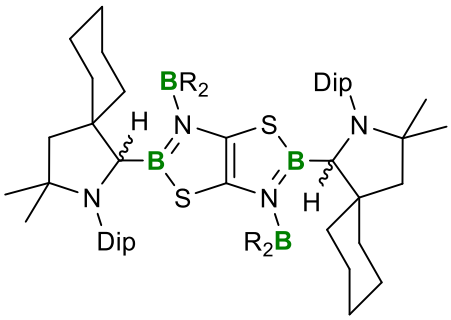

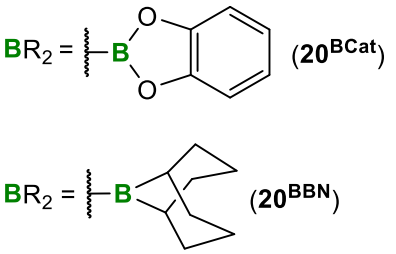

(**20^{BCat}**)

(**20^{BBN}**)

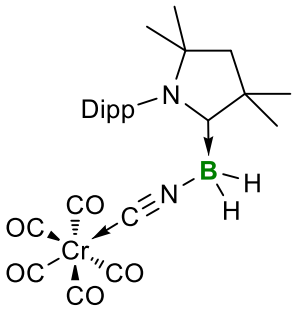

21

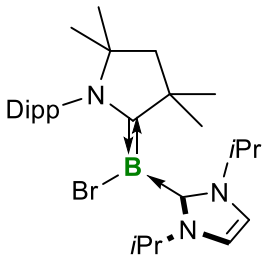

22

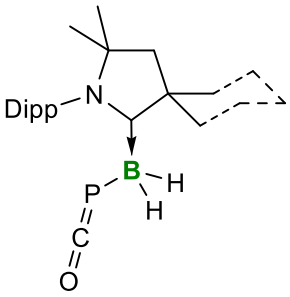

CAAC^{Me} (**23^{Me}**)
CAAC^{Cy} (**23^{Cy}**)

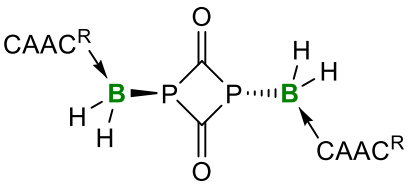

CAAC^{Me} (**24^{Me}**)
CAAC^{Cy} (**24^{Cy}**)

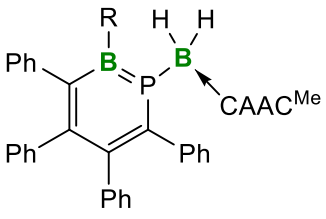

R = Ph (**25^{Ph}**)
2-thienyl (Tn) (**25^{Tn}**)
Mes (**25^{Mes}**)

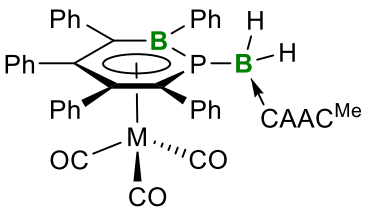

M = Cr (**25^{Ph}-Cr**)
Mo (**25^{Ph}-Mo**)
W (**25^{Ph}-W**)

5.2. Synthesis and Characterization

5.2.1 Synthesis of Triflatoboranes and Boronium Cations

(CAAC^{Me})BH$_2$(OTf) (1^{Me})

MeOTf (2.03 mL, 18.5 mmol, 1.50 equiv) was added slowly to a solution of (CAAC^{Me})BH$_3$ (**VIII**^{Me}) (3.70 g, 12.3 mmol) in 60 mL of benzene whereupon a gas evolution occurred. The reaction mixture was stirred overnight prior to removal of volatiles. The residue was washed with hexane and dried *in vacuo* to yield **1^{Me}** as a white solid (5.30 g, 11.8 mmol, 96% yield). Colorless single crystals were obtained by vapor diffusion of hexane into a saturated benzene solution.

^{1}H{^{11}B} NMR (500 MHz, C_6D_6, 297 K): δ = 7.06 (t, ^3J = 7.8 Hz, 1H, *p*-Ar*H*), 6.92 (d, ^3J = 7.8 Hz, 2H, *m*-Ar*H*), 3.28 (broad s, 2H, BH_2), 2.42 (sept, ^3J = 6.7 Hz, 2H, *i*Pr-C*H*), 1.41 (s, 6H, NC(CH_3)$_2$), 1.33 (s, 2H, CH_2), 1.25 (d, ^3J = 6.7 Hz, 6H, *i*Pr-CH_3), 1.02 (d, ^3J = 6.7 Hz, 6H, *i*Pr-CH_3), 0.71 (s, 6H, C(CH_3)$_2$) ppm.

^{13}C{^{1}H} NMR (126 MHz, C_6D_6, 297 K): δ = 193.0 ($C_{carbene}$, identified by HMBC), 144.7 (*i*-Ar*C*), 131.7 (*o*-Ar*C*), 130.2 (*p*-Ar*C*), 125.3 (*m*-Ar*C*), 120.2 (q, $^1J_{CF}$ = 319 Hz, *C*F$_3$), 78.3 (N*C*(CH$_3$)$_2$), 52.5 (*C*(CH$_3$)$_2$), 51.1 (*C*H$_2$), 29.4 (*i*Pr-*C*H), 28.3 (NC(*C*H$_3$)$_2$), 28.2 (C(*C*H$_3$)$_2$), 25.8 (*i*Pr-*C*H$_3$), 23.7 (*i*Pr-*C*H$_3$) ppm.

^{11}B NMR (160 MHz, C_6D_6, 297 K): δ = –6.3 (br s) ppm.

^{19}F NMR (471 MHz, C_6D_6, 297 K): δ = –76.2 (s) ppm.

Elemental analysis for [$C_{21}H_{33}BF_3NO_3S$] (M_w = 447.36 g mol^{-1}): calcd. C 56.38, H 7.44, N 3.13, S 7.17%; found C 56.71, H 7.59, N 3.36, S 6.82%.

(CAAC^{Cy})BH$_2$(OTf) (1^{Cy})

MeOTf (3.53 mL, 31.2 mmol, 1.50 equiv) was added slowly to a solution of (CAAC^{Cy})BH$_3$ (**VIII**^{Cy}) (7.06 g, 20.8 mmol) in 60 mL of benzene whereupon evolution of gas was observed. After stirring overnight at room temperature volatiles were removed *in vacuo* and the residue was washed with hexane. Drying *in vacuo* afforded **1^{Cy}** as a white solid (10.9 g, 22.4 mmol, 93% yield). Colorless single crystals were obtained by vapor diffusion of hexane into a saturated benzene solution.

^{1}H{^{11}B} NMR (500 MHz, C_6D_6, 297 K): δ = 7.10 (t, ^3J = 7.8 Hz, 1H, *p*-Ar*H*), 6.95 (d, ^3J = 7.8 Hz, 2H, *m*-Ar*H*), 3.28 (br s, 2H, BH_2), 2.54 (dt, ^2J = 13.5 Hz, ^3J = 3.5 Hz, 2H, Cy-CH_2), 2.45 (sept, ^3J = 6.7 Hz, 2H, *i*Pr-C*H*), 1.54–1.52 (m, 2H, Cy-CH_2), 1.49 (s, 2H, CH_2), 1.43–1.36

(m, 2H, Cy-CH_2), 1.34–1.32 (m, 2H, Cy-CH_2), 1.27 (d, ^3J = 6.6 Hz, 6H, *i*Pr-CH_3), 1.06 (d, ^3J = 6.7 Hz, 6H, *i*Pr-CH_3), 1.04–0.96 (m, 2H, Cy-CH_2), 0.75 (s, 6H, NC(CH_3)$_2$) ppm.

^{13}C{^{1}H} NMR (126 MHz, C_6D_6, 297 K): δ = 227.5 ($C_{carbene}$, identified by HMBC), 144.6 (*o*-Ar*C*), 132.0 (*i*-Ar*C*), 130.2 (*p*-Ar*C*), 125.2 (*m*-Ar*C*), 120.1 (q, $^1J_{CF}$ = 319 Hz, *C*F$_3$), 78.5 (N*C*(CH$_3$)$_2$), 58.2 (*C*(C$_5$H$_{10}$)), 45.8 (*C*H$_2$), 34.6 (Cy-*C*H$_2$), 29.4 (*i*Pr-*C*H), 28.8 (NC(*C*H$_3$)$_2$), 25.7 (*i*Pr-*C*H$_3$), 25.1 (Cy-*C*H$_2$), 23.7 (*i*Pr-*C*H$_3$), 22.2 (Cy-*C*H$_2$) ppm.

^{11}B NMR (160 MHz, C_6D_6, 297 K): δ = –6.1 (br s) ppm.

^{19}F NMR (471 MHz, C_6D_6, 297 K): δ = –76.2 (s) ppm.

Elemental analysis for [$C_{24}H_{37}BF_3NO_3S$] (M_w = 487.43 g mol^{-1}): calcd. C 59.14, H 7.65, N 2.87, S 6.58%; found C 58.49, H 7.65, N 2.84, S 6.65%.

[(CAAC^{Me})(CAAC^{Me})BH$_2$][OTf] (2-CAAC^{Me})

Route A. Compound **1^{Me}** (1.30 g, 2.91 mmol) and CAAC^{Me} (1.00 g, 3.49 mmol, 1.20 equiv) were dissolved in 30 mL of benzene and subsequently heated to 75 °C for 2 d. The resulting suspension was filtered and the solid obtained was washed with hexane. Drying *in vacuo* yielded **2-CAAC^{Me}** as a white solid (2.00 g, 2.73 mmol, 94% yield). Colorless single crystals were obtained by vapor diffusion of hexane in a saturated chloroform solution.

Route B. A solution of (CAAC^{Me})BH$_2$(CAAC^{Me}H) (20.0 mg, 34.2 μmol) in 1 mL of benzene was treated with an excess of MeOTf (5–10 equiv). Within 2 d at room temperature a suspension was formed and complete consumption of (CAAC^{Me})BH$_2$(CAAC^{Me}H) was observed by ^{11}B NMR spectroscopy. After filtration the solid obtained was washed with benzene and dried *in vacuo* affording **2-CAAC^{Me}** (22.8 mg, 31.1 μmol, 91% yield). The NMR spectra of the isolated solid were identical with those from route A.

^{1}H NMR (500 MHz, $CDCl_3$, 238 K): δ = 7.27–7.17 (m, 4H, *m*-Ar*H*), 7.03 (s, 1H, *p*-Ar*H*), 7.01 (s, 1H, *p*-Ar*H*), 2.50 (sept, ^3J = 6.1 Hz, 2H, *i*Pr-C*H*), 2.34 (d, ^2J = 13.2 Hz, 2H, CH_2), 2.02 (d, ^2J = 13.1 Hz, 2H, CH_2), 1.90 (m, 2H, *i*Pr-C*H*), 1.88 (s, 6H, NC(CH_3)$_2$), 1.53 (s, 6H, NC(CH_3)$_2$), 1.44 (s, 6H, C(CH_3)$_2$), 1.31 (d, ^3J = 6.5 Hz, 6H, *i*Pr-CH_3), 1.12–1.07 (m, 18H, C(CH_3)$_2$ + two *i*Pr-CH_3), 0.07 (d, ^3J = 6.4 Hz, 6H, *i*Pr-CH_3) ppm.

^{13}C{^{1}H} NMR (126 MHz, $CDCl_3$, 297 K): δ = 193.2 ($C_{carbene}$, identified by HMBC), 144.8 (*i*-Ar*C*), 142.6 (*i*-Ar*C*), 132.7 (*o*-Ar*C*), 129.7 (*p*-Ar*C*), 125.8 (*m*-Ar*C*), 121.2 (q, $^1J_{13C\text{-}19F}$ = 321 Hz, *C*F$_3$), 79.2 (N*C*(CH$_3$)$_2$), 53.6 (*C*H$_2$), 51.9 (*C*(CH$_3$)$_2$), 29.8 (*i*Pr-*C*H), 29.4 (NC(*C*H$_3$)$_2$), 29.1 (C(*C*H$_3$)$_2$), 28.8 (C(*C*H$_3$)$_2$), 28.6 (NC(*C*H$_3$)$_2$), 27.2 (*i*Pr-*C*H$_3$), 25.7 (*i*Pr-*C*H$_3$), 24.4 (*i*Pr-*C*H$_3$), 24.3 (*i*Pr-*C*H$_3$) ppm.

^{11}B NMR (160 MHz, $CDCl_3$, 297 K): δ = –22.4 (t, $^1J_{BH}$ = 85.3 Hz) ppm.

^{19}F NMR (471 MHz, $CDCl_3$, 297 K): δ = –78.0 (s) ppm.

FT-IR (solid-state): $\tilde{\nu}$(B–H) = 2403 cm^{-1}.

Elemental analysis for [$C_{41}H_{64}BF_3N_2O_3S$] (M_w = 732.84 g mol^{-1}): calcd. C 67.20, H 8.80, N 3.82, S 4.37%; found C 68.22, H 8.48, N 3.41, S 4.15%.

HRMS LIFDI for $[C_{40}H_{64}BN_2]^+ = [M – SO_3CF_3]^+$: calcd. 583.5157; found 583.5140.

[(CAAC^{Me})(IMe^{Me})BH$_2$][OTf] (**2-IMe^{Me}**)

A solution of **1^{Me}** (100 mg, 0.22 mmol) and IMe^{Me} (27.8 mg, 0.22 mmol) in 10 mL of benzene was stirred at 60 °C overnight. The resulting suspension was cooled to room temperature and hexane was added to further induce precipitation. After filtration the white solid was washed with hexane and dried *in vacuo* yielding **2-IMe^{Me}** (109 mg, 0.19 mmol, 87% yield).

^{1}H{^{11}B} NMR (500 MHz, $CDCl_3$, 297 K): δ = 7.46 (t, ^3J = 7.8 Hz, 1H, *p*-Ar*H*), 7.33 (d, ^3J = 7.8 Hz, 2H, *m*-Ar*H*), 3.60 (s, 6H, IMe^{Me}-NC*H*$_3$), 2.66 (sept, ^3J = 6.6 Hz, 2H, *i*Pr-C*H*), 2.22 (s, 6H, IMe^{Me}-CC*H*$_3$), 2.17 (s, 2H, C*H*$_2$), 1.81 (s, 2H, B*H*$_2$), 1.41 (s, 6H, NC(C*H*$_3$)$_2$), 1.38 (d, ^3J = 6.6 Hz, 12H, *i*Pr-C*H*$_3$), 1.26 (s, 6H, C(C*H*$_3$)$_2$) ppm.

^{13}C{^{1}H} NMR (126 MHz, $CDCl_3$, 297 K): δ = 230.5 (CAAC-$C_{carbene}$, identified by HMBC), 159.1 (NHC-$C_{carbene}$, identified by HMBC), 144.7 (*i*-Ar*C*), 132.0 (*o*-Ar*C*), 130.1 (*p*-Ar*C*), 126.2(*C*CH$_3$), 125.8 (*m*-Ar*C*), 121.1 (q, $^1J_{CF}$ = 321 Hz, *C*F$_3$), 79.1 (N*C*(CH$_3$)$_2$), 52.9 (*C*(CH$_3$)$_2$), 50.9 (*C*H$_2$), 33.9 (N*C*H$_3$), 29.4 (NC(*C*H$_3$)$_2$), 29.2 (*i*Pr-*C*H), 28.2 (C(*C*H$_3$)$_2$), 26.8 (*i*Pr-*C*H$_3$), 24.7 (*i*Pr-*C*H$_3$), 9.1 (C*C*H$_3$) ppm.

^{11}B NMR (160 MHz, $CDCl_3$, 297 K): δ = –29.2 (t, $^1J_{BH}$ = 87.8 Hz) ppm.

^{19}F NMR (471 MHz, $CDCl_3$, 297 K): δ = –78.1 (s) ppm.

Elemental analysis for [$C_{28}H_{45}BF_3N_3O_3S$] (M_w = 571.55 g mol^{-1}): calcd. C 58.84, H 7.94, N 7.35, S 5.61%; found C 58.45, H 7.92, N 7.75, S 5.42%.

HRMS LIFDI for $[C_{27}H_{45}BN_3]^+ = [M – SO_3CF_3]^+$: calcd. 422.3701; found 422.3678.

[(CAAC^{Me})(PMe$_3$)BH$_2$][OTf] (**2-PMe$_3$**)

A solution of **1^{Me}** (100 mg, 0.22 mmol) and PMe_3 (0.03 mL, 0.27 mmol, 1.20 equiv) in 3 mL of benzene was stirred overnight at room temperature. After removal of all volatiles, the solid obtained was washed with hexane and dried *in vacuo* to afford **2-PMe$_3$** (110 mg, 0.21 mmol, 95% yield).

^{1}H{^{11}B} NMR (500 MHz, CD_2Cl_2, 297 K): δ = 7.49 (t, ^3J = 7.8 Hz, 1H, *p*-Ar*H*), 7.33 (d, ^3J = 7.8 Hz, 2H, *m*-Ar*H*), 2.50 (sept, ^3J = 6.6 Hz, 2H, *i*Pr-C*H*), 2.23 (s, 2H, C*H*$_2$), 1.56 (s, 6H,

NCH_3), 1.55 (d, $^2J_{HP}$ = 11.4 Hz, 9H, P(CH_3)$_3$), 1.46 (d, $^2J_{HP}$ = 23.5 Hz, 2H, PBH_2), 1.34 (d, ^3J = 6.6 Hz, 6H, *i*Pr-CH_3), 1.17 (d, ^3J = 6.6 Hz, 6H, *i*Pr-CH_3) ppm.

^{13}C{^{1}H} NMR (126 MHz, CD_2Cl_2, 297 K): δ = 223.8 ($C_{carbene}$, identified by HMBC), 143.0 (*i*-Ar*C*), 130.7 (*o*-Ar*C*), 129.2 (*p*-Ar*C*), 124.1 (*m*-Ar*C*), 119.9 (q, $^1J_{CF}$ = 321 Hz, *C*F$_3$), 79.6 (N*C*(CH$_3$)$_2$), 51.3 (*C*(CH$_3$)$_2$), 49.4 (*C*H$_2$), 28.1 (*i*Pr-*C*H), 27.8 (NC(*C*H$_3$)$_2$), 27.7 (C(*C*H$_3$)$_2$), 25.0 (*i*Pr-*C*H$_3$), 22.1 (*i*Pr-*C*H$_3$), 11.9 (d, $^1J_{CP}$ = 44.1 Hz, P(*C*H$_3$)$_3$) ppm.

^{11}B NMR (160 MHz, CD_2Cl_2, 297 K): δ = –27.8 (dt, $^1J_{BP}$ = 81.5 Hz, $^1J_{BH}$ = 89.8 Hz, determined by selective ^{1}H and ^{31}P-decoupling experiments) ppm.

^{19}F NMR (471 MHz, CD_2Cl_2, 297 K): δ = –78.9 (s) ppm.

^{31}P{^{1}H} NMR (202 MHz, CD_2Cl_2, 297 K): δ = –10.6 (br m) ppm.

Elemental analysis for [$C_{24}H_{42}BF_3NO_3PS$] (M_w = 523.44 g mol^{-1}): calcd. C 55.07, H 8.09, N 2.68, S 6.12%; found C 54.99, H 7.71, N 3.00, S 5.67%.

[(CAAC^{Me})(pyr)BH$_2$][OTf] (**2-Pyr**)

To a solution of **1^{Me}** (100 mg, 0.22 mmol) in 3 mL of benzene pyridine (17.7 mg, 0.22 mmol) diluted in 1 mL of benzene was added dropwise. After stirring for 3 d at room temperature a suspension was formed and subsequently volatiles were removed *in vacuo*. The residue was washed with hexane and dried *in vacuo* to obtain **2-Pyr** as a white solid (105 mg, 0.20 mmol, 91% yield). Colorless single crystals were obtained by vapor diffusion of hexane in a saturated chloroform solution.

^{1}H{^{11}B} NMR (500 MHz, $CDCl_3$, 297 K): δ = 8.59 (d, ^3J = 5.3 Hz, 2H, Py-C^2*H*), 8.27 (t, ^3J = 7.8 Hz, 1H, Py-C^4*H*), 7.97 (t, ^3J = 7.8 Hz, 2H, Py-C^3*H*), 7.46 (t, ^3J = 7.8 Hz, 1H, *p*-Ar*H*), 7.32 (d, ^3J = 7.8 Hz, 2H, *m*-Ar*H*), 2.93 (br s, 2H, BH_2), 2.76 (sept, ^3J = 6.6 Hz, 2H, *i*Pr-C*H*), 2.20 (s, 2H, CH_2), 1.42 (s, 6H, NC(CH_3)$_2$), 1.39 (d, ^3J = 6.5 Hz, 6H, *i*Pr-CH_3), 1.30 (d, ^3J = 6.6 Hz, 6H, *i*Pr-CH_3), 1.23 (s, 6H, C(CH_3)$_2$) ppm.

^{13}C{^{1}H} NMR (126 MHz, $CDCl_3$, 297 K): δ = 224.5 ($C_{carbene}$, identified by HMBC), 149.0 (Py-*C*^{2}), 144.7 (*i*-Ar*C*), 143.1 (Py-*C*^{4}), 131.5 (*o*-Ar*C*), 130.4 (*p*-Ar*C*), 127.7 (Py-*C*^{3}), 125.5 (*m*-Ar*C*), 121.1 (q, $^1J_{CF}$ = 321 Hz, *C*F$_3$), 79.8 (N*C*(CH$_3$)$_2$), 53.5 (*C*(CH$_3$)$_2$), 50.8 (*C*H$_2$), 29.2 (*i*Pr-*C*H), 29.1 (C(*C*H$_3$)$_2$), 28.9 (NC(*C*H$_3$)$_2$), 26.4 (*i*Pr-*C*H$_3$), 23.9 (*i*Pr-*C*H$_3$) ppm.

^{11}B NMR (160 MHz, $CDCl_3$, 297 K): δ = –9.3 (br s) ppm.

^{19}F NMR (471 MHz, $CDCl_3$, 297 K): δ = –78.1 (s) ppm.

Elemental analysis for [$C_{26}H_{38}BF_3N_2O_3S$] (M_w = 526.47 g mol^{-1}): calcd. C 59.32, H 7.28, N 5.32, S 6.09%; found C 59.47, H 7.26, N 5.73, S 5.72%.

HRMS LIFDI for [$C_{25}H_{38}BN_2$]$^+$ = [M – SO_3CF_3]$^+$: calcd. 377.3123; found 377.3099.

[(CAAC^{Me})(DMAP)BH$_2$][OTf] (2-DMAP)

To a solution of **1^{Me}** (100 mg, 0.22 mmol) in 3 mL of THF DMAP (27.3 mg, 0.22 mmol) dissolved in 1 mL of THF was added dropwise. The mixture was stirred for 3 d at room temperature prior to removal of volatiles. The solid obtained was washed with hexane and dried *in vacuo* to yield **2-DMAP** (111 mg, 0.19 mmol, 89% yield). Colorless single crystals were obtained by vapor diffusion of hexane in a saturated THF solution. *Note: The reaction with 1.00 equiv DMAP in benzene instead of THF also results in the formation of **3-DMAP** (see below), while 50% of **1^{Me}** remain unreacted. While **3-DMAP** crystallizes quantitatively, **1^{Me}** remains in solution, thus enabling separation.*

^{1}H NMR (500 MHz, $CDCl_3$, 297 K): δ = 7.83 (d, ^3J = 7.5 Hz, 2H, *o*-DMAP-*H*), 7.44 (t, ^3J = 7.8 Hz, 1H, *p*-Ar*H*), 7.30 (d, ^3J = 7.8 Hz, 2H, *m*-Ar*H*), 6.79 (d, ^3J = 7.5 Hz, 2H, *m*-DMAP-*H*), 3.17 (s, 6H, DMAP-CH_3), 2.66 (sept, ^3J = 6.6 Hz, 2H, *i*Pr-C*H*), 2.13 (s, 2H, CH_2), 1.37 (s, 6H, NC(CH_3)$_2$), 1.36 (d, ^3J = 6.6 Hz, 6H, *i*Pr-CH_3), 1.30 (d, ^3J = 6.6 Hz, 6H, *i*Pr-CH_3), 1.26 (s, 6H, C(CH_3)$_2$) ppm.

^{13}C{^{1}H} NMR (126 MHz, $CDCl_3$, 297 K): δ = 227.8 ($C_{carbene}$, identified by HMBC), 155.8 (*i*-Ar*C*), 147.3 (*o*-DMAP-*C*), 144.5 (*o*-Ar*C*), 131.6 (*p*-DMAP-*C*), 130.2 (*p*-Ar*C*), 125.4 (*m*-Ar*C*), 121.2 (q, $^1J_{CF}$ = 321 Hz, *C*F$_3$), 107.8 (*m*-DMAP-*C*), 79.2 (N*C*(CH$_3$)$_2$), 53.1 (*C*(CH$_3$)$_2$), 51.4 (*C*H$_2$), 39.9 (DMAP-*C*H$_3$), 29.3 (*i*Pr-*C*H), 29.0 (C(*C*H$_3$)$_2$), 28.9 (C(*C*H$_3$)$_2$), 26.4 (*i*Pr-*C*H$_3$), 24.0 (*i*Pr-*C*H$_3$) ppm.

^{11}B NMR (160 MHz, $CDCl_3$, 297 K): δ = –10.6 (br s) ppm.

^{19}F NMR (471 MHz, $CDCl_3$, 297 K): δ = –78.0 (s) ppm.

HRMS LIFDI for $[C_{27}H_{43}BN_3]^+ = [M - SO_3CF_3]^+$: calcd. 420.3545; found 420.3525.

[(CAAC^{Me}H)(DMAP)$_2$BH$_2$][OTf] (3-DMAP)

A solution of **1^{Me}** (100 mg, 0.22 mmol) and DMAP (54.6 mg, 0.44 mmol, 2.00 equiv) in 4 mL of THF was stirred for 3 d at room temperature. The formed suspension was evaporated to dryness and the solid obtained was washed with hexane yielding **3-DMAP** as a colorless powder (142 mg, 0.20 mmol, 93% yield). Colorless single crystals were obtained by vapor diffusion of hexane in a saturated THF solution.

^{1}H NMR (400 MHz, $CDCl_3$, 297 K): δ = 7.73 (d, ^3J = 6.5 Hz, 2H, *m*-DMAP-*H*), 7.72 (br s, 2H, *o*-DMAP-*H*), 7.01 (d, ^3J = 7.3 Hz, 1H, *m*-Ar*H*), 7.03 (app. t, ^3J = 7.5 Hz, 1H, *p*-Ar*H*), 6.79 (d, ^3J = 7.6 Hz, 1H, *m*-Ar*H*), 6.52 (d, ^3J = 6.8 Hz, 2H, *m*-DMAP-*H*), 6.21 (d, ^3J = 6.5 Hz, 2H, *m*-DMAP-*H*), 3.75 (sept, ^3J = 6.4 Hz, 1H, *i*Pr-C*H*), 3.51 (d, ^3J = 5.7 Hz, 1H, BC*H*), 3.36 (sept, ^3J = 6.7 Hz, 1H, *i*Pr-C*H*), 3.08 (s, 6H, DMAP-CH_3), 3.00 (s, 6H, DMAP-CH_3), 2.24 (d,

^{2}J = 12.5 Hz, 1H, CH_2), 1.84 (d, ^{2}J = 12.5 Hz, 1H, CH_2), 1.53 (s, 3H, N(CH_3)$_3$), 1.49 (d, ^{3}J = 6.4 Hz, 3H, *i*Pr-CH_3), 1.24 (d, ^{3}J = 6.7 Hz, 3H, *i*Pr-CH_3), 1.15 (s, 3H, N(CH_3)$_3$), 1.05 (d, ^{3}J = 6.7 Hz, 3H, *i*Pr-CH_3), 1.00 (s, 3H, C(CH_3)$_2$), 0.92 (s, 3H, C(CH_3)$_2$), 0.59 (d, ^{3}J = 6.4 Hz, 3H, *i*Pr-CH_3) ppm.

^{13}C{^{1}H} NMR (126 MHz, $CDCl_3$, 297 K): δ = 156.2 (*p*-DMAP-*C*), 155.9 (*p*-DMAP-*C*), 151.9 (*o*-Ar*C*), 149.2 (*o*-Ar*C*), 146.5 (*i*-Ar*C*), 144.8 (*o*-DMAP-*C*), 144.5 (*o*-DMAP-*C*), 126.2 (*p*-Ar*C*), 125.8 (*m*-Ar*C*), 124.1 (*m*-Ar*C*), 121.4 (q, $^{1}J_{CF}$ = 321 Hz, *C*F_3), 107.5 (*m*-DMAP-*C*), 107.0 (*m*-DMAP-*C*), 67.9 (B*C*H), 63.3 (N*C*(CH$_3$)$_2$), 61.6 (*C*H$_2$), 41.6 (*C*(CH$_3$)$_2$), 39.9 (DMAP-*C*H$_3$), 39.9 (DMAP-*C*H$_3$), 33.8 (C(*C*H$_3$)$_2$), 33.2 (C(*C*H$_3$)$_2$), 29.0 (*i*Pr-*C*H), 28.5 (C(*C*H$_3$)$_2$), 28.4 (C(*C*H$_3$)$_2$), 27.3 (*i*Pr-*C*H), 27.1 (*i*Pr-*C*H$_3$), 25.9 (*i*Pr-*C*H$_3$), 25.0 (*i*Pr-*C*H$_3$), 24.0 (*i*Pr-*C*H$_3$) ppm.

^{11}B NMR (160 MHz, $CDCl_3$, 297 K): δ = 4.2 (br s) ppm.

^{19}F NMR (471 MHz, $CDCl_3$, 297 K): δ = –78.9 (s) ppm.

HRMS LIFDI for $[C_{34}H_{53}BN_5]^+$ = $[M – SO_3CF_3]^+$: calcd. 542.4389; found 542.4363; $[C_{27}H_{43}BN_3]^+$ = $[M – SO_3CF_3 – DMAP]^+$: calcd. 420.3545; found 420.3525.

[(CAAC^{Me}H)(Pyr)$_2$BH$_2$][OTf] (**3-Pyr**)

Compound **1^{Me}** (20.0 mg, 45 µmol) was dissolved in 0.5 mL of pyridine. ^{11}B NMR data recorded after 15 min at rt show a ca. 1:1 mixture of **2-Pyr** (δ_{11B} = –9.1 ppm) as well as a second species (δ_{11B} = 6.9 ppm, very br s) attributable to the pyridine analogue of **3-DMAP**, [(CAAC^{Me}H)BH(Pyr)$_2$]OTf (**3-Pyr**), by analogy. Heating at 80 °C for 1 day resulted in a maximum conversion of ca. 75% to **3-Pyr**. Attempts to isolate this compound failed as removal of the pyridine solvent also results in removal of the second bound pyridine ligand and isolation of **2-Pyr**.

[(CAAC^{Me})(4,4'-Bipy)BH$_2$]$_2$[OTf]$_2$ (**4-Bipy**)

To a solution of **1^{Me}** (200 mg, 0.45 mmol, 2.00 equiv) in 4 mL of benzene 4,4'-bipyridine (35.0 mg, 0.22 mmol) dissolved in 1 mL of benzene was added dropwise. The reaction mixture instantly turned red accompanied by the formation of a precipitate. After stirring for 1 d at room temperature the suspension was filtered. The off-white solid was washed with benzene and hexane and dried *in vacuo* to afford **4-Bipy** (196 mg, 0.18 mmol, 85% yield).

^{1}H{^{11}B} NMR (500 MHz, $CDCl_3$, 297 K): δ = 8.79 (d, ^{3}J = 6.9 Hz, 4H, *o*-Bipy*H*), 8.70 (d, ^{3}J = 6.9 Hz, 4H, *m*-Bipy*H*), 7.48 (t, ^{3}J = 7.7 Hz, 2H, *p*-Ar*H*), 7.33 (d, ^{3}J = 7.6 Hz, 4H, *m*-Ar*H*), 2.96 (s, 4H, BH_2), 2.69 (sept, ^{3}J = 6.6 Hz, 4H, *i*Pr-C*H*), 2.16 (s, 4H, CH_2), 1.41 (s, 12H,

NC(CH_3)$_2$), 1.39 (d, ^3J = 6.8 Hz, 12H, *i*Pr-CH_3), 1.32 (d, ^3J = 6.5 Hz, 12H, *i*Pr-CH_3), 1.23 (s, 12H, C(CH_3)$_2$) ppm.

^{13}C{^{1}H} NMR (126 MHz, $CDCl_3$, 297 K): δ = 224.7 ($C_{carbene}$), 150.0 (*m*-Bipy-*C*), 147.8 (*p*-Bipy-*C*), 144.5 (*o*-Ar*C*), 131.3 (*i*-Ar*C*), 130.5 (*p*-Ar*C*), 126.4 (*o*-Bipy-*C*), 125.5 (*m*-Ar*C*), 121.0 (q, $^1J_{CF}$ = 320 Hz, *C*F$_3$), 79.7 (N*C*(CH$_3$)$_2$), 53.4 (*C*(CH$_3$)$_2$), 51.3 (*C*H$_2$), 29.4 (*i*Pr-*C*H), 29.2 (C(*C*H$_3$)$_2$), 29.0 (NC(*C*H$_3$)$_2$), 26.4 (*i*Pr-*C*H$_3$), 23.9 (*i*Pr-*C*H$_3$) ppm.

^{11}B NMR (160 MHz, $CDCl_3$, 297 K): δ = –8.6 (very br s) ppm.

^{19}F NMR (471 MHz, $CDCl_3$, 297 K): δ = –78.2 (s) ppm.

Elemental analysis for [$C_{52}H_{74}B_2F_6N_4O_6S_2$] ($M_w$ = 1050.92 g mol^{-1}): calcd. C 59.43, H 7.10, N 5.33, S 6.10%; found C 58.33, H 6.97, N 5.35, S 5.97%.

5.2.2 Synthesis and Reactivity of Boryl Anions and a Hydroboryl Radical

[(CAAC^{Me}H)(CAAC^{Me})BH][K] (**5**)

Route A. Compound **2-CAAC^{Me}** (20.0 mg, 27.3 µmol) and KC_8 (8.00 mg, 60.0 µmol, 2.20 equiv) were suspended in 0.6 mL of C_6D_6. After 1 min, the suspension was filtered yielding an intense red solution of **5** in analytically pure quality sufficient for NMR spectroscopic analysis. The solution was concentrated *in vacuo*. Bright orange single crystals of **5** were obtained by slow evaporation of the solvent at rt. *Note: Evaporation of the solvent in vacuo resulted in some protonation yielding the known compound [(CAAC^{Me})BH$_2$(CAAC^{Me}H)].*[74]

Route B. 2-CAAC^{Me} (100 mg, 0.14 mmol) and KC_8 (40.0 mg, 0.30 mmol, 2.20 equiv) were suspended in 3 mL of hexane for one minute prior to filtration. Complete evaporation of the solvent under atmospheric pressure afforded **5** as a red solid in essentially quantitative yield (86 mg, 0.13 mmol, 99% yield).

^{1}H{^{11}B} NMR (500 MHz, C_6D_6, 297 K): δ = 7.03–7.01 (m, 1H, Ar*H*), 6.84–6.80 (m, 2H, Ar*H*), 6.73–6.69 (m, 2H, Ar*H*), 6.67–6.64 (m, 1H, Ar*H*), 4.38 (d, ^3J = 6.6 Hz, 1H, BC*H*), 4.08 (sept, ^3J = 6.7 Hz, 1H, *i*Pr-C*H*), 3.83 (sept, ^3J = 6.8 Hz, 1H, *i*Pr-C*H*), 3.63 (sept, ^3J = 6.7 Hz, 1H, *i*Pr-C*H*), 3.37 (sept, ^3J = 6.8 Hz, 1H, *i*Pr-C*H*), 2.09 (d, ^2J = 11.7 Hz, 1H, CH_2), 2.02 (d, ^2J = 8.6 Hz, 1H, CH_2), 2.00 (s, 3H, NC(CH_3)$_2$), 1.96 (d, ^2J = 11.8 Hz, 1H, CH_2), 1.95 (d, ^2J = 11.5 Hz, 1H, CH_2), 1.90 (d , ^3J = 6.6 Hz, 1H, B*H*), 1.66 (s, 6H, NC(CH_3)$_2$), 1.48 (d, ^3J = 6.7 Hz, 3H, *i*Pr-CH_3), 1.47 (s, 3H, NC(CH_3)$_2$), 1.36 (s, 3H), 1.34–1.32 (m, 6H), 1.22 (d, ^3J = 6.8 Hz, 3H, *i*Pr-CH_3), 1.16–1.15 (m, 9H), 1.14–1.13 (m, 3H), 1.08–1.06 (m, 6H), 0.82 (d, ^3J = 7.1 Hz, 3H, *i*Pr-CH_3) ppm.

^{13}C{^{1}H} NMR (126 MHz, C_6D_6, 297 K): δ = 155.9, 155.7, 155.2, 150.1 ($C_{carbene}$), 149.7, 147.7, 145.5, 125.2, 124.8, 124.5, 123.4, 123.4, 123.2 (= 12 C Aryl), 67.1 (B*C*H), 62.0 (*C*H$_2$), 61.6

(CH_2), 61.2 (NC(CH_3)$_2$), 60.9 (NC(CH_3)$_2$), 43.5, 43.1, 38.8, 37.9, 33.1, 32.0, 32.0, 29.1, 28.3, 28.2, 27.9, 27.6, 27.5, 27.2, 27.1, 26.5, 26.2, 26.1, 25.3, 25.2, 24.8 ppm.

^{11}B NMR (160 MHz, C_6D_6, 297 K): δ = 16.7 (br s) ppm.

FT-IR (solid-state): $\tilde{\nu}$(B–H) = 2329 cm^{-1}.

UV-vis (THF, 25 °C): λ_{max} = 502 nm.

Elemental analysis for [$C_{40}H_{64}BKN_2$] (M_w = 622.87 g mol^{-1}): calcd. C 77.13, H 10.36, N 4.50%; found C 77.35, H 11.06, N 4.36%.

[(CAAC^{Me}H)(CAAC^{Me})BH][K](thf)$_3$ (5-thf)

2-CAAC^{Me} (50.0 mg, 54.6 μmol) and KC_8 (20.0 mg, 15.0 μmol, 2.20 equiv) were suspended in 3 mL of a 1:5 THF/hexane solvent mixture for one minute prior to filtration. The filtrate was stored at –25 °C for several days providing a crop of red crystals (25.0 mg, 29.8 μmol, 55% yield) suitable for X-ray structural analysis.

^{1}H NMR (400 MHz, C_6D_6, 297 K): δ = 7.02 (d, ^3J = 7.5 Hz, 1H, ArH), 6.86 (d, ^3J = 7.5 Hz, 1H, ArH), 6.81 (t, ^3J = 7.8 Hz, 1H, ArH), 6.75–6.72 (m, 2H, ArH), 6.69 (t, ^3J = 7.6 Hz, 1H, ArH), 4.39 (d, ^3J = 6.6 Hz, 1H, BCH), 4.11 (sept, ^3J = 6.7 Hz, 1H, iPr-CH), 3.84 (sept, ^3J = 6.8 Hz, 1H, iPr-CH), 3.65 (sept, ^3J = 6.7 Hz, 1H, iPr-CH), 3.55 (m, 12H, THF-OCH_2), 3.43 (sept, ^3J = 6.8 Hz, 1H, iPr-CH), 2.10 (d, ^2J = 11.8 Hz, 1H, CH_2), 2.04 (d, ^2J = 8.6 Hz, 1H, CH_2), 2.00 (s, 3H, NC(CH_3)$_2$), 1.98–1.93 (m, 2H, CH_2), 1.66 (s, 3H, NC(CH_3)$_2$), 1.65 (s, 3H, NC(CH_3)$_2$), 1.50 (d, ^3J = 6.7 Hz, 3H, iPr-CH_3), 1.46 (s, 3H, NC(CH_3)$_2$), 1.43–1.39 (m, 12H, THF-CH_2), 1.36–1.35 (m, 6H), 1.32 (s, 3H), 1.22 (d, ^3J = 6.7 Hz, 3H, iPr-CH_3), 1.17–1.13 (m, 12H), 1.11–1.09 (m, 6H), 0.85 (d, ^3J = 6.9 Hz, 3H, iPr-CH_3) ppm.

^{11}B NMR (128 MHz, C_6D_6, 297 K): δ = 16.8 (br s) ppm.

FT-IR (solid-state): $\tilde{\nu}$(B–H) = 2269 cm^{-1}.

UV-vis (THF, 25 °C): λ_{max} = 502 nm.

Elemental analysis for [$C_{52}H_{88}BKN_2O_3$] (M_w = 839.19 g mol^{-1}): calcd. C 74.43, H 10.57, N 3.34%; found C 74.54, H 10.33, N 3.87%.

[(CAAC^{Me}H)$_2$(Me)B] (6)

2-CAAC^{Me} (20.0 mg, 27.3 μmol) and KC_8 (8.00 mg, 60.0 μmol, 2.20 equiv) were suspended in 1 mL of hexane for 1 min prior to filtration. The red filtrate was treated with MeOTf (4.50 mg, 27.3 μmol), whereupon the mixture instantly turned colorless accompanied by formation of a precipitate. After filtration and evaporation of the solvent *in vacuo*, the residue was dissolved in 0.6 mL of C_6D_6 and NMR-spectroscopic analysis showed **6** in analytically

pure quality. After freeze-drying **6** was obtained as a colorless solid (13.0 mg, 21.7 µmol, 80% yield).

^{1}H NMR (500 MHz, C_6D_6, 297 K): δ = 7.14–7.07 (m, 6H, Ar*H*), 4.35 (sept, ^{3}J = 6.8 Hz, 2H, *i*Pr-C*H*), 3.65 (s, 2H, BC*H*), 3.23 (sept, ^{3}J = 6.7 Hz, 2H, *i*Pr-C*H*), 2.09 (d, ^{2}J = 12.6 Hz, 2H, CH_2), 1.66 (s, 3H, BCH_3), 1.57 (s, 6H, NC(CH_3)$_2$), 1.54 (d, ^{3}J = 6.7 Hz, 6H, *i*Pr-CH_3), 1.40 (d, ^{2}J = 12.8 Hz, 2H, CH_2), 1.37 (d, ^{3}J = 6.9 Hz, 6H, *i*Pr-CH_3), 1.23 (d, ^{3}J = 7.0 Hz, 6H, *i*Pr-CH_3), 1.19 (s, 6H, NC(CH_3)$_2$), 1.16 (d, ^{3}J = 6.7 Hz, 6H, *i*Pr-CH_3), 0.98 (s, 6H, C(CH_3)$_2$), 0.58 (s, 6H, C(CH_3)$_2$) ppm.

^{13}C{^{1}H} NMR (126 MHz, C_6D_6, 297 K): δ = 151.3 (*o*-Ar*C*), 149.1 (*o*-Ar*C*), 146.6 (*i*-Ar*C*), 126.3 (*m*-Ar*C*), 125.9 (*m*-Ar*C*), 124.2 (*p*-Ar*C*), 77.5 (B*C*H), 64.2 (N*C*(CH$_3$)$_2$), 60.8 (*C*H$_2$), 42.5 (*C*(CH$_3$)$_2$), 34.2 (NC(*C*H$_3$)$_2$), 33.1 (NC(*C*H$_3$)$_2$), 29.9 (C(*C*H$_3$)$_2$), 28.7 (*i*Pr-*C*H), 28.2 (C(*C*H$_3$)$_2$), 27.5 (*i*Pr-*C*H), 27.0 (*i*Pr-*C*H$_3$), 26.6 (*i*Pr-*C*H$_3$), 24.7 (*i*Pr-*C*H$_3$), 24.7 (*i*Pr-*C*H$_3$), 14.1 (B*C*H$_3$) ppm.

^{11}B NMR (160 MHz, C_6D_6, 297 K): δ = 93.9 (very br s) ppm.

Elemental analysis for [$C_{41}H_{67}BN_2$] (M_w = 598.81 g mol^{-1}): calcd. C 82.24, H 11.28, N 4.68%; found C 82.52, H 11.67, N 4.92%.

HRMS ASAP pos for [$C_{41}H_{68}BN_2$] = [M + H]: calcd. 599.5470; found 599.5468.

[(CAAC^{Me})$_2$BH$_2$](S$_n$)$_{0.5}$ (7)

To a solution of **5** (100 mg, 0.16 mmol) in 3 mL of benzene elemental sulfur (33.0 mg, 1.28 mmol, 64.0 equiv) was added. The reaction mixture turned dark orange accompanied by formation of an off-white precipitate. After stirring for 2 h at room temperature the suspension was filtered. The residue was washed with benzene and hexane affording **7** as an off-white solid (104 mg, 0.12 mmol, 72%). The ^{1}H and ^{11}B NMR spectra of **7** were essentially identical with those of **2-CAAC^{Me}**, indicating the formation of the [(CAAC^{Me})$_2$BH$_2$]$^{+}$ cation, presumably with a S_n^{2-} counteranion.

^{1}H{^{11}B} NMR (500 MHz, $CDCl_3$, 297 K): δ = 7.27 (t, ^{3}J = 7.7 Hz, 2H, *p*-Ar*H*), 7.24–7.18 (m, 2H, *m*-Ar*H*), 7.07–7.02 (m, 2H, *m*-Ar*H*), 2.57 (br s, 2H, *i*Pr-C*H*), 2.43 (d, ^{2}J = 12.0 Hz, 2H, CH_2), 2.04 (d, ^{2}J = 11.4 Hz, 2H, CH_2), 1.93 (br s, 8H, two *i*Pr-C*H* and NC(CH_3)$_2$), 1.70 (s, 2H, BH_2), 1.57 (s, 6H, NC(CH_3)$_2$), 1.49 (s, 6H, C(CH_3)$_2$), 1.33 (s, 6H, *i*Pr-CH_3), 1.14 (br s, 18H, C(CH_3)$_2$ and two *i*Pr-CH_3), 0.17 (s, 6H, *i*Pr-CH_3) ppm.

^{13}C{^{1}H} NMR (126 MHz, $CDCl_3$, 297 K): δ = 192.7 ($C_{carbenes}$), 144.8 (*i*-Ar*C*), 142.6 (*i*-Ar*C*), 132.7 (*o*-Ar*C*), 129.8 (*p*-Ar*C*), 125.9 (*m*-Ar*C*), 79.3 (N*C*(CH$_3$)$_2$), 53.7 (*C*H$_2$), 52.0 (*C*(CH$_3$)$_2$),

29.9 (*i*Pr-*C*H), 29.4 (NC(*C*H$_3$)$_2$), 29.2 (C(*C*H$_3$)$_2$), 28.9 (C(*C*H$_3$)$_2$), 28.7 (NC(*C*H$_3$)$_2$), 27.2 (*i*Pr-*C*H$_3$), 25.7 (*i*Pr-*C*H$_3$), 24.5 (*i*Pr-*C*H$_3$), 24.3 (*i*Pr-*C*H$_3$) ppm.

^{11}B NMR (160 MHz, $CDCl_3$, 297 K): δ = –22.4 (t, $^1J_{BH}$ = 84.7 Hz) ppm.

HRMS LIFDI-pos. for $[C_{40}H_{64}BN_2]^+ = [M]^+$: calcd. 583.5157; found 583.5140.

[(CAAC^{Me})BH(CAAC^{Me}H)]$^{\bullet}$ (8)

A solution of **5-thf** (100 mg, 0.16 mmol) in 5 mL of THF was added dropwise to a solution of **2-CAAC^{Me}** (117 mg, 0.16 mmol) in 3 mL of THF. The reaction mixture instantly turned intense purple and a colorless precipitate was formed. The ^{11}B NMR spectrum of the filtrate was silent indicating the presence of a radical species. After evaporation of the solvent under atmospheric pressure the product was extracted with hexane. Complete removal of hexane under atmospheric pressure afforded **8** as bright orange crystals (166 mg, 0.28 mmol, 89% yield) suitable for X-ray structure analysis.

EPR (CW, X-band, hexane, rt): g_{iso} = 2.0027, a(^{11}B) = 9.7 MHz, a(^{14}N) = 18.5 MHz, a($^1H_{H1}$) = 13.6 MHz, a($^1H_{H2}$) = 4.8 MHz.

FT-IR (solid-state): $\tilde{\nu}$(B–H) = 2533 cm^{-1}.

UV-vis (THF, 25 °C): λ_{max} = 523 nm.

Elemental analysis for $[C_{40}H_{64}BN_2]$ (M_w = 583.78 g mol^{-1}): calcd. C 82.30, H 11.05, N 4.80%; found C 82.08, H 11.35, N 4.75%.

5.2.3 Synthesis of Isothiocyanatoboranes

(CAAC^{Me})BH$_2$(NCS) (9^{Me})

To a suspension of **1^{Me}** (2.00 g, 4.47 mmol) in 40 mL of benzene NaSCN (362 mg, 4.47 mmol) dissolved in 30 mL of THF was added dropwise. The resulting solution was stirred for 1 h at room temperature prior to removal of volatiles. The residue obtained was washed with hexane and subsequently **9^{Me}** was extracted with benzene. Drying *in vacuo* yielded **9^{Me}** (1.47 g, 4.11 mmol, 92% yield) as a colorless solid. Colorless single crystals were obtained by vapor diffusion of hexane in a saturated benzene solution.

^{1}H{^{11}B} NMR (500 MHz, C_6D_6, 297 K): δ = 7.17 (t, ^3J = 7.8 Hz, 1H, *p*-Ar*H*), 7.04 (d, ^3J = 7.7 Hz, 2H, *m*-Ar*H*), 2.78 (br s, 2H, B*H*$_2$), 2.47 (sept, ^3J = 6.7 Hz, 2H, *i*Pr-C*H*), 1.36 (s, 6H, NC(C*H*$_3$)$_2$), 1.33 (s, 2H, C*H*$_2$), 1.30 (d, ^3J = 6.7 Hz, 6H, *i*Pr-C*H*$_3$), 1.06 (d, ^3J = 6.7 Hz, 6H, *i*Pr-C*H*$_3$), 0.74 (s, 6H, C(C*H*$_3$)$_2$) ppm.

^{13}C{^{1}H} NMR (126 MHz, C_6D_6, 297 K): δ = 229.5 (*C*$_{carbene}$, identified by HMBC), 142.7 (*o*-Ar*C*), 129.8 (*i*-Ar*C*), 128.5 (*p*-Ar*C*), 123.3 (*m*-Ar*C*), 75.9 (N*C*(CH$_3$)$_2$), 50.3 (*C*(CH$_3$)$_2$), 48.7

(CH$_2$), 27.5 (*i*Pr-CH), 27.0 (NC(CH$_3$)$_2$), 26.1 (C(CH$_3$)$_2$), 23.4 (*i*Pr-CH$_3$), 21.6 (*i*Pr-CH$_3$) ppm. *Note: the C_{NCS} resonance was not detected.*

^{11}B NMR (160 MHz, C$_6$D$_6$, 297 K): δ = –20.4 (br t, $^1J_{BH}$ = 86.7 Hz) ppm.

FT-IR (solid-state): $\tilde{\nu}$(NCS) = 2148, 2112 cm^{-1}.

Elemental analysis for [C$_{21}$H$_{33}$BN$_2$S] (M_w = 356.38 g mol^{-1}): calcd. C 70.78, H 9.33, N 7.86, S 9.00%; found C 70.73, H 9.56, N 7.49, S 8.84%.

HRMS LIFDI for [C$_{21}$H$_{34}$BN$_2$S]$^+$ = [M + H]$^+$: calcd. 357.2530; found 357.2529.

(CAAC^{Cy})BH$_2$(NCS) (**9^{Cy}**)

NaSCN (333 mg, 4.10 mmol) dissolved in 30 mL of THF was added slowly to a suspension of **1^{Cy}** (2.00 g, 4.10 mmol) in 40 mL of benzene. After stirring for 1 h at room temperature, all volatiles were removed *in vacuo* and the residue was washed with hexane. Extraction with benzene, solvent removal and drying *in vacuo* afforded **9^{Cy}** (1.45 g, 3.65 mmol, 89% yield). Colorless single crystals were obtained by vapor diffusion of hexane in a saturated benzene solution.

^{1}H{^{11}B} NMR (500 MHz, C$_6$D$_6$, 297 K): δ = 7.18 (t, ^3J = 7.8 Hz, 1H, *p*-ArH), 7.05 (d, ^3J = 7.7 Hz, 2H, *m*-ArH), 2.79 (br s, 2H, BH_2), 2.49 (sept, ^3J = 6.7 Hz, 2H, *i*Pr-CH), 2.45–2.40 (m, 2H, Cy-CH_2), 1.54–1.49 (m, 3H, Cy-CH_2), 1.44 (s, 2H, CH_2), 1.42–1.33 (m, 1H, Cy-CH_2), 1.32 (d, ^3J = 6.7 Hz, 6H, *i*Pr-CH_3), 1.29–1.28 (m, 2H, Cy-CH_2), 1.08 (d, ^3J = 6.7 Hz, 6H, *i*Pr-CH_3), 1.04–0.94 (m, 2H, Cy-CH_2), 0.74 (s, 6H, NC(CH_3)$_2$) ppm.

^{13}C{^{1}H} NMR (126 MHz, C$_6$D$_6$, 297 K): δ = 229.4 ($C_{carbene}$, identified by HMBC), 144.7 (*o*-ArC), 132.0 (*i*-ArC), 130.5 (*p*-ArC), 125.3 (*m*-ArC), 78.0 (NC(CH$_3$)$_2$), 57.9 (C(C$_5$H$_{10}$)), 45.4 (CH$_2$), 35.5 (Cy-CH$_2$), 29.5 (*i*Pr-CH), 28.7 (NC(CH$_3$)$_2$), 25.4 (*i*Pr-CH$_3$), 25.2 (Cy-CH$_2$), 23.6 (*i*Pr-CH$_3$), 22.4 (Cy-CH$_2$) ppm. *Note: the C_{NCS} resonance was not detected.*

^{11}B NMR (160 MHz, C$_6$D$_6$, 297 K): δ = –20.1 (br t, $^1J_{BH}$ = 87.4 Hz) ppm.

FT-IR (solid-state): $\tilde{\nu}$(NCS) = 2154 cm^{-1}.

Elemental analysis for [C$_{24}$H$_{37}$BN$_2$S] (M_w = 396.44 g mol^{-1}): calcd. C 72.71, H 9.41, N 7.07, S 8.09%; found C 72.74, H 9.60, N 7.09, S 8.06%.

(CAAC^{Me})BBr$_2$(NCS) (**10^{Me}**)

Elemental bromine (0.52 mL, 9.82 mmol, 2.50 equiv) was added dropwise to a solution of **9^{Me}** (1.40 g, 3.93 mmol) in 25 mL of DCM, whereupon evolution of gas was observed. The reaction mixture was stirred overnight at room temperature prior to removal of all volatiles. The residue was washed with pentane and dried *in vacuo* to afford **10^{Me}** (1.94 g, 3.77 mmol, 96% yield) as

a pale yellow solid. Colorless single crystals were obtained by vapor diffusion of hexane in a saturated benzene solution.

^{1}H NMR (500 MHz, C_6D_6, 297 K): δ = 7.15–7.12 (m, 3H, *p*-Ar*H*, *m*-Ar*H*), 2.63 (sept, ^{3}J = 6.6 Hz, 2H, *i*Pr-C*H*), 1.74 (s, 6H, NC(CH_3)$_2$), 1.54 (d, ^{3}J = 6.5 Hz, 6H, *i*Pr-CH_3), 1.33 (s, 2H, CH_2), 1.05 (d, ^{3}J = 6.6 Hz, 6H, *i*Pr-CH_3), 0.69 (s, 6H, C(CH_3)$_2$) ppm.

^{13}C{^{1}H} NMR (126 MHz, C_6D_6, 297 K): δ = 209.1 ($C_{carbene}$, identified by HMBC), 145.1 (*o*-Ar*C*), 131.4 (*p*-Ar*C*), 131.1 (*i*-Ar*C*), 126.5 (*m*-Ar*C*), 79.3 (N*C*(CH$_3$)$_2$), 53.9 (*C*(CH$_3$)$_2$), 51.1 (*C*H$_2$), 31.9 (NC(*C*H$_3$)$_2$), 29.5 (*i*Pr-*C*H), 28.1 (C(*C*H$_3$)$_2$), 26.6 (*i*Pr-*C*H$_3$), 24.3 (*i*Pr-*C*H$_3$) ppm. *Note: the C_{NCS} resonance was not detected.*

^{11}B NMR (160 MHz, C_6D_6, 297 K): δ = –13.6 (s) ppm.

FT-IR (solid-state): $\tilde{\nu}$(NCS) = 2129, 2093 cm^{-1}.

Elemental analysis for [$C_{21}H_{31}BBr_2N_2S$] (M_w = 514.17 g mol^{-1}): calcd. C 49.06, H 6.08, N 5.45, S 6.24%; found C 49.53, H 6.14, N 5.54, S 6.71%.

(CAAC^{Cy})BBr$_2$(NCS) (**10^{Cy}**)

To a solution of **9^{Cy}** (1.40 g, 3.53 mmol) in 30 mL of DCM elemental bromine (0.47 mL, 8.83 mmol, 2.50 equiv) was added slowly, whereupon evolution of gas was observed. After stirring overnight at room temperature all volatiles were removed *in vacuo*. The residue was washed with pentane and dried *in vacuo*, yielding **10^{Cy}** (1.84 g, 3.32 mmol, 94% yield) as a pale yellow solid. Colorless single crystals of **10^{Cy}** were obtained by vapor diffusion of hexane in a saturated benzene solution.

^{1}H NMR (500 MHz, C_6D_6, 297 K): δ = 7.18–7.13 (m, 3H, *p*-Ar*H*, *m*-Ar*H*, overlapping with C_6H_6), 3.16 (dt, ^{2}J = 13.5 Hz, ^{3}J = 3.5 Hz, 2H, Cy-CH_2), 2.68 (sept, ^{3}J = 6.6 Hz, 2H, *i*Pr-C*H*), 1.81–1.78 (m, 2H, Cy-CH_2), 1.56 (d, ^{3}J = 6.5 Hz, 6H, *i*Pr-CH_3), 1.52–1.41 (m, 4H, Cy-CH_2), 1.48 (s, 2H, CH_2), 1.29–1.17 (m, 2H, Cy-CH_2), 1.07 (d, ^{3}J = 6.6 Hz, 6H, *i*Pr-CH_3), 1.04–0.95 (m, 2H, Cy-CH_2), 0.71 (s, 6H, NC(CH_3)$_2$) ppm.

^{13}C{^{1}H} NMR (126 MHz, C_6D_6, 297 K): δ = 145.1 (*o*-Ar*C*), 131.4 (*p*-Ar*C*), 128.6 (*i*-Ar*C*), 126.5 (*m*-Ar*C*), 79.8 (N*C*(CH$_3$)$_2$), 59.7 (*C*(C$_5$H$_{10}$)), 43.9 (*C*H$_2$), 37.1 (Cy-*C*H$_2$), 29.5 (*i*Pr-*C*H), 28.6 (NC(*C*H$_3$)$_2$), 26.7 (*i*Pr-*C*H$_3$), 24.8 (Cy-*C*H$_2$), 24.4 (*i*Pr-*C*H$_3$), 22.9 (Cy-*C*H$_2$) ppm. *Note: the $C_{carbene}$ and C_{NCS} resonances were not detected, even by HMBC.*

^{11}B NMR (160 MHz, C_6D_6, 297 K): δ = –13.4 (s) ppm.

FT-IR (solid-state): $\tilde{\nu}$(NCS) = 2143, 2104 cm^{-1}.

Elemental analysis for [$C_{24}H_{35}BBr_2N_2S$] (M_w = 554.24 g mol^{-1}): calcd. C 52.01, H 6.37, N 5.05, S 5.78%; found C 52.34, H 6.40, N 5.20, S 6.12%.

5.2.4 Synthesis of Isothiocyanato- and Cyanoborylenes

(CAAC^{Me})(I*i*Pr)B(NCS) (11^{Me})

I*i*Pr (326 mg, 2.14 mmol, 2.20 equiv) and KC_8 (289 mg, 2.14 mmol, 2.20 equiv) were combined in 2 mL of benzene at room temperature. A dilute solution of **10^{Me}** (500 mg, 0.97 mmol) in 20 mL of benzene was added dropwise to this mixture under vigorous stirring. The resulting red suspension was stirred for 2 h at room temperature prior to filtration. The ^{11}B NMR spectrum of the filtrate showed a mixture of both isomers in a ratio of (*E*):(*Z*) 22:78. After concentration of the filtrate to 5 mL *in vacuo*, slow evaporation of the solvent afforded a large crop of orange crystals of **(*Z*)-11^{Me}** (304 mg, 0.60 mmol, 62% yield). Further crystallization yielded a second crop of crystals of **(*E*)-11^{Me}** (55.7 mg, 0.11 mmol, 11% yield; overall yield of both isomers: 0.71 mmol, 73%).

NMR data for **(*E*)-11^{Me}**:

^{1}H NMR (500 MHz, C_6D_6, 297 K): δ = 6.98 (br, 1H, *m*-Ar*H*), 6.92 (t, ^{3}J = 7.7 Hz, 1H, *p*-Ar*H*), 6.73 (br, 1H, *m*-Ar*H*), 6.01 (br, 1H, I*i*Pr-C*H*), 5.91 (br, 1H, I^{i}Pr-C*H*), 5.30 (br, 1H, I^{i}Pr-C*H*(CH$_3$)$_2$), 3.60 (br, 1H, I^{i}Pr-C*H*(CH$_3$)$_2$), 3.47 (br, 1H, *i*Pr-C*H*), 3.14 (br, 1H, *i*Pr-C*H*), 2.02 (br, 3H, I*i*Pr-CH(C*H*$_3$)$_2$) 1.93 (br, 3H, I*i*Pr-CH(C*H*$_3$)$_2$), 1.87 (br, 2H, C*H*$_2$), 1.48 (br, 3H, C(C*H*$_3$)$_2$), 1.44 (br, 3H, I*i*Pr-CH(C*H*$_3$)$_2$), 1.24 (br, 3H, I*i*Pr-CH(C*H*$_3$)$_2$), 1.12 (br, 6H, C(C*H*$_3$)$_2$), 1.04 (br, 3H, C(C*H*$_3$)$_2$), 0.89 (br, 3H, *i*Pr-C*H*$_3$), 0.83 (br, 3H, *i*Pr-C*H*$_3$), 0.33 (br, 3H, *i*Pr-C*H*$_3$), 0.14 (br, 3H, *i*Pr-C*H*$_3$) ppm.

^{13}C{^{1}H} NMR (126 MHz, C_6D_6, 297 K): δ = 149.9 (*o*-Ar*C*), 149.0 (*o*-Ar*C*), 145.3 (*i*-Ar*C*), 125.7 (*p*-Ar*C*), 123.1 (*m*-Ar*C*), 116.5 (I^{i}Pr-*C*H), 115.8 (I^{i}Pr-*C*H), 63.4 (N*C*(CH$_3$)$_2$), 59.0 (*C*H$_2$), 50.7 (I*i*Pr-*C*H(CH$_3$)$_2$), 45.4 (*C*(CH$_3$)$_2$), 33.2 (I*i*Pr-CH(*C*H$_3$)$_2$), 32.0 (I*i*Pr-CH(*C*H$_3$)$_2$), 31.1 (C(*C*H$_3$)$_2$), 27.8 (*i*Pr-*C*H), 27.1 (*i*Pr-*C*H$_3$), 26.6 (C(*C*H$_3$)$_2$), 24.8 (*i*Pr-*C*H$_3$), 24.2 (*i*Pr-*C*H$_3$), 23.9 (C(*C*H$_3$)$_2$), 21.5 (C(*C*H$_3$)$_2$), 21.1 (*i*Pr-*C*H$_3$) ppm. *Note: the $C_{carbene}$ and C_{NCS} resonances were not detected, even by HMBC.*

^{11}B NMR (160 MHz, C_6D_6, 297 K): δ = 3.8 (s) ppm.

NMR data for **(*Z*)-11^{Me}**:

^{1}H NMR (500 MHz, C_6D_6, 297 K): δ = 7.50–7.44 (m, 3H, *p*-Ar*H*, *m*-Ar*H*), 6.11 (s, 2H, I*i*Pr-C*H*), 5.28 (sept, ^{3}J = 6.7 Hz, 2H, I*i*Pr-C*H*(CH$_3$)$_2$), 3.73 (sept, ^{3}J = 6.6 Hz, 2H, *i*Pr-C*H*), 1.92 (s, 2H, C*H*$_2$), 1.70 (d, ^{3}J = 6.7 Hz, 6H, *i*Pr-C*H*$_3$), 1.50 (d, ^{3}J = 6.8 Hz, 6H, *i*Pr-C*H*$_3$), 1.31 (s, 6H, NC(C*H*$_3$)$_2$), 1.06 (d, ^{3}J = 6.7 Hz, 6H, I*i*Pr-CH(C*H*$_3$)$_2$), 1.06 (s, 6H, C(C*H*$_3$)$_2$), 0.93 (d, ^{3}J = 6.7 Hz, 6H, I*i*Pr-CH(C*H*$_3$)$_2$) ppm.

^{13}C{^{1}H} NMR (126 MHz, C_6D_6, 297 K): δ = 149.9 (*o*-Ar*C*), 138.2 (*i*-Ar*C*), 128.6 (*p*-Ar*C*), 124.8 (*m*-Ar*C*), 116.2 (I*i*Pr-*C*H), 63.7 (N*C*(CH$_3$)$_2$), 58.2 (*C*H$_2$), 50.9 (I*i*Pr-*C*H(CH$_3$)$_2$), 42.4 (*C*(CH$_3$)$_2$), 33.4 (NC(*C*H$_3$)$_2$), 30.1 (NC(*C*H$_3$)$_2$), 28.9 (*i*Pr-*C*H), 26.1 (*i*Pr-*C*H$_3$), 25.1 (*i*Pr-*C*H$_3$), 24.8 (*i*Pr-*C*H$_3$), 20.8 (*i*Pr-*C*H$_3$) ppm. *Note: the $C_{carbene}$ and C_{NCS} resonances were not detected, even by HMBC.*

^{11}B NMR (160 MHz, C_6D_6, 297 K): δ = –2.6 (s) ppm.

FT-IR (solid-state): $\tilde{\nu}$(NCS) = 2101 cm^{-1}.

UV-vis (C_6H_6, 25 °C): λ_{max} = 342 nm, λ = 390 nm (shoulder).

Elemental analysis for [$C_{30}H_{47}BN_4S$] (M_w = 506.60 g mol^{-1}): calcd. C 71.13, H 9.35, N 11.06, S 6.33%; found C 72.17, H 9.56, N 10.74, S 5.71%.

HRMS LIFDI for [$C_{30}H_{47}BN_4S$] = [M]: calcd. 506.3609; found 506.3603.

(CAAC^{Cy})(I*i*Pr)B(NCS) (**11^{Cy}**)

To a suspension of I*i*Pr (60.4 mg, 0.40 mmol, 2.20 equiv) and KC_8 (53.7 mg, 0.40 mmol, 2.20 equiv) in 1 mL of benzene a dilute benzene solution of **10^{Cy}** (100 mg, 0.18 mmol) was added dropwise under vigorous stirring. The resulting red suspension was stirred for 2 h at room temperature prior to filtration. The ^{11}B NMR spectrum of the filtrate showed a mixture of both isomers in a ratio of (*E*):(*Z*) 15:85. Fractional crystallization yielded two crops of orange crystals of **(*Z*)-11^{Cy}** (66.7 mg, 0.12 mmol, 68% yield) and **(*E*)-11^{Cy}** (9.90 mg, 18.0 μmol, 10% yield; overall yield of both isomers: 0.14 mmol, 78%) suitable for X-ray diffraction analysis.

NMR data for **(*E*)-11^{Cy}**:

^{1}H NMR (400 MHz, C_6D_6, 297 K): δ = 6.99 (br, 1H, *m*-Ar*H*), 6.92 (t, ^{3}J = 7.6 Hz, 1H, *p*-Ar*H*), 6.73 (br, 1H, *m*-Ar*H*), 6.01 (br, 1H, I*i*Pr-C*H*), 5.89 (br, 1H, I*i*Pr-C*H*), 5.37 (br, 1H, I*i*Pr-C*H*(CH$_3$)$_2$), 3.62 (br, 1H, I*i*Pr-C*H*(CH$_3$)$_2$), 3.50 (br, 1H, *i*Pr-C*H*), 3.13 (br, 1H, *i*Pr-C*H*), 2.96 (br, 1H, Cy-C*H*$_2$), 2.57 (br, 1H, Cy-C*H*$_2$), 2.25 (br, 2H, Cy-C*H*$_2$), 2.14 (br, 2H, Cy-C*H*$_2$), 1.98 (br, 2H, Cy-C*H*$_2$), 1.87 (br, 2H, C*H*$_2$), 1.77 (br, 3H, Cy-C*H*$_2$), 1.48 (br, 6H, I*i*Pr-CH(C*H*$_3$)$_2$, 1.23 (br, 3H, I*i*Pr-CH(C*H*$_3$)$_2$), 1.12 (br, 6H, NC(C*H*$_3$)$_2$), 1.05 (br, 3H, I*i*Pr-CH(C*H*$_3$)$_2$), 0.91 (br, 3H, *i*Pr-C*H*$_3$), 0.87 (br, 3H, *i*Pr-C*H*$_3$), 0.33 (br, 3H, *i*Pr-C*H*$_3$), 0.15 (br, 3H, *i*Pr-C*H*$_3$) ppm.

^{11}B NMR (128 MHz, C_6D_6, 297 K): δ = 3.9 (s) ppm.

NMR data for **(*Z*)-11^{Cy}**:

^{1}H NMR (500 MHz, C_6D_6, 297 K): δ = 7.50–7.44 (m, 3H, *p*-Ar*H*, *m*-Ar*H*), 6.12 (s, 2H, I*i*Pr-C*H*), 5.32 (sept, ^{3}J = 6.9 Hz, 2H, I*i*Pr-C*H*(CH$_3$)$_2$), 3.71 (sept, ^{3}J = 6.9 Hz, 2H, *i*Pr-C*H*), 1.91 (s, 2H, C*H*$_2$), 1.86 (d, ^{2}J = 12.1 Hz, 2H, Cy-C*H*$_2$), 1.70 (d, ^{3}J = 6.7 Hz, 6H, *i*Pr-C*H*$_3$), 1.58–1.56 (m, 1H, Cy-C*H*$_2$), 1.50 (d, ^{3}J = 6.8 Hz, 6H, *i*Pr-C*H*$_3$), 1.45–1.37 (m, 4H, Cy-C*H*$_2$), 1.28 (s,

6H, NC(CH_3)$_2$), 1.06 (d, ^3J = 6.7 Hz, 6H, I*i*Pr-CH(CH_3)$_2$), 0.95 (d, ^3J = 6.9 Hz, 6H, I^{i}Pr-CH(CH_3)$_2$), 0.77 (dt, ^2J = 12.6 Hz, ^3J = 4.7 Hz, 2H, Cy-CH_2), 0.73–0.65 (m, 1H, Cy-CH_2) ppm.

^{13}C{^{1}H} NMR (126 MHz, C_6D_6, 297 K): δ = 150.0 (*o*-Ar*C*), 138.2 (*i*-Ar*C*), 124.8 (*p*-Ar*C*), 124.8 (*m*-Ar*C*), 116.3 (I*i*Pr-*C*H), 63.9 (N*C*(CH$_3$)$_2$), 51.0 (I*i*Pr-*C*H(CH$_3$)$_2$), 50.4 (*C*H$_2$), 47.3 (*C*(C$_5$H$_{10}$)), 41.7 (Cy-CH_2), 30.4 (NC(*C*H$_3$)$_2$), 28.9 (*i*Pr-*C*H), 27.0 (Cy-CH_2), 26.1 (*i*Pr-*C*H$_3$), 25.2 (*i*Pr-*C*H$_3$), 24.7 (I*i*Pr-CH(*C*H$_3$)$_2$), 24.2 (Cy-CH_2), 21.0 (I*i*Pr-CH(*C*H$_3$)$_2$) ppm. *Note: the $C_{carbene}$ and C_{NCS} resonances were not detected, even by HMBC.*

^{11}B NMR (160 MHz, C_6D_6, 297 K): δ = –2.3 (s) ppm.

FT-IR (solid-state): $\tilde{\nu}$(NCS) = 2101 cm^{-1}.

HRMS LIFDI for [$C_{33}H_{51}BN_4S$] = [M]: calcd. 546.3922; found 546.3915.

(CAAC^{Me})(I*i*Pr)B(CN) (**12**)

To a suspension of I*i*Pr (174 mg, 1.14 mmol, 2.20 equiv) and KC_8 (154 mg, 1.41 mmol, 2.20 equiv) in 5 mL of benzene a dilute solution of (CAAC^{Me})BBr_2(CN) (**XXV**) (250 mg, 0.52 mmol) in 10 mL of benzene was added dropwise under vigorous stirring. The resulting dark yellow suspension was stirred for 2 h at room temperature prior to filtration. After concentration of the filtrate to 5 mL *in vacuo*, slow evaporation of the solvent afforded **12** (200 mg, 0.42 mmol, 81% yield) as yellow crystals suitable for X-ray diffraction analysis.

^{1}H NMR (500 MHz, C_6D_6, 297 K): δ = 7.47–7.44 (m, 1H, *p*-Ar*H*), 7.40–7.38 (m, 2H, *m*-Ar*H*), 6.22 (s, 2H, I*i*Pr-C*H*), 5.32 (sept, ^3J = 6.8 Hz, 2H, I*i*Pr-C*H*(CH$_3$)$_2$), 3.63 (sept, ^3J = 6.8 Hz, 2H, *i*Pr-C*H*), 1.91 (s, 2H, CH_2), 1.80 (d, ^3J = 6.7 Hz, 6H, *i*Pr-CH_3), 1.48 (d, ^3J = 6.7 Hz, 6H, *i*Pr-CH_3), 1.32 (s, 6H, NC(CH_3)$_2$), 1.13 (d, ^3J = 6.7 Hz, 6H, I*i*Pr-CH(CH_3)$_2$), 1.09 (s, 6H, C(CH_3)$_2$), 0.98 (d, ^3J = 6.9 Hz, 6H, I*i*Pr-CH(CH_3)$_2$) ppm.

^{13}C{^{1}H} NMR (126 MHz, C_6D_6, 297 K): δ = 151.4 (*o*-Ar*C*), 138.1 (*i*-Ar*C*), 128.6 (*p*-Ar*C*), 124.8 (*m*-Ar*C*), 116.3 (I*i*Pr-*C*H), 63.8 (N*C*(CH$_3$)$_2$), 57.8 (*C*H$_2$), 51.0 (I*i*Pr-*C*H(CH$_3$)$_2$), 43.7 (*C*(CH$_3$)$_2$), 33.0 (C(*C*H$_3$)$_2$), 30.3 (NC(*C*H$_3$)$_2$), 28.8 (*i*Pr-*C*H), 26.7 (*i*Pr-*C*H$_3$), 25.4 (*i*Pr-*C*H$_3$), 24.1 (I*i*Pr-CH(*C*H$_3$)$_2$), 20.8 (I*i*Pr-CH(*C*H$_3$)$_2$) ppm. *Note: the $C_{carbene}$ and C_{CN} resonances were not detected, even by HMBC.*

^{11}B NMR (160 MHz, C_6D_6, 297 K): δ = –12.1 (s) ppm.

FT-IR (solid-state): $\tilde{\nu}$(CN) = 2119 cm^{-1}.

UV-vis (C_6H_6, 25 °C): λ_{max} = 313 nm, λ = 446 nm.

Elemental analysis for [$C_{30}H_{47}BN_4$] (M_w = 474.54 g mol^{-1}): calcd. C 75.93, H 9.98, N 11.81%; found C 76.34, H 9.88, N 11.27%.

5.2.5 Reactivity of Isothiocyanato- and Cyanoborylenes

[(CAAC^{Me})(I*i*Pr)B(NCS)]$^{\bullet+}$[OTf]$^-$ ([(*Z*)-11$^{Me\bullet+}$][OTf$^-$])

11^{Me} (50.0 mg, 98.7 μmol) and AgOTf (25.4 mg, 98.7 μmol) were suspended in 2 mL of benzene for five minutes at room temperature. Filtration and evaporation of the solvent under atmospheric pressure afforded **[(*Z*)-11$^{Me\bullet+}$][OTf$^-$]** (52.4 mg, 79.9 μmol, 81% yield) as yellow crystals suitable for X-ray diffraction analysis.

EPR (CW, X-band, C_6H_6, rt): g_{iso} = 2.003 (peak-to-peak linewidth: 1.9 mT).

FT-IR (solid-state): $\tilde{\nu}$(NCS) = 2056 cm^{-1}.

UV-vis (C_6H_6, 25 °C): λ = 318 nm (shoulder), λ_{max} = 364 nm, λ = 433 nm, λ = 460 nm.

HRMS LIFDI for $[C_{30}H_{47}BN_4S]^{\bullet+}$ = $[M]^{\bullet+}$: calcd. 506.3609; found 506.3606.

[(CAAC^{Me})(I*i*Pr)B(CN)]$^{\bullet+}$[OTf]$^-$ ([12$^{\bullet+}$][OTf$^-$])

Cyanoborylene **12** (100 mg, 0.211 mmol) and AgOTf (54.2 mg, 0.211 mmol) were suspended in 5 mL of benzene for five minutes at room temperature, whereupon a black precipitate was formed. Filtration and evaporation of the solvent under atmospheric pressure afforded a large crop of yellow crystals of **[12$^{\bullet+}$][OTf$^-$]** (111 mg, 0.178 mmol, 85% yield) suitable for X-ray diffraction analysis.

EPR (CW, X-band, C_6H_6, rt): g_{iso} = 2.0025, a(^{10,11}B) = 9.0 MHz, a(^{14}N) = 21.7 MHz, a(^{14}N) = 18.0 MHz.

FT-IR (solid-state): $\tilde{\nu}$(CN) = 2145 cm^{-1}.

UV-vis (C_6H_6, 25 °C): λ_{max} = 313 nm, λ = 452 nm.

HRMS LIFDI for $[C_{30}H_{48}BN_4]$ = $[M + H]^+$: calcd. 475.3967; found 475.3959.

(CAAC^{Me})(I*i*Pr)B(NCS)(Cr(CO)$_5$) (**11^{Me}-Cr**)

A solution of $[Cr(CO)_6]$ (10.4 mg, 47.4 μmol, 1.20 equiv) in 0.4 mL of THF was irradiated for 3 h and subsequently added to **11^{Me}** (20.0 mg, 39.5 μmol) dissolved in 0.4 mL of THF. The color instantly changed from orange to red. After evaporation of the solvent, the residue was washed with hexane and dried *in vacuo* to afford **11^{Me}-Cr** (23.7 mg, 34.0 μmol, 86% yield) as a brown solid. *Note: all attempts to crystallize **11^{Me}-Cr** resulted in the recovery of **11^{Me}**.*

^{1}H NMR (500 MHz, C_6D_6, 297 K): δ = 7.35–7.28 (m, 3H, *p*-Ar*H*, *m*-Ar*H*), 6.10 (s, 2H, I*i*Pr-C*H*), 5.06 (sept, ^3J = 6.8 Hz, 2H, I*i*Pr-C*H*(CH$_3$)$_2$), 3.50 (sept, ^3J = 6.7 Hz, 2H, *i*Pr-C*H*), 1.79 (s, 2H, C*H*$_2$), 1.54 (d, ^3J = 6.7 Hz, 6H, *i*Pr-C*H*$_3$), 1.39 (d, ^3J = 6.8 Hz, 6H, *i*Pr-C*H*$_3$), 1.19 (s, 6H, NC(C*H*$_3$)$_2$), 1.15 (d, ^3J = 6.6 Hz, 6H, I*i*Pr-CH(C*H*$_3$)$_2$), 0.93 (s, 6H, C(C*H*$_3$)$_2$), 0.90 (d, ^3J = 6.8 Hz, 6H, I*i*Pr-CH(C*H*$_3$)$_2$) ppm.

^{13}C{^{1}H} NMR (126 MHz, C_6D_6, 297 K): δ = 223.8 (*C*O), 216.6 (*C*O), 149.4 (*o*-Ar*C*), 136.9 (*i*-Ar*C*), 129.2 (*p*-Ar*C*), 125.0 (*m*-Ar*C*), 116.9 (I*i*Pr-*C*H), 64.6 (N*C*(CH$_3$)$_2$), 57.3 (*C*H$_2$), 51.2 (I*i*Pr-*C*H(CH$_3$)$_2$), 43.1 (*C*(CH$_3$)$_2$), 32.8 (C(*C*H$_3$)$_2$), 29.9 (NC(*C*H$_3$)$_2$), 28.8 (*i*Pr-*C*H), 26.1 (I*i*Pr-CH(*C*H$_3$)$_2$), 24.9 (*i*Pr-*C*H$_3$), 24.8 (I*i*Pr-CH(*C*H$_3$)$_2$), 20.9 (*i*Pr-*C*H$_3$) ppm. *Note: the $C_{carbene}$ and C_{NCS} resonances were not detected, even by HMBC.*

^{11}B NMR (160 MHz, C_6D_6, 297 K): δ = –3.8 (s) ppm.

FT-IR (solid-state): $\tilde{\nu}$(NCS) = 2108 cm^{-1}; $\tilde{\nu}$(CO) = 2057, 1968, 1932, 1903 cm^{-1}.

UV-vis (C_6H_6, 25 °C): λ_{max} = 365 nm.

Elemental analysis for [$C_{35}H_{47}BCrN_4O_5S$] (M_w = 698.65 g mol^{-1}): calcd. C 60.17, H 6.78, N 8.02, S 4.59%; found C 60.67, H 7.14, N 8.17, S 4.77%. *Note: HMRS only provided a peak for the **11^{Me}** borylene.*

(CAAC^{Me})(I*i*Pr)B(NCS)(W(CO)$_5$) (11^{Me}-W)

[W(CO)$_6$] (16.7 mg, 47.4 µmol, 1.20 equiv) dissolved in 0.4 mL of THF was irradiated for 3 h and added to a solution of **11^{Me}** (20.0 mg, 39.5 µmol) in 0.4 mL of THF. After a color change from orange to red the solvent was removed *in vacuo*. The residue was washed with hexane and dried *in vacuo* yielding **11^{Me}-W** (26.9 mg, 32.4 µmol, 82% yield) as a brown solid. *Note: all attempts to crystallize **11^{Me}-W** resulted in the recovery of **11^{Me}**.*

^{1}H NMR (500 MHz, C_6D_6, 297 K): δ = 7.35–7.28 (m, 3H, *p*-Ar*H*, *m*-Ar*H*), 6.13 (s, 2H, I*i*Pr-C*H*), 5.05 (sept, ^3J = 6.8 Hz, 2H, I*i*Pr-C*H*(CH$_3$)$_2$), 3.49 (sept, ^3J = 6.8 Hz, 2H, *i*Pr-C*H*), 1.78 (s, 2H, C*H*$_2$), 1.53 (d, ^3J = 6.8 Hz, 6H, *i*Pr-C*H*$_3$), 1.38 (d, ^3J = 6.8 Hz, 6H, *i*Pr-C*H*$_3$), 1.18 (s, 6H, NC(C*H*$_3$)$_2$), 1.13 (d, ^3J = 6.7 Hz, 6H, I*i*Pr-CH(C*H*$_3$)$_2$), 0.92 (s, 6H, C(C*H*$_3$)$_2$), 0.91 (d, ^3J = 6.9 Hz, 6H, I*i*Pr-CH(C*H*$_3$)$_2$) ppm.

^{13}C{^{1}H} NMR (126 MHz, C_6D_6, 297 K): δ = 201.5 (*C*O), 198.8 (*C*O), 149.4 (*o*-Ar*C*), 136.9 (*i*-Ar*C*), 129.3 (*p*-Ar*C*), 125.0 (*m*-Ar*C*), 117.0 (I*i*Pr-*C*H), 64.7 (N*C*(CH$_3$)$_2$), 57.2 (*C*H$_2$), 51.2 (I*i*Pr-*C*H(CH$_3$)$_2$), 43.2 (*C*(CH$_3$)$_2$), 32.8 (C(*C*H$_3$)$_2$), 29.9 (NC(*C*H$_3$)$_2$), 28.8 (*i*Pr-*C*H), 26.1 (I*i*Pr-CH(*C*H$_3$)$_2$), 25.0 (*i*Pr-*C*H$_3$), 24.9 (I*i*Pr-CH(*C*H$_3$)$_2$), 20.8 (*i*Pr-*C*H$_3$) ppm. *Note: the $C_{carbene}$ and C_{NCS} resonances were not detected, even by HMBC.*

^{11}B NMR (160 MHz, C_6D_6, 297 K): δ = –3.9 (s) ppm.

FT-IR (solid-state): $\tilde{\nu}$(NCS) = 2106 cm^{-1}; $\tilde{\nu}$(CO) = 2066, 1972, 1911, 1880 cm^{-1}.

UV-vis (C_6H_6, 25 °C): λ_{max} = 367 nm.

Elemental analysis for [$C_{35}H_{47}BN_4O_5SW$] (M_w = 830.49 g mol^{-1}): calcd. C 50.62, H 5.70, N 6.75, S 3.86%; found C 50.98, H 6.14, N 6.92, S 4.11%. *Note: HMRS only provided a peak for the **11^{Me}** borylene.*

(CAAC^{Me})(I*i*Pr)B(CN)(Cr(CO)$_5$) (12-Cr)

A solution of [Cr(CO)$_6$] (11.1 mg, 50.5 μmol, 1.20 equiv) in 0.4 mL of THF was irradiated for 3 h and added to **12** (20.0 mg, 42.1 μmol) dissolved in 0.4 mL of THF, whereupon the yellow color intensified. After evaporation of the solvent, the solid residue was washed with a 9:1 mixture of hexane/benzene. Drying *in vacuo* afforded **12-Cr** (25.5 mg, 38.3 μmol, 91% yield) as a yellow solid and as the (*Z*)-isomer only. Single crystals of **(*Z*)-12-Cr** were obtained by vapour diffusion of hexane into a saturated benzene solution.

^{1}H NMR (500 MHz, C_6D_6, 297 K): δ = 7.57 (t, ^3J = 7.7 Hz, 1H, *p*-Ar*H*), 7.40 (d, ^3J = 7.7 Hz, 1H, *p*-Ar*H*), 6.09 (s, 2H, I*i*Pr-C*H*), 5.07 (sept, ^3J = 6.8 Hz, 2H, I*i*Pr-C*H*(CH$_3$)$_2$), 3.34 (sept, ^3J = 6.7 Hz, 2H, *i*Pr-C*H*), 1.76 (s, 2H, CH_2), 1.61 (d, ^3J = 6.7 Hz, 6H, *i*Pr-CH_3), 1.39 (d, ^3J = 6.8 Hz, 6H, *i*Pr-CH_3), 1.17 (s, 6H, NC(CH_3)$_2$), 1.14 (d, ^3J = 6.7 Hz, 6H, I*i*Pr-CH(CH_3)$_2$), 0.92 (s, 6H, C(CH_3)$_2$), 0.90 (d, ^3J = 6.9 Hz, 6H, I*i*Pr-CH(CH_3)$_2$) ppm.

^{13}C{^{1}H} NMR (126 MHz, C_6D_6, 297 K): δ = 220.4 (*C*O), 215.4 (*C*O), 150.0 (*o*-Ar*C*), 136.4 (*i*-Ar*C*), 129.2 (*p*-Ar*C*), 125.6 (*m*-Ar*C*), 116.4 (I*i*Pr-*C*H), 64.6 (N*C*(CH$_3$)$_2$), 56.9 (*C*H$_2$), 51.0 (I*i*Pr-*C*H(CH$_3$)$_2$), 43.9 (*C*(CH$_3$)$_2$), 32.4 (C(*C*H$_3$)$_2$), 30.1 (NC(*C*H$_3$)$_2$), 28.8 (*i*Pr-*C*H), 26.6 (I*i*Pr-CH(*C*H$_3$)$_2$), 25.0 (*i*Pr-*C*H$_3$), 24.4 (I*i*Pr-CH(*C*H$_3$)$_2$), 20.6 (*i*Pr-*C*H$_3$) ppm. *Note: the $C_{carbene}$ and C_{CN} resonances were not detected, even by HMBC.*

^{11}B NMR (160 MHz, C_6D_6, 297 K): δ = –13.2 (s) ppm.

FT-IR (solid-state): $\tilde{\nu}$(CN) = 2134 cm^{-1}; $\tilde{\nu}$(CO) = 2064, 1975, 1928, 1884, 1862 cm^{-1}.

UV-vis (C_6H_6, 25 °C): λ_{max} = 340 nm.

Elemental analysis for [$C_{35}H_{47}BCrN_4O_5$] (M_w = 666.59 g mol^{-1}): calcd. C 63.06, H 7.11, N 8.41%; found C 62.59, H 7.16, N 7.92%.

HRMS LIFDI for [$C_{35}H_{47}BCrN_4O_5$] = [M]: calcd. 666.3039; found 666.3031.

(CAAC^{Me})(I*i*Pr)B(CN)(Mo(CO)$_5$) (12-Mo)

[Mo(CO)$_6$] (13.3 mg, 50.5 μmol, 1.20 equiv) dissolved in 0.4 mL of THF was irradiated for 3 h and added to a solution of **12** (20.0 mg, 42.1 μmol) in 0.4 mL of THF. The yellow color immediately intensified and subsequently, the solvent was evaporated. The residue was washed with a 9:1 mixture of hexane/benzene and dried *in vacuo* yielding **12-Mo** (26.7 mg, 37.5 μmol, 89% yield) as a yellow solid in a 95:5 (*Z*)/(*E*) ratio. Single crystals of **(*Z*)-12-Mo** were obtained by vapor diffusion of hexane into a saturated benzene solution.

^{1}H NMR (500 MHz, C_6D_6, 297 K): δ = 7.56 (t, ^3J = 7.7 Hz, 1H, *p*-Ar*H*), 7.39 (d, ^3J = 7.7 Hz, 1H, *p*-Ar*H*), 6.10 (s, 2H, I*i*Pr-C*H*), 5.06 (sept, ^3J = 6.8 Hz, 2H, I*i*Pr-C*H*(CH$_3$)$_2$), 3.34 (sept, ^3J = 6.8 Hz, 2H, *i*Pr-C*H*), 1.76 (s, 2H, CH_2), 1.60 (d, ^3J = 6.7 Hz, 6H, *i*Pr-CH_3), 1.38 (d,

^3J = 6.7 Hz, 6H, *i*Pr-CH_3), 1.17 (s, 6H, NC(CH_3)$_2$), 1.12 (d, ^3J = 6.7 Hz, 6H, I*i*Pr-CH(CH_3)$_2$), 0.92 (s, 6H, C(CH_3)$_2$), 0.90 (d, ^3J = 6.9 Hz, 6H, I*i*Pr-CH(CH_3)$_2$) ppm.

^{13}C{^{1}H} NMR (126 MHz, C_6D_6, 297 K): δ = 212.9 (*C*O), 204.9 (*C*O), 150.1 (*o*-Ar*C*), 136.5 (*i*-Ar*C*), 129.2 (*p*-Ar*C*), 125.6 (*m*-Ar*C*), 116.5 (I*i*Pr-*C*H), 64.8 (N*C*(CH$_3$)$_2$), 56.8 (*C*H$_2$), 51.1 (I*i*Pr-*C*H(CH$_3$)$_2$), 44.0 (*C*(CH$_3$)$_2$), 32.4 (C(*C*H$_3$)$_2$), 30.1 (NC(*C*H$_3$)$_2$), 28.8 (*i*Pr-*C*H), 26.6 (I*i*Pr-CH(*C*H$_3$)$_2$), 25.0 (*i*Pr-*C*H$_3$), 24.3 (I*i*Pr-CH(*C*H$_3$)$_2$), 20.6 (*i*Pr-*C*H$_3$) ppm. *Note: the $C_{carbene}$ and C_{CN} resonances were not detected, even by HMBC.*

^{11}B NMR (160 MHz, C_6D_6, 297 K): δ = –13.6 (s) ppm.

FT-IR (solid-state): $\tilde{\nu}$(CN) = 2126 cm^{-1}; $\tilde{\nu}$(CO) = 2067, 1976, 1926, 1858 cm^{-1}.

UV-vis (C_6H_6, 25 °C): λ_{max} = 345 nm.

HRMS LIFDI for [$C_{35}H_{47}BMoN_4O_5$] = [M]: calcd. 712.2688; found 712.2682.

(CAAC^{Me})(I*i*Pr)B(CN)(W(CO)$_5$) (**12-W**)

A solution of [W(CO)$_6$] (17.8 mg, 50.5 μmol, 1.20 equiv) in 0.4 mL of THF was irradiated for 3 h and added to **12** (20.0 mg, 42.1 μmol) dissolved in 0.4 mL of THF, whereupon the yellow colour intensified. After evaporation of the solvent the residue was washed with a 9:1 mixture of hexane/benzene and dried *in vacuo*. **12-W** was isolated as a 9:1 (*Z*)/(*E*) mixture (29.2 mg, 36.6 μmol, 87% yield), which isomerized to a 2:3 (*Z*)/(*E*) equilibrium ratio after heating for 10 d at 60 °C in C_6D_6, as determined by NMR-spectroscopic analysis. Single crystals of **(*E*)-12-W** were obtained by slow evaporation of this solution.

NMR data for **(*Z*)-12-W**:

^{1}H NMR (500 MHz, C_6D_6, 297 K): δ = 7.58 (t, ^3J = 7.6 Hz, 1H, *p*-Ar*H*), 7.40 (d, ^3J = 7.7 Hz, 2H, *m*-Ar*H*), 6.08 (s, 2H, I*i*Pr-C*H*), 5.04 (sept, ^3J = 6.8 Hz, 2H, I*i*Pr-C*H*(CH$_3$)$_2$), 3.31 (sept, ^3J = 6.8 Hz, 2H, *i*Pr-C*H*), 1.74 (s, 2H, C*H*$_2$), 1.60 (d, ^3J = 6.7 Hz, 6H, *i*Pr-C*H*$_3$), 1.37 (d, ^3J = 6.8 Hz, 6H, *i*Pr-C*H*$_3$), 1.15 (s, 6H, NC(C*H*$_3$)$_2$), 1.11 (d, ^3J = 6.7 Hz, 6H, *i*Pr-C*H*$_3$), 0.91 (s, 6H, C(C*H*$_3$)$_2$), 0.89 (d, ^3J = 6.8 Hz, 6H, *i*Pr-C*H*$_3$) ppm.

^{13}C{^{1}H} NMR (126 MHz, C_6D_6, 297 K): δ = 201.9 (*C*O), 197.9 (*C*O), 150.0 (*o*-Ar*C*), 136.3 (*i*-Ar*C*), 129.4 (*p*-Ar*C*), 125.8 (*m*-Ar*C*), 116.6 (I*i*Pr-*C*H), 64.3 (N*C*(CH$_3$)$_2$), 56.7 (*C*H$_2$), 51.1 (I*i*Pr-*C*H(CH$_3$)$_2$), 44.1 (*C*(CH$_3$)$_2$), 32.3 (C(*C*H$_3$)$_2$), 30.1 (NC(*C*H$_3$)$_2$), 28.8 (*i*Pr-*C*H), 26.6 (I*i*Pr-CH(*C*H$_3$)$_2$), 25.0 (*i*Pr-*C*H$_3$), 24.4 (I*i*Pr-CH(*C*H$_3$)$_2$), 20.6 (*i*Pr-*C*H$_3$) ppm. *Note: the $C_{carbene}$ and C_{CN} resonances were not detected, even by HMBC.*

^{11}B NMR (160 MHz, C_6D_6, 297 K): δ = –13.9 (s) ppm.

NMR data for **(*E*)-12-W**: *Note: due to the very broad and partially overlapping resonances of **(E)-12-W**, its ^{1}H and $^{13}C\{^{1}H\}$ NMR spectra were not assigned.*

^{11}B NMR (160 MHz, C_6D_6, 297 K): δ = –8.4 (s) ppm.

FT-IR (solid-state): $\tilde{\nu}$(CN) = 2143 (**(*E*)-12-W**), 2121 (**(*Z*)-12-W**) cm^{-1}; $\tilde{\nu}$(CO) = 2066, 1978, 1914, 1856 cm^{-1}. *Note: generous washing of the original 9:1 (Z)/(E) mixture of **12-W** with a 3:2 mixture of hexane/THF and subsequent drying in vacuo afforded a few milligrams of pure **(Z)-12-W**, enabling the assignment of $\tilde{\nu}$(CN) in the solid-state IR spectrum.*

UV-vis (C_6H_6, 25 °C): λ_{max} = 354 nm.

HRMS LIFDI for $[C_{35}H_{47}BN_4O_5W]$ = [M]: calcd. 798.3143; found 798.3136.

[(CAAC)(I*i*Pr)BH(NCS)][SPh] (13^{NCS}) and (CAACH)(I*i*Pr)B(NCS)(SPh) (14^{NCS})

A solution of **11^{Me}** (100 mg, 197 µmol) and thiophenol (26.1 mg, 237 µmol, 1.20 equiv) in 5 mL of benzene was stirred overnight at room temperature resulting in a colorless solution, the ^{1}H and ^{11}B NMR spectra of which showed the formation of a 2:3 mixture of **13^{NCS}** and **14^{NCS}**. Further stirring for 3 days at room temperature led to the formation of a colorless precipitate. The solvent was removed *in vacuo* and the solid residue was washed with hexane. Drying *in vacuo* afforded an 85:15 mixture of diastereomers of **14^{NCS}** (99.6 mg, 162 µmol, 82% yield). Colorless single crystals of the (*R*,*R*)/(*S*,*S*) diastereomer of **14^{NCS}** were obtained by vapor diffusion of hexane in a saturated benzene solution.

NMR data for **13^{NCS}**: *Note: due to its continuous conversion to **14^{NCS}** at room temperature in solution, **13^{NCS}** could not be isolated and only its ^{1}H and ^{11}B NMR data recorded in situ could be obtained.*

^{1}H{^{11}B} NMR (400 MHz, C_6D_6, 297 K): δ = 8.47–8.23 (m, 1H, *p*-Ar*H*), 8.06–7.76 (m, 2H, *m*-Ar*H*), 7.36–6.76 (m, 5H, SC_6H_5, overlapping with residual thiophenol), 4.73 (br s, 1H, I*i*Pr-C*H*$(CH_3)_2$), 4.29 (br s, 1H, I*i*Pr-C*H*$(CH_3)_2$), 3.76 (s, 1H, B*H*), 2.90 (sept, ^{3}J = 6.7 Hz, 1H, *i*Pr-C*H*), 2.63 (sept, ^{3}J = 6.6 Hz, 1H, *i*Pr-C*H*), 2.33 (d, ^{2}J = 13.5 Hz, 1H, CH_2), 2.00 (d, ^{2}J = 13.5 Hz, 1H, CH_2),1.70–0.95 (m, 37H, BH_2, NC(CH_3)$_2$, C(CH_3)$_2$, I*i*Pr-CH(CH_3)$_2$, *i*Pr-CH_3) ppm.

^{11}B NMR (128 MHz, C_6D_6, 297 K): δ = –18.9 (br s) ppm.

NMR data for the minor diastereomer of **14^{NCS}** (15%): *Note: for the minor diastereomer of **14^{NCS}** only the ^{1}H NMR data are provided.*

^{1}H NMR (500 MHz, C_6D_6, 297 K): δ = 7.48–7.40 (m, Ar*H*), 7.01–6.92 (m, Ar*H*), 6.20 (s, I*i*Pr-C*H*), 6.14 (s, I*i*Pr-C*H*), 5.44 (br s, *i*Pr-C*H*), 5.20 (br s, *i*Pr-C*H*), 4.14 (sept, ^{3}J = 6.7 Hz, *i*Pr-C*H*), 3.79 (s, 1H, BC*H*), 1.95 (br s, NC(CH_3)$_2$), 1.76–1.74 (m), 1.57–1.54 (m), 1.44–1.42

(m), 1.32 (d, ^3J = 6.7 Hz, *i*Pr-C*H*$_3$), 1.29–1.15 (m), 0.88–0.86 (m), 0.79 (s), 0.51 (d, ^3J = 6.5 Hz, *i*Pr-C*H*$_3$) ppm.

NMR data for the major diastereomer of **14^{NCS}** (85%):

^{1}H NMR (500 MHz, C_6D_6, 297 K): δ = 7.37 (dd, ^3J = 7.6 Hz, ^2J = 1.8 Hz, 1H, Ar*H*), 7.28 (t, ^3J = 7.6 Hz, 1H, Ar*H*), 7.18–7.17 (m, 1H, Ar*H*), 7.10–7.09 (m, 1H, Ar*H*), 7.08–7.07 (m, 1H, Ar*H*), 6.89 (t, ^3J = 7.7 Hz, 2H, Ar*H*), 6.80–6.76 (m, 1H, Ar*H*), 6.06 (d, ^3J = 2.2 Hz, 1H, I*i*Pr-C*H*), 6.05 (d, ^3J = 2.2 Hz, 1H, I*i*Pr-C*H*), 5.57 (sept, ^3J = 6.6 Hz, 1H, *i*Pr-C*H*), 5.49 (sept, ^3J = 6.6 Hz, 1H, *i*Pr-C*H*), 4.82 (sept, ^3J = 6.8 Hz, 1H, *i*Pr-C*H*), 3.70 (s, 1H, BC*H*), 3.45 (sept, ^3J = 6.8 Hz, 1H, *i*Pr-C*H*), 2.22 (d, ^2J = 12.2 Hz, 1H, C*H*$_2$), 2.02 (d, ^3J = 6.7 Hz, 3H, *i*Pr-C*H*$_3$), 2.01 (s, 3H, NC(C*H*$_3$)$_2$), 1.80 (d, ^2J = 12.2 Hz, 1H, C*H*$_2$), 1.61 (d, ^3J = 6.8 Hz, 3H, *i*Pr-C*H*$_3$), 1.48 (d, ^3J = 6.7 Hz, 3H, *i*Pr-C*H*$_3$), 1.41 (s, 3H, NC(C*H*$_3$)$_2$), 1.39 (d, ^3J = 6.6 Hz, 3H, *i*Pr-C*H*$_3$), 1.10 (s, 3H, NC(C*H*$_3$)$_2$), 1.08 (d, ^3J = 6.5 Hz, 3H, *i*Pr-C*H*$_3$), 1.00 (d, ^3J = 6.8 Hz, 3H, *i*Pr-C*H*$_3$), 0.91 (d, ^3J = 6.7 Hz, 3H, *i*Pr-C*H*$_3$), 0.90 (d, ^3J = 6.6 Hz, 3H, *i*Pr-C*H*$_3$), 0.89 (s, 3H, C(C*H*$_3$)$_2$) ppm.

^{13}C{^{1}H} NMR (126 MHz, C_6D_6, 297 K): δ = 153.8 (Ar*C*), 147.8 (Ar*C*), 145.9 (Ar*C*), 140.8 (Ar*C*), 132.7 (Ar*C*), 126.3 (Ar*C*), 125.0 (Ar*C*), 124.6 (Ar*C*), 124.5 (Ar*C*), 117.5 (I*i*Pr-*C*H), 117.4 (I*i*Pr-*C*H), 72.1 (B*C*H), 63.2 (N*C*(CH$_3$)$_2$), 61.4 (*C*H$_2$), 51.5 (*i*Pr-*C*H), 50.8 (*i*Pr-*C*H), 41.9 (*C*(CH$_3$)$_2$), 35.4 (*C*(CH$_3$)$_2$), 33.4 (NC(*C*H$_3$)$_2$), 29.5 (C(*C*H$_3$)$_2$), 28.9 (NC(*C*H$_3$)$_2$), 28.6 (C(*C*H$_3$)$_2$), 28.0 (C(*C*H$_3$)$_2$), 27.5 (*i*Pr-*C*H$_3$), 25.7 (*i*Pr-*C*H$_3$), 25.6 (*i*Pr-*C*H$_3$), 25.5 (*i*Pr-*C*H$_3$), 24.1 (*i*Pr-*C*H$_3$), 23.8 (*i*Pr-*C*H$_3$), 23.1 (*i*Pr-*C*H$_3$), 22.8 (*i*Pr-*C*H$_3$) ppm. *Note: the $C_{carbene}$ and C_{NCS} resonances were not detected, even by HMBC.*

^{11}B NMR (160 MHz, C_6D_6, 297 K): δ = –6.0 (s) ppm.

FT-IR (solid-state): $\tilde{\nu}$(NCS) = 2137 cm^{-1}.

HRMS LIFDI for $[C_{36}H_{52}BN_4S_2]$ = $[M - H]^-$: calcd. 615.3721; found 615.3715.

[(CAAC^{Me})(I*i*Pr)BH(CN)][SPh] (13^{CN})

Treatment of a solution of **12** (20.0 mg, 42.1 μmol) in 0.5 mL of C_6D_6 with thiophenol (10.2 mg, 92.7 μmol, 2.20 equiv) led to partial fading of the yellow color of the solution. The reaction mixture was monitored *in situ* by ^{11}B, ^{11}B{^{1}H}, ^{1}H and ^{1}H{^{11}B} NMR spectroscopy. After 15 min at room temperature, the NMR spectra showed ca. 85% conversion of **12** to **13^{CN}**. The ratio of the mixture did not change over a course of 1 d, whereupon various attempts to isolate **13^{CN}** were made.

Attempt A. Prolonged heating of the reaction mixture at 80 °C afforded a 65:35 ratio of **12** and **13^{CN}**, suggesting an equilibrium between **12** and **13^{CN}**. Upon cooling a few colorless single

crystals of **13^{CN}** suitable for X-ray diffraction analysis were obtained. *Note: due to the very weak diffraction, the X-ray crystallographic data was of insufficient quality for structural discussion but provided proof of connectivity.*

Attempt B. After removal of the solvent *in vacuo*, the residual yellow solid was dried *in vacuo* at 60 °C for 4 h. Redissolving this solid in 0.5 mL of C_6D_6 resulted in almost quantitative recovery of **12**.

Attempt C. The reaction mixture was left undisturbed overnight, yielding colorless crystals of **13^{CN}**, the supernatant of which was decanted. Subsequently, the crystals of **13^{CN}** were washed with small amounts of hexane (2 × 0.3 mL) and dried under atmospheric pressure for 1 h. Redissolving these crystals in 0.5 mL of C_6D_6 afforded **12** and residual thiophenol.

VT-NMR experiment: 12 (9.30 mg, 0.20 mmol) in 0.5 mL of d^8-toluene was treated with an excess of thiophenol (ca. 2–5 equiv), whereupon the yellow color vanished and a colorless solid precipitated. The mixture was monitored *in situ* by ^{11}B and ^{1}H NMR spectroscopy while heating stepwise from room temperature to 100 °C. Upon cooling, colorless single crystals of **13^{CN}** suitable for X-ray diffraction analysis were obtained.

NMR data for **13^{CN}**: *Note: due to its continuous partial conversion to **12** at room temperature in solution, only the ^{1}H and ^{11}B NMR data of **13^{CN}** recorded in situ could be obtained. Further conversion of **13^{CN}** to the **14^{CN}** analogue of **14^{NCS}** was not observed, even in the presence of a vast excess of thiophenol.*

^{1}H{^{11}B} NMR (400 MHz, C_6D_6, 297 K): δ = 8.53–7.79 (m, 3H, Ar*H*), 4.77 (br s, 1H, I*i*Pr-C*H*(CH_3)$_2$), 4.34 (br s, 1H, I*i*Pr-C*H*(CH_3)$_2$), 3.02 (s, 1H, B*H*), 2.93 (sept, ^{3}J = 6.7 Hz, 1H, *i*Pr-C*H*), 2.62 (sept, ^{3}J = 6.6 Hz, 1H, *i*Pr-C*H*), 2.40 (d, ^{2}J = 13.5 Hz, 1H, CH_2), 2.03 (d, ^{2}J = 13.5 Hz, 1H, CH_2) ppm.

^{11}B NMR (128 MHz, C_6D_6, 297 K): δ = –29.3 (br s) ppm.

HRMS LIFDI for [$C_{30}H_{48}BN_4$] = [M – C_6H_5S]$^+$: calcd. 475.3967; found 475.3959.

(CAAC^{Me}H)B(SPh)$_2$ (15)

Route A. A solution of **11^{Me}** (100 mg, 197 µmol) and thiophenol (47.8 mg, 434 µmol, 2.20 equiv) in 5 mL of benzene was stirred for 6 d at 60 °C, until the orange color disappeared. After evaporation of the solvent the residue was extracted with hexane. Removal of the solvent and drying *in vacuo* yielded **15** (75.0 mg, 146 µmol, 74% yield) as a colorless solid.

Route B. 14^{NCS} (10.0 mg, 16 µmol) and thiophenol (2.10 mg, 19 µmol, 1.2 equiv) were combined in 0.6 mL of benzene and heated at 60 °C. After 6 d, the ^{11}B NMR spectrum showed full conversion to **15**.

^{1}H NMR (500 MHz, C_6D_6, 297 K): δ = 7.49–7.47 (m, 2H, Ar*H*), 7.26–7.18 (m, 3H, Ar*H*), 6.94–6.81 (m, 6H, Ar*H*), 6.71–6.69 (m, 2H, Ar*H*), 3.64 (sept, ^{3}J = 6.7 Hz, 1H, *i*Pr-C*H*), 3.44 (sept, ^{3}J = 6.7 Hz, 1H, *i*Pr-C*H*), 2.91 (d, ^{3}J = 2.8 Hz, 1H, BC*H*), 2.55 (d, ^{2}J = 14.3 Hz, 1H, CH_2), 1.72 (d, ^{3}J = 6.7 Hz, 3H, *i*Pr-CH_3), 1.63 (d, ^{3}J = 6.7 Hz, 3H, *i*Pr-CH_3), 1.37 (d, ^{3}J = 6.7 Hz, 6H, *i*Pr-CH_3), 1.32 (s, 3H, NC(CH_3)$_2$), 1.30 (d, ^{2}J = 11.5 Hz, 1H, CH_2), 1.15 (s, 3H, NC(CH_3)$_2$), 1.09 (s, 3H, C(CH_3)$_2$), 0.89 (s, 3H, C(CH_3)$_2$) ppm.

^{13}C{^{1}H} NMR (126 MHz, C_6D_6, 297 K): δ = 149.4 (Ar*C*), 147.8 (Ar*C*), 140.1 (Ar*C*), 137.2 (Ar*C*), 136.2 (Ar*C*), 134.2 (Ar*C*), 129.0 (Ar*C*), 128.6 (Ar*C*), 127.0 (Ar*C*), 125.1 (Ar*C*), 125.1 (Ar*C*), 125.0 (Ar*C*), 59.3 (N*C*(CH$_3$)$_2$), 49.6 (*C*H$_2$), 43.6 (B*C*H), 35.3 (*C*(CH$_3$)$_2$), 33.0 (C(*C*H$_3$)$_2$), 30.4 (NC(*C*H$_3$)$_2$), 30.0 (C(*C*H$_3$)$_2$), 29.5 (NC(*C*H$_3$)$_2$), 29.4 (*i*Pr-*C*H), 29.1 (*i*Pr-*C*H), 27.1 (*i*Pr-*C*H$_3$), 27.0 (*i*Pr-*C*H$_3$), 24.5 (*i*Pr-*C*H$_3$), 24.1 (*i*Pr-*C*H$_3$) ppm.

^{11}B NMR (160 MHz, C_6D_6, 297 K): δ = 42.6 (br s) ppm.

HRMS LIFDI for [$C_{32}H_{42}BNS2$] = [M]: calcd. 515.2846; found 515.2843.

5.2.6 Synthesis and Reactivity of Boron-doped Thiazolothiazoles

[(CAAC^{Me})B(NCS)]$_2$ (16^{Me})

Addition of 2 mL of benzene to a mixture of **10^{Me}** (50.0 mg, 97.2 µmol) and KC_8 (28.9 mg, 214 µmol, 2.20 equiv) resulted in an intense blue suspension, which was stirred for 2 h at room temperature. Filtration and slow evaporation of the solvent under atmospheric pressure afforded a few blue single crystals of **16^{Me}** (13.0 mg, 36.6 µmol, 38% yield). *Note: the low crystalline yield of **16^{Me}** is due to the high solubility of the compound.*

^{1}H NMR (500 MHz, CD_2Cl_2, 297 K): δ = 7.51 (t, ^{3}J = 7.8 Hz, 2H, *p*-Ar*H*), 7.35 (d, overlapping with residual C_6H_6, 4H, *m*-Ar*H*), 2.76 (sept, ^{3}J = 6.7 Hz, 4H, *i*Pr-C*H*), 2.21 (s, 2H, CH_2), 1.92 (s, 12H, NC(CH_3)$_2$), 1.44 (s, 12H, C(CH_3)$_2$), 1.25 (d, ^{3}J = 6.7 Hz, 12H, *i*Pr-CH_3), 1.08 (d, ^{3}J = 6.7 Hz, 12H, *i*Pr-CH_3) ppm.

^{13}C{^{1}H} NMR (126 MHz, CD_2Cl_2, 297 K): δ = 199.1 ($C_{carbene}$, identified by HMBC), 146.4 (*o*-Ar*C*), 133.8 (*i*-Ar*C*), 130.4 (*p*-Ar*C*), 126.8 (*m*-Ar*C*), 76.1 (N*C*(CH$_3$)$_2$), 53.7 (*C*H$_2$), 51.6 (*C*(CH$_3$)$_2$), 32.8 (NC(*C*H$_3$)$_2$), 29.5 (C(*C*H$_3$)$_2$), 29.5 (*i*Pr-*C*H), 26.4 (*i*Pr-*C*H$_3$), 25.2 (*i*Pr-*C*H$_3$) ppm. *Note: the C_{NCS} resonance was not detected.*

^{11}B NMR (160 MHz, CD_2Cl_2, 297 K): δ = 32.3 (br s) ppm.

UV-vis (DCM, 25 °C): λ = 453 nm (ε = 4000 M^{-1} cm^{-1}), λ = 630 nm (ε = 27000 M^{-1} cm^{-1}), λ_{max} = 680 nm (ε = 66200 M^{-1} cm^{-1}).

HRMS LIFDI for [$C_{42}H_{63}B_2N_4S_2$]$^{+}$ = [M + H]$^{+}$: calcd. 709.4675; found 709.4658.

[(CAAC^{Cy})B(NCS)]$_2$ (16^{Cy})

10^{Cy} (300 mg, 0.54 mmol) and KC_8 (161 mg, 1.19 mmol, 2.20 equiv) were combined in 10 mL of benzene. The intense blue suspension was stirred for 2 h at room temperature prior to filtration. Evaporation of the solvent under atmospheric pressure afforded **16^{Cy}** (143 mg, 0.18 mmol, 67% yield) as dark blue crystals suitable for X-ray diffraction analysis.

^{1}H NMR (500 MHz, CD_2Cl_2, 297 K): δ = 7.53 (t, ^3J = 7.7 Hz, 2H, *p*-Ar*H*), 7.36 (d, overlapping with residual C_6H_6, 4H, *m*-Ar*H*), 3.28–3.22 (m, 4H, Cy-CH_2), 2.77 (sept, ^3J = 6.4 Hz, 4H, *i*Pr-C*H*), 2.29 (s, 4H, CH_2), 1.81 (d, ^2J = 13.0 Hz, 4H, Cy-CH_2), 1.75 (d, ^2J = 12.3 Hz, 4H, Cy-CH_2), 1.65–1.55 (m, 2H, Cy-CH_2), 1.51–1.44 (m, 3H, Cy-CH_2), 1.43 (s, 12H, NC(CH_3)$_2$), 1.38–1.27 (m, 3H, Cy-CH_2), 1.23 (d, ^3J = 6.7 Hz, 12H, *i*Pr-CH_3), 1.07 (d, ^3J = 6.6 Hz, 12H, *i*Pr-CH_3) ppm.

^{13}C{^{1}H} NMR (126 MHz, CD_2Cl_2, 297 K): δ = 199.1 ($C_{carbene}$, identified by HMBC), 146.6 (*o*-Ar*C*), 134.1 (*i*-Ar*C*), 130.3 (*p*-Ar*C*), 126.8 (*m*-Ar*C*), 76.0 (N*C*(CH$_3$)$_2$), 57.1 (*C*(C$_5$H$_{10}$)), 47.7 (*C*H$_2$), 39.2 (Cy-*C*H$_2$), 29.9 (NC(*C*H$_3$)$_2$), 29.5 (*i*Pr-*C*H), 26.4 (*i*Pr-*C*H$_3$), 25.5 (Cy-*C*H$_2$), 25.2 (*i*Pr-*C*H$_3$), 23.2 (Cy-*C*H$_2$) ppm. *Note: the C_{NCS} resonance was not detected.*

^{11}B NMR (160 MHz, CD_2Cl_2, 297 K): δ = 32.5 (br s) ppm.

UV-vis (DCM, 25 °C): λ = 455 nm (ε = 2800 M^{-1} cm^{-1}), λ = 632 nm (ε = 29500 M^{-1} cm^{-1}), λ_{max} = 680 nm (ε = 83300 M^{-1} cm^{-1}).

HRMS LIFDI for $[C_{48}H_{71}B_2N_4S_2]^+ = [M + H]^+$: calcd. 789.5301; found 789.5286.

[(CAAC^{Cy})BN(CuC$_6$F$_5$)CS]$_2$ (17)

16^{Cy} (50.0 mg, 63.4 µmol) and $[CuC_6F_5]_4$ (32.1 mg, 34.9 µmol, 0.55 equiv) were combined in 1 mL of DCM whereupon an intense purple solution was obtained. Slow evaporation of the solvent yielded a large crop of dark blue crystals of **17** (72.9 mg, 58.3 µmol, 92% yield) suitable for X-ray diffraction analysis.

^{1}H NMR (500 MHz, CD_2Cl_2, 297 K): δ = 7.46 (t, ^3J = 7.7 Hz, 2H, *p*-Ar*H*), 7.30 (d, ^3J = 7.8 Hz, 4H, *m*-Ar*H*), 3.16–3.11 (m, 4H, Cy-CH_2), 2.71 (sept, ^3J = 6.7 Hz, 4H, *i*Pr-C*H*), 2.35 (s, 4H, CH_2), 1.97 (d, ^2J = 12.9 Hz, 4H, Cy-CH_2), 1.83 (d, ^2J = 12.9 Hz, 4H, Cy-CH_2), 1.78–1.61 (m, 2H, Cy-CH_2), 1.59–1.43 (m, 4H, Cy-CH_2), 1.48 (s, 12H, NC(CH_3)$_2$), 1.41–1.29 (m, 2H, Cy-CH_2), 1.24 (d, ^3J = 6.6 Hz, 12H, *i*Pr-CH_3), 1.00 (d, ^3J = 6.7 Hz, 12H, *i*Pr-CH_3) ppm.

^{13}C{^{1}H} NMR (126 MHz, CD_2Cl_2, 297 K): δ = 204.2 ($C_{carbene}$, identified by HMBC), 149.9 (*C*F), 145.4 (*o*-Ar*C*), 137.3 (*C*F), 132.3 (*i*-Ar*C*), 131.4 (*p*-Ar*C*), 127.1 (*m*-Ar*C*), 125.8 (*C*F), 80.4 (N*C*(CH$_3$)$_2$), 58.5 (*C*(C$_5$H$_{10}$)), 46.3 (*C*H$_2$), 38.5 (Cy-*C*H$_2$), 29.9 (NC(*C*H$_3$)$_2$), 29.7

(*i*Pr-*C*H), 26.4 (*i*Pr-*C*H$_3$), 25.0 (Cy-*C*H$_2$), 24.7 (*i*Pr-*C*H$_3$), 22.5 (Cy-*C*H$_2$) ppm. *Note: the C_{NCS} and C_{CuC} resonances were not detected.*

^{11}B NMR (128 MHz, CD_2Cl_2, 297 K): δ = 33.0 (br s) ppm.

^{19}F NMR (471 MHz, CD_2Cl_2, 297 K): δ = –111.1 – –111.3 (m, 2F, *o*-C*F*), –162.5 – –162.6 (m, 1F, *p*-C*F*), –164.3 – –164.5 (m, 2F, *m*-C*F*) ppm.

UV-vis (DCM, 25 °C): λ = 378 nm, λ_{max} = 573 nm, λ = 621 nm.

Elemental analysis for $[C_{60}H_{70}B_2Cu_2F_{10}N_4S_2]$ (M_w = 1250.06 g mol^{-1}): calcd. C 57.65, H 5.64, N 4.48, S 5.13%; found C 57.35, H 5.64, N 4.54, S 4.86%.

[{(CAAC^{Cy})BNHCS}$_2^{2+}$][Cl$^-$]$_2$ (18-Cl)

Route A. To a solution of **16^{Cy}** (100 mg, 0.13 μmol) in 3 mL of DCM HCl·toluene (2.60 mL, 0.10 M, 0.26 μmol, 2.00 equiv) was added dropwise under vigorous stirring at room temperature. The resulting red solution was treated with 15 mL of pentane to induce precipitation. The suspension was filtered and the solid obtained was washed with pentane. Drying under atmospheric pressure yielded **18-Cl** (93.9 mg, 0.11 mmol, 86% yield) as red solid. Single crystals suitable for X-ray diffraction analysis were obtained by vapor diffusion of hexane into a saturated dichloromethane solution.

Route B. A solution of **16^{Cy}** (75.0 mg, 95.1 μmol) in 1 mL of dichloromethane was treated with thiophenol (23.0 mg, 0.21 mmol, 2.20 eq.) whereupon the color changed from blue to red over a course of 1 h. Subsequently, 10 mL of pentane were added yielding a red precipitate which was filtered off and washed with pentane. Drying under atmospheric pressure afforded **18-Cl** (65.5 mg, 76.1 μmol, 80% yield) as an intense red solid. The NMR spectra were identical with those from Route A.

^{1}H NMR (500 MHz, CD_2Cl_2, 297 K): δ = 13.0 (br s, 2H, N*H*), 7.60 (t, ^3J = 7.8 Hz, 2H, *p*-Ar*H*), 7.38 (d, ^3J = 7.9 Hz, 4H, *m*-Ar*H*), 2.76 (sept, ^3J = 6.6 Hz, 4H, *i*Pr-C*H*), 2.51–2.45 (m, 4H, Cy-C*H*$_2$), 2.43 (s, 4H, C*H*$_2$), 2.00 (br d, ^3J = 12.8 Hz, 4H, Cy-C*H*$_2$), 1.94–1.85 (m, 2H, Cy-C*H*$_2$), 1.90 (br d, ^3J = 12.6 Hz, 4H, Cy-C*H*$_2$), 1.69–1.64 (m, 2H, Cy-C*H*$_2$), 1.57 (s, 12H, NC(C*H*$_3$)$_2$), 1.50–1.41 (m, 4H, Cy-C*H*$_2$), 1.29 (d, ^3J = 6.6 Hz, 12H, *i*Pr-C*H*$_3$), 0.98 (d, ^3J = 6.6 Hz, 12H, *i*Pr-C*H*$_3$) ppm.

^{13}C{^{1}H} NMR (126 MHz, CD_2Cl_2, 297 K): δ = 204.3 ($C_{carbene}$, identified by HMBC), 145.1 (*o*-Ar*C*), 132.7 (*i*-Ar*C*), 132.2 (*p*-Ar*C*), 131.3 (*p*-Ar*C*), 127.3 (*m*-Ar*C*), 83.4 (N*C*(CH$_3$)$_2$), 59.4 (*C*(C$_5$H$_{10}$)), 45.4 (*C*H$_2$), 36.0 (Cy-*C*H$_2$), 29.8 (NC(*C*H$_3$)$_2$), 29.6 (*i*Pr-*C*H), 26.3 (*i*Pr-*C*H$_3$), 24.8 (*i*Pr-*C*H$_3$), 23.9 (Cy-*C*H$_2$), 22.3 (Cy-*C*H$_2$) ppm. *Note: the C_{NCS} resonance was not detected.*

^{11}B NMR (128 MHz, CD_2Cl_2, 297 K): δ = 32.8 (br s) ppm.

FT-IR (solid-state): $\tilde{\nu}$(NH) = 3061 cm^{-1}.

UV-vis (DCM, 25 °C): λ = 470 nm (shoulder), λ_{max} = 493 nm.

Fluorescence (DCM, 25 °C): λ = 580 nm (for λ_{ex} = 493 nm, Φ_{fl} = ND).

Elemental analysis for [$C_{48}H_{72}B_2Cl_2N_4S_2$] ($M_w$ = 861.77 g mol^{-1}): calcd. C 66.90, H 8.42, N 6.50, S 7.44%; found C 65.24, H 8.44, N 6.17, S 8.06%.

HRMS LIFDI for [$C_{48}H_{71}B_2N_4S_2$] = [M – Cl_2 – H]$^+$: calcd. 789.5301; found 789.5279.

[{(CAAC^{Cy})BNHCS}$_2^{2+}$] [OTf$^-$]$_2$ (18-OTf)

Route A. HOTf (19.0 mg, 126.8 µmol, 2.00 equiv) diluted in 0.5 mL of DCM was added dropwise to a stirred solution of **16^{Cy}** (50.0 mg, 63.4 µmol) in 2 mL of DCM, whereupon the color changed from intense blue to bright orange. After addition was completed, the solvent was allowed to evaporate under atmospheric pressure yielding orange crystals of **18-OTf** (60.0 mg, 55.2 µmol, 87% yield) suitable for X-ray diffraction analysis.

Route B. 18-Cl (15.0 mg, 17.4 µmol) and AgOTf (8.95 mg, 34.8 µmol, 2.00 equiv) were combined in 0.5 mL of CD_2Cl_2, whereupon the color changed from red to orange accompanied by formation of a colorless precipitate. After 5 min, the suspension was filtered yielding an intense orange solution of **18-OTf** in analytically pure quality for NMR spectroscopic analysis. The NMR spectra were identical with those from Route A.

Route C. 18-OTf·HOTf (15.0 mg, 10.8 µmol) and **16^{Cy}** (17.0 mg, 21.6 µmol, 2.00 equiv) were combined in 0.5 mL of CD_2Cl_2. The NMR spectra of the resulting orange solution of **18-OTf** were identical with those from Routes A and B.

^{1}H NMR (500 MHz, CD_2Cl_2, 297 K): δ = 10.5 (br s, 2H, N*H*), 7.62 (t, ^3J = 7.8 Hz, 2H, *p*-Ar*H*), 7.40 (d, ^3J = 7.9 Hz, 4H, *m*-Ar*H*), 2.57 (sept, ^3J = 6.6 Hz, 4H, *i*Pr-C*H*), 2.45 (s, 4H, CH_2), 2.19 (dt, ^2J = 13.4 Hz, ^3J = 3.4 Hz, 4H, Cy-CH_2), 1.96–1.88 (m, 8H, Cy-CH_2), 1.79–1.72 (m, 2H, Cy-CH_2), 1.67–1.36 (m, 6H, Cy-CH_2), 1.57 (s, 12H, NC(CH_3)$_2$), 1.30 (d, ^3J = 6.6 Hz, 12H, *i*Pr-CH_3), 0.93 (d, ^3J = 6.6 Hz, 12H, *i*Pr-CH_3) ppm.

^{13}C{^{1}H} NMR (126 MHz, CD_2Cl_2, 297 K): δ = 202.2 ($C_{carbene}$, identified by HMBC), 144.8 (*o*-Ar*C*), 132.7 (*i*-Ar*C*), 132.1 (*p*-Ar*C*), 131.0 (*p*-Ar*C*), 127.5 (*m*-Ar*C*), 84.0 (N*C*(CH_3)$_2$), 59.3 (*C*(C_5H_{10})), 45.4 (*C*H_2), 35.9 (Cy-*C*H_2), 29.8 (NC(*C*H_3)$_2$), 29.7 (*i*Pr-*C*H), 25.9 (*i*Pr-*C*H_3), 24.8 (*i*Pr-*C*H_3), 24.1 (Cy-*C*H_2), 21.9 (Cy-*C*H_2) ppm. *Note: the C_{NCS} and C_{CF3} resonances were not detected.*

^{11}B NMR (128 MHz, CD_2Cl_2, 297 K): δ = 33.1 (br s) ppm.

^{19}F NMR (471 MHz, CD_2Cl_2, 297 K): δ = –78.5 (s) ppm.

FT-IR (solid-state): $\tilde{\nu}$(NH) = 3170 cm^{-1}.

UV-vis (DCM, 25 °C): λ_{max} = 474 nm.

Fluorescence (DCM, 25 °C): λ = 566 nm (for λ_{ex} = 474 nm, Φ_{fl} = 23%).

Elemental analysis for [$C_{50}H_{72}B_2F_6N_4O_6S_4$] ($M_w$ = 1089.00 g mol^{-1}): calcd. C 55.15, H 6.66, N 5.14, S 11.78%; found C 54.48, H 6.73, N 5.08, S 11.73%.

[{(CAAC^{Cy})BNHCS}$_2^{2+}$][OTf(HOTf)$^-$]$_2$ (18-OTf·HOTf)

To a solution of **16^{Cy}** (50.0 mg, 63.4 μmol) in 2 mL of DCM an excess of HOTf (ca. 5 equiv) was added dropwise. The solvent of the resulting yellow solution was allowed to evaporate under atmospheric pressure yielding yellow single crystals of **18-OTf·HOTf** (65.2 mg, 46.9 μmol, 74% yield).

^{1}H NMR (500 MHz, CD_2Cl_2, 297 K): δ = 15.6 (very br s, 2H, *H*OTf), 9.20 (br s, 2H, N*H*), 7.66 (t, ^3J = 7.8 Hz, 2H, *p*-Ar*H*), 7.43 (d, ^3J = 7.9 Hz, 4H, *m*-Ar*H*), 2.53 (sept, ^3J = 6.7 Hz, 4H, *i*Pr-C*H*), 2.48 (s, 4H, CH_2), 2.17–2.11 (m, 4H, Cy-CH_2), 1.95–1.87 (m, 8H, Cy-CH_2), 1.84–1.78 (m, 2H, Cy-CH_2), 1.58 (s, 12H, NC(CH_3)$_2$), 1.55–1.47 (m, 6H, Cy-CH_2), 1.30 (d, ^3J = 6.6 Hz, 12H, *i*Pr-CH_3), 0.89 (d, ^3J = 6.6 Hz, 12H, *i*Pr-CH_3) ppm.

^{13}C{^{1}H} NMR (126 MHz, CD_2Cl_2, 297 K): δ = 200.5 ($C_{carbene}$, identified by HMBC), 144.6 (*o*-Ar*C*), 133.0 (*i*-Ar*C*), 131.6 (*p*-Ar*C*), 130.9 (*p*-Ar*C*), 127.8 (*m*-Ar*C*), 119.7 (q, $^1J_{CF}$ = 318 Hz, *C*F$_3$), 83.3 (N*C*(CH$_3$)$_2$), 59.3 (*C*(C$_5$H$_{10}$)), 45.4 (*C*H$_2$), 36.3 (Cy-*C*H$_2$), 29.8 (NC(*C*H$_3$)$_2$), 29.8 (*i*Pr-*C*H), 25.7 (*i*Pr-*C*H$_3$), 24.7 (*i*Pr-*C*H$_3$), 24.3 (Cy-*C*H$_2$), 21.8 (Cy-*C*H$_2$) ppm. *Note: the C_{NCS} resonance was not detected.*

^{11}B NMR (128 MHz, CD_2Cl_2, 297 K): δ = 33.5 (br s) ppm.

^{19}F NMR (471 MHz, CD_2Cl_2, 297 K): δ = –78.3 (s) ppm.

FT-IR (solid-state): $\tilde{\nu}$(NH) = 3288 cm^{-1}.

UV-vis (DCM, 25 °C): λ_{max} = 471 nm.

Fluorescence (DCM, 25 °C): λ = 562 nm (for λ_{ex} = 471 nm, Φ_{fl} = 27%).

Elemental analysis for [$C_{52}H_{74}B_2F_{12}N_4O_{12}S_6$] ($M_w$ = 1389.14 g mol^{-1}): calcd. C 44.96, H 5.37, N 4.03, S 13.85%; found C 45.28, H 5.14, N 4.22, S 14.31%.

[{(CAAC^{Cy})BNHCS}$_2^{2+}$][BAr$^F{}_4^-$]$_2$ (18-[BAr$^F{}_4$]·Et$_2$O) and **(18-[BAr$^F{}_4$])**

[H(OEt$_2$)$_2$][BAr$^F{}_4$] (Brookhart's acid) (128 mg, 127 μmol, 2.00 equiv) dissolved in 1 mL of Et$_2$O was added dropwise to a stirred suspension of **16^{Cy}** (50.0 mg, 63.4 μmol) in 1 mL of Et$_2$O whereupon the reaction mixture turned bright yellow. After five minutes of stirring the resulting solution was left undisturbed and the solvent was allowed to evaporate under atmospheric pressure yielding a large crop of bright yellow crystals of **18-[BAr$^F{}_4$]·Et$_2$O** (154 mg, 57.7 μmol,

91% yield) suitable for X-ray diffraction analysis. *Note: solvent removal in vacuo and redissolving of Et_2O-free **18-[BAr$^F_4$]** in CD_2Cl_2 led to partial decomposition. Slow evaporation of this solution afforded a few single crystals of **18-[BAr$^F_4$]** suitable for X-ray diffraction analysis.*

NMR data for **18-[BAr$^F_4$]·Et$_2$O**:

^{1}H NMR (500 MHz, CD_2Cl_2, 297 K): δ = 7.72–7.68 (m, 18H, *o*-(3,5-C$_6$*H*$_3$(CF$_3$)$_2$) + *m*-Ar*H*), 7.56 (br s, 8H, *p*-(3,5-C$_6$*H*$_3$(CF$_3$)$_2$), 7.48 (d, ^3J = 7.9 Hz, 4H, *p*-Ar*H*), 6.89 (br s, 2H, N*H*), 3.44 (q, ^3J = 7.0 Hz, 8H, O(C*H*$_2$CH$_3$)$_2$), 2.53–2.45 (m, 8H, *i*Pr-C*H* + C*H*$_2$), 2.04 (dt, ^2J = 12.7 Hz, ^3J = 3.5 Hz, 4H, Cy-C*H*$_2$), 1.89–1.85 (m, 10H, Cy-C*H*$_2$), 1.59 (s, 12H, NC(C*H*$_3$)$_2$), 1.55–1.46 (m, 4H, Cy-C*H*$_2$), 1.36–1.26 (m, 2H, Cy-C*H*$_2$), 1.30 (d, ^3J = 6.7 Hz, 12H, *i*Pr-C*H*$_3$), 1.15 (t, ^3J = 7.0 Hz, 12H, O(CH$_2$C*H*$_3$)$_2$), 0.79 (d, ^3J = 6.7 Hz, 12H, *i*Pr-C*H*$_3$) ppm.

^{13}C{^{1}H} NMR (126 MHz, CD_2Cl_2, 297 K): δ = 197.8 (*C*$_{carbene}$, identified by HMBC), 162.1 (1:1:1:1 q, $^1J_{BC}$ = 49.8 Hz, *i*-(3,5-*C*$_6$H$_3$(CF$_3$)$_2$)), 144.5 (*o*-Ar*C*), 135.2 (br s, *o*-(3,5-*C*$_6$H$_3$(CF$_3$)$_2$)), 133.7 (*i*-Ar*C*), 130.9 (*p*-Ar*C*), 130.5 (*p*-Ar*C*), 129.3 (qq, $^2J_{CF}$ = 31.5 Hz, $^4J_{CF}$ = 2.9 Hz, *m*-(3,5-*C*$_6$H$_3$(CF$_3$)$_2$)), 128.2 (*m*-Ar*C*), 125.0 (q, $^1J_{CF}$ = 272.4 Hz, *C*F$_3$), 117.9 (sept, $^3J_{CF}$ = 4.0 Hz, *p* (3,5-*C*$_6$H$_3$(CF$_3$)$_2$)), 85.1 (N*C*(CH$_3$)$_2$), 66.1 (O(*C*H$_2$CH$_3$)$_2$), 59.3 (*C*(C$_5$H$_{10}$)), 45.5 (*C*H$_2$), 37.3 (Cy-*C*H$_2$), 29.9 (NC(*C*H$_3$)$_2$), 29.7 (*i*Pr-*C*H), 25.5 (*i*Pr-*C*H$_3$), 24.7 (Cy-*C*H$_2$), 24.3 (*i*Pr-*C*H$_3$), 21.8 (Cy-*C*H$_2$), 15.5 (O(CH$_2$*C*H$_3$)$_2$) ppm. *Note: the C_{NCS} resonance was not detected.*

^{11}B NMR (128 MHz, CD_2Cl_2, 297 K): δ = 33.7 (br s, *B*NCS), –6.6 (s, *B*Ar$^F_4$) ppm.

^{19}F NMR (471 MHz, CD_2Cl_2, 297 K): δ = –62.8 (s) ppm.

NMR data for **18-[BAr$^F_4$]**:

^{1}H NMR (500 MHz, CD_2Cl_2, 297 K): δ = 7.72–7.68 (m, 18H, *o*-(3,5-C$_6$*H*$_3$(CF$_3$)$_2$) + *m*-Ar*H*), 7.56 (br s, 8H, *p*-(3,5-C$_6$*H*$_3$(CF$_3$)$_2$), 7.48 (d, ^3J = 7.9 Hz, 4H, *p*-Ar*H*), 6.84 (br s, 2H, N*H*), 2.53–2.45 (m, 8H, *i*Pr-C*H* + C*H*$_2$), 2.08–2.01 (m, 4H, Cy-C*H*$_2$), 1.91–1.85 (m, 10H, Cy-C*H*$_2$), 1.59 (s, 12H, NC(C*H*$_3$)$_2$), 1.57–1.44 (m, 4H, Cy-C*H*$_2$), 1.33–1.26 (m, 2H, Cy-C*H*$_2$), 1.30 (d, ^3J = 6.7 Hz, 12H, *i*Pr-C*H*$_3$), 0.79 (d, ^3J = 6.6 Hz, 12H, *i*Pr-C*H*$_3$) ppm.

^{13}C{^{1}H} NMR (126 MHz, CD_2Cl_2, 297 K): δ = 197.8 (*C*$_{carbene}$, identified by HMBC), 162.1 (1:1:1:1 q, $^1J_{BC}$ = 49.8 Hz, *i*-(3,5-*C*$_6$H$_3$(CF$_3$)$_2$)), 144.5 (*o*-Ar*C*), 135.2 (br s, *o*-(3,5-*C*$_6$H$_3$(CF$_3$)$_2$)), 133.7 (*i*-Ar*C*), 130.9 (*p*-Ar*C*), 130.5 (*p*-Ar*C*), 129.3 (qq, $^2J_{CF}$ = 31.5 Hz, $^4J_{CF}$ = 2.9 Hz, *m*-(3,5-*C*$_6$H$_3$(CF$_3$)$_2$)), 128.2 (*m*-Ar*C*), 125.0 (q, $^1J_{CF}$ = 272.4 Hz, *C*F$_3$), 117.9 (sept, $^3J_{CF}$ = 4.0 Hz, *p*-(3,5-*C*$_6$H$_3$(CF$_3$)$_2$)), 85.1 (N*C*(CH$_3$)$_2$), 59.3 (*C*(C$_5$H$_{10}$)), 45.5 (*C*H$_2$), 37.3 (Cy-*C*H$_2$), 29.9 (NC(*C*H$_3$)$_2$), 29.7 (*i*Pr-*C*H), 25.5 (*i*Pr-*C*H$_3$), 24.6 (*i*Pr-*C*H$_3$), 24.3 (Cy-*C*H$_2$), 21.8 (Cy-*C*H$_2$) ppm. *Note: the C_{NCS} resonance was not detected.*

^{11}B NMR (128 MHz, CD_2Cl_2, 297 K): δ = 33.9 (br s, *B*NCS), –6.6 (s, *B*Ar$^F_4$) ppm.

^{19}F NMR (471 MHz, CD_2Cl_2, 297 K): δ = –62.8 (s) ppm.

FT-IR (solid-state): $\tilde{\nu}$(NH) = 3396 cm^{-1}.

UV-vis (DCM, 25 °C): λ_{max} = 450 nm, λ = 473 nm (shoulder).

Fluorescence (DCM, 25 °C): λ = 539 nm (for λ_{ex} = 450 nm, Φ_{fl} = 33%).

Elemental analysis for [$C_{112}H_{96}B_4F_{48}N_4S_2$] ($M_w$ = 2517.31 g mol^{-1}): calcd. C 53.44, H 3.84, N 2.23, S 2.55%; found C 54.35, H 3.41, N 2.53, S 2.23%.

[(CAAC^{Cy})(BNHCS)(BNCS)(CAAC^{Cy})$^+$][Cl$^-$] (19-Cl)

18-Cl (15.0 mg, 17.4 μmol) and **16^{Cy}** (13.7 mg, 17.4 μmol) were combined in 0.5 mL of CD_2Cl_2 yielding an intense blue solution of **19-Cl** in analytically pure quality for NMR spectroscopic analysis. Slow evaporation of the solvent under atmospheric pressure afforded **19-Cl** (27.0 mg, 32.7 μmol, 94% yield) as dark blue solid.

^{1}H NMR (500 MHz, CD_2Cl_2, 297 K): δ = 9.42 (br s, 1H, N*H*), 7.64–7.58 (m, 2H, *p*-Ar*H*), 7.41–7.38 (m, 4H, *p*-Ar*H*), 3.18 (t, ^2J = 12.0 Hz, 2H, Cy-CH_2), 2.79–2.58 (m, 4H, *i*Pr-C*H*), 2.50–2.38 (m, 4H, Cy-CH_2 + CH_2), 2.34 (s, 2H, CH_2), 2.01–1.63 (m, 10H, Cy-CH_2), 1.59–1.40 (m, 18H, Cy-CH_2 + NC(CH_3)$_2$), 1.31–1.23 (m, 12H, *i*Pr-CH_3), 0.98–0.86 (m, 12H, *i*Pr-CH_3) ppm.

^{13}C{^{1}H} NMR (126 MHz, CD_2Cl_2, 297 K): δ = 145.5 (*o*-Ar*C*), 145.4 (*o*-Ar*C*), 132.6 (*i*-Ar*C*), 132.0 (*p*-Ar*C*), 131.9 (*i*-Ar*C*), 131.2 (*p*-Ar*C*), 127.3 (*m*-Ar*C*), 127.1 (*m*-Ar*C*), 81.8 (N*C*(CH$_3$)$_2$), 79.1 (N*C*(CH$_3$)$_2$), 58.6 (*C*(C$_5$H$_{10}$)), 58.4 (*C*(C$_5$H$_{10}$)), 46.8 (*C*H$_2$), 45.9 (*C*H$_2$), 38.2 (Cy-*C*H$_2$), 37.6 (Cy-*C*H$_2$), 29.8 (NC(*C*H$_3$)$_2$), 29.6 (NC(*C*H$_3$)$_2$), 26.1 (*i*Pr-*C*H$_3$), 25.9 (*i*Pr-*C*H$_3$), 25.4 (Cy-*C*H$_2$), 25.0 (*i*Pr-*C*H$_3$), 24.6 (*i*Pr-*C*H$_3$), 22.8 (Cy-*C*H$_2$), 22.5 (Cy-*C*H$_2$) ppm. *Note: the $C_{carbene}$ and C_{NCS} resonances were not detected, even by HMBC.*

^{11}B NMR (128 MHz, CD_2Cl_2, 297 K): δ = 32.0 (br s) ppm. *Note: both ^{11}B NMR signals overlapped.*

FT-IR (solid-state): $\tilde{\nu}$(NH) = 3403 cm^{-1}.

UV-vis (DCM, 25 °C): λ = 370 nm, λ = 458 nm (shoulder), λ = 495 nm, λ = 699 nm, λ_{max} = 763 nm.

Elemental analysis for [$C_{48}H_{71}B_2ClN_4S_2$·(CH_2Cl_2)$_{0.5}$] (M_w = 867.78 g mol^{-1}): calcd. C 67.13, H 8.36, N 6.46, S 7.39%; found C 67.17, H 8.42, N 6.48, S 7.31%. *Note: the elemental analyses have repeatedly contained 0.5 equivalents of residual CH_2Cl_2, which could not be removed as drying in vacuo afforded partial decomposition of **19-Cl**.*

[(CAAC^{Cy})(BNHCS)(BNCS)(CAAC^{Cy})$^{+}$][OTf^{-}] (19-OTf)

Route A. 19-Cl (15.0 mg, 18.2 μmol) and AgOTf (4.67 mg, 18.2 μmol) were combined in 0.5 mL of CD_2Cl_2. After 1 min, the resulting suspension was filtered yielding an intense blue solution of **19-OTf** in analytically pure quality for NMR spectroscopic analysis. Slow evaporation of the solvent under atmospheric pressure afforded **19-OTf** (16.4 mg, 17.5 μmol, 96% yield) as dark blue solid.

Route B. 18-OTf (10.0 mg, 9.18 μmol) and **16^{Cy}** (14.5 mg, 18.4 μmol, 2.00 equiv) were combined in 0.5 mL of CD_2Cl_2. The NMR spectra of the resulting blue solution of **19-OTf** were identical with those from Route A.

^{1}H NMR (500 MHz, CD_2Cl_2, 297 K): δ = 7.69 (t, ^{3}J = 7.9 Hz, 1H, *p*-Ar*H*), 7.57 (t, ^{3}J = 7.9 Hz, 1H, *p*-Ar*H*), 7.47 (d, ^{3}J = 7.8 Hz, 1H, *m*-Ar*H*), 7.37 (d, ^{3}J = 7.8 Hz, 1H, *m*-Ar*H*), 7.13 (br s, 1H, N*H*), 3.23–3.13 (m, 2H, Cy-CH_2), 2.61 (sept, ^{3}J = 6.6 Hz, 4H, *i*Pr-C*H*), 2.45 (s, 2H, CH_2), 2.40–2.31 (m, 3H, Cy-CH_2 + CH_2), 1.94–1.67 (m, 9H, Cy-CH_2), 1.58–1.43 (m, 18H, Cy-CH_2 + NC(CH_3)$_2$), 1.34–1.23 (m, 14H, Cy-CH_2 + *i*Pr-CH_3), 0.92 (s, 3H, *i*Pr-CH_3), 0.90 (s, 3H, *i*Pr-CH_3), 0.84 (s, 3H, *i*Pr-CH_3), 0.83 (s, 3H, *i*Pr-CH_3) ppm.

^{13}C{^{1}H} NMR (126 MHz, CD_2Cl_2, 297 K): δ = 145.4 (*o*-Ar*C*), 145.2 (*o*-Ar*C*), 132.6 (*p*-Ar*C*), 132.5 (*i*-Ar*C*), 131.8 (*i*-Ar*C*), 131.3 (*p*-Ar*C*), 127.7 (*m*-Ar*C*), 127.2 (*m*-Ar*C*), 119.9 (q, $^{1}J_{CF}$ = 320 Hz, *C*F$_3$), 81.7 (N*C*(CH$_3$)$_2$), 79.8 (N*C*(CH$_3$)$_2$), 58.7 (*C*(C$_5$H$_{10}$)), 58.4 (*C*(C$_5$H$_{10}$)), 46.7 (*C*H$_2$), 46.2 (*C*H$_2$), 38.5 (Cy-*C*H$_2$), 38.0 (Cy-*C*H$_2$), 29.8 (NC(*C*H$_3$)$_2$), 29.7 (NC(*C*H$_3$)$_2$), 29.6 (NC(*C*H$_3$)$_2$), 26.0 (*i*Pr-*C*H$_3$), 25.6 (*i*Pr-*C*H$_3$), 25.4 (Cy-*C*H$_2$), 25.1 (*i*Pr-*C*H$_3$), 24.9 (*i*Pr-*C*H$_3$), 24.4 (Cy-*C*H$_2$), 22.7 (Cy-*C*H$_2$), 22.4 (Cy-*C*H$_2$) ppm. *Note: the $C_{carbene}$ and C_{NCS} resonances were not detected, even by HMBC.*

^{11}B NMR (128 MHz, CD_2Cl_2, 297 K): δ = 32.5 (br s), 31.5 (br s) ppm.

^{19}F NMR (471 MHz, CD_2Cl_2, 297 K): δ = –78.8 (s) ppm.

FT-IR (solid-state): $\tilde{\nu}$(NH) = 3401 cm^{-1}.

UV-vis (DCM, 25 °C): λ = 482 nm, λ_{max} = 688 nm, λ = 761 nm.

Elemental analysis for [$C_{49}H_{71}B_2F_3N_4O_3S_3$·($CH_2Cl_2$)] ($M_w$ = 1023.85 g mol^{-1}): calcd. C 58.66, H 7.62, N 5.97, S 10.24%; found C 58.81, H 7.22, N 5.56, S 9.74%. *Note: the elemental analyses have repeatedly contained one equivalent of residual CH_2Cl_2, which could not be removed as drying in vacuo afforded partial decomposition of **19-OTf**.*

[(CAAC^{Cy})(BNHCS)(BNCS)(CAAC^{Cy})$^{+}$][BAr$^{F}_{4}$$^{-}$]·Et$_2$O (19-[BAr$^{F}_{4}$]·Et$_2$O)

18-[BAr$^{F}_{4}$]·Et$_2$O (32.0 mg, 12.0 μmol) dissolved in 1 mL of DCM was added dropwise to a suspension of **16^{Cy}** (9.47 mg, 12.0 μmol) in 1 mL of Et$_2$O. The resulting blue solution was

stirred for five minutes at room temperature. Slow evaporation of the solvent under atmospheric pressure yielded **19-[BAr$^{F}_{4}$]·Et$_2$O** (41.2 mg, 24.9 µmol, 94% yield) as dark blue solid.

^{1}H NMR (500 MHz, CD_2Cl_2, 297 K): δ = 7.75–7.72 (m, 8H, *o*-(3,5-$C_6H_3(CF_3)_2$)), 7.69–7.64 (m, 1H, *p*-Ar*H*), 7.60–7.52 (m, 1H *p*-Ar*H*), 7.57 (br s, 4H, *p*-(3,5-$C_6H_3(CF_3)_2$), 7.46 (d, ^3J = 7.8 Hz, 2H, *m*-Ar*H*), 7.36 (d, ^3J = 7.8 Hz, 2H, *m*-Ar*H*), 6.88 (br s, 1H, N*H*), 3.44 (q, ^3J = 7.0 Hz, 4H, O(CH_2CH_3)$_2$), 3.21–3.16 (m, 2H, Cy-CH_2), 2.64–2.56 (m, 4H, *i*Pr-C*H*), 2.47–2.34 (m, 6H, Cy-CH_2 + CH_2), 1.97–1.69 (m, 10H, Cy-CH_2 + CH_2), 1.60–1.42 (m, 18H, Cy-CH_2 + NC(CH_3)$_2$), 1.30–1.25 (m, 12H, *i*Pr-CH_3), 1.16 (t, ^3J = 7.0 Hz, 6H, O(CH_2CH_3)$_2$), 0.92–0.87 (m, 6H, *i*Pr-CH_3), 0.82 (d, ^3J = 6.6 Hz, 12H, *i*Pr-CH_3) ppm.

^{13}C{^{1}H} NMR (126 MHz, CD_2Cl_2, 297 K): δ = 188.0 ($C_{carbene}$, identified by HMBC), 162.2 (1:1:1:1 q, $^1J_{BC}$ = 49.9 Hz, *i*-(3,5-$C_6H_3(CF_3)_2$)), 145.5 (*o*-Ar*C*), 145.1 (*o*-Ar*C*), 135.2 (br s, *o*-(3,5-$C_6H_3(CF_3)_2$)), 132.7 (*p*-Ar*C*), 132.5 (*i*-Ar*C*), 131.8 (*i*-Ar*C*), 131.3 (*p*-Ar*C*), 129.3 (qq, $^2J_{CF}$ = 31.5 Hz, $^4J_{CF}$ = 2.9 Hz, *m*-(3,5-$C_6H_3(CF_3)_2$)), 127.8 (*m*-Ar*C*), 127.2 (*m*-Ar*C*), 125.0 (q, $^1J_{CF}$ = 272.4 Hz, *C*F_3), 117.9 (sept, $^3J_{CF}$ = 4.0 Hz, *p*-(3,5-$C_6H_3(CF_3)_2$)), 81.5 (N*C*(CH_3)$_2$), 80.0 (N*C*(CH_3)$_2$), 66.1 (O(*C*H_2CH_3)$_2$), 58.8 (*C*(C_5H_{10})), 58.4 (*C*(C_5H_{10})), 46.7 (*C*H_2), 46.3 (*C*H_2), 38.7 (Cy-*C*H_2), 38.0 (Cy-*C*H_2), 30.2 (*i*Pr-*C*H), 29.8 (NC(*C*H_3)$_2$), 29.8 (NC(*C*H_3)$_2$), 29.7 (NC(*C*H_3)$_2$), 29.2 (*i*Pr-*C*H), 26.5 (*i*Pr-*C*H_3), 26.0 (*i*Pr-*C*H_3), 25.6 (*i*Pr-*C*H_3), 25.4 (Cy-*C*H_2), 25.1 (Cy-*C*H_2), 24.9 (*i*Pr-*C*H_3), 24.6 (*i*Pr-*C*H_3), 24.3 (*i*Pr-*C*H_3), 22.8 (Cy-*C*H_2), 22.4 (Cy-*C*H_2), 22.0 (Cy-*C*H_2), 21.6 (Cy-*C*H_2), 15.5 (O(CH_2CH_3)$_2$) ppm. *Note: the C_{NCS} resonance was not detected.*

^{11}B NMR (128 MHz, CD_2Cl_2, 297 K): δ = 32.2 (br s), 31.2 (br s), –6.6 (s, *B*Ar$^{F}_{4}$) ppm.

^{19}F NMR (471 MHz, CD_2Cl_2, 297 K): δ = –62.8 (s) ppm.

FT-IR (solid-state): $\tilde{\nu}$(NH) = 3401 cm^{-1}.

UV-vis (DCM, 25 °C): λ = 482 nm (shoulder), λ = 513 nm, λ_{max} = 635 nm, λ = 770 nm (shoulder).

Elemental analysis for [$C_{80}H_{83}B_3F_{24}N_4S_2$] ($M_w$ = 1653.08 g mol^{-1}): calcd. C 58.13, H 5.06, N 3.39, S 3.88%; found C 57.67, H 5.54, N 3.43, S 3.32%.

[(CAAC^{Cy}H)B(N^{BCat})(CS)]$_2$ (**20^{BCat}**)

A solution of **16^{Cy}** (50.0 mg, 63.4 µmol) in 1 mL of DCM was treated with catecholborane (HBCat) (19.0 mg, 0.16 mmol, 2.50 equiv), whereupon the intense blue color vanished and an off-white solid precipitated. After removal of all volatiles, the solid residue was washed with a 1:10 benzene/hexane mixture (3 × 1 mL). Removal of the solvent and drying *in vacuo* yielded

20^{BCat} as an off-white solid (58.9 mg, 57.1 μmol, 90% yield). Colorless single crystals of **20^{BCat}** were obtained by vapor diffusion of hexane in a saturated DCM solution.

^{1}H NMR (500 MHz, C_6D_6, 297 K): δ = 7.24 (d, ^{3}J = 7.5 Hz, 2H, *m*-Ar*H*), 7.23 (d, ^{3}J = 7.5 Hz, 2H, *m*-Ar*H*), 7.08 (t, ^{3}J = 7.6 Hz, 2H, *p*-Ar*H*), 7.05–7.02 (m, 6H, Cat*H* + *m*-Ar*H*), 6.83–6.60 (m, 4H, Cat*H*), 5.01 (s, 2H, BC*H*), 4.49 (sept, ^{3}J = 6.7 Hz, 2H, *i*Pr-C*H*), 3.68 (sept, ^{3}J = 6.7 Hz, 2H, *i*Pr-C*H*), 2.43–2.40 (m, 2H, Cy-CH_2), 2.20 (d, ^{2}J = 12.8 Hz, 2H, CH_2), 1.97–1.94 (m, 2H, Cy-CH_2), 1.89 (d, ^{2}J = 12.8 Hz, 2H, CH_2), 1.70 (d, ^{3}J = 6.6 Hz, 6H, *i*Pr-CH_3), 1.63–1.55 (m, 3H, Cy-CH_2), 1.58 (s, 6H, NC(CH_3)$_2$), 1.48 (d, ^{3}J = 6.7 Hz, 6H, *i*Pr-CH_3), 1.47–1.43 (m, 3H, Cy-CH_2), 1.41–1.33 (m, 6H, Cy-CH_2), 1.31 (d, ^{3}J = 6.6 Hz, 6H, *i*Pr-CH_3), 1.27 (d, ^{3}J = 6.7 Hz, 6H, *i*Pr-CH_3), 1.25–1.20 (m, 2H, Cy-CH_2), 1.23 (s, 6H, NC(CH_3)$_2$), 0.71–0.66 (m, 2H, Cy-CH_2) ppm.

^{13}C{^{1}H} NMR (126 MHz, C_6D_6, 297 K): δ = 152.3 (*o*-Ar*C*), 149.9 (*o*-Ar*C*), 147.9 (Cat-*C*O), 142.4 (*i*-Ar*C*), 126.7 (*p*-Ar*C*), 126.5 (*p*-Ar*C*), 125.5 (*m*-Ar*C*), 125.1 (*m*-Ar*C*), 123.2 (Cat-*C*H), 112.5 (Cat-*C*H), 67.4 (B*C*H), 64.3 (N*C*(CH$_3$)$_2$), 52.5 (*C*H$_2$), 46.7 (*C*(C$_5$H$_{10}$)), 40.5 (Cy-*C*H$_2$), 38.4 (Cy-*C*H$_2$), 32.8 (NC(*C*H$_3$)$_2$), 29.0 (*i*Pr-*C*H), 28.2 (*i*Pr-*C*H), 27.3 (NC(*C*H$_3$)$_2$), 27.0 (*i*Pr-*C*H$_3$), 26.7 (*i*Pr-*C*H$_3$), 26.1 (Cy-*C*H$_2$), 25.8 (*i*Pr-*C*H$_3$), 25.3 (*i*Pr-*C*H$_3$), 24.8 (Cy-*C*H$_2$), 23.4 (Cy-*C*H$_2$) ppm. *Note: the C_{NCS} resonance was not detected.*

^{11}B NMR (128 MHz, C_6D_6, 297 K): δ = 52.2 (very br s, *B*NCS), 26.1 (br s, N*B*Cat) ppm.

Elemental analysis for [$C_{60}H_{80}B_4N_4O_4S_2$] (M_w = 1028.68 g mol^{-1}): calcd. C 70.06, H 7.84, N 5.45, S 6.23%; found C 70.16, H 8.04, N 5.28, S 5.79%.

HRMS LIFDI for [$C_{60}H_{80}B_4N_4O_4S_2$] = [M]: calcd. 1028.6021; found 1028.6001.

[(CAAC^{Cy}H)B(N^{BBN})(CS)]$_2$ (20^{BBN})

16^{Cy} (50.0 mg, 63.4 μmol) and [9-BBN]$_2$ (23.2 mg, 95.1 μmol, 1.50 equiv) were combined in 2 mL of DCM. Over a course of 1 d, the color changed from intense blue to brownish. After addition of 5 mL of pentane, the solvent was allowed to evaporate slowly under atmospheric pressure yielding colorless crystals of **20^{BBN}** (54.4 mg, 52.6 μmol, 83% yield) suitable for X-ray diffraction analysis.

^{1}H NMR (500 MHz, C_6D_6, 297 K): δ = 7.16–7.08 (m, 6H, *m*-Ar*H* + *p*-Ar*H*), 4.41 (sept, ^{3}J = 6.8 Hz, 2H, *i*Pr-C*H*), 4.31 (s, 2H, BC*H*), 3.50 (sept, ^{3}J = 6.8 Hz, 2H, *i*Pr-C*H*), 2.32–2.20 (m, 12H, Cy-CH_2 + CH_2 + BBN-*H*), 2.04–1.84 (m, 18H, Cy-CH_2 + CH_2+ BBN-*H*), 1.80–1.63 (m, 9H, Cy-CH_2 + BBN-*H*), 1.60 (s, 6H, NC(CH_3)$_2$), 1.52–1.36 (m, 12H, Cy-CH_2 + BBN-*H*), 1.34 (d, ^{3}J = 6.7 Hz, 6H, *i*Pr-CH_3), 1.32–1.28 (m, 3H, Cy-CH_2 + BBN-*H*), 1.27–1.22 (m, 20H, *i*Pr-CH_3 + BBN-*H*), 1.16 (s, 6H, NC(CH_3)$_2$), 1.12–1.02 (m, 2H, Cy-CH_2) ppm.

$^{13}C\{^{1}H\}$ NMR (126 MHz, C_6D_6, 297 K): δ = 152.5 (*o*-Ar*C*), 150.5 (*o*-Ar*C*), 141.8 (*i*-Ar*C*), 129.9 (*p*-Ar*C*), 126.8 (*p*-Ar*C*), 125.3 (*m*-Ar*C*), 125.2 (*m*-Ar*C*), 68.9 (B*C*H), 64.4 (N*C*(CH_3)$_2$), 52.1 (*C*H_2), 46.6 (*C*(C_5H_{10})), 41.3 (Cy-*C*H_2), 39.0 (Cy-*C*H_2), 34.5 (BBN-*C*H_2), 34.2 (BBN-*C*H_2), 32.1 (NC(*C*H_3)$_2$), 28.8 (BBN-*C*H), 28.6 (*i*Pr-*C*H), 28.3 (*i*Pr-*C*H), 28.0 (NC(*C*H_3)$_2$), 26.7 (*i*Pr-*C*H_3), 26.5 (BBN-*C*H_2), 25.9 (*i*Pr-*C*H_3), 25.9 (*i*Pr-*C*H_3), 25.5 (BBN-*C*H_2), 24.8 (Cy-*C*H_2), 24.0 (Cy-*C*H_2), 23.1 (Cy-*C*H_2) ppm. *Note: the C_{NCS} resonance was not detected.*

^{11}B NMR (128 MHz, CD_2Cl_2, 297 K): δ = 66.0 (very br s, NB^{BBN}), 52.2 (br s, *B*NCS) ppm.

Elemental analysis for [$C_{64}H_{100}B_4N_4S_2$] (M_w = 1032.89 g mol^{-1}): calcd. C 74.42, H 9.76, N 5.42, S 6.21%; found C 74.52, H 9.78, N 5.17, S 5.63%.

HRMS LIFDI for [$C_{64}H_{100}B_4N_4S_2$] = [M]: calcd. 1032.7756; found 1032.7766.

5.2.7 Synthesis of Compounds 21 and 22

[(CAAC^{Me})BH_2(NC)Cr(CO)$_5$] (**21**)

To a solution of **1^{Me}** (200 mg, 447 μmol) dissolved in 50 mL of benzene Na[Cr(CO)$_5$(CN)] (120 mg, 447 μmol) dissolved in 10 mL of THF was added dropwise. The resulting yellow solution was stirred for 20 min prior to removal of the solvent *in vacuo* and the solid obtained was washed with hexane. Extraction with DCM, filtration and slow evaporation of the solvent under atmospheric pressure afforded a large crop of colorless crystals of **21** (172 mg, 333 μmol, 75% yield) suitable for X-ray diffraction analysis.

$^{1}H\{^{11}B\}$ NMR (500 MHz, $CDCl_3$, 297 K): δ = 7.45 (t, ^3J = 7.8 Hz, 1H, *p*-Ar*H*), 7.28 (d, ^3J = 7.9 Hz, 2H, *m*-Ar*H*), 2.60 (sept, ^3J = 6.7 Hz, 2H, *i*Pr-C*H*), 2.22 (br s, 2H, BH_2), 2.13 (s, 2H, CH_2), 1.65 (s, 6H, NC(CH_3)$_2$), 1.37 (s, 6H, C(CH_3)$_2$), 1.31 (d, ^3J = 6.7 Hz, 6H, *i*Pr-CH_3), 1.24 (d, ^3J = 6.7 Hz, 6H, *i*Pr-CH_3) ppm.

$^{13}C\{^{1}H\}$ NMR (126 MHz, $CDCl_3$, 297 K): δ = 227.9 ($C_{carbene}$, identified by HMBC), 219.2 (*C*O), 216.2 (*C*O), 165.3 (BN*C*), 144.7 (*o*-Ar*C*), 131.9 (*i*-Ar*C*), 130.3 (*p*-Ar*C*), 125.3 (*m*-Ar*C*), 78.6 (N*C*(CH_3)$_2$), 52.6 (*C*(CH_3)$_2$), 51.3 (*C*H_2), 29.5 (*i*Pr-*C*H), 29.1 (NC(*C*H_3)$_2$), 28.8 (C(*C*H_3)$_2$), 25.4 (*i*Pr-*C*H_3), 23.7 (*i*Pr-*C*H_3) ppm.

^{11}B NMR (160 MHz, $CDCl_3$, 297 K): δ = –21.6 (br t) ppm.

FT-IR (solid-state): $\tilde{\nu}$(BH) = 2431, 2333 cm^{-1}; $\tilde{\nu}$(NC) = 2165 cm^{-1}; $\tilde{\nu}$(CO) = 2066, 2003, 1895 cm^{-1}.

Elemental analysis for [$C_{26}H_{33}BCrN_2O_5$] (M_w = 516.37 g mol^{-1}): calcd. C 60.48, H 6.44, N 5.43%; found C 60.33, H 6.48, N 5.45%.

(CAAC^{Me})(I*i*Pr)BBr (22)

I*i*Pr (66.5 mg, 0.44 mmol, 1.50 equiv) and KC_8 (86.6 mg, 0.64 mmol, 2.20 equiv) were combined in 1 mL of benzene at room temperature. A dilute solution of (CAAC^{Me})BBr_3 (**VI^{Me}**) (150 mg, 0.29 mmol) in 10 mL of benzene was added dropwise to this mixture under vigorous stirring. The resulting red suspension was stirred for 2 h at room temperature prior to filtration. After removal of all volatiles *in vacuo*, **22** was extracted with pentane. Slow evaporation of the solvent at –30 °C yielded red single crystals of **22** (99.6 mg, 0.19 mmol, 65% yield) suitable for X-ray diffraction analysis.

^{1}H NMR (500 MHz, C_6D_6, 297 K): δ = 7.38–7.35 (m, 1H, *p*-Ar*H*), 7.31–7.30 (m, 2H, *m*-Ar*H*), 6.10 (s, 2H, I*i*Pr-C*H*), 5.41 (sept, ^3J = 6.8 Hz, 2H, I*i*Pr-C*H*$(CH_3)_2$), 3.91 (sept, ^3J = 6.8 Hz, 2H, *i*Pr-C*H*), 2.03 (s, 2H, CH_2), 1.77 (d, ^3J = 6.8 Hz, 6H, *i*Pr-CH_3), 1.49 (d, ^3J = 6.8 Hz, 6H, *i*Pr-CH_3), 1.43 (s, 6H, NC(CH_3)$_2$), 1.23 (s, 6H, C(CH_3)$_2$), 1.16 (d, ^3J = 6.6 Hz, 6H, I*i*Pr-CH(CH_3)$_2$), 0.98 (d, ^3J = 6.9 Hz, 6H, I*i*Pr-CH(CH_3)$_2$) ppm.

^{13}C{^{1}H} NMR (126 MHz, C_6D_6, 297 K): δ = 151.3 (*o*-Ar*C*), 141.4 (*i*-Ar*C*), 126.5 (*p*-Ar*C*), 124.0 (*m*-Ar*C*), 115.8 (I*i*Pr-*C*H), 63.0 (N*C*$(CH_3)_2$), 59.8 (*C*H_2), 50.7 (I*i*Pr-*C*H$(CH_3)_2$), 43.8 (*C*$(CH_3)_2$), 34.2 (C(*C*H_3)$_2$), 30.1 (NC(*C*H_3)$_2$), 28.6 (*i*Pr-*C*H), 26.0 (*i*Pr-*C*H_3), 25.8 (*i*Pr-*C*H_3), 23.8 (I*i*Pr-CH(*C*H_3)$_2$), 21.1 (I*i*Pr-CH(*C*H_3)$_2$) ppm. *Note: the $C_{carbene}$ resonances were not detected, even by HMBC.*

^{11}B NMR (160 MHz, C_6D_6, 297 K): δ = 0.7 (s) ppm.

UV-vis (C_6H_6, 25 °C): λ_{max} = 365 nm (shoulder), λ = 499 nm.

Elemental analysis for [$C_{29}H_{47}BBrN_3$] (M_w = 528.43 g mol^{-1}): calcd. C 65.92, H 8.97, N 7.95%; found C 65.64, H 9.14, N 7.83%.

5.2.8 Synthesis of Boraphosphaketenes and their Dimers

(CAAC^{Me})BH_2(PCO) (23^{Me})

Na(OCP)·$(dioxane)_{2.5}$ (1.35 g, 4.47 mmol) dissolved in 30 mL of THF was added dropwise to a suspension of **1^{Me}** (2.00 g, 4.47 mmol) in 40 mL of benzene. The resulting yellow solution was stirred for 1 h at room temperature prior to removal of volatiles. The residue obtained was washed with hexane and **23^{Me}** was subsequently extracted with benzene. Drying *in vacuo* yielded **23^{Me}** (1.30 g, 3.64 mmol, 81% yield) as a yellow solid, which was stored at –30 °C under exclusion of light. *Note: attempts to obtain single crystals of **23^{Me}** from slow evaporation of a toluene solution at –30 °C resulted in the isolation of **24^{Me}**.*

^{1}H{^{11}B} NMR (500 MHz, C_6D_6, 297 K): δ = 7.12 (t, ^3J = 7.8 Hz, 1H, *p*-Ar*H*), 6.99 (d, ^3J = 7.6 Hz, 2H, *m*-Ar*H*), 2.54 (sept, ^3J = 6.5 Hz, 2H, *i*Pr-C*H*), 2.28 (d, $^2J_{HP}$ = 4.3 Hz, 2H, BH_2),

1.62 (s, 6H, NC(CH_3)$_2$), 1.48 (s, 2H, CH_2), 1.29 (d, ^3J = 6.5 Hz, 6H, *i*Pr-CH_3), 1.10 (d, ^3J = 6.6 Hz, 6H, *i*Pr-CH_3), 0.83 (s, 6H, C(CH_3)$_2$) ppm.

^{13}C{^{1}H} NMR (126 MHz, C_6D_6, 297 K): δ = 234.5 ($C_{carbene}$), 192.8 (d, $^1J_{CP}$ = 44.4 Hz, P*C*O), 145.0 (*o*-Ar*C*), 133.2 (*i*-Ar*C*), 129.7 (*p*-Ar*C*), 124.9 (*m*-Ar*C*), 76.8 (N*C*(CH$_3$)$_2$), 53.0 (*C*(CH$_3$)$_2$), 51.7 (*C*H$_2$), 30.5 (NC(*C*H$_3$)$_2$), 30.4 (NC(*C*H$_3$)$_2$), 29.4 (*i*Pr-*C*H), 28.2 (C(*C*H$_3$)$_2$), 26.4 (*i*Pr-*C*H$_3$), 26.4 (*i*Pr-*C*H$_3$), 23.4 (*i*Pr-*C*H$_3$) ppm.

^{11}B NMR (160 MHz, C_6D_6, 297 K): δ = –27.3 (t, $^1J_{BH}$ = 101 Hz) ppm.

^{31}P NMR (202 MHz, C_6D_6, 297 K): δ = –336.6 (s) ppm.

FT-IR (solid-state): $\tilde{\nu}$(BH) = 2434, 2361 cm^{-1}; $\tilde{\nu}$(PCO) = 1899, 1859 cm^{-1}.

UV-vis (C_6H_6, 25 °C): λ_{max} = 406 nm.

Elemental analysis for [$C_{21}H_{33}BNOP$] (M_w = 357.28 g mol^{-1}): calcd. C 70.60, H 9.31, N 3.92%; found C 68.69, H 9.29, N 3.70%.

HRMS LIFDI for [$C_{21}H_{34}BNOP$]$^+$ = [M + H]$^+$: calcd. 358.2466; found 358.2462.

[(CAAC^{Me})BH$_2$(PCO)]$_2$ (24^{Me})

A solution of **23^{Me}** (50.0 mg, 0.14 mmol) in 2 mL of toluene was left undisturbed for two weeks at –30 °C yielding a crop of yellow crystals (36.5 mg, 25.6 µmol, 73% yield) suitable for X-ray structural analysis.

^{1}H{^{11}B} NMR (500 MHz, CD_2Cl_2, 297 K): δ = 7.41 (t, ^3J = 7.8 Hz, 2H, *p*-Ar*H*), 7.26 (d, ^3J = 7.8 Hz, 4H, *m*-Ar*H*), 2.52 (sept, ^3J = 6.6 Hz, 4H, *i*Pr-C*H*), 2.03 (s, 4H, CH_2), 1.74 (br s, 4H, BH_2), 1.26 (s, 12H, NC(CH_3)$_2$), 1.26 (d, ^3J = 6.4 Hz, 12H, *i*Pr-CH_3), 1.13 (d, ^3J = 6.6 Hz, 12H, *i*Pr-CH_3) ppm.

^{13}C{^{1}H} NMR (126 MHz, CD_2Cl_2, 297 K): δ = 242.7 (overlapping dd, P*C*O), 229.7 ($C_{carbene}$, identified by HMBC), 145.4 (*o*-Ar*C*), 133.1 (*i*-Ar*C*), 129.8 (*p*-Ar*C*), 125.1 (*m*-Ar*C*), 77.6 (N*C*(CH$_3$)$_2$), 53.0 (*C*(CH$_3$)$_2$), 51.8 (*C*H$_2$), 30.0 (NC(*C*H$_3$)$_2$), 29.4 (*i*Pr-*C*H), 28.9 (C(*C*H$_3$)$_2$), 26.3 (*i*Pr-*C*H$_3$), 23.6 (*i*Pr-*C*H$_3$) ppm.

^{11}B NMR (160 MHz, CD_2Cl_2, 297 K): δ = –24.1 (br s) ppm.

^{31}P NMR (202 MHz, CD_2Cl_2, 297 K): δ = 125.3 (s) ppm.

FT-IR (solid-state): $\tilde{\nu}$(BH) = 2426, 2402 cm^{-1}; $\tilde{\nu}$(CO) = 1613 cm^{-1}.

Elemental analysis for [$C_{42}H_{66}B_2N_2O_2P_2$] (M_w = 714.57 g mol^{-1}): calcd. C 70.60, H 9.31, N 3.92%; found C 68.79, H 9.42, N 3.77%.

[(CAAC^{Cy})BH$_2$(PCO)]$_2$ (24^{Cy})

Na(OCP)·(dioxane)$_{2.5}$ (124 mg, 0.41 mmol) dissolved in 10 mL of THF was added dropwise to a suspension of **1^{Cy}** (200 mg, 0.41 mmol) in 5 mL of benzene. The resulting yellow solution was stirred for 1 h at room temperature prior to removal of volatiles. The residue obtained was washed with hexane and **24^{Cy}** was subsequently extracted with DCM. Slow evaporation of the solvent at ambient temperature under the exclusion of light afforded a large crop of yellow crystals (137 mg, 17.2 mmol, 84% yield) suitable for X-ray diffraction analysis.

^{1}H{^{11}B} NMR (500 MHz, CD_2Cl_2, 297 K): δ = 7.40 (t, ^3J = 7.8 Hz, 2H, *p*-Ar*H*), 7.25 (d, ^3J = 7.7 Hz, 4H, *m*-Ar*H*), 2.52 (sept, ^3J = 6.6 Hz, 4H, *i*Pr-C*H*), 2.37 (dt, ^2J = 13.3 Hz, ^3J = 3.4 Hz, 4H, Cy-CH_2), 2.10 (s, 4H, CH_2), 1.82–1.69 (m, 10H, Cy-CH_2 + BH_2), 1.63–1.54 (m, 2H, Cy-CH_2), 1.51–1.49 (m, 4H, Cy-CH_2), 1.42–1.33 (m, 4H, Cy-CH_2), 1.26 (s, 12H, NC(CH_3)$_2$), 1.25 (d, ^3J = 6.8 Hz, 12H, *i*Pr-CH_3), 1.13 (d, ^3J = 6.7 Hz, 12H, *i*Pr-CH_3) ppm.

^{13}C{^{1}H} NMR (126 MHz, CD_2Cl_2, 297 K): δ = 242.6 (overlapping dd, P*C*O), 229.2 ($C_{carbene}$, identified by HMBC), 145.3 (*o*-Ar*C*), 133.2 (*i*-Ar*C*), 129.7 (*p*-Ar*C*), 125.0 (*m*-Ar*C*), 77.7 (N*C*(CH$_3$)$_2$), 58.4 (*C*(C$_5$H$_{10}$)), 45.9 (*C*H$_2$), 36.7 (Cy-*C*H$_2$), 29.4 (*i*Pr-*C*H), 29.4 (NC(*C*H$_3$)$_2$), 26.3 (*i*Pr-*C*H$_3$), 25.3 (Cy-*C*H$_2$), 23.6 (*i*Pr-*C*H$_3$), 22.8 (Cy-*C*H$_2$) ppm.

^{11}B NMR (160 MHz, CD_2Cl_2, 297 K): δ = –23.8 (br s) ppm.

^{31}P NMR (202 MHz, CD_2Cl_2, 297 K): δ = 125.3 (s) ppm.

FT-IR (solid-state): $\tilde{\nu}$(BH) = 2410, 2361 cm^{-1}; $\tilde{\nu}$(CO) = 1606 cm^{-1}.

Elemental analysis for [C$_{48}$H$_{74}$B$_2$N$_2$O$_2$P$_2$] (M_w = 794.70 g mol^{-1}): calcd. C 72.55, H 9.39, N 3.53%; found C 72.33, H 9.48, N 3.40%.

5.2.9 Synthesis and Coordination Chemistry of 1,2-Phosphaborinines

(CAAC^{Me})BH$_2$(PBC$_4$Ph$_5$) (25^{Ph})

A solution of **21^{Me}** (201 mg, 0.56 mmol) in 5 mL of benzene was added dropwise to [PhBC$_4$Ph$_4$] (250 mg, 0.56 mmol) dissolved in 5 mL of benzene. The reaction mixture was stirred for 10 min at room temperature and turned yellow accompanied by evolution of gas. After evaporation of all volatiles, the residue was washed with hexane. Drying *in vacuo* yielded **25^{Ph}** (403 mg, 0.52 mmol, 93% yield) as a yellow solid. Yellow single crystals were obtained by slow evaporation of a concentrated benzene solution.

^{1}H{^{11}B} NMR (500 MHz, C_6D_6, 297 K): δ = 7.77 (d, ^3J = 7.9 Hz, 2H, Ar*H*), 7.33–7.31 (m, 2H, Ar*H*), 7.77 (d, ^3J = 7.7 Hz, 2H, Ar*H*), 7.22 (t, ^3J = 7.5 Hz, 2H, Ar*H*), 7.18–7.14 (m, 4H, Ar*H*), 7.14–7.10 (m, 1H, Ar*H*), 7.03–7.00 (m, 1H, Ar*H*), 6.97–6.92 (m, 6H, Ar*H*), 6.82–6.77 (m, 6H, Ar*H*), 6.65–6.61 (m, 2H, Ar*H*), 2.44 (sept, ^3J = 6.6 Hz, 2H, *i*Pr-C*H*), 2.38 (d, $^2J_{HP}$ = 19.5 Hz,

2H, BH_2), 1.23 (s, 2H, CH_2), 1.20 (s, 6H, NC(CH_3)$_2$), 1.13 (d, ^3J = 6.5 Hz, 6H, *i*Pr-CH_3), 1.09 (d, ^3J = 6.6 Hz, 6H, *i*Pr-CH_3), 0.67 (s, 6H, C(CH_3)$_2$) ppm.

^{13}C{^{1}H} NMR (126 MHz, C_6D_6, 297 K): δ = 233.0 ($C_{carbene}$, identified by HMBC), 152.1 (d, J_{CP} = 24.4 Hz, Ar*C*), 150.4 (br s, Ar*C*), 148.6 (d, J_{CP} = 5.3 Hz, Ar*C*), 148.6 (d, J_{CP} = 1.6 Hz, Ar*C*), 147.7 (br s, Ar*C*), 145.8 (d, J_{CP} = 3.8 Hz, Ar*C*), 145.2 (d, J_{CP} = 8.4 Hz, Ar*C*), 144.9 (s, Ar*C*), 144.5 (d, J_{CP} = 3.6 Hz, Ar*C*), 141.1 (d, J_{CP} = 3.1 Hz, Ar*C*), 135.0 (d, J_{CP} = 9.1 Hz, Ar*C*), 132.8 (s, Ar*C*), 132.7 (s, Ar*C*), 132.2 (d, J_{CP} = 2.5 Hz, Ar*C*), 131.9 (s, Ar*C*), 131.4 (d, J_{CP} = 5.9 Hz, Ar*C*), 129.8 (s, Ar*C*), 127.0 (s, Ar*C*), 126.9 (d, J_{CP} = 5.1 Hz, Ar*C*), 126.5 (d, J_{CP} = 4.1 Hz, Ar*C*), 125.7 (d, J_{CP} = 1.6 Hz, Ar*C*), 125.4 (s, Ar*C*), 125.3 (s, Ar*C*), 124.6 (d, J_{CP} = 5.2 Hz, Ar*C*), 123.9 (s, Ar*C*), 76.9 (N*C*(CH$_3$)$_2$), 53.0 (*C*(CH$_3$)$_2$), 52.1 (*C*H$_2$), 29.2 (*i*Pr-*C*H), 29.1 (NC(*C*H$_3$)$_2$), 29.0 (NC(*C*H$_3$)$_2$), 28.4 (C(*C*H$_3$)$_2$), 27.0 (*i*Pr-*C*H$_3$), 24.3 (*i*Pr-*C*H$_3$) ppm.

^{11}B NMR (160 MHz, C_6D_6, 297 K): δ = 42.8 (br s, Ph*B*P), –28.0 (br s, P*B*H$_2$) ppm.

^{31}P NMR (202 MHz, C_6D_6, 297 K): δ = 81.0 (s) ppm.

FT-IR (solid-state): $\tilde{\nu}$(BH) = 2415, 2389 cm^{-1}.

UV-vis (C_6H_6, 25 °C): λ_{max} = 361 nm.

Elemental analysis for [$C_{54}H_{58}B_2NP$] (M_w = 773.66 g mol^{-1}): calcd. C 83.83, H 7.56, N 1.81%; found C 82.61, H 7.61, N 1.73%.

HRMS LIFDI for [$C_{54}H_{58}B_2NP$] = [M]: calcd. 773.4487; found 773.4469.

(CAAC^{Me})BH$_2$(PB(2-thienyl)C$_4$Ph$_4$) (25^{Tn})

23^{Me} (15.0 mg, 42.0 μmol) and [(2-thienyl)BC_4Ph_4] (18.9 mg, 42.0 μmol) were combined in 0.6 mL of benzene, whereupon evolution of gas and a color change from purple to yellow was observed. After 5 min at room temperature, ^{11}B and ^{31}P NMR spectroscopy showed full consumption of both starting materials. The solvent was removed *in vacuo* and the residue was washed with hexane. Drying *in vacuo* yielded **25^{Tn}** (29.1 mg, 37.4 μmol, 89% yield) as a yellow solid.

^{1}H{^{11}B} NMR (500 MHz, C_6D_6, 297 K): δ = 7.54–7.53 (m, 1H, Ar*H*), 7.42–7.40 (m, 2H, Ar*H*), 7.29 (d, ^3J = 7.7 Hz, 2H, Ar*H*), 7.26–7.25 (m, 1H, Ar*H*), 7.18–7.13 (m, 4H, Ar*H*), 7.09–6.98 (m, 4H, Ar*H*), 6.96–6.91 (m, 5H, Ar*H*), 6.83–6.77 (m, 5H, Ar*H*), 6.65–6.59 (m, 2H, Ar*H*), 2.53 (sept, ^3J = 6.6 Hz, 2H, *i*Pr-C*H*), 2.41 (d, $^2J_{HP}$ = 19.1 Hz, 2H, BH_2), 1.31 (s, 6H, NC(CH_3)$_2$), 1.28 (s, 2H, CH_2), 1.13 (d, ^3J = 6.5 Hz, 6H, *i*Pr-CH_3), 1.10 (d, ^3J = 6.6 Hz, 6H, *i*Pr-CH_3), 0.74 (s, 6H, C(CH_3)$_2$) ppm.

^{13}C{^{1}H} NMR (126 MHz, C_6D_6, 297 K): δ = 233.2 ($C_{carbene}$, identified by HMBC), 152.1 (d, J_{CP} = 24.6 Hz, Ar*C*), 150.3 (br s, Ar*C*), 148.8 (s, Ar*C*), 148.5 (s, Ar*C*), 148.6 (d, J_{CP} = 10.6 Hz,

Ar*C*), 147.5 (br s, Ar*C*), 145.5 (d, J_{CP} = 3.7 Hz, Ar*C*), 145.1 (s, Ar*C*), 145.0 (s, Ar*C*), 145.0 (s, Ar*C*), 144.2 (d, J_{CP} = 3.9 Hz, Ar*C*), 141.0 (d, J_{CP} = 3.4 Hz, Ar*C*), 133.1 (d, J_{CP} = 9.8 Hz, Ar*C*), 133.0 (s, Ar*C*), 132.6 (s, Ar*C*), 131.9 (d, J_{CP} = 2.6 Hz, Ar*C*), 131.8 (s, Ar*C*), 131.4 (d, J_{CP} = 5.9 Hz, Ar*C*), 129.8 (s, Ar*C*), 129.2 (d, J_{CP} = 2.5 Hz, Ar*C*), 127.2 (s, Ar*C*), 127.0 (s, Ar*C*), 126.6 (s, Ar*C*), 126.6 (s, Ar*C*), 126.5 (s, Ar*C*), 126.5 (s, Ar*C*), 125.4 (s, Ar*C*), 125.3 (s, Ar*C*), 124.7 (d, J_{CP} = 5.2 Hz, Ar*C*), 124.6 (s, Ar*C*), 77.0 (N*C*(CH_3)$_2$), 53.3 (*C*(CH_3)$_2$), 52.2 (*C*H_2), 29.2 (*i*Pr-*C*H), 29.2 (NC(*C*H_3)$_2$), 29.2 (NC(*C*H_3)$_2$), 28.4 (C(*C*H_3)$_2$), 27.2 (*i*Pr-*C*H_3), 24.3 (*i*Pr-*C*H_3) ppm.

^{11}B NMR (160 MHz, C_6D_6, 297 K): δ = 39.7 (br s, Thio*B*P), –27.9 (br s, P*B*H_2) ppm.

^{31}P NMR (202 MHz, C_6D_6, 297 K): δ = 80.4 (s) ppm.

FT-IR (solid-state): $\tilde{\nu}$(BH) = 2418, 2390 cm^{-1}.

UV-vis (C_6H_6, 25 °C): λ_{max} = 320 nm (shoulder), λ = 367 nm.

Elemental analysis for [$C_{52}H_{56}B_2NPS$] (M_w = 779.68 g mol^{-1}): calcd. C 80.11, H 7.24, N 1.80, S 4.11%; found C 78.37, H 7.16, N 1.68, S 4.14%.

HRMS LIFDI for [$C_{52}H_{56}B_2NPS$] = [M]: calcd. 779.4052; found 779.4033.

(CAAC^{Me})BH_2(PB(Mes)C_4Ph$_4$) (**25^{Mes}**)

23^{Me} (20.0 mg, 60.0 µmol) and [MesBC_4Ph$_4$] (27.2 mg, 60.0 µmol) were combined in 0.6 mL of benzene. The solution turned yellow over a period of 30 min and evolution of gas occurred. Removal of the solvent *in vacuo*, washing with hexane and drying *in vacuo* afforded **25^{Mes}** (42.1 mg, 51.6 µmol, 86% yield) as a pale yellow solid.

^{1}H{^{11}B} NMR (500 MHz, C_6D_6, 297 K): δ = 7.33 (d, ^3J = 7.8 Hz, 2H, Ar*H*), 7.31–7.29 (m, 2H, Ar*H*), 7.20–7.18 (m, 2H, Ar*H*), 7.07–7.05 (m, 2H, Ar*H*), 7.03–7.01 (m, 1H, Ar*H*), 6.97–6.89 (m, 6H, Ar*H*), 6.83–6.74 (m, 7H, Ar*H*), 6.69–6.66 (m, 1H, Ar*H*), 6.62–6.59 (m, 2H, Ar*H*), 2.57 (s, 6H, *o*-MesCH_3), 2.31 (d, $^2J_{HP}$ = 17.6 Hz, 2H, BH_2), 2.20 (sept, ^3J = 6.6 Hz, 2H, *i*Pr-C*H*), 2.17 (s, 3H, *p*-MesCH_3), 1.35 (s, 6H, NC(CH_3)$_2$), 1.24 (s, 2H, CH_2), 1.02 (d, ^3J = 6.6 Hz, 6H, *i*Pr-CH_3), 1.00 (d, ^3J = 6.6 Hz, 6H, *i*Pr-CH_3), 0.63 (s, 6H, C(CH_3)$_2$) ppm.

^{13}C{^{1}H} NMR (126 MHz, C_6D_6, 297 K): δ = 232.3 ($C_{carbene}$, identified by HMBC), 151.6 (d, J_{CP} = 17.3 Hz, Ar*C*), 150.4 (br s, Ar*C*), 149.0 (d, J_{CP} = 9.0 Hz, Ar*C*), 148.9 (d, J_{CP} = 15.2 Hz, Ar*C*), 146.0 (d, J_{CP} = 3.8 Hz, Ar*C*), 145.3 (d, J_{CP} = 8.2 Hz, Ar*C*), 145.1 (s, Ar*C*), 144.8 (d, J_{CP} = 4.2 Hz, Ar*C*), 143.1 (br s, Ar*C*), 141.1 (d, J_{CP} = 2.6 Hz, Ar*C*), 139.3 (d, J_{CP} = 6.3 Hz, Ar*C*), 134.5 (d, J_{CP} = 2.0 Hz, Ar*C*), 133.0 (s, Ar*C*), 132.6 (s, Ar*C*), 132.4 (d, J_{CP} = 2.4 Hz, Ar*C*), 132.0 (d, J_{CP} = 5.6 Hz, Ar*C*), 130.7 (s, Ar*C*), 129.9 (s, Ar*C*), 127.3 (s, Ar*C*), 126.9 (s, Ar*C*), 126.4 (d, J_{CP} = 2.2 Hz, Ar*C*), 126.4 (s, Ar*C*), 125.3 (s, Ar*C*), 125.3 (s, Ar*C*), 124.5 (d, J_{CP} = 5.5 Hz, Ar*C*),

123.8 (s, Ar*C*), 77.0 (N*C*(CH$_3$)$_2$), 53.0 (*C*(CH$_3$)$_2$), 52.1 (*C*H$_2$), 29.3 (*i*Pr-*C*H), 29.0 (NC(*C*H$_3$)$_2$), 29.0 (NC(*C*H$_3$)$_2$), 28.7 (C(*C*H$_3$)$_2$), 26.5 (*i*Pr-*C*H$_3$), 25.1 (*o*-Mes*C*H$_3$), 24.4 (*i*Pr-*C*H$_3$), 21.4 (*p*-Mes*C*H$_3$) ppm.

^{11}B NMR (160 MHz, C$_6$D$_6$, 297 K): δ = 45.7 (br s, Mes*B*P), –28.1 (br s, P*B*H$_2$) ppm.

^{31}P NMR (202 MHz, C$_6$D$_6$, 297 K): δ = 72.1 (s) ppm.

FT-IR (solid-state): $\tilde{\nu}$(BH) = 2412, 2385 cm^{-1}.

UV-vis (C$_6$H$_6$, 25 °C): λ_{max} = 364 nm.

Elemental analysis for [C$_{57}$H$_{64}$BN$_2$P] (M_w = 815.74 g mol^{-1}): calcd. C 83.93, H 7.91, N 1.72%; found C 81.52, H 7.98, N 1.77%.

HRMS LIFDI for [C$_{57}$H$_{64}$B$_2$NP] = [M]: calcd. 815.4957; found 815.4941.

(CAAC^{Me})BH$_2$(PBC$_4$Ph$_5$)Cr(CO)$_3$ (25^{Ph}-Cr)

A solution of **25^{Ph}** (40.0 mg, 51.7 µmol) and [Cr(CH$_3$CN)$_3$(CO)$_3$] (40.2 mg, 155 µmol, 3.00 equiv) in 0.6 mL of THF was stirred for two days at room temperature. After removal of the solvent *in vacuo*, the red residue was washed with a 9:1 mixture of hexane/THF (3 × 2 mL) and dried *in vacuo* yielding **25^{Ph}-Cr** (42.8 mg, 47.0 µmol, 91% yield) as a yellow solid. Yellow single crystals were obtained by slow evaporation of a saturated benzene solution.

^{1}H{^{11}B} NMR (500 MHz, CD$_2$Cl$_2$, 297 K): δ = 7.42 (t, ^3J = 7.8 Hz, 1H, Ar*H*), 7.32–7.28 (m, 4H, Ar*H*), 7.23–7.16 (m, 3H, Ar*H*), 7.12–7.04 (m, 5H, Ar*H*), 7.01–6.93 (m, 1H, Ar*H*), 6.90–6.87 (m, 2H, Ar*H*), 6.84–6.75 (m, 6H, Ar*H*), 6.72–6.64 (m, 6H, Ar*H*), 2.51 (sept, ^3J = 6.5 Hz, 1H, *i*Pr-C*H*), 2.38 (sept, ^3J = 6.5 Hz, 1H, *i*Pr-C*H*), 2.00 (t, $^2J_{HP}$ = 20.0 Hz, 1H, B*H*$_2$), 1.91–1.85 (m, 2H, C*H*$_2$), 1.65 (t, $^2J_{HP}$ = 20.0 Hz, 1H, B*H*$_2$), 1.37 (s, 3H, C(C*H*$_3$)$_2$), 1.32 (d, ^3J = 6.6 Hz, 3H, *i*Pr-C*H*$_3$), 1.27 (d, ^3J = 6.6 Hz, 3H, *i*Pr-C*H*$_3$), 1.20 (s, 3H, NC(C*H*$_3$)$_2$), 1.16 (d, ^3J = 6.6 Hz, 3H, *i*Pr-C*H*$_3$), 1.15 (s, 3H, NC(C*H*$_3$)$_2$), 1.06 (s, 3H, C(C*H*$_3$)$_2$), 0.85 (d, ^3J = 6.6 Hz, 3H, *i*Pr-C*H*$_3$) ppm.

^{13}C{^{1}H} NMR (126 MHz, CD$_2$Cl$_2$, 297 K): δ = 234.7 (*C*O), 228.7 ($C_{carbene}$, identified by HMBC), 144.9 (d, J_{CP} = 8.7 Hz, Ar*C*), 143.8 (d, J_{CP} = 9.1 Hz, Ar*C*), 142.1 (br s, Ar*C*), 140.3 (s, Ar*C*), 140.3 (d, J_{CP} = 5.7 Hz, Ar*C*), 139.1 (d, J_{CP} = 4.1 Hz, Ar*C*), 135.6 (d, J_{CP} = 6.9 Hz, Ar*C*), 134.2 (s, Ar*C*), 133.4 (s, Ar*C*), 133.1 (d, J_{CP} = 11.2 Hz, Ar*C*), 132.9 (d, J_{CP} = 3.2 Hz, Ar*C*), 132.5 (d, J_{CP} = 8.2 Hz, Ar*C*), 132.4 (s, Ar*C*), 130.1 (s, Ar*C*), 127.4 (br s, Ar*C*), 127.2 (s, Ar*C*), 126.9 (s, Ar*C*), 126.8 (s, Ar*C*), 126.8 (d, J_{CP} = 6.4 Hz, Ar*C*), 126.6 (s, Ar*C*), 126.1 (s, Ar*C*), 126.0 (s, Ar*C*), 125.9 (s, Ar*C*), 125.7 (d, J_{CP} = 3.3 Hz, Ar*C*), 125.4 (d, J_{CP} = 7.6 Hz, Ar*C*), 124.7 (s, Ar*C*), 122.2 (d, J_{CP} = 5.2 Hz, Ar*C*), 121.3 (d, J_{CP} = 2.7 Hz, Ar*C*), 115.2 (br s, Ar*C*), 114.1 (s, Ar*C*), 78.9 (N*C*(CH$_3$)$_2$), 53.3 (*C*(CH$_3$)$_2$), 51.6 (*C*H$_2$), 29.7 (NC(*C*H$_3$)$_2$), 29.4 (*i*Pr-*C*H),

29.3 (*i*Pr-*C*H), 29.1 (C(*C*H$_3$)$_2$), 29.0 (C(*C*H$_3$)$_2$), 28.8 (NC(*C*H$_3$)$_2$), 26.9 (*i*Pr-*C*H$_3$), 26.8 (*i*Pr-*C*H$_3$), 24.3 (*i*Pr-*C*H$_3$), 24.0 (*i*Pr-*C*H$_3$) ppm.

^{11}B NMR (160 MHz, CD_2Cl_2, 297 K): δ = 27.5 (br s, Ph*B*P), –28.5 (br s, P*B*H$_2$) ppm.

^{31}P NMR (202 MHz, CD_2Cl_2, 297 K): δ = –12.6 (s) ppm.

FT-IR (solid-state): $\tilde{\nu}$(BH) = 2453, 2410 cm^{-1}; $\tilde{\nu}$(CO) = 1936, 1872, 1850 cm^{-1}.

UV-vis (C_6H_6, 25 °C): λ_{max} = 346 nm.

HRMS LIFDI for [$C_{57}H_{58}B_2CrNO_3P$] = [M]: calcd. 909.3740; found 909.3728.

(CAAC^{Me})BH$_2$(PBC$_4$Ph$_5$)Mo(CO)$_3$ (25^{Ph}-Mo)

25^{Ph} (40.0 mg, 51.7 µmol) and [Mo(CH$_3$CN)$_3$(CO)$_3$] (23.5 mg, 77.6 µmol, 1.50 equiv) were combined in 0.6 mL of THF and the solution was stirred overnight at room temperature. The solvent was evaporated and the residue was washed with a 9:1 mixture of hexane/THF (3 × 1 mL). Drying *in vacuo* afforded **25^{Ph}-Mo** (46.8 mg, 49.1 µmol, 94% yield) as a yellow solid.

^{1}H{^{11}B} NMR (500 MHz, CD_2Cl_2, 297 K): δ = 7.43 (t, ^3J = 7.8 Hz, 1H, Ar*H*), 7.28–7.24 (m, 4H, Ar*H*), 7.14–7.01 (m, 6H, Ar*H*), 6.96–6.94 (m, 1H, Ar*H*), 6.90–6.81 (m, 8H, Ar*H*), 6.78–6.62 (m, 8H, Ar*H*), 2.52 (sept, ^3J = 6.6 Hz, 1H, *i*Pr-C*H*), 2.37 (sept, ^3J = 6.6 Hz, 1H, *i*Pr-C*H*), 1.99–1.76 (m, 4H, C*H*$_2$ + B*H*$_2$), 1.33 (d, ^3J = 6.6 Hz, 3H, *i*Pr-C*H*$_3$), 1.26 (d, ^3J = 6.6 Hz, 3H, *i*Pr-C*H*$_3$), 1.20 (s, 3H, NC(C*H*$_3$)$_2$), 1.19 (s, 3H, NC(C*H*$_3$)$_2$), 1.17 (s, 3H, C(C*H*$_3$)$_2$), 1.14 (s, 3H, C(C*H*$_3$)$_2$), 1.04 (d, ^3J = 6.6 Hz, 3H, *i*Pr-C*H*$_3$), 0.96 (d, ^3J = 6.5 Hz, 3H, *i*Pr-C*H*$_3$) ppm.

^{13}C{^{1}H} NMR (126 MHz, CD_2Cl_2, 297 K): δ = 228.7 (*C*$_{carbene}$, identified by HMBC), 223.7 (*C*O), 145.2 (s, Ar*C*), 144.7 (s, Ar*C*), 143.4 (d, J_{CP} = 8.8 Hz, Ar*C*), 142.1 (br s, Ar*C*), 139.9 (s, Ar*C*), 139.6 (d, J_{CP} = 4.9 Hz, Ar*C*), 138.8 (d, J_{CP} = 4.3 Hz, Ar*C*), 136.0 (s, Ar*C*), 135.5 (d, J_{CP} = 7.3 Hz, Ar*C*), 134.3 (s, Ar*C*), 134.1 (s, Ar*C*), 133.5 (br s, Ar*C*), 133.0 (s, Ar*C*), 133.0 (s, Ar*C*), 132.6 (br s, Ar*C*), 132.5 (s, Ar*C*), 132.2 (s, Ar*C*), 130.1 (s, Ar*C*), 127.6 (br s, Ar*C*), 127.1 (s, Ar*C*), 126.9 (s, Ar*C*), 126.8 (s, Ar*C*), 126.7 (s, Ar*C*), 126.7 (s, Ar*C*), 126.1 (s, Ar*C*), 126.0 (s, Ar*C*), 125.8 (s, Ar*C*), 125.7 (s, Ar*C*), 125.6 (s, Ar*C*), 125.5 (s, Ar*C*), 125.1 (d, J_{CP} = 5.2 Hz, Ar*C*), 124.8 (s, Ar*C*), 123.5 (d, J_{CP} = 5.1 Hz, Ar*C*), 119.7 (br s, Ar*C*), 117.9 (s, Ar*C*), 79.1 (N*C*(CH$_3$)$_2$), 53.5 (*C*(CH$_3$)$_2$), 51.7 (*C*H$_2$), 29.5 (C(*C*H$_3$)$_2$), 29.5 (*i*Pr-*C*H), 29.3 (NC(*C*H$_3$)$_2$), 29.3 (*i*Pr-*C*H), 29.1 (C(*C*H$_3$)$_2$), 28.8 (NC(*C*H$_3$)$_2$), 27.2 (*i*Pr-*C*H$_3$), 26.7 (*i*Pr-*C*H$_3$), 24.1 (*i*Pr-*C*H$_3$), 24.1 (*i*Pr-*C*H$_3$) ppm.

^{11}B NMR (160 MHz, CD_2Cl_2, 297 K): δ = 27.1 (br s, Ph*B*P), –28.3 (br s, P*B*H$_2$) ppm.

^{31}P NMR (202 MHz, CD_2Cl_2, 297 K): δ = –4.59 (s) ppm.

FT-IR (solid-state): $\tilde{\nu}$(BH) = 2409 cm^{-1}; $\tilde{\nu}$(CO) = 1943, 1855 cm^{-1}.

UV-vis (C_6H_6, 25 °C): λ_{max} = 347 nm, λ = 405 nm (shoulder).

HRMS LIFDI for [$C_{57}H_{58}B_2MoNO_3P$] = [M]: calcd. 954.3427; found 954.3410.

(CAAC^{Me})BH$_2$(PBC$_4$Ph$_5$)W(CO)$_3$ (25^{Ph}-W)

A solution of **25^{Ph}** (20.0 mg, 25.9 μmol) and [W(CH$_3$CN)$_3$(CO)$_3$] (20.3 mg, 51.8 μmol, 2.00 equiv) in 0.6 mL of THF was heated at 60 °C for two days. The solvent was removed *in vacuo* and the red residue was washed with a 9:1 mixture of hexane/THF (3 × 1 mL). Drying *in vacuo* yielded **25^{Ph}-W** (21.5 mg, 20.7 μmol, 83% yield) as a yellow solid.

^{1}H{^{11}B} NMR (500 MHz, CD_2Cl_2, 297 K): δ = 7.43 (t, ^3J = 7.8 Hz, 1H, Ar*H*), 7.27–7.23 (m, 4H, Ar*H*), 7.11–7.01 (m, 6H, Ar*H*), 6.95–6.89 (m, 9H, Ar*H*), 6.77–6.62 (m, 8H, Ar*H*), 2.49 (sept, ^3J = 6.6 Hz, 1H, *i*Pr-C*H*), 2.36 (sept, ^3J = 6.6 Hz, 1H, *i*Pr-C*H*), 2.07–1.97 (m, 1H, BH_2), 1.89–1.81 (m, 3H, CH_2 + BH_2), 1.31 (d, ^3J = 6.6 Hz, 3H, *i*Pr-CH_3), 1.26 (d, ^3J = 6.6 Hz, 3H, *i*Pr-CH_3), 1.21 (s, 3H, NC(CH_3)$_2$), 1.16 (d, ^3J = 6.6 Hz, 3H, *i*Pr-CH_3), 1.16 (s, 3H, NC(CH_3)$_2$), 1.14 (s, 3H, C(CH_3)$_2$), 1.01 (d, ^3J = 6.6 Hz, 3H, *i*Pr-CH_3), 0.97 (d, ^3J = 6.5 Hz, 3H, *i*Pr-CH_3) ppm.

^{13}C{^{1}H} NMR (126 MHz, CD_2Cl_2, 297 K): δ = 228.4 ($C_{carbene}$, identified by HMBC), 213.8 (*C*O), 145.1 (s, Ar*C*), 144.7 (s, Ar*C*), 143.1 (d, J_{CP} = 8.7 Hz, Ar*C*), 141.3 (br s, Ar*C*), 139.4 (s, Ar*C*), 139.3 (d, J_{CP} = 4.6 Hz, Ar*C*), 138.3 (d, J_{CP} = 4.3 Hz, Ar*C*), 136.6 (s, Ar*C*), 135.9 (d, J_{CP} = 7.1 Hz, Ar*C*), 135.0 (s, Ar*C*), 134.7 (s, Ar*C*), 134.3 (br s, Ar*C*), 133.2 (s, Ar*C*), 132.9 (s, Ar*C*), 132.4 (s, Ar*C*), 132.2 (s, Ar*C*), 130.1 (s, Ar*C*), 128.7 (s, Ar*C*), 127.7 (br s, Ar*C*), 127.3 (s, Ar*C*), 127.2 (s, Ar*C*), 127.1 (s, Ar*C*), 126.9 (s, Ar*C*), 126.9 (s, Ar*C*), 126.9 (s, Ar*C*), 126.2 (s, Ar*C*), 126.2 (s, Ar*C*), 126.1 (s, Ar*C*), 125.9 (s, Ar*C*), 125.7 (s, Ar*C*), 125.7 (s, Ar*C*), 125.5 (s, Ar*C*), 124.9 (s, Ar*C*), 121.1 (d, J_{CP} = 4.7 Hz, Ar*C*), 118.0 (d, J_{CP} = 8.3 Hz, Ar*C*), 114.8 (s, Ar*C*), 79.1 (N*C*(CH$_3$)$_2$), 53.4 (*C*(CH$_3$)$_2$), 51.7 (*C*H$_2$), 29.5 (*i*Pr-*C*H), 29.4 (C(*C*H$_3$)$_2$), 29.3 (*i*Pr-*C*H), 29.2 (NC(*C*H$_3$)$_2$), 29.2 (C(*C*H$_3$)$_2$), 28.8 (NC(*C*H$_3$)$_2$), 27.1 (*i*Pr-*C*H$_3$), 26.7 (*i*Pr-*C*H$_3$), 24.1 (*i*Pr-*C*H$_3$), 24.0 (*i*Pr-*C*H$_3$) ppm.

^{11}B NMR (160 MHz, CD_2Cl_2, 297 K): δ = 25.2 (br s, Ph*B*P), –28.3 (br s, P*B*H$_2$) ppm.

^{31}P NMR (202 MHz, CD_2Cl_2, 297 K): δ = –21.3 (s) ppm.

FT-IR (solid-state): $\tilde{\nu}$(BH) = 2416 cm^{-1}; $\tilde{\nu}$(CO) = 1936, 1870, 1845 cm^{-1}.

UV-vis (C_6H_6, 25 °C): λ_{max} = 342 nm.

HRMS LIFDI for [$C_{57}H_{58}B_2NO_3PW$] = [M]: calcd. 1041.3871; found 1041.3849.

VI Appendix

6.1 Figures of other Solid-state Structures

In the following, solid-state structures are shown, which have not been illustrated in the chapter "Results and Discussion".

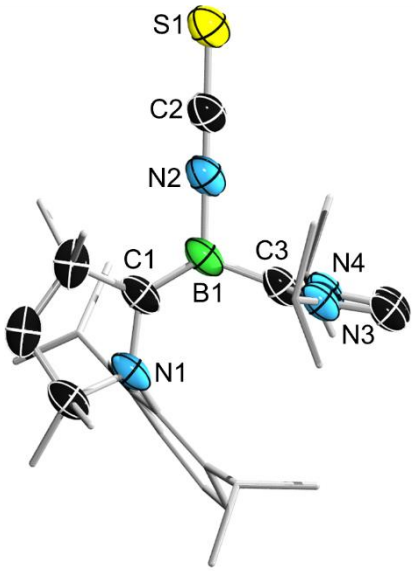

Figure 60. Crystallographically-derived molecular structure of **(*E*)-11^{Me}**. Atomic displacement ellipsoids are shown at the 50% probability level. Ellipsoids of the ligand peripheries and hydrogen atoms have been omitted for clarity. Structural proof of connectivity and of the (*E*)-configuration only.

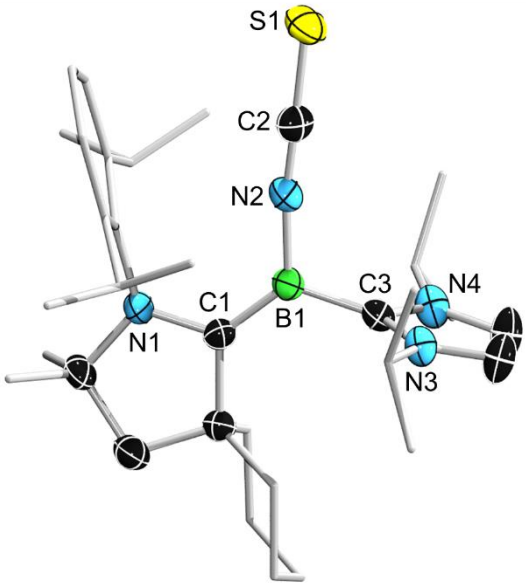

Figure 61. Crystallographically-derived molecular structure of **(*Z*)-11^{Cy}**. Atomic displacement ellipsoids are shown at the 50% probability level. Ellipsoids of the ligand peripheries and hydrogen atoms have been omitted for clarity. Selected bond lengths (Å) and angles (°): N1–C1 1.424(3), C1–B1 1.458(3), B1–N2 1.492(3), N2–C2 1.182(3), C2–S1 1.613(2), B1–C3 1.598(3), B1–N2–C2 170.9(2), N2–C2–S1 178.4(2), C1–B1–C3 125.94(18), N2–B1–C3–N3 85.6(2).

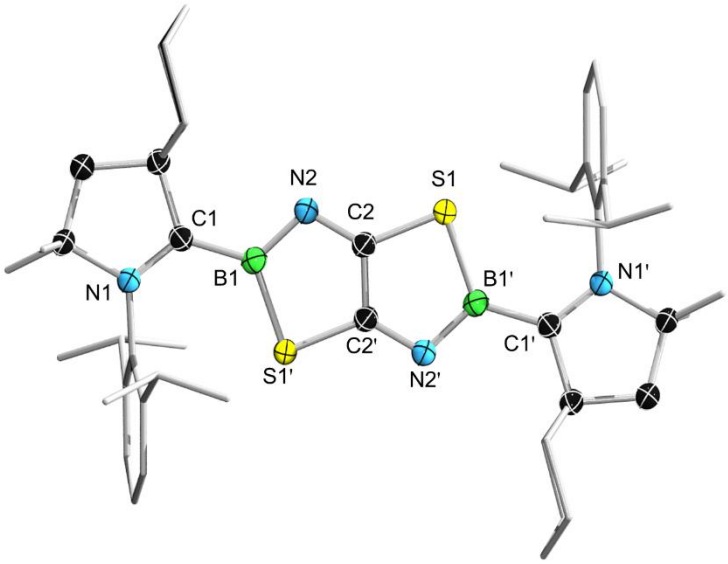

Figure 62. Crystallographically-derived molecular structure of **16**^{Cy}. Atomic displacement ellipsoids are shown at the 50% probability level. Ellipsoids of the ligand peripheries and hydrogen atoms have been omitted for clarity. Selected bond lengths (Å) and angles (°): N1–C1 1.3236(19), C1–B1 1.545(2), B1–N2 1.418(2), N2–C2 1.3318(19), C2–C2' 1.421(3), C2–S1 1.7481(14), S1'–B1 1.8594(17), C1–B1–N2 121.64(13), N2–B1–S1' 112.31(11), N2–C2–S1 129.75(11), B1–N2–C2 108.88(12), C2'–C2–S1 109.53(14), C2'–S1'–B1 88.55(7).

6.2 Figures of other UV-vis Spectra

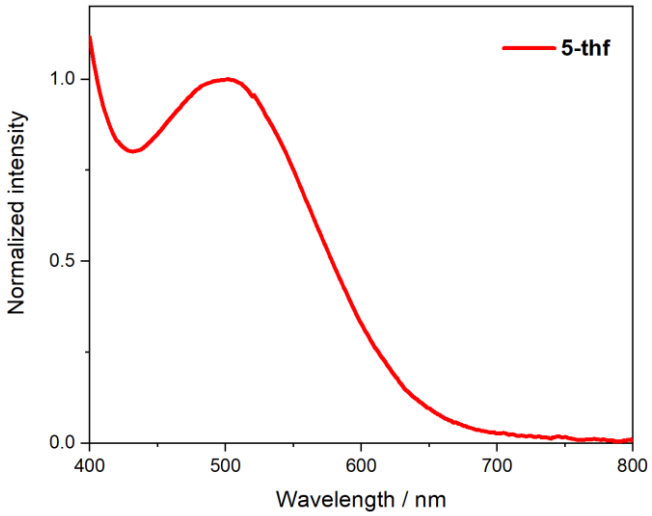

Figure 63. UV-vis absorption spectrum of the boryl anion **5-thf** in THF at 25 °C. **5-thf**: λ_{max} = 502 nm.

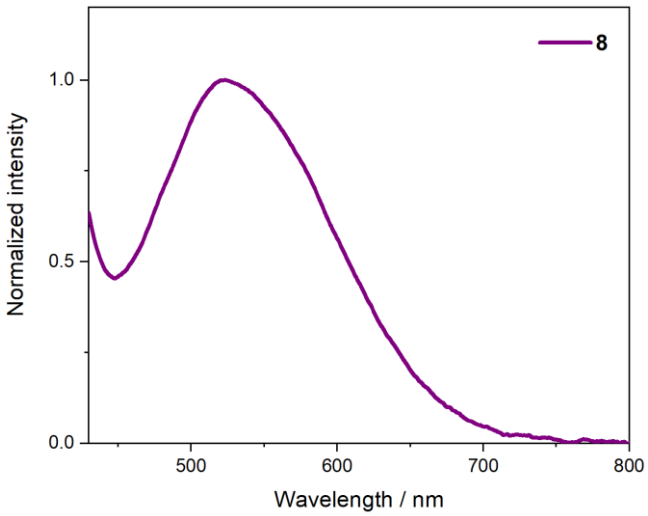

Figure 64. UV-vis absorption spectrum of the boryl radical **8** in benzene at 25 °C. **8**: λ_{max} = 523 nm.

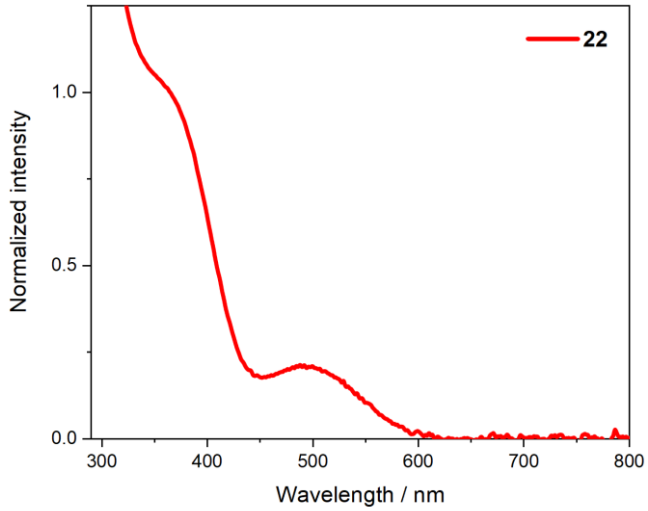

Figure 65. UV-vis absorption spectrum of the bromoborylene **22** in benzene at 25 °C. **22**: λ_{max} = 365 nm (shoulder), λ = 499 nm.

6.3 Crystal Data and Parameters

Compound	1^{Me}	1^{Cy}	2-$CAAC^{Me}$
CCDC number	1956853	2045411	1956849
Empirical formula	$C_{21}H_{33}BF_3NO_3S$	$C_{24}H_{37}BF_3NO_3S$	$C_{42}H_{65}BCl_3F_3N_2O_3S$
Formula weight (g mol^{-1})	447.35	487.41	852.18
Temperature (K)	102(2)	100(2)	296(2)
Radiation, λ (Å)	$Mo_{K\alpha}$ 0.71073	$Mo_{K\alpha}$ 0.71073	$Mo_{K\alpha}$ 0.71073
Crystal system	Monoclinic	Triclinic	Monoclinic
Space group	$P2_1/n$	$P\ \bar{1}$	$P2_1$
Unit cell dimensions			
a (Å)	8.2118(7)	9.9965(4)	9.1335(4)
b (Å)	16.9590(13)	11.1570(5)	22.0651(8)
c (Å)	16.6506(12)	11.9864(5)	21.9639(8)
α (°)	90	103.463(2)	90
β (°)	95.196(3)	98.667(2)	94.994(2)
γ (°)	90	99.398(2)	90
Volume (Å^3)	2309.3(3)	1257.61(9)	4409.6(3)
Z	4	2	4
Calculated density (Mg m^{-3})	1.287	1.287	1.284
Absorbtion coefficient (mm^{-1})	0.186	0.176	0.307
F(000)	952	520	1816
Theta range for collection	2.402 to 26.017°	2.247 to 26.022°	1.846 to 27.103°
Reflections collected	41839	38575	69525
Independent reflections	4544	4966	18321
Minimum/maximum transmission	0.7109/0.7454	0.7018/0.7454	0.3688/0.7456
Refinement method	Full-matrix least-squares on F^2	Full-matrix least-squares on F^2	Full-matrix least-squares on F^2
Data / parameters / restrains	4544 / 287 / 0	4966 / 312 / 0	18321 / 1148 / 966
Goodness-of-fit on F^2	1.036	1.034	1.018
Final R indices [I>2σ(I)]	R_1 = 0.0369, wR^2 = 0.0816	R_1 = 0.0404, wR^2 = 0.0942	R_1 = 0.0621, wR^2 = 0.1254
R indices (all data)	R_1 = 0.0523, wR^2 = 0.0889	R_1 = 0.0475, wR^2 = 0.0998	R_1 = 0.0893, wR^2 = 0.1403
Maximum/minimum residual electron density (e Å^{-3})	0.300 / –0.395	0.663 / –0.450	0.438 / –0.393

Compound	2-Pyr	2-DMAP	3-DMAP
CCDC number	1956847	1956848	1956850
Empirical formula	$C_{26}H_{38}BF_3N_2O_3S$	$C_{28}H_{43}BF_3N_3O_3S$	$C_{43}H_{69}BF_3N_5O_5S$
Formula weight (g mol^{-1})	526.45	569.52	835.90
Temperature (K)	101(2)	101(2)	101(2)
Radiation, λ (Å)	$Mo_{K\alpha}$ 0.71073	$Mo_{K\alpha}$ 0.71073	$Mo_{K\alpha}$0.71073
Crystal system	Triclinic	Triclinic	Triclinic
Space group	$P\ \bar{1}$	$P\ \bar{1}$	$P\ \bar{1}$
Unit cell dimensions			
a (Å)	10.1404(6)	10.6577(12)	8.7125(7)
b (Å)	10.7992(7)	10.6616(15)	12.5555(11)
c (Å)	14.1434(10)	13.7408(18)	22.1845(19)
α (°)	109.794(2)	88.486(6)	78.804(3)
β (°)	104.440(2)	79.875(5)	81.554(3)
γ (°)	99.480(2)	81.424(6)	73.644(3)
Volume (Å^3)	1357.49(15)	1519.8(3)	2273.2(3)
Z	2	2	2
Calculated density (Mg m^{-3})	1.288	1.244	1.221
Absorbtion coefficient (mm^{-1})	0.170	0.158	0.131
F(000)	560	608	900
Theta range for collection	2.556 to 27.138°	2.449 to 27.861°	0.940 to 26.022°
Reflections collected	22441	29943	29636
Independent reflections	5991	7144	8965
Minimum/maximum transmission	0.6657/0.7455	0.6420/0.7456	0.6001/0.7454
Refinement method	Full-matrix least-squares on F^2	Full-matrix least-squares on F^2	Full-matrix least-squares on F^2
Data / parameters / restrains	5991 / 488 / 184	7144 / 443 / 103	8965 / 493 / 0
Goodness-of-fit on F^2	1.025	1.040	2.366
Final R indices [I>2σ(I)]	R_1 = 0.0488, wR^2 = 0.1035	R_1 = 0.0576, wR^2 = 0.1196	R_1 = 0.1223, wR^2 = 0.3243
R indices (all data)	R_1 = 0.0786, wR^2 = 0.1212	R_1 = 0.0926, wR^2 = 0.1409	R_1 = 0.1579, wR^2 = 0.3323
Maximum/minimum residual electron density (e Å^{-3})	0.291 / –0.287	0.330 / –0.394	3.750 / –0.410

Compound	**5**	**5-thf**	**8**
CCDC number	1956854	1956851	1956852
Empirical formula	$C_{52}H_{76}BKN_2$	$C_{52}H_{88}BKN_2O_3$	$C_{43}H_{67}BN_2$
Formula weight (g mol^{-1})	779.05	839.15	622.79
Temperature (K)	102(2)	102(2)	100(2)
Radiation, λ (Å)	$Mo_{K\alpha}$ 0.71073	$Mo_{K\alpha}$ 0.71073	$Mo_{K\alpha}$ 0.71073
Crystal system	Monoclinic	Triclinic	Triclinic
Space group	*C*2/*c*	$P\ \bar{1}$	$P\ \bar{1}$
Unit cell dimensions			
a (Å)	22.753(9)	10.337(2)	9.1257(3)
b (Å)	9.854(5)	12.573(3)	11.7040(3)
c (Å)	20.638(7)	20.686(6)	18.4845(5)
α (°)	90	106.736(9)	97.5860(10)
β (°)	93.074(15)	90.380(17)	103.7760(10)
γ (°)	90	97.258(10)	91.7560(10)
Volume (Å^3)	4621(4)	2551.4(11)	1896.75(9)
Z	4	2	2
Calculated density (Mg m^{-3})	1.120	1.092	1.090
Absorbtion coefficient (mm^{-1})	0.151	0.145	0.061
F(000)	1704	924	688
Theta range for collection	2.253 to 26.753°	2.235 to 26.021°	2.233 to 27.144°
Reflections collected	30179	55956	60189
Independent reflections	4914	10054	8317
Minimum/maximum transmission	0.6213/0.7454	0.7017/0.7454	0.7095/0.7455
Refinement method	Full-matrix least-squares on F^2	Full-matrix least-squares on F^2	Full-matrix least-squares on F^2
Data / parameters / restrains	4914 / 279 / 18	10054 / 643 / 120	8317 / 435 / 0
Goodness-of-fit on F^2	1.058	1.023	1.035
Final R indices [I>2σ(I)]	R_1 = 0.0452, wR^2 = 0.0952	R_1 = 0.0414, wR^2 = 0.0992	R_1 = 0.0465, wR^2 = 0.1157
R indices (all data)	R_1 = 0.0700, wR^2 = 0.1073	R_1 = 0.0592, wR^2 = 0.1075	R_1 = 0.0536, wR^2 = 0.1215
Maximum/minimum residual electron density (e Å^{-3})	0.290 / –0.339	0.346 / –0.298	0.422 / –0.295

Compound	**9^{Me}**	**9^{Cy}**	**10^{Me}**
CCDC number	2045417	2045412	2045418
Empirical formula	$C_{21}H_{33}BN_2S$	$C_{24}H_{37}BN_2S$	$C_{21}H_{31}BBr_2N_2S$
Formula weight (g mol^{-1})	356.36	396.42	514.17
Temperature (K)	103(2)	103(2)	100(2)
Radiation, λ (Å)	$Mo_{K\alpha}$ 0.71073	$Mo_{K\alpha}$ 0.71073	$Mo_{K\alpha}$ 0.71073
Crystal system	Monoclinic	Triclinic	Orthorhombic
Space group	$P2_1/c$	$P\ \bar{1}$	*Pbca*
Unit cell dimensions			
a (Å)	15.454(4)	10.291(2)	16.133(3)
b (Å)	7.5569(13)	10.4748(19)	16.511(8)
c (Å)	19.789(3)	11.880(8)	17.790(4)
α (°)	90	88.016(17)	90
β (°)	111.261(11)	65.57(2)	90
γ (°)	90	82.230(14)	90
Volume (Å^3)	2153.7(8)	1154.9(8)	4739(3)
Z	4	2	8
Calculated density (Mg m^{-3})	1.099	1.140	1.441
Absorbtion coefficient (mm^{-1})	0.156	0.152	3.518
F(000)	776	432	2096
Theta range for collection	1.414 to 26.021°	1.883 to 26.021°	2.104 to 27.126°
Reflections collected	35860	19198	45673
Independent reflections	4251	4546	5231
Minimum/maximum transmission	0.7072/0.7454	0.6567/0.7454	0.5654/0.8667
Refinement method	Full-matrix least-squares on F^2	Full-matrix least-squares on F^2	Full-matrix least-squares on F^2
Data / parameters / restrains	4251 / 240 / 0	4546 / 267 / 0	5231 / 252 / 0
Goodness-of-fit on F^2	1.048	1.062	1.036
Final R indices [I>2σ(I)]	R_1 = 0.0417, wR^2 = 0.0990	R_1 = 0.0445, wR^2 = 0.1152	R_1 = 0.0602, wR^2 = 0.1549
R indices (all data)	R_1 = 0.0541, wR^2 = 0.1049	R_1 = 0.0526, wR^2 = 0.1221	R_1 = 0.0780, wR^2 = 0.1660
Maximum/minimum residual electron density (e Å^{-3})	0.369 / –0.389	0.358 / –0.318	0.438 / –0.393

Compound	**10^{Cy}**	**(*E*)-11^{Me}**	**(*Z*)-11^{Me}**
CCDC number	2045413	2045410	2045415
Empirical formula	$C_{24}H_{35}BBr_2N_2S$	$C_{33}H_{50}BN_4S$	$C_{36}H_{53}BN_4S$
Formula weight (g mol^{-1})	554.23	545.66	584.69
Temperature (K)	103(2)	99.99(18)	100(2)
Radiation, λ (Å)	$Mo_{K\alpha}$ 0.71073	$Cu_{K\alpha}$1.54184	$Mo_{K\alpha}$ 0.71073
Crystal system	Orthorhombic	Triclinic	Monoclinic
Space group	*Pbca*	$P\ \bar{1}$	$P2_1/c$
Unit cell dimensions			
a (Å)	16.362(3)	10.8346(7)	15.7019(18)
b (Å)	16.987(3)	16.8397(19)	11.9233(11)
c (Å)	18.158(3)	19.1961(13)	38.077(4)
α (°)	90	80.925(7)	90
β (°)	90	74.130(6)	94.116(8)
γ (°)	90	89.280(7)	90
Volume (Å^3)	5046.7(16)	3325.0(5)	7110.3(13)
Z	8	2	8
Calculated density (Mg m^{-3})	1.459	3.246	1.092
Absorbtion coefficient (mm^{-1})	3.309	14.754	0.120
F(000)	2272	3255	2544
Theta range for collection	2.060 to 26.022°	4.244 to 51.958°	1.744 to 27.885°
Reflections collected	55108	6114	88589
Independent reflections	4972	4331	16942
Minimum/maximum transmission	0.3456/0.4532	0.83512/1.00000	0.6800/0.7456
Refinement method	Full-matrix least-squares on F^2	Full-matrix least-squares on F^2	Full-matrix least-squares on F^2
Data / parameters / restrains	4972 / 277 / 0	4331 / 337 / 0	16942 / 939 / 181
Goodness-of-fit on F^2	1.041	2.115	1.027
Final R indices [I>2σ(I)]	R_1 = 0.0321, wR^2 = 0.0801	R_1 = 0.0958, wR^2 = 0.2866	R_1 = 0.0414, wR^2 = 0.1047
R indices (all data)	R_1 = 0.0422, wR^2 = 0.0849	R_1 = 0.1110, wR^2 = 0.2929	R_1 = 0.0530, wR^2 = 0.1114
Maximum/minimum residual electron density (e Å^{-3})	1.427 / –0.693	0.357 / –0.540	0.368 / –0.233

Compound	**(*E*)-11^{Cy}**	**(*Z*)-11^{Cy}**	**12**
CCDC number	2045409	2045416	2071474
Empirical formula	$C_{36}H_{54}BN_4S$	$C_{33}H_{51}BN_4S$	$C_{66}H_{100}B_2N_8$
Formula weight (g mol^{-1})	585.70	546.64	1027.15
Temperature (K)	100(2)	100(2)	99.99(11)
Radiation, λ (Å)	$Mo_{K\alpha}$ 0.71073	$Mo_{K\alpha}$ 0.71073	$Cu_{K\alpha}$1.54184
Crystal system	Triclinic	Triclinic	Monoclinic
Space group	$P\ \bar{1}$	$P\ \bar{1}$	$P2_1/c$
Unit cell dimensions			
a (Å)	9.7239(10)	9.668(6)	32.7131(2)
b (Å)	10.4152(12)	11.565(7)	9.67986(7)
c (Å)	18.702(3)	16.440(9)	21.35114(15)
α (°)	102.314(4)	94.779(18)	90
β (°)	97.686(4)	90.772(19)	108.9322(8)
γ (°)	109.094(3)	112.396(19)	90
Volume (Å^3)	1705.7(4)	1691.6(18)	6395.27(8)
Z	2	2	4
Calculated density (Mg m^{-3})	1.140	1.073	1.067
Absorbtion coefficient (mm^{-1})	0.125	0.122	0.467
F(000)	638	596	2248
Theta range for collection	1.143 to 26.021°	2.349 to 26.021°	2.1876 to 77.467°
Reflections collected	26113	29937	60303
Independent reflections	6716	6664	13395
Minimum/maximum transmission	0.6460/0.7454	0.6507/0.7454	0.756/1.000
Refinement method	Full-matrix least-squares on F^2	Full-matrix least-squares on F^2	Full-matrix least-squares on F^2
Data / parameters / restrains	6716 / 389 / 0	6664 / 362 / 0	13395 / 709 / 66
Goodness-of-fit on F^2	1.031	1.052	1.055
Final R indices [I>2σ(I)]	R_1 = 0.0461, wR^2 = 0.1176	R_1 = 0.0493, wR^2 = 0.1131	R_1 = 0.0471, wR^2 = 0.1217
R indices (all data)	R_1 = 0.0632, wR^2 = 0.1290	R_1 = 0.0994, wR^2 = 0.1469	R_1 = 0.0555, wR^2 = 0.1275
Maximum/minimum residual electron density (e Å^{-3})	0.321 / –0.328	0.214 / –0.319	0.698 / –0.372

Compound	**[(*Z*)-11$^{Me•+}$][OTf$^-$]**	**[12$^{•+}$][OTf$^-$]**	**(*Z*)-12-Cr**
CCDC number	2071477	2071475	2071473
Empirical formula	$C_{31}H_{47}BF_3N_4O_3S_2$	$C_{34}H_{50}BF_3N_4O_3S$	$C_{35}H_{47}BCrN_4O_5$
Formula weight (g mol^{-1})	655.65	663.92	666.57
Temperature (K)	99.9(6)	99(2)	100(2)
Radiation, λ (Å)	$Cu_{K\alpha}$1.54184	$Mo_{K\alpha}$ 0.71073	$Mo_{K\alpha}$ 0.71073
Crystal system	Orthorhombic	Triclinic	Monoclinic
Space group	*Pbca*	$P\ \bar{1}$	$P2_1/c$
Unit cell dimensions			
a (Å)	12.31193(8)	9.430(7)	19.185(7)
b (Å)	15.53996(11)	9.763(7)	11.123(4)
c (Å)	36.3830(2)	20.736(15)	19.623(6)
α (°)	90.0	95.574(13)	90
β (°)	90.0	96.19(3)	118.54(2)
γ (°)	90.0	101.684(14)	90
Volume (Å^3)	6961.04(8)	1845(2)	3679(2)
Z	8	2	4
Calculated density (Mg m^{-3})	1.251	1.195	1.204
Absorbtion coefficient (mm^{-1})	1.827	0.140	0.354
F(000)	2792.000	709	1416
Theta range for collection	2.4288 to 72.118°	1.991 to 26.020°	2.077 to 26.022°
Reflections collected	58073	7258	37289
Independent reflections	6847	7258	7245
Minimum/maximum transmission	0.360/1.000	0.5953/0.7454	0.5957/0.7454
Refinement method	Full-matrix least-squares on F^2	Full-matrix least-squares on F^2	Full-matrix least-squares on F^2
Data / parameters / restrains	6847 / 409 / 0	7258 / 517 / 211	7245 / 427 / 0
Goodness-of-fit on F^2	1.071	1.159	1.022
Final R indices [I>2σ(I)]	R_1 = 0.0444, wR^2 = 0.1172	R_1 = 0.1063, wR^2 = 0.2839	R_1 = 0.0403, wR^2 = 0.0977
R indices (all data)	R_1 = 0.0464, wR^2 = 0.1188	R_1 = 0.1210, wR^2 = 0.2898	R_1 = 0.0528, wR^2 = 0.1044
Maximum/minimum residual electron density (e Å^{-3})	0.356 / –0.927	0.826 / –0.556	0.318 / –0.532

Compound	**(*Z*)-12-Mo**	**(*E*)-12-W**	**13^{CN}**
CCDC number	2071470	2071471	2071476
Empirical formula	$C_{41}H_{53}BMoN_4O_5$	$C_{35}H_{47}BN_4O_5W$	$C_{36}H_{53}BN_4S\cdot(C_7H_8)_{0.5}$
Formula weight (g mol^{-1})	788.62	798.42	630.76
Temperature (K)	100(2)	100(2)	99.8(8)
Radiation, λ (Å)	$Mo_{K\alpha}$ 0.71073	$Mo_{K\alpha}$ 0.71073	$Cu_{K\alpha}$1.54184
Crystal system	Orthorhombic	Triclinic	Triclinic
Space group	$P2_12_12_1$	$P\ \bar{1}$	$P\ \bar{1}$
Unit cell dimensions			
a (Å)	13.190(6)	9.653(4)	9.78460(10)
b (Å)	14.868(5)	10.588(7)	11.33740(10)
c (Å)	21.174(7)	19.881(9)	17.2083(2)
α (°)	90	78.11(2)	95.3960(10)
β (°)	90	83.576(15)	95.5070(10)
γ (°)	90	67.077(16)	99.3500(10)
Volume (Å^3)	4152(3)	1830.2(17)	1863.18(3)
Z	4	2	2
Calculated density (Mg m^{-3})	1.261	1.449	1.124
Absorbtion coefficient (mm^{-1})	0.361	3.200	0.997
F(000)	1656	808	686
Theta range for collection	1.674 to 26.022°	1.047 to 26.022°	2.596 to 78.007°
Reflections collected	26955	30853	79195
Independent reflections	8028	7190	7909
Minimum/maximum transmission	0.5079/0.7454	0.4106/0.7454	0.34689/1.00000
Refinement method	Full-matrix least-squares on F^2	Full-matrix least-squares on F^2	Full-matrix least-squares on F^2
Data / parameters / restrains	8028 / 481 / 0	7190 / 427 / 0	7909 / 488 / 327
Goodness-of-fit on F^2	1.016	1.016	1.093
Final R indices [I>2σ(I)]	R_1 = 0.0357, wR^2 = 0.0708	R_1 = 0.0349, wR^2 = 0.0759	R_1 = 0.0537, wR^2 = 0.1507
R indices (all data)	R_1 = 0.0463, wR^2 = 0.0746	R_1 = 0.0411, wR^2 = 0.0786	R_1 = 0.0575, wR^2 = 0.1544
Maximum/minimum residual electron density (e Å^{-3})	0.525 / –0.441	1.652 / –1.839	0.580 / –0.354

Compound	**14^{NCS}**	**16^{Me}**	**16^{Cy}**
CCDC number	2071472	2045414	2045419
Empirical formula	$C_{42}H_{59}BN_4S_2$	$C_{54}H_{74}B_2N_4S_2$	$C_{72}H_{94}B_2N_4S_2$
Formula weight (g mol^{-1})	694.86	864.91	1101.25
Temperature (K)	100(2)	100(2)	99.97(18)
Radiation, λ (Å)	$Mo_{K\alpha}$ 0.71073	$Mo_{K\alpha}$ 0.71073	$Cu_{K\alpha}$1.54184
Crystal system	Monoclinic	Monoclinic	Triclinic
Space group	*Pc*	*C*2/*c*	$P\ \bar{1}$
Unit cell dimensions			
a (Å)	10.657(7)	19.577(5)	9.6331(2)
b (Å)	16.337(11)	17.036(3)	13.2465(3)
c (Å)	11.950(9)	16.371(4)	14.0946(3)
α (°)	90	90	112.401(2)
β (°)	106.86(2)	115.215(12)	101.422(2)
γ (°)	90	90	93.354(2)
Volume (Å^3)	1991(2)	4940(2)	1611.98(7)
Z	2	4	1
Calculated density (Mg m^{-3})	1.159	1.163	1.134
Absorbtion coefficient (mm^{-1})	0.168	0.148	1.070
F(000)	752	1872	596
Theta range for collection	2.354 to 26.020°	2.391 to 26.021°	3.493 to 72.129°
Reflections collected	36025	39860	32397
Independent reflections	7672	4863	6331
Minimum/maximum transmission	0.6890/0.7454	0.7027/0.7454	0.84199/1.00000
Refinement method	Full-matrix least-squares on F^2	Full-matrix least-squares on F^2	Full-matrix least-squares on F^2
Data / parameters / restrains	7672 / 485 / 254	4863 / 317 / 108	6331 / 398 / 72
Goodness-of-fit on F^2	1.038	1.031	1.061
Final R indices [I>2σ(I)]	R_1 = 0.0335, wR^2 = 0.0725	R_1 = 0.0333, wR^2 = 0.0795	R_1 = 0.0505, wR^2 = 0.1408
R indices (all data)	R_1 = 0.0369, wR^2 = 0.0740	R_1 = 0.0401, wR^2 = 0.0828	R_1 = 0.0553, wR^2 = 0.1451
Maximum/minimum residual electron density (e Å^{-3})	0.174 / –0.207	0.278 / –0.275	0.511 / –0.384

Compound	17	18-Cl	18-OTf
CCDC number	–	–	–
Empirical formula	$C_{62}H_{74}B_2Cl_4Cu_2F_{10}N_4S_2$	$C_{52}H_{80}B_2Cl_{10}N_4S_2$	$C_{50}H_{72}B_2F_6N_4O_6S_4$
Formula weight (g mol^{-1})	1419.87	1201.44	1088.97
Temperature (K)	100.0(3)	100(2)	99.9(8)
Radiation, λ (Å)	$Cu_{K\alpha}$1.54184	$Mo_{K\alpha}$ 0.71073	$Cu_{K\alpha}$1.54184
Crystal system	Monoclinic	Triclinic	Triclinic
Space group	$P2_1/n$	$P\ \bar{1}$	$P\ \bar{1}$
Unit cell dimensions			
a (Å)	9.88691(5)	9.349(3)	9.4490(3)
b (Å)	23.13953(13)	11.782(3)	10.6687(3)
c (Å)	13.87825(7)	15.284(3)	13.2878(4)
α (°)	90.0	100.027(14)	80.966(2)
β (°)	99.4769(5)	106.935(13)	89.074(2)
γ (°)	90.0	105.492(13)	86.747(2)
Volume (Å^3)	3131.71(3)	1493.1(7)	1320.74(7)
Z	2	1	1
Calculated density (Mg m^{-3})	1.506	1.336	1.369
Absorbtion coefficient (mm^{-1})	3.654	0.575	2.272
F(000)	1464	632	576
Theta range for collection	3.752 to 72.126°	2.024 to 26.020°	3.368 to 72.125°
Reflections collected	72424	41850	26931
Independent reflections	6181	5851	5209
Minimum/maximum transmission	0.69186/1.00000	0.6615/0.7454	0.819/1.000
Refinement method	Full-matrix least-squares on F^2	Full-matrix least-squares on F^2	Full-matrix least-squares on F^2
Data / parameters / restrains	6181 / 394 / 0	5851 / 326 / 0	5209 / 427 / 328
Goodness-of-fit on F^2	1.049	1.057	1.027
Final R indices [I>2σ(I)]	R_1 = 0.0378, wR^2 = 0.0999	R_1 = 0.0430, wR^2 = 0.1070	R_1 = 0.0577, wR^2 = 0.1424
R indices (all data)	R_1 = 0.0384, wR^2 = 0.1004	R_1 = 0.0485, wR^2 = 0.1113	R_1 = 0.0678, wR^2 = 0.1485
Maximum/minimum residual electron density (e Å^{-3})	1.089 / –0.802	1.608 / –1.228	0.362 / –0.534

Compound	18-OTf·HOTf	18-[BAr$^F_4$]·Et$_2$O	18-[BAr$^F_4$]
CCDC number	–	–	–
Empirical formula	$C_{54}H_{78}B_2Cl_4F_{12}N_4O_{12}S_6$	$C_{64}H_{68}B_2F_{24}N_2O_2S$	$C_{112}H_{96}B_4F_{48}N_4S_2$
Formula weight (g mol^{-1})	1558.98	1406.88	2517.28
Temperature (K)	101(2)	98(2)	99.9(6)
Radiation, λ (Å)	Mo$_{K\alpha}$0.71073	Mo$_{K\alpha}$ 0.71073	Cu$_{K\alpha}$1.54184
Crystal system	Triclinic	Triclinic	Triclinic
Space group	$P\ \bar{1}$	$P\ \bar{1}$	$P\ \bar{1}$
Unit cell dimensions			
a (Å)	9.577(4)	13.254(7)	13.69288(11)
b (Å)	10.746(4)	14.011(7)	13.92081(11)
c (Å)	17.956(12)	19.110(10)	17.10886(11)
α (°)	78.701(9)	103.44(2)	101.5941(6)
β (°)	77.36(2)	101.23(4)	107.8323(7)
γ (°)	88.871(9)	100.81(4)	106.7535(7)
Volume (Å^3)	1767.7(16)	3283(3)	2819.14(4)
Z	1	2	1
Calculated density (Mg m^{-3})	1.464	1.423	1.483
Absorbtion coefficient (mm^{-1})	0.434	0.162	1.590
F(000)	808	1448	1280
Theta range for collection	1.185 to 26.021°	1.131 to 26.021°	2.861 to 72.128°
Reflections collected	30059	54925	118728
Independent reflections	6964	12940	11100
Minimum/maximum transmission	0.6919/0.7454	0.6612/0.7454	0.405/1.000
Refinement method	Full-matrix least-squares on F^2	Full-matrix least-squares on F^2	Full-matrix least-squares on F^2
Data / parameters / restrains	6964 / 509 / 253	12940 / 870 / 0	11100 / 945 / 653
Goodness-of-fit on F^2	1.051	1.062	1.037
Final R indices [I>2σ(I)]	R_1 = 0.0373, wR^2 = 0.0858	R_1 = 0.0591, wR^2 = 0.1539	R_1 = 0.0436, wR^2 = 0.1055
R indices (all data)	R_1 = 0.0556, wR^2 = 0.0930	R_1 = 0.0913, wR^2 = 0.1738	R_1 = 0.0466, wR^2 = 0.1076
Maximum/minimum residual electron density (e Å^{-3})	0.549 / –0.443	0.981 / –0.622	0.539 / –0.395

Compound	**20^{Bcat}**	**20^{BBN}**	**21**
CCDC number	–	–	–
Empirical formula	$C_{60}H_{80}B_4N_4O_4S_2$	$C_{64}H_{100}B_4N_4S_2$	$C_{26}H_{33}BCrN_2O_5$
Formula weight (g mol^{-1})	1028.64	1032.83	516.35
Temperature (K)	100(2)	100(2)	100(2)
Radiation, λ (Å)	$Mo_{K\alpha}$ 0.71073	$Mo_{K\alpha}$ 0.71073	$Mo_{K\alpha}$ 0.71073
Crystal system	Triclinic	Monoclinic	Triclinic
Space group	$P\ \bar{1}$	$P2_1/n$	$P\ \bar{1}$
Unit cell dimensions			
a (Å)	9.487(2)	16.093(7)	9.6050(13)
b (Å)	14.575(5)	11.4147(19)	11.9696(14)
c (Å)	21.898(8)	16.144(8)	12.476(5)
α (°)	109.05(2)	90	104.67(4)
β (°)	90.346(9)	97.09(2)	95.958(13)
γ (°)	93.630(15)	90	103.391(7)
Volume (Å^3)	2855.2(17)	2943(2)	1329.6(6)
Z	2	2	2
Calculated density (Mg m^{-3})	1.196	1.166	1.290
Absorbtion coefficient (mm^{-1})	0.143	0.134	0.467
F(000)	1104	1128	544
Theta range for collection	2.341 to 26.021°	2.191 to 26.021°	1.713 to 26.019°
Reflections collected	84055	51874	22084
Independent reflections	11224	5793	5250
Minimum/maximum transmission	0.6736/0.7454	0.6469/0.7454	0.6332/0.7454
Refinement method	Full-matrix least-squares on F^2	Full-matrix least-squares on F^2	Full-matrix least-squares on F^2
Data / parameters / restrains	11224 / 679 / 0	5793 / 344 / 0	5250 / 332 / 0
Goodness-of-fit on F^2	1.043	1.019	1.024
Final R indices [I>2σ(I)]	R_1 = 0.0514, wR^2 = 0.1010	R_1 = 0.0355, wR^2 = 0.0862	R_1 = 0.0287, wR^2 = 0.0774
R indices (all data)	R_1 = 0.0760, wR^2 = 0.1099	R_1 = 0.0443, wR^2 = 0.0926	R_1 = 0.0320, wR^2 = 0.0793
Maximum/minimum residual electron density (e Å^{-3})	0.351 / –0.298	0.297 / –0.264	0.384 / –0.317

Compound	**22**	**24^{Me}**	**24^{Cy}**
CCDC number	–	2044881	2044883
Empirical formula	$C_{29}H_{47}BBrN_3$	$C_{49}H_{74}B_2N_2O_2P_2$	$C_{50}H_{78}B_2Cl_4N_2O_2P_2$
Formula weight (g mol^{-1})	528.41	806.66	964.50
Temperature (K)	100(2)	100.00(10)	100(2)
Radiation, λ (Å)	$Mo_{K\alpha}$ 0.71073	$Cu_{K\alpha}$1.54184	$Mo_{K\alpha}$ 0.71073
Crystal system	Monoclinic	Triclinic	Monoclinic
Space group	$P2_1/c$	$P\ \bar{1}$	$P2_1/c$
Unit cell dimensions			
a (Å)	22.454(4)	8.64108(16)	15.095(7)
b (Å)	14.221(2)	11.9691(3)	12.104(3)
c (Å)	18.158(11)	12.4567(3)	15.552(3)
α (°)	90	67.204(2)	90
β (°)	94.03(3)	80.2643(19)	113.731(18)
γ (°)	90	89.3387(16)	90
Volume (Å^3)	5784(4)	1168.54(5)	2601.2(15)
Z	8	1	2
Calculated density (Mg m^{-3})	1.214	1.146	1.231
Absorbtion coefficient (mm^{-1})	1.442	1.134	0.329
F(000)	2256	438	1032
Theta range for collection	2.517 to 26.022°	3.912 to 72.115°	2.209 to 26.022°
Reflections collected	59134	25215	24506
Independent reflections	11385	4605	5116
Minimum/maximum transmission	0.6008/0.7453	0.49919/1.00000	0.6421/0.7454
Refinement method	Full-matrix least-squares on F^2	Full-matrix least-squares on F^2	Full-matrix least-squares on F^2
Data / parameters / restrains	11385 / 723 / 252	4605 / 388 / 252	5116 / 294 / 0
Goodness-of-fit on F^2	1.028	1.051	1.030
Final R indices [I>2σ(I)]	R_1 = 0.0282, wR^2 = 0.0647	R_1 = 0.0371, wR^2 = 0.0969	R_1 = 0.0346, wR^2 = 0.0832
R indices (all data)	R_1 = 0.0373, wR^2 = 0.0686	R_1 = 0.0407, wR^2 = 0.0995	R_1 = 0.0434, wR^2 = 0.0889
Maximum/minimum residual electron density (e Å^{-3})	0.339 / –0.480	0.331 / –0.243	0.433 / –0.434

Compound	**25^{Ph}**	**25^{Ph}-Cr**
CCDC number	2044882	2044884
Empirical formula	$C_{54}H_{58}B_2NP$	$C_{123}H_{125}B_4Cr_2N_2O_6P_2$
Formula weight (g mol^{-1})	773.60	1936.42
Temperature (K)	99.98(19)	100(2)
Radiation, λ (Å)	$Cu_{K\alpha}$1.54184	$Mo_{K\alpha}$ 0.71073
Crystal system	Monoclinic	Triclinic
Space group	$P2_1/n$	$P\ \bar{1}$
Unit cell dimensions		
a (Å)	14.70993(9)	11.8302(18)
b (Å)	11.47947(8)	22.906(4)
c (Å)	26.29888(19)	24.371(4)
α (°)	90.0	62.350(13)
β (°)	94.4600(6)	88.527(14)
γ (°)	90.0	75.955(11)
Volume (Å^3)	4427.44(6)	5645.8(18)
Z	4	2
Calculated density (Mg m^{-3})	1.161	1.139
Absorbtion coefficient (mm^{-1})	0.816	0.274
F(000)	1656	2046
Theta range for collection	3.337 to 72.122°	2.049 to 26.022°
Reflections collected	104240	322472
Independent reflections	8718	22247
Minimum/maximum transmission	0.901/1.000	0.6379/0.7454
Refinement method	Full-matrix least-squares on F^2	Full-matrix least-squares on F^2
Data / parameters / restrains	8718 / 537 / 0	22247 / 1309 / 445
Goodness-of-fit on F^2	1.128	1.038
Final R indices [I>2σ(I)]	R_1 = 0.0439, wR^2 = 0.0967	R_1 = 0.0708, wR^2 = 0.1825
R indices (all data)	R_1 = 0.0479, wR^2 = 0.0986	R_1 = 0.0936, wR^2 = 0.2011
Maximum/minimum residual electron density (e Å^{-3})	0.347 / –0.309	0.926 / –0.740

VII References

[1] S. Hagspiel, *Masterarbeit* **2018**, Julius-Maximilians-Universität Würzburg.

[2] D. Himmel, I. Krossing, A. Schnepf, *Angew. Chem. Int. Ed.* **2014**, *53*, 370–374.

[3] G. Frenking, *Angew. Chem. Int. Ed.* **2014**, *53*, 6040–6046.

[4] D. Himmel, I. Krossing, A. Schnepf, *Angew. Chem. Int. Ed.* **2014**, *53*, 6047–6048.

[5] M. N. Hopkinson, C. Richter, M. Schedler, F. Glorius, *Nature* **2014**, *510*, 485–496.

[6] S. Díez-González, *N-Heterocyclic Carbenes: From Laboratory Curiosities to Efficient Synthetic Tools, Vol. 27*, Royal Society of Chemistry, **2016**.

[7] E. O. Fischer, A. Maasböl, *Angew. Chem. Int. Ed.* **1964**, *3*, 580–581.

[8] R. R. Schrock, *J. Am. Chem. Soc.* **1975**, *97*, 6577–6578.

[9] A. J. Arduengo III, R. L. Harlow, M. Kline, *J. Am. Chem. Soc.* **1991**, *113*, 361–363.

[10] S. Würtemberger-Pietsch, U. Radius, T. B. Marder, *Dalton Trans.* **2016**, *45*, 5880–5895.

[11] K. M. Hindi, M. J. Panzner, C. A. Tessier, C. L. Cannon, W. J. Youngs, *Chem. Rev.* **2009**, *109*, 3859–3884.

[12] R. Visbal, M. C. Gimeno, *Chem. Soc. Rev.* **2014**, *43*, 3551–3574.

[13] S. Díez-González, N. Marion, S. P. Nolan, *Chem. Rev.* **2009**, *109*, 3612–3676.

[14] F. E. Hahn, M. C. Jahnke, *Angew. Chem. Int. Ed.* **2008**, *47*, 3122–3172.

[15] D. Enders, O. Niemeier, A. Henseler, *Chem. Rev.* **2007**, *107*, 5606–5655.

[16] E. A. B. Kantchev, C. J. O'Brien, M. G. Organ, *Angew. Chem. Int. Ed.* **2007**, *46*, 2768–2813.

[17] F. Wang, L.-j. Liu, W. Wang, S. Li, M. Shi, *Coord. Chem. Rev.* **2012**, *256*, 804–853.

[18] P. Teo, R. H. Grubbs, *Organometallics* **2010**, *29*, 6045–6050.

[19] C. Samojłowicz, M. Bieniek, K. Grela, *Chem. Rev.* **2009**, *109*, 3708–3742.

[20] V. Lavallo, Y. Canac, C. Präsang, B. Donnadieu, G. Bertrand, *Angew. Chem. Int. Ed.* **2005**, *44*, 5705–5709.

[21] D. Martin, M. Soleilhavoup, G. Bertrand, *Chem. Sci.* **2011**, *2*, 389–399.

[22] V. Lavallo, Y. Canac, B. Donnadieu, W. W. Schoeller, G. Bertrand, *Angew. Chem. Int. Ed.* **2006**, *45*, 3488–3491.

[23] S. Kundu, S. Sinhababu, V. Chandrasekhar, H. W. Roesky, *Chem. Sci.* **2019**, *10*, 4727–4741.

[24] U. S. D. Paul, M. J. Krahfuß, U. Radius, *Chem. Unserer Zeit* **2019**, *53*, 212–223.

[25] M. Melaimi, R. Jazzar, M. Soleilhavoup, G. Bertrand, *Angew. Chem. Int. Ed.* **2017**, *56*, 10046–10068.

[26] M. Soleilhavoup, G. Bertrand, *Acc. Chem. Res.* **2015**, *48*, 256–266.

[27] Y. Mizuhata, T. Sasamori, N. Tokitoh, *Chem. Rev.* **2009**, *109*, 3479–3511.

[28] M. Soleilhavoup, G. Bertrand, *Angew. Chem. Int. Ed.* **2017**, *56*, 10282–10292.

[29] M. Krasowska, M. Edelmann, H. F. Bettinger, *J. Phys. Chem. A* **2016**, *120*, 6332–6341.

[30] M. Krasowska, H. F. Bettinger, *J. Am. Chem. Soc.* **2012**, *134*, 17094–17103.

[31] C. A. Thompson, L. Andrews, J. M. L. Martin, J. El-Yazal, *J. Phys. Chem.* **1995**, *99*, 13839–13849.

[32] P. L. Timms, *Acc. Chem. Res.* **1973**, *6*, 118–123.

[33] P. L. Timms, *J. Am. Chem. Soc.* **1967**, *89*, 1629–1632.

[34] J. W. C. Johns, F. A. Grimm, R. F. Porter, *J. Mol. Spectrosc.* **1967**, *22*, 435–451.

[35] H. F. Bettinger, *J. Am. Chem. Soc.* **2006**, *128*, 2534–2535.

[36] L. Andrews, P. Hassanzadeh, J. M. L. Martin, P. R. Taylor, *J. Phys. Chem.* **1993**, *97*, 5839–5847.

[37] M. Ito, N. Tokitoh, T. Kawashima, R. Okazaki, *Tetrahedron Lett.* **1999**, *40*, 5557–5560.

[38] W. J. Grigsby, P. P. Power, *J. Am. Chem. Soc.* **1996**, *118*, 7981–7988.

[39] A. Meller, U. Seebold, W. Maringgele, M. Noltemeyer, G. M. Sheldrick, *J. Am. Chem. Soc.* **1989**, *111*, 8299–8300.

[40] P. L. Timms, *J. Am. Chem. Soc.* **1968**, *90*, 4585–4589.

[41] B. Pachaly, R. West, *Angew. Chem. Int. Ed.* **1984**, *23*, 454–455.

[42] H. Braunschweig, T. Wagner, *Angew. Chem. Int. Ed.* **1995**, *34*, 825–826.

[43] H. Braunschweig, C. Kollann, U. Englert, *Angew. Chem. Int. Ed.* **1998**, *37*, 3179–3180.

[44] H. Braunschweig, R. D. Dewhurst, V. H. Gessner, *Chem. Soc. Rev.* **2013**, *42*, 3197–3208.

[45] Y. Wang, B. Quillian, P. Wei, C. S. Wannere, Y. Xie, R. B. King, H. F. Schaefer, P. v. R. Schleyer, G. H. Robinson, *J. Am. Chem. Soc.* **2007**, *129*, 12412–12413.

[46] R. Kinjo, B. Donnadieu, M. A. Celik, G. Frenking, G. Bertrand, *Science* **2011**, *333*, 610–613.

[47] D. A. Ruiz, M. Melaimi, G. Bertrand, *Chem. Commun.* **2014**, *50*, 7837–7839.

[48] L. Kong, Y. Li, R. Ganguly, D. Vidovic, R. Kinjo, *Angew. Chem. Int. Ed.* **2014**, *53*, 9280–9283.

[49] C. E. Anderson, H. Braunschweig, R. D. Dewhurst, *Organometallics* **2008**, *27*, 6381–6389.

[50] H. Braunschweig, R. D. Dewhurst, F. Hupp, M. Nutz, K. Radacki, C. W. Tate, A. Vargas, Q. Ye, *Nature* **2015**, *522*, 327–330.

[51] H. Braunschweig, I. Krummenacher, M.-A. Légaré, A. Matler, K. Radacki, Q. Ye, *J. Am. Chem. Soc.* **2017**, *139*, 1802–1805.

[52] P. Bissinger, H. Braunschweig, A. Damme, I. Krummenacher, A. K. Phukan, K. Radacki, S. Sugawara, *Angew. Chem. Int. Ed.* **2014**, *53*, 7360–7363.

[53] M.-A. Légaré, G. Bélanger-Chabot, R. D. Dewhurst, E. Welz, I. Krummenacher, B. Engels, H. Braunschweig, *Science* **2018**, *359*, 896–900.

[54] K. Edel, M. Krieg, D. Grote, H. F. Bettinger, *J. Am. Chem. Soc.* **2017**, *139*, 15151–15159.

[55] Y. Nishibayashi, *Transition metal-dinitrogen complexes: preparation and reactivity*, John Wiley & Sons, **2019**.

[56] J. Huheey, E. Keiter, R. Keiter, *Anorganische Chemie*, *Frontmatter*, De Gruyter, **2014**.

[57] M.-A. Légaré, C. Pranckevicius, H. Braunschweig, *Chem. Rev.* **2019**, *119*, 8231–8261.

[58] B. Rösch, T. X. Gentner, J. Langer, C. Färber, J. Eyselein, L. Zhao, C. Ding, G. Frenking, S. Harder, *Science* **2021**, *371*, 1125–1128.

[59] B. Xu, H. Beckers, H. Ye, Y. Lu, J. Cheng, X. Wang, S. Riedel, *Angew. Chem. Int. Ed.* **2021**, *60*, 17205–17210.

[60] M.-A. Légaré, M. Rang, G. Bélanger-Chabot, J. I. Schweizer, I. Krummenacher, R. Bertermann, M. Arrowsmith, M. C. Holthausen, H. Braunschweig, *Science* **2019**, *363*, 1329–1332.

[61] M.-A. Légaré, G. Bélanger-Chabot, M. Rang, R. D. Dewhurst, I. Krummenacher, R. Bertermann, H. Braunschweig, *Nature Chem.* **2020**, *12*, 1076–1080.

[62] M. Arrowsmith, D. Auerhammer, R. Bertermann, H. Braunschweig, G. Bringmann, M. A. Celik, R. D. Dewhurst, M. Finze, M. Grüne, M. Hailmann, T. Hertle, I. Krummenacher, *Angew. Chem. Int. Ed.* **2016**, *55*, 14464–14468.

[63] H. Wang, L. Wu, Z. Lin, Z. Xie, *J. Am. Chem. Soc.* **2017**, *139*, 13680–13683.

[64] M. Arrowsmith, J. I. Schweizer, M. Heinz, M. Härterich, I. Krummenacher, M. C. Holthausen, H. Braunschweig, *Chem. Sci.* **2019**, *10*, 5095–5103.

[65] S. K. Sarkar, M. M. Siddiqui, S. Kundu, M. Ghosh, J. Kretsch, P. Stollberg, R. Herbst-Irmer, D. Stalke, A. C. Stückl, B. Schwederski, W. Kaim, S. Ghorai, E. D. Jemmis, H. W. Roesky, *Dalton Trans.* **2019**, *48*, 8551–8555.

[66] C. Pranckevicius, C. Herok, F. Fantuzzi, B. Engels, H. Braunschweig, *Angew. Chem. Int. Ed.* **2019**, *58*, 12893–12897.

[67] S. Morisako, R. Shang, Y. Yamamoto, H. Matsui, M. Nakano, *Angew. Chem. Int. Ed.* **2017**, *56*, 15234–15240.

[68] F. Dahcheh, D. Martin, D. W. Stephan, G. Bertrand, *Angew. Chem. Int. Ed.* **2014**, *53*, 13159–13163.

[69] A. D. Ledet, T. W. Hudnall, *Dalton Trans.* **2016**, *45*, 9820–9826.

[70] M. Arrowsmith, J. Böhnke, H. Braunschweig, H. Gao, M.-A. Légaré, V. Paprocki, J. Seufert, *Chem. Eur. J.* **2017**, *23*, 12210–12217.

[71] D. P. Curran, A. Boussonnière, S. J. Geib, E. Lacôte, *Angew. Chem. Int. Ed.* **2012**, *51*, 1602–1605.

[72] Y. Wang, G. H. Robinson, *Inorg. Chem.* **2011**, *50*, 12326–12337.

[73] P. Bissinger, H. Braunschweig, A. Damme, R. D. Dewhurst, T. Kupfer, K. Radacki, K. Wagner, *J. Am. Chem. Soc.* **2011**, *133*, 19044–19047.

[74] D. Auerhammer, M. Arrowsmith, H. Braunschweig, R. D. Dewhurst, J. O. C. Jimenez-Halla, T. Kupfer, *Chem. Sci.* **2017**, *8*, 7066–7071.

[75] C. Pranckevicius, M. Weber, I. Krummenacher, A. K. Phukan, H. Braunschweig, *Chem. Sci.* **2020**, *11*, 11055–11059.

[76] T. W. Hudnall, C. W. Bielawski, *J. Am. Chem. Soc.* **2009**, *131*, 16039–16041.

[77] L. Kong, W. Lu, Y. Li, R. Ganguly, R. Kinjo, *J. Am. Chem. Soc.* **2016**, *138*, 8623–8629.

[78] L. Kong, R. Ganguly, Y. Li, R. Kinjo, *Chem. Sci.* **2015**, *6*, 2893–2902.

[79] H. Braunschweig, R. D. Dewhurst, L. Pentecost, K. Radacki, A. Vargas, Q. Ye, *Angew. Chem. Int. Ed.* **2016**, *55*, 436–440.

[80] H. V. Huynh, *Chem. Rev.* **2018**, *118*, 9457–9492.

[81] H. Clavier, S. P. Nolan, *Chem. Commun.* **2010**, *46*, 841–861.

[82] I. Ghesner, W. E. Piers, M. Parvez, R. McDonald, *Can. J. Chem.* **2006**, *84*, 81–92.

[83] M. F. Dubreuil, N. G. Farcy, E. J. Goethals, *Macromol. Rapid Commun.* **1999**, *20*, 383–386.

[84] M. Arrowsmith, J. D. Mattock, S. Hagspiel, I. Krummenacher, A. Vargas, H. Braunschweig, *Angew. Chem. Int. Ed.* **2018**, *57*, 15272–15275.

[85] M. Arrowsmith, D. Auerhammer, R. Bertermann, H. Braunschweig, M. A. Celik, J. Erdmannsdörfer, I. Krummenacher, T. Kupfer, *Angew. Chem. Int. Ed.* **2017**, *56*, 11263–11267.

[86] D. A. Ruiz, G. Ung, M. Melaimi, G. Bertrand, *Angew. Chem. Int. Ed.* **2013**, *52*, 7590–7592.

[87] M. Wagner, N. J. R. van Eikema Hommes, H. Noeth, P. v. R. Schleyer, *Inorg. Chem.* **1995**, *34*, 607–614.

[88] L. M. Sachs, M. Geller, J. J. Kaufman, *J. Chem. Phys.* **1970**, *52*, 974–977.

[89] J. Monot, A. Solovyev, H. Bonin-Dubarle, É. Derat, D. P. Curran, M. Robert, L. Fensterbank, M. Malacria, E. Lacôte, *Angew. Chem. Int. Ed.* **2010**, *49*, 9166–9169.

[90] M. Yamashita, K. Nozaki, *Boryl Anions, Synthesis and Application of Organoboron Compounds. Topics in Organometallic Chemistry, Vol. 49*, Springer, Cham, **2015**.

[91] H. C. Brown, R. Liotta, C. G. Scouten, *J. Am. Chem. Soc.* **1976**, *98*, 5297–5301.

[92] G. W. Kramer, H. C. Brown, *J. Organomet. Chem.* **1977**, *132*, 9–27.

[93] S. Akiyama, K. Yamada, M. Yamashita, *Angew. Chem. Int. Ed.* **2019**, *58*, 11806–11810.

[94] Y. Su, R. Kinjo, *Coord. Chem. Rev.* **2017**, *352*, 346–378.

[95] A. Deissenberger, E. Welz, R. Drescher, I. Krummenacher, R. D. Dewhurst, B. Engels, H. Braunschweig, *Angew. Chem. Int. Ed.* **2019**, *58*, 1842–1846.

[96] J. Böhnke, T. Dellermann, M. A. Celik, I. Krummenacher, R. D. Dewhurst, S. Demeshko, W. C. Ewing, K. Hammond, M. Heß, E. Bill, E. Welz, M. I. S. Röhr, R. Mitrić, B. Engels, F. Meyer, H. Braunschweig, *Nat. Commun.* **2018**, *9*, 1197.

[97] T. Peymann, C. B. Knobler, M. Frederick Hawthorne, *Chem. Commun.* **1999**, 2039–2040.

[98] A. Solovyev, Q. Chu, S. J. Geib, L. Fensterbank, M. Malacria, E. Lacôte, D. P. Curran, *J. Am. Chem. Soc.* **2010**, *132*, 15072–15080.

[99] W. Preetz, B. Steuer, *Z. Naturforsch. B* **1996**, *51*, 551–556.

[100] F. L. Hirshfeld, *Theor. Chim. Acta* **1977**, *44*, 129–138.

[101] C. Lee, W. Yang, R. G. Parr, *Phys. Rev. B* **1988**, *37*, 785–789.

[102] B. Miehlich, A. Savin, H. Stoll, H. Preuss, *Chem. Phys. Lett.* **1989**, *157*, 200–206.

[103] N. C. Handy, A. J. Cohen, *Mol. Phys.* **2001**, *99*, 403–412.

[104] W.-M. Hoe, A. J. Cohen, N. C. Handy, *Chem. Phys. Lett.* **2001**, *341*, 319–328.

[105] J. Böhnke, M. Arrowsmith, H. Braunschweig, *J. Am. Chem. Soc.* **2018**, *140*, 10368–10373.

[106] L. Kong, W. Lu, L. Yongxin, R. Ganguly, R. Kinjo, *Inorg. Chem.* **2017**, *56*, 5586–5593.

[107] M. Nutz, B. Borthakur, C. Pranckevicius, R. D. Dewhurst, M. Schäfer, T. Dellermann, F. Glaab, M. Thaler, A. K. Phukan, H. Braunschweig, *Chem. Eur. J.* **2018**, *24*, 6843–6847.

[108] R. E. Bachman, K. H. Whitmire, *Inorg. Chem.* **1995**, *34*, 1542–1551.

[109] F. Biesemeier, K. Harms, U. Müller, *Z. Kristallogr. NCS* **2003**, *218*, 419–420.

[110] A. Trummal, L. Lipping, I. Kaljurand, I. A. Koppel, I. Leito, *J. Phys. Chem. A* **2016**, *120*, 3663–3669.

[111] F. G. Bordwell, D. L. Hughes, *J. Org. Chem.* **1982**, *47*, 3224–3232.

[112] A. K. Chandra, P.-C. Nam, M. T. Nguyen, *J. Phys. Chem. A* **2003**, *107*, 9182–9188.

[113] E. P. L. Hunter, S. G. Lias, *J. Phys. Chem. Ref. Data* **1998**, *27*, 413–656.

[114] R. Tonner, G. Heydenrych, G. Frenking, *ChemPhysChem* **2008**, *9*, 1474–1481.

[115] P. Bissinger, H. Braunschweig, K. Kraft, T. Kupfer, *Angew. Chem. Int. Ed.* **2011**, *50*, 4704–4707.

[116] B. P. Biswal, D. Becker, N. Chandrasekhar, J. S. Seenath, S. Paasch, S. Machill, F. Hennersdorf, E. Brunner, J. J. Weigand, R. Berger, X. Feng, *Chem. Eur. J.* **2018**, *24*, 10868–10875.

[117] M. T. Mock, R. G. Potter, D. M. Camaioni, J. Li, W. G. Dougherty, W. S. Kassel, B. Twamley, D. L. DuBois, *J. Am. Chem. Soc.* **2009**, *131*, 14454–14465.

[118] D. K. Roy, T. Tröster, F. Fantuzzi, R. D. Dewhurst, C. Lenczyk, K. Radacki, C. Pranckevicius, B. Engels, H. Braunschweig, *Angew. Chem. Int. Ed.* **2021**, *60*, 3812–3819.

[119] K. E. Horner, P. B. Karadakov, *J. Org. Chem.* **2015**, *80*, 7150–7157.

[120] R. Herges, D. Geuenich, *J. Phys. Chem. A* **2001**, *105*, 3214–3220.

[121] D. Geuenich, K. Hess, F. Köhler, R. Herges, *Chem. Rev.* **2005**, *105*, 3758–3772.

[122] P. v. R. Schleyer, C. Maerker, A. Dransfeld, H. Jiao, N. J. R. van Eikema Hommes, *J. Am. Chem. Soc.* **1996**, *118*, 6317–6318.

[123] Z. Chen, C. S. Wannere, C. Corminboeuf, R. Puchta, P. v. R. Schleyer, *Chem. Rev.* **2005**, *105*, 3842–3888.

[124] T. Tao, J. Geng, L. Hong, W. Huang, H. Tanaka, D. Tanaka, T. Ogawa, *J. Phys. Chem. C* **2013**, *117*, 25325–25333.

[125] A. Dessì, M. Calamante, A. Mordini, L. Zani, M. Taddei, G. Reginato, *RSC Advances* **2014**, *4*, 1322–1328.

[126] P. Wagner, M. Kubicki, *Acta Crystallogr. C* **2003**, *59*, o91–o92.

[127] M. Moral, A. Garzón, J. Canales-Vázquez, J. C. Sancho-García, *J. Phys. Chem. C* **2016**, *120*, 24583–24596.

[128] A. Fitri, A. T. Benjelloun, M. Benzakour, M. McHarfi, M. Sfaira, M. Hamidi, M. Bouachrine, *Res. Chem. Intermed.* **2013**, *39*, 2679–2695.

[129] P. Zahradník, P. Magdolen, P. Zahradník, *Tetrahedron Lett.* **2010**, *51*, 5819–5821.

[130] J. Wu, G. Li, J. Fang, X. Guo, L. Zhu, B. Guo, Y. Wang, G. Zhang, L. Arunagiri, F. Liu, H. Yan, M. Zhang, Y. Li, *Nat. Commun.* **2020**, *11*, 4612.

[131] A. Dessì, M. Calamante, A. Sinicropi, M. L. Parisi, L. Vesce, P. Mariani, B. Taheri, M. Ciocca, A. Di Carlo, L. Zani, A. Mordini, G. Reginato, *Sustain. Energy Fuels* **2020**, *4*, 2309–2321.

[132] S. Ameen, M. S. Akhtar, M. Nazim, M. K. Nazeeruddin, H.-S. Shin, *Nano Energy* **2018**, *49*, 372–379.

[133] W. Li, X. Huang, T. Zeng, Y. A. Liu, W. Hu, H. Yang, Y.-B. Zhang, K. Wen, *Angew. Chem. Int. Ed.* **2021**, *60*, 1869–1874.

[134] Y. Wang, H. Liu, Q. Pan, N. Ding, C. Yang, Z. Zhang, C. Jia, Z. Li, J. Liu, Y. Zhao, *ACS Appl. Mater. Interfaces* **2020**, *12*, 46483–46489.

[135] A. Khatun, D. K. Panda, N. Sayresmith, M. G. Walter, S. Saha, *Inorg. Chem.* **2019**, *58*, 12707–12715.

[136] J. Y. Jung, M. Kang, J. Chun, J. Lee, J. Kim, J. Kim, Y. Kim, S.-J. Kim, C. Lee, J. Yoon, *Chem. Commun.* **2013**, *49*, 176–178.

[137] J. Y. Jung, S. J. Han, J. Chun, C. Lee, J. Yoon, *Dyes Pigm.* **2012**, *94*, 423–426.

[138] S. Safaei, J. Wang, P. C. Junk, *J. Solid State Chem.* **2021**, *294*, 121762.

[139] G. Sathiyan, S. Chatterjee, P. Sen, A. Garg, R. K. Gupta, A. Singh, *ChemistrySelect* **2019**, *4*, 11718–11725.

[140] M. R. Pinto, Y. Takahata, T. D. Z. Atvars, *J. Photochem. Photobiol. A: Chem.* **2001**, *143*, 119–127.

[141] U. Olgun, M. Gülfen, *RSC Advances* **2014**, *4*, 25165–25171.

[142] J. T. Goettel, H. Braunschweig, *Coord. Chem. Rev.* **2019**, *380*, 184–200.

[143] H. Araki, K. Tsuge, Y. Sasaki, S. Ishizaka, N. Kitamura, *Inorg. Chem.* **2005**, *44*, 9667–9675.

[144] X.-S. Wang, H. Zhao, Y.-H. Li, R.-G. Xiong, X.-Z. You, *Top. Catal.* **2005**, *35*, 43–61.

[145] M. A. Bennett, *Chem. Rev.* **1962**, *62*, 611–652.

[146] F. Jäkle, *Dalton Trans.* **2007**, 2851–2858.

[147] A. Sundararaman, R. A. Lalancette, L. N. Zakharov, A. L. Rheingold, F. Jäkle, *Organometallics* **2003**, *22*, 3526–3532.

[148] A. Doshi, A. Sundararaman, K. Venkatasubbaiah, L. N. Zakharov, A. L. Rheingold, M. Myahkostupov, P. Piotrowiak, F. Jäkle, *Organometallics* **2012**, *31*, 1546–1558.

[149] K. Wang, S. Huang, Y. Zhang, S. Zhao, H. Zhang, Y. Wang, *Chem. Sci.* **2013**, *4*, 3288–3293.

[150] E. Bulak, T. Varnal, P. Paetzold, U. Englert, *Z. Anorg. Allg. Chem.* **1999**, *625*, 3–5.

[151] J. A. Soderquist, H. C. Brown, *J. Org. Chem.* **1981**, *46*, 4599–4600.

[152] S. Sulzer-Mossé, A. Alexakis, J. Mareda, G. Bollot, G. Bernardinelli, Y. Filinchuk, *Chem. Eur. J.* **2009**, *15*, 3204–3220.

[153] Y.-J. Cao, Y.-Y. Lai, H. Cao, X.-N. Xing, X. Wang, W.-J. Xiao, *Can. J. Chem.* **2006**, *84*, 1529–1533.

[154] J. Xia, R. Yao, M. Cai, *Appl. Organomet. Chem.* **2015**, *29*, 221–225.

[155] J. M. Khurana, P. K. Sahoo, *Synth. Commun.* **1992**, *22*, 1691–1702.

[156] M. Breugst, H.-U. Reissig, *Angew. Chem. Int. Ed.* **2020**, *59*, 12293–12307.

[157] Y.-C. Wang, X.-J. Lai, K. Huang, S. Yadav, G. Qiu, L. Zhang, H. Zhou, *Org. Chem. Front.* **2021**, *8*, 1677–1693.

[158] E. Merling, V. Lamm, S. J. Geib, E. Lacôte, D. P. Curran, *Org. Lett.* **2012**, *14*, 2690–2693.

[159] A. K. Swarnakar, C. Hering-Junghans, M. J. Ferguson, R. McDonald, E. Rivard, *Chem. Sci.* **2017**, *8*, 2337–2343.

[160] N. Zhu, H. Vahrenkamp, *Angew. Chem. Int. Ed.* **1994**, *33*, 2090–2091.

[161] *Science of Synthesis*, *Category 1, Organometallics, Vol. 2*, Georg Thieme Verlag, Stuttgart, **2003**.

[162] J. L. Vidal, G. E. Ryschkewitsch, *Inorg. Chem.* **1977**, *16*, 1898–1906.

[163] R. B. King, M. S. Saran, *Inorg. Chem.* **1974**, *13*, 74–78.

[164] J. M. Goicoechea, H. Grützmacher, *Angew. Chem. Int. Ed.* **2018**, *57*, 16968–16994.

[165] G. Becker, W. Schwarz, N. Seidler, M. Westerhausen, *Z. Anorg. Allg. Chem.* **1992**, *612*, 72–82.

[166] L. Weber, *Eur. J. Inorg. Chem.* **2018**, *2018*, 2175–2227.

[167] D. W. N. Wilson, M. P. Franco, W. K. Myers, J. E. McGrady, J. M. Goicoechea, *Chem. Sci.* **2020**, *11*, 862–869.

[168] W. Yang, K. E. Krantz, D. A. Dickie, A. Molino, D. J. D. Wilson, R. J. Gilliard Jr., *Angew. Chem. Int. Ed.* **2020**, *59*, 3971–3975.

[169] D. W. N. Wilson, A. Hinz, J. M. Goicoechea, *Angew. Chem. Int. Ed.* **2018**, *57*, 2188–2193.

[170] A. Hinz, R. Labbow, C. Rennick, A. Schulz, J. M. Goicoechea, *Angew. Chem. Int. Ed.* **2017**, *56*, 3911–3915.

[171] D. Heift, Z. Benkő, H. Grützmacher, *Dalton Trans.* **2014**, *43*, 831–840.

[172] J. H. Barnard, P. A. Brown, K. L. Shuford, C. D. Martin, *Angew. Chem. Int. Ed.* **2015**, *54*, 12083–12086.

[173] H. Braunschweig, F. Hupp, I. Krummenacher, L. Mailänder, F. Rauch, *Chem. Eur. J.* **2015**, *21*, 17844–17849.

[174] J. H. Barnard, S. Yruegas, K. Huang, C. D. Martin, *Chem. Commun.* **2016**, *52*, 9985–9991.

[175] S. Yruegas, C. D. Martin, *Chem. Eur. J.* **2016**, *22*, 18358–18361.

[176] H. Braunschweig, M. A. Celik, T. Dellermann, G. Frenking, K. Hammond, F. Hupp, H. Kelch, I. Krummenacher, F. Lindl, L. Mailänder, J. H. Müssig, A. Ruppert, *Chem. Eur. J.* **2017**, *23*, 8006–8013.

[177] G. Bélanger-Chabot, H. Braunschweig, D. K. Roy, *Eur. J. Inorg. Chem.* **2017**, 4353–4368.

[178] X. Su, J. J. Baker, C. D. Martin, *Chem. Sci.* **2020**, *11*, 126–131.

[179] B. Mailvaganam, B. G. Sayer, M. J. McGlinchey, *J. Organomet. Chem.* **1990**, *395*, 177–185.

[180] A. J. Ashe, X. Fang, X. Fang, J. W. Kampf, *Organometallics* **2001**, *20*, 5413–5418.

[181] E. Ardestani, R. Ghiasi, J. M. Tabatabai, *J. Struct. Chem.* **2018**, *59*, 1784–1790.

[182] F. Feixas, J. O. C. Jiménez-Halla, E. Matito, J. Poater, M. Solà, *Pol. J. Chem.* **2007**, *81*, 783–797.

[183] G. Sheldrick, *Acta Crystallogr. A* **2015**, *71*, 3–8.

[184] G. Sheldrick, *Acta Crystallogr. A* **2008**, *64*, 112–122.

[185] G. D. Frey, J. D. Masuda, B. Donnadieu, G. Bertrand, *Angew. Chem. Int. Ed.* **2010**, *49*, 9444–9447.

[186] M. Niehues, G. Erker, G. Kehr, P. Schwab, R. Fröhlich, O. Blacque, H. Berke, *Organometallics* **2002**, *21*, 2905–2911.

[187] D. Savoia, E. Tagliavini, C. Trombini, A. Umani-Ronchi, *J. Org. Chem.* **1981**, *46*, 5344–5348.

[188] N. Kuhn, T. Kratz, *Synthesis* **1993**, *1993*, 561–562.

[189] M. Brookhart, B. Grant, A. F. Volpe, *Organometallics* **1992**, *11*, 3920–3922.

[190] J. J. Eisch, J. E. Galle, S. Kozima, *J. Am. Chem. Soc.* **1986**, *108*, 379–385.

[191] H. Braunschweig, A. Damme, J. O. C. Jimenez-Halla, C. Hörl, I. Krummenacher, T. Kupfer, L. Mailänder, K. Radacki, *J. Am. Chem. Soc.* **2012**, *134*, 20169–20177.

[192] H. Braunschweig, V. Dyakonov, J. O. C. Jimenez-Halla, K. Kraft, I. Krummenacher, K. Radacki, A. Sperlich, J. Wahler, *Angew. Chem. Int. Ed.* **2012**, *51*, 2977–2980.

[193] D. P. Tate, W. R. Knipple, J. M. Augl, *Inorg. Chem.* **1962**, *1*, 433–434.

Danksagung

Zuallererst möchte ich meinem Doktorvater **Prof. Dr. Holger Braunschweig** für die Möglichkeit danken, meine Dissertation in seinem Arbeitskreis anzufertigen. Vielen Dank Holger für die tolle Arbeitsatmosphäre, die du uns bereitest, sowie für das stetige Vertrauen in meine Arbeit und die mir gewährte wissenschaftliche Freiheit. Deine mitreißende Begeisterung für die Chemie hat mich stets motiviert. Danke Holger, dass du mir auch bei meinem weiteren beruflichen Weg so viel Unterstützung zukommen lässt.

Ein großes Dankeschön auch an **Birgit Zepke** für die Unterstützung in bürokratischen Angelegenheiten. Ohne dich wären wir oftmals ganz schön aufgeschmissen!

Außerdem möchte ich mich bei meinen Laborkollegen und all denjenigen bedanken, die bei chemischen Fragestellungen und sonstigen Problemen stets mit Rat und Tat zur Seite standen. Danke für eure Unterstützung in Form von Diskussionen, Ideen, Edukten und Glasgeräten, sowie ganz allgemein für die produktive Zusammenarbeit. An dieser Stelle möchte ich mich auch bei allen bedanken, die unzählige Stunden ihrer Arbeitszeit in die Suche von Einkristallen und die Auswertung der Messdaten investiert haben. Danke für euren Beitrag zu dieser Arbeit!

Ganz besonders möchte ich mich bei **Dr. Merle Arrowsmith**, **Dr. Rian Dewhurst** und **Dr. Ivo Krummenacher** für die gemeinsamen Publikationen bedanken. Vielen Dank Merle, dass du stets so viel Interesse an meiner Chemie gezeigt und du dir immer Zeit für Diskussionen genommen hast. Ich bin dir sehr dankbar, dass du mir beim Verfassen von Manuskripten und Forschungsanträgen so viel beigebracht hast – das weiß ich sehr zu schätzen! Danke Ivo für die Durchführung der cyclovoltammetrischen Messungen und die Aufnahme der ESR-Spektren.

Für die Durchführung der quantenmechanischen Rechnungen danke ich **Dr. Felipe Fantuzzi** und **Dr. Alfredo Vargas**. Danke Felipe, ohne dich wären unsere gemeinsamen Publikationen nicht halb so schön. Ich danke dir vielmals für dein Engagement und wünsche dir für deinen akademischen Werdegang nur das Beste!

Dr. Krzysztof Radacki danke für das Einlernen in die Hohe Kunst der Röntgenstrukturanalyse. Danke Krzys, dass man sich immer hilfesuchend an dich wenden kann. Danke auch für deine Anekdoten, deine Aussprache des Wortes „label“ und dein Fachwissen über Steinobst, wie beispielsweise Mirabellen.

Weiterhin möchte ich mich bei **Dr. Rüdiger Bertermann**, **Marie-Luise Schäfer** und **Laura Wolz** für die Durchführung der NMR-spektroskopischen Messungen danken. **Sabine Timmroth** und **Liselotte Michels** danke ich für die Elementaranalysen. **Christoph Mahler**

gilt mein Dank für die Aufnahme der Massenspektren. Außerdem möchte ich mich bei allen Angestellten der Verwaltungen, Werkstätten und bei der Haustechnik bedanken, die oftmals im Hintergrund arbeiten und einen reibungslosen Laborbetrieb gewährleisten.

Bedanken möchte ich mich auch bei meinen Praktikanten **Dren Elezi** und **Jan Niedens** für deren fleißige Mitarbeit.

Maximilian Fest danke ich vielmals für die Durchführung der Fluoreszenzmessungen.

Ein großer Dank geht auch an **Kai Hammond** und **Carina Heer**. Danke, dass ihr mich stets mit Chemikalien versorgt habt und ich mich bei präparativen Fragen immer an euch wenden konnte.

Ein generelles Dankeschön gilt auch allen aktuellen und ehemaligen Mitgliedern des AK Braunschweig und des AK Lichtenberg für die wunderbare Zeit und die ideale Arbeitsatmosphäre. Danke für die schönen Weihnachtsfeiern, Sommerfeste, sonstige Freizeitaktivitäten und den ein oder anderen Gefährlichen Wochentag.

Außerdem möchte ich allen danken, die zur Fertigstellung dieser Arbeit beigetragen haben. Vielen Dank **Maximilian Dietz**, **Dr. Merle Arrowsmith** und **Dr. Felix Lindl** für das Korrekturlesen dieser Arbeit. Maxi danke ich zudem dafür, dass er sich neben sinnvollen Verbesserungsvorschlägen auch Zeit für wertende Kommentare genommen hat. Vielen Dank Felix für die vielen Diskussionen, neue Ideen und deine ansteckende Freude an der Chemie.

Der vielleicht größte Dank geht an meine Freunde, auch bekannt als „die einzigen Normalen“. **Fabian** (FS, EFES, Schorres, Schnurres, Pico, Ash, Leicht-angedeuteter), **Annalena** (Anna, Anna-Lena, Anna-Lea, Annemarie, Annegret, Annika, ALG, AnGa, Hüterin-der-Synergy, Ganga), **Maximilian** (Maxi, MAXIMILIAN, Max-a-million, Dietrich, Die-CHN-passt-eh-nicht), **Lisa** (LiZzy, LiZzy LiZzard, Butterbirne, Leute-bitte), ich danke euch für die unvergessliche Zeit während des Studiums und der Promotion. Ich werde immer mit Freude auf die gemeinsamen Mittags- und Kaffeepausen, Kochabende, Tagungen und die vielen Freizeitaktivitäten zurückblicken. Ich hoffe ihr wart nicht nur Übergangsfreunde! Außerdem möchte ich **Corinna**, **Dario**, **Jacque**, **Malte**, **Kai**, **Nicola**, **Max R.**, **Peter**, **Silvi**, **Anna L.** und allen, die ich gerade vergessen habe, für die schöne gemeinsame Zeit danken!

Zu guter Letzt möchte ich mich auch bei meiner gesamten **Familie** bedanken. Vielen Dank dafür, dass ihr immer an meiner Seite steht und mich bedingungslos unterstützt.